

**IMAGING STUDIES OF THE CANINE
CERVICAL VERTEBRAL VENOUS PLEXUS**

by

Marcelo A. Gomez Jaramillo, DVM

Dissertation submitted to the faculty of the Virginia Polytechnic Institute and State
University in partial fulfillment of the requirements for the degree of

DOCTOR OF PHILOSOPHY
IN
VETERINARY MEDICAL SCIENCES

Jeryl Jones, Chair
Larry Freeman
Otto Lanz
Karen Inzana
Richard Broadstone

January 14, 2005

Blacksburg, Virginia

Keywords: vertebral venous plexus, computed tomography, CT venography,
digital subtraction venography, cervical spine.

Copyright 2005, Marcelo Gomez Jaramillo

**IMAGING STUDIES OF THE CANINE CERVICAL VERTEBRAL VENOUS
PLEXUS**

by

Marcelo Gomez Jaramillo, DVM

Jeryl Jones, DVM, PhD, Chair

Department of Small Animal Clinical Sciences

(ABSTRACT)

The internal vertebral venous plexus (IVVP) is an extensive vascular network recently implicated in various human and canine spinal disorders. Nevertheless, little recent information is available regarding normal anatomy of canine IVVP and its role in acute spinal injuries. The objectives of the study were; (1) to describe the normal IVVP morphology in the canine cervical region using transverse anatomy sections and computed tomography (CT), (2) to develop a technique for CT examination of the IVVP in vivo, (3) to analyze the quantitative characteristics of the IVVP, and (4) to assess the effect of acute experimental spinal cord compression on IVVP morphology. In the first experiment, CT of the cervical vertebral canal was performed in 6, normal, adult mixed-breed dogs. After dogs were euthanized, a gelatin and iohalamate mixture was injected into the right external jugular vein. Cadavers were then frozen to -8°C , sliced into transverse sections, and compared with CT images. Vascular components such as the IVVP, interarcuate veins, intervertebral veins, and vertebral veins were accurately depicted on CT images. In the second experiment, CT venography

was performed using a biphasic IV injection of iodinated contrast medium. Dimensions of the IVVP and other vertebral canal components were calculated for the C3-C7 vertebral region. Sagittal diameters of the IVVP ranged from 0.6 mm to 3.2 mm. The IVVP area occupied 30.61% of the cervical vertebral epidural space area. When C3-C7 segments were considered as a group, IVVP area dimensions were significantly correlated ($r > 0.7$, $p < 0.0001$) with vertebral canal area and dural sac area. In the last experiment, acute spinal cord compression (ASCC) was induced and maintained for 10 minutes using an angioplasty balloon catheter device over the C3/4 vertebral region in 6 dogs. Dogs were evaluated prior to, during, and after compression using digital subtraction venography (DSV) and CT venography. Results showed that ASCC produced a significant change in diameter of the IVVP at the site of compression. This effect persisted during the post-compression period. In conclusion, findings indicate that CT venography and DSV accurately depict the IVVP in dogs, and that significant changes of the IVVP morphology occur under ASCC conditions.

DEDICATION

I would like to dedicate this thesis to my father Rolando, my mother Marta and my sisters Viviana, Maria Eugenia and my brother Claudio. You are a pillar of strength to me.

Also to my nephews Valentina, Tomas and Claudito

I would never have made it without you.

ACKNOWLEDGMENTS

This research project and dissertation benefited from extensive contributions of some wonderful people. Particularly, I would like to thank:

Dr. Jeryl Jones, my research advisor: for her multiple encouragements, for all the weekly assistance and availability and organizational input that contributed tremendously to the start, continuation and completion of this dissertation.

Dr. Larry Freeman, committee member: for his support and ideas, but especially for his invaluable friendship.

Drs. Otto Lanz, Karen Inzana and Richard Broadstone, committee members: for their priceless contributions.

Dr. Mary Lee Jensen, research collaborator: for her invaluable help on the project and her kind hospitality at UVA.

Pam Arnold, anatomy lab supervisor: for her patience, assistance and ideas on instrumentation and techniques for specimen preparation.

Susie Ayers, John Strauss and Chris Wakley, technical assistants: for their important help and collaboration.

Dan Ward, statistician: for his assistance in the experimental design and statistical analysis.

Dr. Bernard Jortner, neuropathologist: for his assistance on interpretation of histopathologic samples.

Thank you all so much.

TABLE OF CONTENTS

Abstract.....	ii
Dedication.....	iv
Acknowledgments.....	v
Table of Contents.....	vi
List of Tables.....	xii
List of Figures.....	xiii
Chapter 1- Literature Review.....	1
1.1 - Anatomy of the Canine Cervical Spine.....	1
1.1.1 - Developmental anatomy.....	1
1.1.2 - Post-natal development.....	6
1.1.3 - Cervical vertebral column.....	8
1.1.4 - Ligaments and joints of the cervical spine.....	11
1.1.5 - Muscles of the cervical spine.....	16
1.1.6 - Cervical spinal cord and meninges.....	21
1.1.7 - Vascular anatomy of the cervical spinal cord.....	24
1.2 - Canine Vertebral Venous Plexus.....	31
1.2.1 - Historical notes.....	31
1.2.2 - Anatomy of the canine cervical vertebral venous plexus...33	
1.2.3 - Comparative anatomy of the vertebral venous plexus.....	42
1.2.4 - Physiology and clinical aspects of the vertebral venous plexus.....	44
1.3 - Pathophysiologic Mechanisms of Acute Spinal Cord Injury.....	51

1.3.1 - Primary injury.....	52
1.3.2 - Secondary injury.....	53
1.3.2.1 - Biochemical changes.....	54
1.3.2.1.1 - Free radicals.....	54
1.3.2.1.2 - Neurotransmitter excitotoxicity.....	57
1.3.2.1.3 - Endogenous opioids.....	58
1.3.2.1.4 - Electrolyte disturbances.....	59
1.3.2.1.5 - Energy depletion.....	60
1.3.2.2 – Cellular changes.....	61
1.3.2.2.1 - Vascular mechanism.....	61
1.3.2.2.2 - Immune response.....	64
1.3.2.2.3 - Apoptosis.....	65
1.3.3 - Neuropathology of the spinal cord injury.....	67
1.3.4 - Gene expression during spinal cord injury.....	68
1.3.5 - Pharmacology research and clinical trials in spinal cord injury.....	71
1.4 - General Physiologic Effects of Acute Spinal Cord Injury.....	76
1.4.1 - Cardiovascular complications.....	76
1.4.2 - Regulation of perfusion in the spinal cord vasculature.....	80
1.4.3 - Cushing reflex.....	84
1.4.4 - Monro-Kellie hypothesis of cerebrospinal fluid pressure....	84
1.4.5 - Respiratory complications.....	85
1.4.6 - Spinal shock.....	87

1.5 - Imaging of the Cervical Spinal Region in Dogs.....	89
1.5.1 - Principles and technical considerations for imaging	
modalities used in evaluation of the canine cervical spine..	89
1.5.1.1 - Radiology.....	89
1.5.1.2 - Myelography.....	92
1.5.1.3 - Computed tomography.....	95
1.5.1.4 - Magnetic resonance imaging.....	100
1.5.1.5 - Vertebral intraosseous venography.....	104
1.5.1.6 - Epidural venography.....	107
1.5.1.7 - Digital subtraction epidural venography.....	111
1.5.2 – Imaging characteristics of common diseases in the cervical	
spine of the dog.....	113
1.5.2.1 - Congenital anomalies.....	113
1.5.2.1.1 - Radiographic signs of congenital	
anomalies.....	114
1.5.2.1.2 - Myelographic signs of congenital	
anomalies.....	115
1.5.2.1.3 - CT signs of congenital anomalies.....	116
1.5.2.1.4 - MRI signs of congenital anomalies.....	116
1.5.2.2 - Intervertebral disk disease.....	117
1.5.2.2.1 - Radiographic signs of IVD disease.....	118
1.5.2.2.2 - Myelographic signs of IVD disease.....	120
1.5.2.2.3 - CT signs of IVD disease.....	121

1.5.2.2.4 - MRI signs of IVD disease.....	122
1.5.2.3 - Cervical vertebral stenosis.....	124
1.5.2.3.1 - Radiographic signs of CVS.....	125
1.5.2.3.2 - Myelographic signs of CVS.....	126
1.5.2.3.3 - CT signs of CVS.....	127
1.5.2.3.4 - MRI signs of CVS.....	128
1.5.2.4 - Spinal neoplasia.....	129
1.5.2.4.1 - Radiographic signs of spinal neoplasia.	130
1.5.2.4.2 - Myelographic signs of spinal neoplasia.	131
1.5.2.4.3 - CT signs of spinal neoplasia.....	132
1.5.2.4.4 - MRI signs of spinal neoplasia.....	132
1.5.2.5 - Spinal infections.....	134
1.5.2.5.1 - Radiographic signs of spinal infections.	135
1.5.2.5.2 - Myelographic signs of spinal infections.	137
1.5.2.5.3 - CT signs of spinal infections.....	137
1.5.2.5.4 - MRI signs of spinal infections.....	138
1.5.2.6 - Fibrocartilaginous embolism.....	139
1.5.2.6.1 - Radiographic signs of FCE.....	140
1.5.2.6.2 - Myelographic signs of FCE.....	140
1.5.2.6.3 - CT signs of FCE.....	140
1.5.2.6.4 - MRI signs of FCE.....	141
1.5.2.7 - Spinal Trauma.....	141
1.5.2.7.1 - Radiographic signs of spinal trauma....	141

1.5.2.7.2 - CT signs of spinal trauma.....	142
1.5.2.7.3 - MRI signs of spinal trauma.....	143
1.5.2.8 - Arachnoid cysts.....	145
1.5.2.8.1 - Radiographic signs of arachnoid cysts..	145
1.5.2.8.2 - Myelographic signs of arachnoid cysts..	146
1.5.2.8.3 - CT signs of arachnoid cysts.....	146
1.5.2.8.4 - MRI signs of arachnoid cysts.....	147
1.5.2.9 - Schmorl's nodes.....	147
1.5.2.9.1 - Radiographic signs of Schmorl's nodes	148
1.5.2.9.2 - Myelographic signs of Schmorl's nodes	148
1.5.2.9.3 - CT signs of Schmorl's nodes.....	148
1.5.2.9.4 - MRI signs of Schmorl's nodes.....	149
 Chapter 2- Computed Tomographic Anatomy of the Canine Cervical Vertebral Venous System.....	 150
2.1 - Abstract.....	151
2.2 - Introduction.....	152
2.3 - Material and Methods.....	154
2.4 - Results.....	157
2.5 - Discussion.....	175
 Chapter 3- Morphometry of the Vertebral Venous Plexus, Vertebral Canal, Dural Sac, and Vertebral Body in the Normal Canine Cervical Spine: Evaluation Using Non-selective CT Venography.....	 179
3.1 - Abstract.....	180

3.2 - Introduction.....	182
3.3 - Material and Methods.....	185
3.4 - Results.....	190
3.5 - Discussion.....	200
Chapter 4 - Effects of Acute Spinal Cord Compression on The Morphology of the Canine Cervical Vertebral Venous System: Evaluation using CT Venography and Digital Subtraction Venography.....	208
4.1 - Abstract.....	209
4.2 - Introduction.....	211
4.3 - Material and Methods.....	214
4.4 - Results.....	228
4.5 - Discussion.....	248
Chapter 5 - General Conclusions.....	259
Bibliography.....	266
Vita.....	293

LIST OF TABLES

Table 1.1 - Major extravertebral anastomoses of the intervertebral veins in the dog.....	37
Table 1.2 - Synonyms of the standard veterinary and human official nomenclature for the vertebral venous plexus.....	40
Table 3.1 - Dimensions of C3-7 vertebral components in 6 normal adult dogs (mean \pm SD).....	194
Table 3.2 - Correlation between dimensions of the vertebral venous plexus, vertebral canal, dural sac, and vertebral body between C3 and C7 vertebral segments.....	195
Table 4.1 - Imaging and histopathological findings for 6 dogs, after experimental acute cervical spinal cord compression.....	243
Table 4.2 - Physiological parameters recorded during pre-compression, compression, and post-compression.....	245
Table 4.3 - Arterial gas analysis results recorded during pre-compression, compression, and post-compression	246

LIST OF FIGURES

Figure 1.1 - Illustration of the arterial blood supply to the cervical spinal cord in the dog.....	29
Figure 1.2 - Schematic representation of the canine vertebral venous plexus in the dog (dorsal view).....	42
Figure 2.1 - Transverse, contrast-enhanced CT image (A) and anatomic section (B) through C1.....	160
Figure 2.2 - Transverse, contrast-enhanced CT image (A) and anatomic section (B) through C1-C2.....	161
Figure 2.3 - Transverse, contrast-enhanced CT image (A) and anatomic section (B) through C2.....	162
Figure 2.4 - Transverse, contrast-enhanced CT image (A) and anatomic section (B) through C2-C3.....	163
Figure 2.5 - Transverse, contrast-enhanced CT image (A) and anatomic section (B) through C3.....	164
Figure 2.6 - Transverse, contrast-enhanced CT image (A) and anatomic section (B) through C3-C4.....	165
Figure 2.7 – Transverse, contrast-enhanced CT image (A) and anatomic section (B) through C4.....	166
Figure 2.8 – Transverse, contrast-enhanced CT image (A) and anatomic section (B) through C4-C5.....	167

Figure 2.9 - Transverse, contrast-enhanced CT image (A) and anatomic section (B) through C5.....	168
Figure 2.10 - Transverse, contrast-enhanced CT image (A) and anatomic section (B) through C5-C6.....	169
Figure 2.11 - Transverse, contrast-enhanced CT image (A) and anatomic section (B) through C6.....	170
Figure 2.12 - Transverse, contrast-enhanced CT image (A) and anatomic section (B) through C6-C7.....	171
Figure 2.13 -Transverse, contrast-enhanced CT image (A) and anatomic section (B) through C7.....	172
Figure 2.14 - Dorsal plane view of the C5-7 vertebral canal.....	173
Figure 2.15 - Schematic illustration of the vertebral venous plexus.....	174
Figure 3.1 - Illustration demonstrating the diameter and area dimensions measured.....	189
Figure 3.2 - Percent of the C3-7 epidural space area occupied by the vertebral venous plexus.....	196
Figure 3.3 - Mean areas values of the right and left IVVP in the vertebral segments C3 to C7.....	197
Figure 3.4 - Transverse CT images obtained at the mid-vertebral bodies of C4 (A) and C5 (B).....	198
Figure 3.5 - Transverse CT image obtained at the mid-body of C7.....	198
Figure 3.6 - Mean values for sagittal diameters of the vertebral venous plexus, vertebral canal, dural sac and vertebral body from C3 to C7.....	199

Figure 4.1 - Dorsoventral post-contrast radiograph of the cervical region in the first pilot dog	225
Figure 4.2 - Lateral reverse window, digital images of the cervical region from the first pilot dog.....	226
Figure 4.3 - Materials used in spinal cord compression experiment.....	227
Figure 4.4 - Lateral digital radiograph of the lumbosacral area demonstrating a guidewire in place in the lumbar vertebral canal extending from the lumbosacral space.....	235
Figure 4.5 - Lateral digital radiograph of the cervical region in a dog showing the position of the angioplasty balloon catheter at C3/4.....	235
Figure 4.6 - Dorso-ventral digital radiograph of the cervical region demonstrating the position of the angioplasty balloon catheter with its radiopaque markers inside the C3/4 vertebral canal	236
Figure 4.7 - Pre-compression digital subtraction venogram (A) and diagram (B) of the IVVP in the cervical region of a dog.....	237
Figure 4.8 - Magnified pre-compression (A) and compression (B) digital subtraction venograms of the cranial cervical region obtained from the same dog	238
Figure 4.9 - Pre-compression transverse CT venographic image at midportion of C7.....	239
Figure 4.10 - Pre-compression transverse CT venographic image at the midportion of C5.....	239

Figure 4.11 - Pre-compression transverse CT venographic image at midportion of C2.....	240
Figure 4.12 - Transverse CT venographic image at C4 during compression....	241
Figure 4.13 - Transverse views of compressed spinal cord sections obtained at C4 (A) and C5 (B) spinal cord segments from 2 dogs.....	242
Figure 4.14 - Histological images from two compressed spinal cord samples at C4 (Hemtoxyline & eosin).....	242
Figure 4.15 - Mean transverse diameters (mm) of the left IVVP measured from DSV and CT venograms during pre-compression, compression, and post-compression of the cervical spinal cord in 6 dogs.....	244
Figure 4.16 - Mean of arterial blood pressure during pre-compression, compression and post-compression.....	247

CHAPTER 1

LITERATURE REVIEW

1. 1 ANATOMY OF THE CANINE CERVICAL SPINE

The following chapter addresses important aspects related to developmental and macroscopic morphology of the canine cervical spine. All veterinary anatomical nomenclature is in accordance with the *Nomina Embryologica Veterinaria*¹ and *Nomina Anatomica Veterinaria*,¹ and is included in parentheses with italic letters. When human comparisons are made, nomenclature is based on the most recent version of the *Terminologia Anatomica*.² Medical terms are in accordance with the Dorland's Illustrated Medical Dictionary.³

1.1.1 Developmental anatomy

The spinal cord is derived from the embryonic neural tube (*tubus neuralis*) and its wall is derived from three layers; the outer marginal layer (*stratum marginale*), the middle mantle layer (*stratum palliale*), and the central ventricular zone (*stratum ependymale*).^{4,5} The mantle layer is divided into a dorsal component called the alar plate or lamina (*lamina alaris, lamina dorsolateralis*), and a ventral component named the basal plate or lamina (*lamina basalis, lamina ventrolateralis*). Both sides of the embryonic spinal cord are connected dorsally by the roof plate and ventrally by the floor plate. Within the parenchymal of the spinal cord the neural canal is indented laterally by a small longitudinal groove,

the sulcus limitans. This groove constitutes the internal limit between the alar and basal plates. The ventricular zone constitutes the central canal and ependyma of the mature spinal cord. Functionally, neurons from the alar plate possess sensory function and those from the basal plate, motor function.⁴ During maturation the embryonic spinal cord develops a dorsal median sulcus located at the dorsal midline, and the ventral portion develops a well-defined ventral median fissure. Proliferation and migration of immature neurons together in the mantle layer form the gray matter of the mature spinal cord. Later, migration of these primitive neural cells form the distinctive “H” shape of the gray matter with their dorsal and ventral horns seen on transverse section. Development of the limbs in the embryo is associated with enlargements of the embryonic spinal cord areas at these respective levels. Degeneration of immature neural cells in areas that do not participate in the innervation of the limbs accentuates these formations. The spinal cord enlargement related to the thoracic limb is the cervical intumescence, and extends from the 5th cervical segment to the 2nd thoracic spinal cord segment. The spinal cord enlargement associated with the lumbar vertebrae is the lumbar intumescence, and extends between the 4th lumbar and 3rd sacral spinal cord segments in the dog.

The marginal layer constitutes the white matter in the mature spinal cord. It is composed of ascending and descending spinal tracts (*fasciculus* or *tractus*) organized in columns (*funiculus*). The spinal cord is divided in 3 columns: dorsal,

lateral, and ventral. These columns are named based on boundaries given by the emergence of dorsal and ventral nerve rootlets.^{4,5}

Vertebrae are derived from paraxial mesoderm (*mesoderma paraxiale*) that fuses in a segmental fashion to form somites. The cells of the mesodermal structures are organized into three layers: the dorsal (superficial) dermatome (*dermatomi*), the intermediate myotome (*myotomi*), and the inner (deep) sclerotome (*sclerotomus*). Dermatome cells contribute to dermis formation. Myotome cells form the axial, appendicular, and abdominal wall musculature. Sclerotome cells give rise to vertebrae and ribs. Approximately 40 or more somites participate in the formation of the canine vertebral column.⁴

Sclerotomal vertebrae (*vertebra precartilaginosa*) develop in a cranio-caudal fashion in the same sequence as chondrification. However, the ossification process in embryos does not occur sequentially and the cervical vertebrae can ossify later than more caudal segments. The formation of vertebrae involves sclerotomal cells from each somite group in two characteristic populations: a diffuse cranial population, and a more compact caudal group. The classic reorganization theory is that the caudal group of cells in each sclerotome joins with the cranial group of cells of the contiguous sclerotome, and later they form a single vertebra. New evidence suggests this classic organization of the somites is actually formed from a continuous blastema column. From this blastema, the dense population forms the vertebral arch and related parts, and the intervertebral disk. The less dense cell population, which joins the dense

mesenchyme of the adjacent sclerotome will form most of the body of the vertebra that is intersegmental in origin. These new arrangements account for the intervertebral position of spinal nerve ganglia and nerve roots. Myotomes extend from one vertebra to another, and the intrasomitic arteries are now between the pedicles of the vertebral arch. Later, chondrification starts within each sclerotome but ultimately fuses. The cartilaginous precursors from both sides of the vertebral body surround the notochord and later fuse. The remnant of the notochord inside each vertebral unit is almost completely obliterated. However, the notochord within the intervertebral disk persists and expands to form a central core, the nucleus pulposus. Sclerotomal mesenchyme forms the annulus fibrosus that surrounds the nucleus pulposus. Later, during the pre-natal period, the development of the cartilaginous vertebra (*vertebra cartilaginea*) is completed with the lateral growth of the transverse and costal processes and later fusion of the left and right vertebral arch components in the dorsal midline.⁴⁻⁶

In dogs, ossification of the vertebral column begins in the sixth week of gestation. Primary ossification centers appear near the middle of each centrum (vertebral body) and lateral to the spinal cord at the base of each neural arch. The centrum first appears as endochondral nodular condensations, where the neural arches develop from perichondral collars around the base of the cartilaginous arch. In dogs, paired perichondral neural ossification is evident at 38 days of gestation (54 mm embryo length) from C1 to T7.⁷ In dogs and cats born in a relatively immature condition, these ossification centers fuse dorsally

after birth. Secondary ossification centers appear during the post-natal period on the cranial and caudal ends of the body of the vertebra to form the epiphyses and distal tips of transverse processes.⁷

The segmental reorganization of sclerotomal cells in the cranial end of the cervical spine differs from the pattern described for the rest of the vertebral column. The bodies of the atlas and axis form differently from the rest of the cervical spine. Embryologically part of the atlas centrum fuses with that of the axis.⁸ The vertebral body of the atlas is formed by intercentrum I, and the vertebral body of the axis is formed by centrum I, intercentrum II, and centrum II.^{7,8} At birth, the atlas is composed of 3 ossification centers: a pair forming the dorsal arches, and one forming the small vertebral body or ventral arch. In the prenatal period, the axis is composed of 4 bony elements: a bilateral pair of neural arch elements dorsolaterally, centrum II in the main portion of the body of the axis, a relatively smaller centrum I in the base of the dens, and the cranial portion of the body of the axis.⁸ When there is variation in relation to the appearance and fusion of those elements, the intercentrum I of the atlas is found to ossify after day 46 of gestation (92 mm embryo length). All elements of the axis fuse with one another by the 4th month postpartum.⁷

1.1.2 Post-natal development

In post-natal life, separate bony elements of the atlas and axis continue to develop in size and shape.⁸ In addition to elements present at birth (two neural arches, centrum I and centrum II), 3 more separate bony elements develop in the axis: intercentrum II, the ephyphysis, and the centrum of the proatlas. So, the atlanto-axial complex is formed in the post-natal period by 10 bony components; 3 for the atlas and 7 for the axis.⁷ The intercentrum II is present around 30 days after birth. Ossification centers for the vertebral body epiphysis are present in puppies at 22 days of age and older.⁸ The centrum of the proatlas ossifies in puppies around 42 days old. Later, post-natal development consists of additional growth and fusion of separate bony elements to form the mature atlas and axis. Arch elements of the atlas fuse dorsally around 15 weeks of age and these arches fuse to the early vertebral body one week later (115 days).

In relation to the axis, vertebral arch components fuse to each other at approximately 42 days of age. The centrum II starts fusing with vertebral arch components around 7 weeks and is complete at 15 weeks of age.⁸ The centrum of the proatlas fuses with the rest of the dens (centrum I) at 106 days of age.⁸ Fusion of the intercentrum II with centrum I cranially, and centrum II caudally occurs around 22 weeks of age. Epiphyses are the last bony elements of the axis that fuse beginning at 7 months of age, and complete fusion occurs at 13 months of age.⁸

In newborn puppies, primary centers of ossification of the vertebral bodies of the fifth, sixth, and seventh cervical vertebrae are surrounded by hyaline cartilage except at the median point dorsally and ventrally.⁹ In these areas, a cuff of bone is present where blood vessels penetrate to enter the center of the vertebral body. Bone formation occurs by intramembranous ossification under the periosteum later at these sites. Within the primary ossification centers of C5 to C7, hemopoietic tissue fills the spaces between the bone trabeculae. At this stage of development most of the bone trabeculae contain fragments of mineralized cartilage. Dorsolaterally, at the junction of each vertebral arch component with the vertebral body, there is a large vascular foramen containing a thin walled vein which joins the ipsilateral internal vertebral venous plexus. By 7 to 8 weeks of age, bone content of the spinous processes, articular facets and transverse process has increased. During this same period, the transverse foramen in the fifth cervical vertebrae is completely surrounded by bone, but in the sixth vertebrae a band of cartilage is present ventrally. At 10 to 12 weeks of post-natal age, endochondral ossification still occurs in the vertebral bodies, at the cranial and caudal poles of the primary ossification centers, and the junction of the neural arches and vertebral body. At this age, it is possible to observe bony fusion occurring ventral to the transverse foramen.⁹

1.1.3 Cervical vertebral column

Vertebrae are the basic components of the vertebral column or axial skeleton.⁵ Most of these bony structures are formed by a vertebral arch (lamina and pedicles), vertebral body (epiphysis and diaphysis) and processes (spinous process, transverse processes and articular processes), in different degrees of development and appearance.¹⁰ The cervical vertebral column in dogs is formed by 7 vertebrae (*vertebrae cervicales*) in which the first 2 diverge in developmental pattern from the rest of the cervical vertebrae as well as the rest of the vertebral column. Three vertebrae (C3, C4 and C5) present minimal differences among them and usually are difficult to differentiate from each other. The last 2 cervical vertebrae (C6 and C7) are distinctive and easily identifiable.^{5,7,11,12}

Atlas

The first cervical vertebra (C1) or atlas has a distinctive structure and function. Cranially, it articulates with the occipital bone of the skull and caudally with the axis. The atlas is composed of a dorsal and a ventral arch (*arcus dorsalis* and *ventralis*) that gives the vertebra its particular annular appearance. The ventral arch is narrower than its dorsal equivalent. A prominent dorsal tubercle (*tuberculum dorsale*) and a small nodular ventral tubercle (*tuberculum ventrale*) are located in the dorsal and ventral arches respectively. The dorsal tubercle sometimes can present a bifid conformation. The ventral arch is considered the body of the atlas. The lateral portions of the dorsal arch of the

atlas are thick and fused to the body. They are known as lateral masses (*massa lateralis*). From these masses, the transverse processes or wings of the atlas (*ala atlantis*) extend laterally and horizontally. Ventrally the wings have concave surfaces that form the atlantal fossa (*fossa atlantis*). Occasionally, an intraosseous venous canal is observed extending from this fossa into the lateral mass. The cranial borders of the wings, near the dorsal arch, are indented to form the alar notch (*incisura alaris*). Medial to this position in the craniodorsal area of the vertebral arch, the lateral vertebral foramen (*foramen vertebrale laterale*) opens into the vertebral foramen. In some small breeds this lateral vertebral foramen persists as a notch on the cranial border of the atlas.¹³ In the caudal aspect of the atlas, a transverse foramen (*foramen transversarium*) is located at the base of each wing. The atlas articulates cranially with the occipital condyles by the cranial articular surface (*fovea articularis cranialis*) and caudally with the axis via the caudal articular surface (*fovea articularis caudalis*) and the fovea of the dens (*fovea dentis*) located on the dorsal surface of the body of the atlas.^{5,11,12,14}

Axis

In the dog, the second cervical vertebra (C2) or axis is the longest bone of the cervical segment.^{5,7,10} The axis has a prominent spinous process that is blade-like cranially, and expanded caudally.¹⁰ This spinous process extends over the dorsal arch of the atlas cranially and covers a portion of the lamina of the

third cervical vertebra caudally. This spinous process merges with the caudal articular process that faces ventrally. The body of the atlas includes a cranio-ventral eminence called the *dens* or odontoid process. The cranial articular processes of the axis are convex and continuous with the ventral articular surface (*facies articularis ventralis*) of the dens. The dens also contains a dorsal articular area (*facies articularis dorsalis*). Transverse processes of the axis are directed caudally and laterally, and at their bases each is perforated by the transverse foramen. The cranial vertebral notches of the axis with the caudal vertebral notches of the atlas form the large second intervertebral foramina (*foramen intervertebrale*) for the exit of the second pair of cervical spinal nerves and intervertebral vessels. The caudal notches of the axis and the cranial notches from the third cervical vertebra participate in the less prominent third intervertebral foramina.^{5,11,12,14}

Cervical vertebrae 3rd to 7th

Cervical vertebrae 3rd through 7th become progressively shorter toward the thoracic junction.^{5,7} The extremities of the vertebral bodies are more curved than other vertebral regions and are directed obliquely in a dorsoventral fashion. The vertebral arches are prominent and wide, but their spinous processes increase in height and in cranial inclination toward the cervico-thoracic junction.⁷ The transverse processes are large and divided into dorsal and ventral tubercles (*tuberculum dorsale* and *ventrale*). The ventral lamina (*lamina ventralis*) of the

transverse process of C6 replaces the ventral tubercle of the other cervical vertebrae.⁷ This osseous plate extends ventrally below the contour of the vertebral body of C6. Bases of the transverse processes from C3 to C6 are perforated by transverse foramina where the vertebral artery, vein and nerve travel. Cranial and caudal articular facets are large, flat and nearly horizontal.¹⁰ The seventh cervical vertebra (C7) is transitional to those of the thoracic segment and is recognized by its taller spinous process, absence of transverse foramina, and the presence of costal facets (*fovea costalis caudalis*) on the caudal extremity of its body for articulation with the first pair of ribs.^{5,12,14} The intervertebral foramina in the cervical vertebrae are larger than those in other vertebral segments and are directed in a ventrolateral fashion.¹⁵

1.1.4 Ligaments and joints of the cervical spine

Atlanto-occipital joint

The atlanto-occipital joint (*articulatio atlantooccipitalis*) is composed of the occipital condyles and the right and left concave cranial articular surfaces of the atlas.¹⁶ The articular surfaces of the atlas and axis converge ventrally forming a contiguous U-shape joint. This articulation communicates caudally with the atlanto-axial joint cavity and sometimes is referred to as the occipito-atlas-axis joint cavity.¹⁷ The joint capsule of the atlanto-occipital articulation is reinforced by dorsal and ventral atlanto-occipital membranes (*membrana atlantooccipitalis dorsalis* and *ventralis*).¹⁶ The dorsal membrane extends from the dorsal edge of

the foramen magnum to the cranial border of the dorsal arch of the atlas.⁷ The ventral membrane extends from the ventral border of the foramen magnum to the body of the atlas. The lateral ligaments (*ligamenta laterale*) of the atlanto-occipital joint run from the lateral part of the dorsal arch of the atlas to the paracondylar process of the occipital bone.¹⁶ This articulation functions as a ginglymus with movement restricted to flexion and extension in the sagittal plane.^{5,7,12}

Atlanto-axial joint

The atlanto-axial joint (*articulatio atlantoaxialis*) is formed between the caudal aspect of the vertebral body of the atlas and the dens of the axis.^{16,17} This articulation has a thin and loose joint capsule extending from the dorsal part of the cranial articular surface of the axis to the caudal border of the lamina and the vertebral body of the atlas.¹⁷ The atlanto-axial joint communicates cranially with the central portion of the atlanto-occipital joint.¹⁷ A tectorial membrane (*membrana tectoria*) travels from the dorsal surface of the body of the axis to the ventral border of the atlas and foramen magnum. The dorsal atlanto-axial membrane (*membrana atlantoaxialis dorsalis*) connects the dorsal arch of the atlas and the vertebral arch of the axis. The dens (odontoid process) is connected to the occipital bone by 3 ligaments. The apical ligament of the dens (*ligamentum apices dentis*) goes straight from the apex of the dens to the basilar portion of the occipital bone. The other 2 ligaments are the alar ligaments

(*ligamentum alaria*) of the atlas that extend from the lateral borders of the dens to the occipital condyles.^{5,16} A transverse ligament of the atlas (*ligamentum transversus atlantis*) is a strong fibrous band that connects one side of the ventral arch of the atlas to the other. Its travels over the dens and embraces this odontoid process against the vertebral body of the atlas.^{5,12,14} In dogs, a prominent synovial bursa is present between the transverse ligament of the atlas and the dorsal surface of the dens.¹⁷

Caudal to the axis, synovial articulations are found between the cranial and caudal articular processes (*articulationes processum articularium*) of contiguous cervical vertebrae.¹⁶ The capsule of these joints is thick compared with the other vertebral segments. Also, between the caudal body of the seventh cervical vertebra (C7) and the cranial body of the first thoracic vertebra is the articulation with the head of the first rib (*articulatio capitis costae*).^{5,12}

The nuchal ligament (*ligamentum nuchae*) is an elastic band that extends from the caudal aspect of the spinous process of the axis to the beginning of the supraspinous ligament (*ligamentum supraspinale*) at the first thoracic spinous process.^{5,10,16} The dorsal longitudinal ligament (*ligamentum longitudinale dorsale*) is located on the dorsal surfaces of the vertebral bodies within the vertebral canal. Over the intervertebral disks, the ligament is wider at the middle of the vertebral bodies.¹⁶ The dorsal longitudinal ligament attaches to the bony ridges on the dorsal aspect of the vertebral bodies and dorsal anulus fibrosus. This ligament extends from the axis to the terminal portion of the vertebral canal, in

the cranial region of the caudal vertebrae. The ventral longitudinal ligament (*ligamentum longitudinale ventrale*) is developed from the ventral portion of the eighth thoracic vertebra to the sacrum and is poorly developed at the cervical region.¹⁴ The interarcuate or yellow ligaments (*ligamenta flava*) are thin, elastic sheets connecting the lamina of adjacent vertebral arches.^{5,11,12,14}

Intervertebral disk

With the exception of C1 and C2, every intervertebral segment of the cervical spine is united by an intervertebral disk (*discus intervertebralis*) forming an amphiarthrosis of the symphysis type.⁵ The thickness of the disks between the cervical vertebrae is greater than other vertebral levels.¹⁶ Each intervertebral disk is formed by an outer fibrous ring (*annulus fibrosus*) a central, gelatinous and amorphous nucleus pulposus (*nucleus pulposus*). This nucleus pulposus is a gelatinous remnant of the notochord. Cervical intervertebral disks comprise 12% of the cervical spinal column length in the dog.^{12,18}

The annulus fibrosus is formed by concentric fibers that run obliquely from one vertebral endplate to the next. In dogs, the ratio of dorsoventral diameters of the ventral versus dorsal aspects of the annulus is approximately 2.3:1. Functionally, they transmit stresses and strains required for lateral and dorsoventral movements. Other functions of the disks are absorption of compressive (primarily axial) forces and resistance of torsional forces.¹⁹ Viewed cranially or caudally, the disk is oval in shape with the longest dimension

occurring transversely. The annulus fibrosus is composed almost entirely of fibrous tissue; indeed, 70% of its dry weight is collagen. This fibrous tissue is produced and maintained by cellular elements located between the fibrous bundles. Major components of the disk are collagenous and noncollagenous proteins, proteoglycan aggregates, and glycoproteins. The molecular organization of the annulus primarily consists of type I and II collagen. Collagen type I is located in the outer lamellae of the annulus, is more resistant and provides support to the disk in tensile bending.¹⁸ Collagen type II is predominantly in the inner fibers of the annulus and the nucleus. This type of collagen is also found in cartilaginous tissue and is important in load bearing.¹⁸ Chondrocytes, fibrocytes, notochordal cell and intermediate cells are cellular elements present in the fibrous lamellae. In the mature nonchondrodystrophic disk, water content of the nucleus and annulus is 80% and 60%, respectively.^{18,20} Collagen types III, IV, IX, X, and XI have been also identified in intervertebral disks of mature dogs.²¹

The cartilaginous endplates are located cranial and caudal to the intervertebral disk.¹⁸ They are formed by a hyaline-like type of cartilage. The endplates are 1 to 2 mm thick, with the thickness reduced at the center where the nucleus pulposus is located. This level is where most of the nourishment of the disk occurs since this area is permeable and communicates with vessels of the vertebral body.¹⁸

Sensory innervation of the disk is found only in its most peripheral portions. Innervation is supplied by branches of the sinuvertebral nerve

(*meningeal rami*). Presence of neurotransmitters implicated in pain transmission such as substance P and vasoactive intestinal peptide (VIP) in these nerve fibers are indicative of their nociceptive function.⁶ Type III mechanoreceptors are also present in the outer portion of the disk. These types of mechanoreceptors are believed to participate in pain perception and in proprioceptive function

1.1.5 Muscles of the cervical spine

Muscles that attach only to components of the axial skeleton are considered to be intrinsic spinal muscles.²² They are deeply located and represented by a series of fascicles which extend from one vertebra to the other. The spinal musculature can be categorized into epaxial or hypaxial muscle groups, based on location of the muscles above or below the transverse processes of the vertebral column.⁵ Epaxial muscles lie dorsal to transverse processes, are segmentally innervated by dorsal branches of spinal nerves, and produce spinal extension and lateral flexion. Hypaxial muscles are located ventral to the transverse processes, are segmentally innervated by ventral branches of spinal nerves, and produce spinal flexion and lateral flexion. Among the epaxial musculature in the cervical region of the dog are included the m. erector spinae (represented mainly by m. spinalis and longissimus cervicis), the m. transversospinalis (represented by the m. semispinalis capitis, m. semispinalis cervicis, mmm. multifidus cervicis and mm. rotatores) and the m. interspinalis cervicis.^{11,12,22}

Hypoaxial muscles in the cervical region include the longus capitis, longus colli, rectus capitis ventralis and rectus capitis lateralis muscles.²²

Epaxial cervical spinal muscles

The mm. spinalis thoracis, spinalis cervicis and semispinalis thoracis are very close to each other, so they are considered together under the common name m. spinalis thoracis and cervicis (*m. spinalis thoracis et cervicis*).²²

The mm. spinalis and semispinalis thoracis, and spinalis cervicis constitute a strong, partially unsegmented, longitudinal muscle group, located lateral to the spinous processes of the thoracic vertebrae, and dorsomedial to the m. longissimus thoracis (*m. longissimus thoracis*). In the cervical region, this group runs medial to the multifidus muscle (*mm multifidi*) and ventral to the nuchal ligament. The m. spinalis and semispinalis thoracis and cervicis extend from the spinous process of the T11 vertebra to the spinous process of the axis. This combined muscle is separated into lateral and medial parts. The lateral part is the m. spinalis and semispinalis thoracis, and the medial part is the m. spinalis cervicis. The spinalis cervicis is a flat muscle with 4 tendinous inscriptions. It originates from the tendon of the most cranial portion of the m. semispinalis thoracis and from the dorsal border of the first thoracic spinous process. A few bundles also originate from the spinous process of the seventh cervical vertebrae. The spinalis cervicis muscle runs cranially, ventral to the nuchal ligament, and is separated by the muscle of the opposite side only by a median

ligamentous septum. The spinalis cervicis muscle inserts on the spinous process of the fifth to second cervical vertebrae and is covered partially by portions of the mm. multifidus.^{14,22}

The m. semispinalis capitis is the continuation to the head of the m. spinalis and semispinalis thoracis and cervicis. The muscle lies deep, as it extends from the first five thoracic vertebrae and the last cervical vertebrae to the occipital bone. The m. semispinalis capitis is divided in 2 parts; the dorsally located m. biventer cervicis (*m. biventer cervicis*), and the ventrally placed m. complexus (*m. complexus*). Their actions extend the head and neck when functioning together, or flex the head and neck laterally when acting unilaterally. The mm. multifidus is formed by several individual portions that course dorsocranially over several segments in the vertebral column. The mm. multifidus extends from transverse or articular processes of one vertebra to the spinous processes of the cranial ones. Generally, two vertebrae are in contact with each bundle. The multifidus cervicis is covered by the semispinalis capitis. It appears under the ventrolateral border of the m. spinalis and semispinalis thoracis and cervicis, where it extends from the articular process of the second thoracic vertebra to the spinous process of the axis. The multifidus cervicis consists of 6 incompletely separable portions that are partially divided and collectively arise from the articular processes. The action of mm. multifidus with other muscles of the back provides stabilization of the vertebral column when they act bilaterally.²²

The cervical portion of the m. interspinalis runs between contiguous edges of spinous processes of cervical vertebrae. They also participate in fixation of the vertebral column. The intertransversarius muscles (*m. intertransversarii*) are deep segments that originate from the longissimus system. The intertransversarius cervicis (*m. intertransversari cervicis*) is divided into 3 separate muscle bundles: dorsal, intermediate, and ventral. The intertransversarius intermedius cervicis (*mm. intertransversarii intermidii cervicis*) forms a strand which is composed of 5 or 6 distinctly separable parts that extend only between transverse processes. These segments course between the terminal tubercles of the ends of the transverse processes from the T1 vertebra to the axis. At the 6th cervical vertebrae, it is on the transverse process, and, from the 5th cervical vertebra cranially, it is on the caudal branch of the transverse process and the border of the wing of the atlas. The most caudal portion courses under the dorsal mm. intertransversarius of the axis. The intertransversarius ventralis cervicis (*mm. intertransversarii ventrales cervicis*) extends from the ventral border of the transverse process of C6 to insert by 3 separate terminal segments on the caudal branch of the transverse process of C4, C3 and axis.^{11,12,22}

The rectus capitis muscle (*m. rectus capitis*) is formed by 3 portions that run between the axis, atlas and the occipital bone. The 3 portions are rectus capitis dorsalis major, intermedius and minor.²² There are also 2 oblique

muscles, the mm. obliquus capitis caudalis and cranialis that can be considered modifications of the mm. multifidus, or derivatives of the mm. intertransversarius.²²

Hypaxial cervical spinal muscles

The longus capitis muscle (*m. longus capitis*) is a long flat muscle that runs on the lateral and ventral sides of the cervical vertebrae, lateral to the longus colli muscle (*m. longus colli*). The longus capitis originates from the caudal border of the transverse processes of C6 to the axis and extends cranially to the axis. After crossing the atlanto-occipital joint, the longus capitis inserts on the muscular tubercle of the basilar portion of the occipital bone, between the tympanic bulla.

The m. longus colli is a long muscle composed of separate bundles. The right and left portions of the muscle lie together on the vertebral bodies of the first 6 thoracic vertebrae and all of the cervical vertebrae. Each portion divided into thoracic and cervical portions. On the neck the bilateral muscle is flanked by the right and left m. longus capitis. The cervical portion arises on the ventral border of the transverse process of the C6 to C3 vertebrae and ends on the ventral spine of the next preceding vertebra. The cranial segment of the longus colli inserts on the ventral tubercle of the atlas.^{11,12,22}

The m. rectus capitis ventralis is a short strong muscle that lies dorsal to the end of the m. longus capitis. It extends from the ventral arch of the atlas to

the basilar portion of the occipital bone. As the right rectus capitis ventralis crosses the atlanto-occipital joint, it converges with its opposite component.²²

The m. rectus capitis lateralis is a small muscle located lateral to the m. rectus capitis ventralis. The rectus capitis lateralis originates on the ventral surface of the caudal half of the wing of the atlas, and lateral to the m. rectus capitis ventralis. It passes sagittally toward the cranium over the atlanto-occipital joint and inserts on the base of the paracondylar processes of the occipital bone. The rectus capitis ventralis is sometimes considered a special portion of the mm. intertransversarius ventralis.^{5,12,14,22}

1.1.6 Cervical spinal cord and meninges

The spinal cord (*medulla spinalis*) together with the brain are of the components of the central nervous system (CNS).^{5,23} The spinal cord is a elongated cylindrical nervous structure located inside the vertebral canal. The cervical spinal cord (*medulla spinalis pars cervicalis*) emits 8 cervical spinal nerves that are part of the peripheral nervous system.²³ Cervical spinal nerves are formed by the dorsal and ventral spinal roots (*radix dorsalis* and *ventralis*). Those nerve roots originate from bundles called rootlets (*fila radicularia*) that attach along the dorsolateral and ventrolateral grooves (*sulcus lateralis dorsalis* and *ventralis*) of the spinal cord. In addition to the dorsal and ventral spinal roots, the first cranial 7 or 8 cervical segments have rootlets that emerge mid-laterally from the spinal cord and join to form the spinal roots of the accessory nerve

(*radices spinales n. accesorius*). Boundaries of the spinal cord segments are defined by the origins of the most caudal and most cranial rootlets of adjacent dorsal roots.²³ A thickening of the caudal segments of cervical spinal cord and cranial thoracic segments constitutes part of the cervical intumescence (*intumescentia cervicalis*). Specifically the cervical intumescence involve the segments between C6 and T2. Ventral branches of the spinal nerves originating from this enlargement form the brachial plexus (*plexus brachialis*). Spinal cord segments vary in length. The third cervical segment constitutes the longest spinal cord segment. The two cranial cervical spinal cord segments (C1 and C2) are positioned within their respective vertebra; however the rest of the cervical segments lie cranial to their respective vertebral levels.^{5,12,23}

The spinal cord contains a central canal (*canalis centralis*) that constitutes the remnant of the lumen of the embryonic neural tube. Surrounding this canal is the gray matter (*substantia grisea*) that resembles an “H” on tranverse section. It is composed of cell bodies and processes of neurons and glial cells. Dorsal projections of this spinal gray matter are the dorsal (*cornu dorsale*) and ventral horns (*cornu ventralis*). A less developed lateral horn (*cornu laterale*) is interposed between the dorsal and ventral horns, but is not present in the cervical spinal cord. These gray matter formations are united around the central canal by the central intermediate substance (*substantia intermedia centralis*) that includes the gray commissure (*commissura grisea*).²³

The white matter (*substantia alba*) that surrounds the gray matter is divided into 3 funiculi on each half of the spinal cord.²³ The dorsal funiculus is contained between the shallow dorsal median sulcus (*sulcus medianus dorsalis*) and the dorsolateral sulcus (*sulcus lateralis dorsalis*) where the line of origin of the dorsal roots of the spinal nerves are located.²³ The lateral funiculus is located between the dorsal and ventrolateral sulci (*sulcus lateralis ventralis*) where the origins of dorsal and ventral roots exit the spinal cord. The ventral funiculus includes the white matter located between the ventrolateral sulcus and the ventral median fissure (*fissura mediana ventralis*). The funiculi include ascending and descending axons called tracts or fasciculi that convey information from one location to another, and have a common origin, destination, and function.^{12,19,23}

The spinal cord is surrounded and protected by 3 continuous membranes or meninges derived embryologically from somatic mesoderm.²⁴ The external or superficial layer is the dura mater (*dura mater spinalis*) which is strong and fibrous. The spinal dura mater is continuous cranially with the cranial dura mater at the foramen magnum, where it fuses with the periosteum (endosteum) of the vertebral canal within vertebrae C1 and C2. It is also known as the pachymenin (*pachymeninix*) and, with the periosteum of the vertebral canal, limits the epidural space (*cavum epidurale*). The epidural space contains fat and the internal vertebral venous plexus. The spinal arachnoid membrane (*arachnoidea spinalis*) and the pia mater (*pia mater spinalis*) are the deeper leptomeninges (*leptomeninx*). The arachnoid membrane is the most superficial layer of these

two delicate inner membranes. The space between the arachnoid and pia mater is the subarachnoid space (*cavum subarachnoideale*) and contains cerebrospinal fluid (*liquor cerebrospinalis*). The inner most layer, pia mater, is formed by collagen fibers and superficial, flattened, leptomeningeal fibroblasts that line the entire subarachnoid space. Collagen fibers of the pia mater make contact with a basal lamina on the nervous tissue surface. Astrocyte processes of a glial membrane contact the deep surface of the basal lamina. The pia mater collagen is bilaterally thickened along the lateral surface of the spinal cord, forming the denticulate ligament (*ligamentum denticulatum*). Denticulate ligaments have lateral extensions that traverse the subarachnoid space and attach to dura mater, thus suspending the spinal cord in cerebrospinal fluid within the subarachnoid space.^{5,12,14,23}

1.1.7 Vascular anatomy of the cervical spinal cord

Arteries

The major supply of the cervical vertebral canal and spinal cord is provided by branches of the vertebral artery (*a. vertebralis*).¹⁹ The vertebral artery enters the vertebral canal by passing through the lateral foramen of the atlas. It perforates the dura mater and the arachnoid membrane and divides into cranial and caudal branches. These branches anastomose to form the basilar artery cranially (*a. basilaris*). Caudally they form the cranial portion of the ventral spinal artery (*a. spinalis ventralis*). From the medial surface of both vertebral

arteries, at the level of each intervertebral foramen, spinal branches (*rami spinalis*) enter the vertebral canal. The ventral branches or ventral radicular arteries of these spinal arteries join to form the ventral spinal artery. The ventral spinal artery travels along the ventral median fissure of the spinal cord (Fig. 1.1). The ventral spinal artery constitutes the major blood source for the ventral surface of the spinal cord. This unpaired artery sends branches through the ventral median fissure into the gray matter of the spinal cord.

The ventral spinal artery receives a variable number of radicular contributions. Caulkins et al.²⁵ found the radicular contribution (from the vertebral artery) to the ventral spinal artery for the cervical spinal cord in dogs was made by 14 arteries, from a possible 16 for the cervical segments. In human beings, contributions of radicular arteries for the anterior spinal artery in the cervical region are 2 to 6, and around 6 to 8 arteries for all the anterior spinal arterial system.^{26,27} The high level of regression of radicular arteries in human beings indicates a more desegmented pattern of spinal cord blood supply compared to the more segmented pattern of blood supply in dogs.^{25,26} The diameter of the ventral spinal artery in dogs is largest between C1 and C3, with a mean diameter of 0.9 mm at this region.²⁵ Caudal to this region, the diameter of the ventral spinal artery narrows abruptly with a mean diameter of only 0.30 mm throughout the rest of the cervical region. In some dogs the ventral spinal artery is paired for short distances, sometimes from the C1 to C3 level or C6 to C7 level.²⁵ The C1 and C3 radicular arteries are consistently the largest branches, with a mean

diameter of the ventral radicular arteries in the cervical region (excluding C1 and C3) averages 0.2 mm. The mean diameter of the C3 ventral radicular artery is 0.7 mm, and the ventral radicular artery at C1 is 0.8 mm.²⁵

The dorsal surface of the spinal cord is supplied by paired and longitudinal dorsal spinal arteries. For the cervical segments, the main arteries feeding the dorsal spinal arteries are formed by dorsal branches of the ventral radicular arteries.²⁵ For other spinal cord segments, the contribution comes from separate dorsal radicular arteries originating from the spinal arteries. The total contribution of radicular branches for the cervical segment of the dorsal spinal arteries in dogs is 14, similar to that for the ventral spinal artery.²⁵ In human beings, around 4 radicular arteries empty into the posterior spinal arteries of the cervical area.²⁶

The ventral spinal artery gives rise to sulcal arteries, which travel dorsally into the ventral median fissure (Fig 1.1). Sulcal arteries are also known as sulcocommissural, central or middle arteries. The mean number of sulcal arteries in the cervical spinal cord in dogs is around 6 per cm. Tator et al.²⁷ using a silicone rubber microangiographic technique, found similar results for the cervical spinal cord in human cadavers. This density is decreased in the lumbar and thoracic spinal cord. The length of the stems of central arteries in the cervical region in dogs ranges from 2.0 mm to 5.0 mm, with a mean length of 3.5 mm.²⁵ Sulcal arteries enter the spinal cord and supply the right or left half of the spinal cord parenchyma. Normally, one sulcal artery supplies one side of the spinal cord, while the adjacent artery feeds the other side.²⁷ A small percentage (19%)

of sulcal arteries bifurcate in the median ventral sulcus supplying the spinal cord bilaterally.²⁷

In dogs and human beings, circumferential arteries form an irregular arterial ring or pial arterial system around the spinal cord connecting the dorsolateral spinal arteries with the ventral spinal artery. This arterial ring, also known as the vasocorona, receives incoming dorsal root and ventral root arteries. Radial arteries arise from this pial arterial system and supply the outer white matter. Sulcal arteries supply most of the ventral gray matter and the ventral part of the dorsal gray matter. Branches of the sulcal arteries course through the gray matter and supply approximately the inner half of the ventral and lateral funiculi. The base of the dorsal funiculi is also supplied by branches of the sulcal arteries. Microangiographic studies in human beings show that the outer half of the ventral and lateral funiculi is supplied by a centripetal arterial system from the pial arteries.²⁷ Dorsal spinal arteries and their branches supply the dorsal portion of the dorsal funiculi. There is an area of overlap between the sulcal arterial system (centrifugal system) and the pial arterial system (centripetal system) named the watershed zone.²⁷ The angioarchitecture in the white matter has a radial pattern, whereas vessels in the gray matter have a more plexiform pattern (Fig 1.1).²⁸

Capillary networks are more abundant in the gray matter than in the white matter. The number of capillaries per unit area (mm^2) is 5.2 times higher in the gray matter than white matter of canine spinal cord. The number of capillaries is

significantly correlated with the difference in metabolic needs between these two regions.²⁹

The deep cervical artery, a branch of the costocervical trunk, supplies the deep structures of the neck including the semispinalis capitis, spinalis et semispinalis thoracis et cervicis and the terminal cranial portion of the thoracic portion of the longissimus. It anastomoses with dorsal muscular branches of the vertebral artery and, in the cranial part of the neck, with the descending branch of the occipital artery.^{6,25,30}

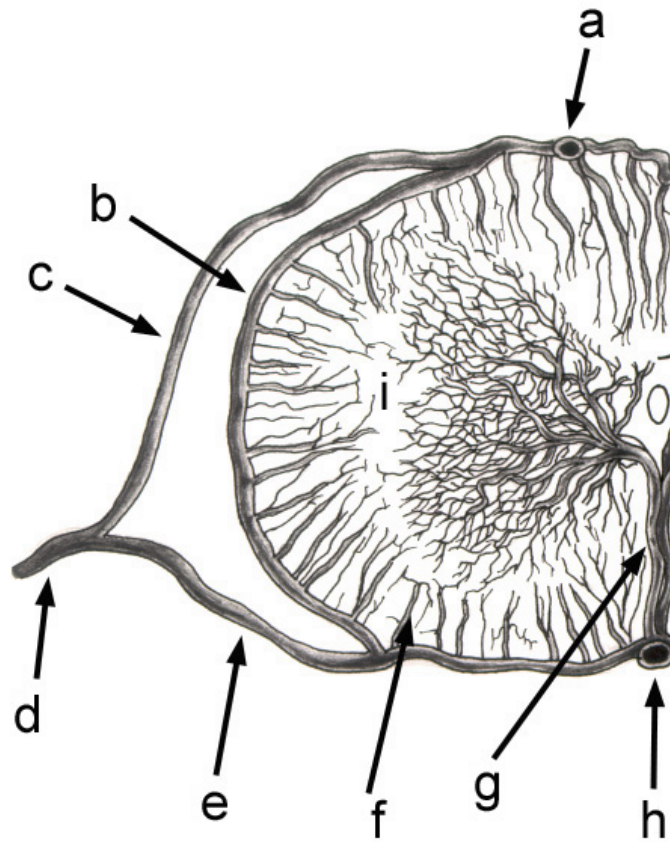


Figure 1.1- Illustration of the arterial blood supply to the cervical spinal cord in the dog (Drawing made by the first author)

Dorsolateral spinal artery (a), Pial arterial system (b), Dorsal radicular artery (c), Spinal artery (d), Ventral radicular artery (e), Radial artery (f), Sulcal (central) artery (g), Ventral spinal artery (h), Watershed zone (i).

Veins

The ventral spinal vein travels along the ventral median fissure on the ventral surface of the spinal cord parallel to the ventral spinal artery.²⁸ In some cases, a duplicate ventral spinal vein courses on either side of the ventral spinal artery. Branches from the circumferential veins (pial venous vessels) and central veins (sulcal veins) run parallel to the artery, drain into the ventral spinal vein.²⁸

In the dorsal surface of the spinal cord, a dorsal spinal vein receives tributaries from the circumferential veins and dorsal central veins, and run longitudinally on the midline region of the dorsal surface of the spinal cord. The dorsal spinal vein is usually larger than the ventral spinal vein. The dorsal spinal vein diameter is largest in the lumbar region, next largest is at the cervical level, and smallest in the thoracic region of the spinal cord segments.²⁸

In a midsagittal section, several central veins run perpendicular to the central canal. The number of central veins emerging from the ventral median fissure is greatest in the cervical level.²⁸ Vessels in the gray matter show a plexus pattern of dense arterioles, capillaries, and venules.²⁸

1.2 CANINE VERTEBRAL VENOUS PLEXUS

Published as a review article in: *Int. J. Morphol.*, 2003, vol. 21, no.3, p.237-244.

1.2.1 Historical notes

Vesalius^a and Sylvius^b are mentioned as the first anatomists to observe emissaries of the vertebral venous plexus in the spine of human cadavers.³¹ Falloppio (1523-1563) visualized the longitudinal vertebral venous sinus inside the cervical region and Vidus-Vidius (1500-1569) was the first to illustrate the longitudinal venous sinuses.³¹ Batson (1957) credits the English anatomist Willis for first describing and illustrating the longitudinal and transverse veins that extend the entire length of the vertebral canal.^{31,32} The first and most complete anatomical studies on the human vertebral venous system was made in the first part of the 19th century by Gilbert Breschet at the Anatomical Laboratory in Paris.^{31,32} During this period, Cruveilhier (1834-1836) underlined the importance of the vertebral venous plexus in human beings as a collateral system after occlusion of the inferior vena cava.³² Following these early findings the knowledge of these veins was ignored or forgotten.³³

In 1940 Batson's two landmark articles, he explained the properties of these veins in the spread of tumor metastases³³ and he was responsible for resurgence of interest in the vertebral venous system.³² Batson, using X-rays and injecting a radiopaque material into the dorsal vein of the penis in *Macacus*

^a Andreas Vesalius (1514-1564), flemish anatomist, author of *De Humani Corporis Fabrica*

^b Jacobus Sylvius (1478-1555), french anatomist, author of the *Hippocratis & Galeni*

rhesus monkeys, demonstrated connections between the pelvic veins and cranial sinuses via vertebral venous plexus.³¹ These experiments provided evidence for understanding prostatic cancer metastases to the vertebral column and the spinal epidural space.³² He also demonstrated a voluminous valveless venous system, eponymically known as Batson's veins, that was capable of replacing the jugular system in cases when the latter was occluded.³³

A number of authors have investigated the venous drainage of the vertebrae in the dog. Hofman made an extensive comparative anatomical study of the veins of the brain, and spinal cord of various representative vertebrates, from *Pisces* to *Perissodactyla*, including *Canis familiaris*.³⁴ Dräger³⁵ made a contribution on the epidural veins on the dog and its relation to others adjacent structures.

Worthman^{36,37} conducted a complete anatomical and physiological study of the vertebral venous sinuses in the dog. He described anastomoses between the basivertebral veins and extravertebral branches of the vertebral veins, and also described external vertebral venous plexuses. In 1962, Reinhardt et al.³⁸ described the ventral internal venous vertebral plexus in the dog and its connections with the occipital, vertebral and deep cervical veins. In 1966, Wieboldt³⁹ described the extravertebral veins of the vertebral column of the dog and cat, without referring to the nutrient vessels. In 1960, Crock⁴⁰ gave a thorough description of the intraosseous venous distribution of the vertebra of the dog, using radiography and clearing techniques.

Descriptions of this venous plexus have also been made in the following species: cats,⁴¹ rabbits,⁴² rats,⁴³ baboons,⁴⁴ goat and sheep,⁴⁵ ox,³⁴ whales and seals,⁴⁶ birds,⁴⁷ and snakes.⁴⁸

1.2.2 Anatomy of the canine vertebral venous plexus

The vertebral venous plexus is a thin-walled, valveless venous network that surrounds the entire length of the vertebral column, terminating cephalad in the cerebral venous sinuses.^{12,49,50} According with its position inside or outside the vertebral canal, this vertebral venous plexus can be divided into 3 intercommunicating divisions: internal vertebral venous plexus, external vertebral venous plexus, and the basivertebral veins.⁵⁰

The external vertebral venous plexus (EVVP) is subdivided into a dorsal and a ventral component.^{12,38,50} The dorsal external vertebral venous plexus (*plexus vertebralis externus dorsalis*) is associated with the external surface of the vertebral arches and anastomoses with extraosseous veins of the adjacent musculature, as well as with interarcual effluents coming from the internal vertebral venous plexus⁵¹ (Fig 1.2). Extraosseous veins that drain the cervical vertebral column in the dog are: the vertebral veins, deep cervical veins, occipital veins, and internal jugular veins.⁴⁹ In the rest of the vertebral column, this external venous plexus is represented by the azygos, left hemiazygos, internal iliac, external iliac and mediam sacral veins.^{12,49,50} The ventral external vertebral venous plexus (*plexus vertebralis externus ventralis*) is not very prominent in the

dog.^{12,38,50} It can be recognized by its anastomoses, ventral to the vertebral bodies, with tributaries of the intervertebral veins and the basivertebral veins.^{36,38,51}

The internal vertebral venous plexus (IVVP) is known as longitudinal spinal sinuses, vertebral sinuses, epidural venous plexus or meningorachidean plexus (Table 1.2). The *Nomina Anatomica Veterinaria*¹ (NAV) recognizes, in domestic animals only, a ventral component of the IVVP or *plexus vertebralis internus ventralis*. The IVVP lies within the vertebral canal, inside the epidural space and along the dorsal surface of the vertebral bodies and intervertebral disks.⁵¹ The IVVP consists of two symmetrical flattened longitudinal sinusoidal venous trunks, of about 2-4 mm in diameter.⁴⁰ Deep transverse connections from one side to the other occur erratically at the junctions between the vertebrae beneath the dorsal longitudinal ligament.^{19,36,38} Cranially the IVVP communicates with the basilar sinuses at the level of the foramen magnum, and caudally it extends to the 4th or 6th caudal vertebra.⁴⁰ Compared with human beings the IVVP in dogs is less complex.³² The human IVVP is formed by the anterior vertebral venous plexus and posterior vertebral venous plexus. The anterior component in human beings is represented by 4 channels, 2 anteriomedial and 2 anterolateral, while the posterior component is formed by 2 longitudinal channels located posterolaterally in the spinal epidural space.³²

The IVVP has a peculiar rhomboidal or segmentally arched appearance^{40,52} (Fig 1.2). At the level of the intervertebral disk space both

longitudinal channels deviate dorso-laterally, contacting with the inner surface of the vertebral pedicles and converging medially over the mid-portion of the dorsal surface of the vertebral bodies.⁴⁰ Each venous trunk is dilated in the middle of the vertebral body and constricted at the intervertebral disk space level.⁴¹ At its origin at the foramen magnum and within the dorsal arch of the atlas, each component of the IVVP appears dilated and larger than at other levels in the vertebral canal.^{12,36,50} At this level, two large sinuses representing the IVVP are positioned against the vertebral arch of the atlas so the spinal cord passes between them in contact with the dorsal surface of the dens.³⁶ In human beings, the internal vertebral venous plexus at this level protects the dural sac from compression during atlanto-axial rotation due to reduction of the epidural space.⁵³ In dogs, the diameter of the IVVP is reported to be smaller within the C3 vertebra than throughout the rest of the cervical region.³⁶ The caliber of the plexus decreases at the thoracic inlet region (C7-T1) and remains constant to the level of 4th or 5th lumbar vertebra.³⁸ From C5, a progressive and marked reduction of the IVVP begins. Vessels fuse within the 4th to 6th caudal vertebrae or terminate as small venules in the tail musculature.^{36,50}

The interarcuate branches (*rami interarcuales*) are dorsal anastomoses of the internal vertebral venous plexus within the vertebral canal.⁵¹ These connections are prominent in the cervical and thoracic region and are located approximately at the level of the intervertebral disk.⁵⁰ In the cervical region, immediately ventral to the cranial border of the dorsal arch of the atlas, the first

interarcual effluents are seen as complete dorsal connections between the two longitudinal trunks of the IVVP.^{36,38} At the atlantoaxial level, these branches have a similar pattern and occasionally between the second and third cervical vertebrae.³⁶ In the rest of the vertebral canal these dorsal anastomoses are often incomplete.³⁶ At intervertebral spaces, the interarcuate veins perforate the ligamenta flava and receive tributaries from the dorsal external vertebral venous plexus or interspinous veins.⁵⁰ The interarcuate branches of the IVVP in the dog resemble the human venous rings that circle the lumen of each vertebral segment and interconnect the IVVP.^{36,54} Some authors consider the interarcuate branches in the dogs as part of a dorsal IVVP.^{51,55}

At each intervertebral foramen, intervertebral veins (*Vv intervertebrales*) connect the IVVP with the EVVP.⁴⁰ These veins receive the spinal branches (*rami spinales*) that drain the spinal cord, dura mater, and the spinal nerve roots.⁵¹ In human beings, the intervertebral veins are also known as pedicular veins or foraminal veins (Table 1.2).^{49,56} With the exception of the first cervical intervertebral veins most of the intervertebral veins are double.^{12,36,50} These connections may sometimes form a plexus, as a venous cushion, around the emerging roots of the spinal nerve, protecting them from injury.^{5,34} The intervertebral veins receive the name and numeration according with the intervertebral foramen through which they pass.⁵⁰ However, the first two sacral intervertebral veins pass through the two ventral sacral foramina on each side.

TABLE 1.1 - Major extravertebral anastomoses of the intervertebral veins in the dog⁵⁰.

Intervertebral veins	Extravertebral Connections
Cervical I	Vertebral vein/Occipital vein
Cervical II to VIII	Vertebral vein
Thoracic I,II, III	Costocervical vein and thoracic vertebral vein
Thoracic IV (left)	Thoracic vertebral vein or right azygos vein
Thoracic IV (right)	Right azygos vein
Thoracic V to IX	Right azygos vein
Thoracic X to XIII (left)	Left hemiazygos vein
Thoracic X to XIII (right)	Right azygos vein
Lumbar I to III	Right azygos vein
Lumbar IV(V) to V(VI)	Caudal vena cava
Lumbar VI to VII	Internal iliac vein, common iliac vein or caudal vena cava
Lumbar VII	Internal iliac
Sacral I (II)	Craneal gluteal vein
Sacral II (III)	Internal pudendal vein
Caudal I to IV	Middle sacral vein or internal iliac vein

The basivertebral veins (*Vv. Basivertebrales*) are single or double veins that pass through channels within the bodies of the vertebrae and connect the IVVP with extravertebral veins of the region.³⁶ They emerge through variable foramina which lie just to the right, or left, of the midline on the ventral surface of the vertebral bodies. They are found in all regions of the vertebral column.^{38,50} In the lumbar region both right and left foramina find some degree of regularity. When 2 foramina are present in any vertebral segment, they usually have different diameter.³⁶ When one or more foramina are present on the ventral side of the vertebra, basivertebral veins always travel through the body of the vertebra by bony channels and join both right and left components of the IVVP via transverse anastomoses.^{36,38}

In the cervical region, basivertebral veins connect with branches of the vertebral veins for the *longus colli* muscle.³⁶ Dorsal to the vertebral bodies these veins empty into the IVVP; ventro-laterally they empty into the vertebral veins; and ventrally some branches join the EVVP.³⁶ Basivertebral veins are not evident in the cranial thoracic segments, and in the caudal thoracic portion they usually join the intercostal veins.³⁸ In the lumbar region, basivertebral veins are paired, larger, and connect ventrally to the lumbar vertebral bodies with the lumbar veins.^{12,36,50} The sacral and caudal vertebrae usually do not have basivertebral veins; however, if they are present they emerge from the ventral surface of the vertebrae as a single vein to enter into the caudal sacral vein.³⁶

Inside the vertebral body, basivertebral veins receive tributaries arranged predominantly at right angles to their main axis.⁴⁰ These branches originate a short distance from the metaphyseal zones of the vertebra from which they course centrally toward the basivertebral vein or veins.⁴⁰ Close to the vertebral endplates, epiphyseal veins are arranged parallel when viewed in longitudinal sections.⁵⁷ These epiphyseal veins drain dorsally into the right and left components of the IVVP. These arborizing epiphyseal veins drain into the EVVP on the ventro-lateral aspects of the vertebral bodies.⁵⁷ These epiphyseal veins constitute the subarticular collecting venous system of the adult canine vertebral body.⁵⁷

Innervation of the vertebral venous plexus is provided by the sinuvertebral nerve (*ramus meningeus*). In human beings, the cranial IVVP may receive branches from the trigeminal nerve and upper cervical sensory nerve fibers.⁵⁸

TABLE 1.2 - Synonyms of standard veterinary and human nomenclature for the vertebral venous plexus.

Standard Nomenclature ^{a,b}	Synonyms
<p>Internal vertebral venous plexus <i>(Plexus vertebralis internus ventralis)</i>^a <i>(Plexus venosus vertebralis internus anterior et posterior)</i>^b</p>	<ul style="list-style-type: none"> • Epidural venous plexus^{59*} • Epidural veins⁶⁰ • Meningorachidean venous plexus*⁶¹ • Longitudinal spinal sinuses¹⁹ • Longitudinal vertebral veins⁶² • Extrathecal venous plexus*⁶³ • Vertebral sinuses^{64,65} • Intrarachideal venous plexus⁶⁶ • Columnar vertebral sinuses¹¹ • Batson's plexus^{67*} • <i>Circelli venosi</i>⁴⁵ • Intraspinial veins⁶⁸
<p>External vertebral venous plexus <i>(Plexus vertebralis externus dorsalis et ventralis)</i>^a <i>(Plexus venosus vertebralis externus anterior et posterior)</i>^b</p>	<ul style="list-style-type: none"> • Paravertebral venous plexus^{48*} • Prevertebral longitudinal veins⁶⁹ • Extrarachidean venous plexus⁶⁶

^a Nomina Anatomica Veterinaria, 1994

^b Terminologia Anatomica, 1998

<p>Intervertebral veins (<i>Vv. intervertebrales</i>)^{a,b}</p>	<ul style="list-style-type: none"> • Radicular veins⁷⁰ • Pedicular veins (supra e infra)⁵⁶ • Veins of the lateral foramina⁶⁰ • Foraminal veins⁷¹ • Transvertebral veins⁷²
<p>Basivertebral veins (<i>Vv. basivertebrales</i>)^{a,b}</p>	<ul style="list-style-type: none"> • Intraosseous vertebral veins⁷³ • Basilar veins⁷⁴

* Also used as synonyms for the vertebral venous plexus

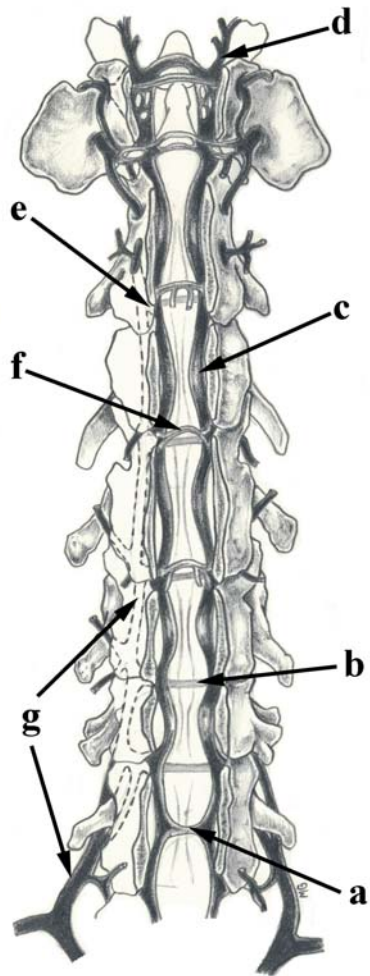


Figure 1.2 - Schematic representation of the canine vertebral venous plexus in the dog (dorsal view) (Drawing made by the first author). Transverse branch (a), intervertebral disk (b), internal vertebral venous plexus (c), basilar plexus (d), intervertebral vein (e), interarcual vein (f), vertebral vein (g).

1.2.3 Comparative anatomy of the vertebral venous plexus

The IVVP in other domestic mammals presents a similar pattern of arrangement as in dogs, however some small differences can be observed.⁵⁵ In ruminants, between the first and third cervical vertebrae, the vertebral venous plexus sometimes can be represented by 4 major channels.⁵⁵ Connections between the right and left component of the IVVP occur by segmental transverse anastomoses lying dorsal and ventral to the dorsal longitudinal ligament.^{34,55} As in dogs, there is absence of a dorsal IVVP. Thoracic intervertebral veins empty into the left azygos and right azygos veins.⁵⁵

In horses, the IVVP is located in paramedian grooves on the bodies of the cervical vertebrae and the connections between the components are made by anastomoses that pass along the middle of the vertebral bodies, along the dorsal longitudinal ligament or in bony channels within the bone. In horses, basivertebral veins are well developed in the cervical region.⁵⁵ The left and right basivertebral veins are connected by large anastomoses lying ventral to the dorsal longitudinal ligament and under cover of the bony bridges on the dorsal surfaces of the vertebral bodies.⁵⁵ Spinal branches arise irregularly within each segment of the IVVP or from the intervertebral veins. A poorly developed dorsal internal vertebral venous plexus is present in horses.⁵⁵

In pigs, anastomoses between the right and left components of the IVVP are less common but are seen more frequently between basivertebral veins of both sides along the ventral aspect of the dorsal longitudinal ligament.⁵⁵ Thoracic

intervertebral veins in pigs empty into the supreme intercostal vein, left azygos vein, and right azygos veins when present. The dorsal IVVP is not developed in the pig.⁵⁵

1.2.4 Physiology and clinical aspects of the vertebral venous plexus

The vertebral venous plexus drains blood from the vertebral column, the paravertebral musculature, the spinal cord, the meninges, and nerve roots of the spinal nerves.⁷⁵ Together with the normal drainage function, this vascular network can also be a collateral pathway for blood return toward the heart in cases of occlusion or ligation of the caval venous system.⁵² The plexus also acts as a vascular bypass during transient increases in thoracoabdominal pressures induced by coughing, defecation,³¹ micturition,⁴¹ lifting, and the Valsalva maneuver.^{31,76} Suzuki et al.⁷⁷ using fluoroscopy, demonstrated that intra-abdominal pressures above 25 mm Hg are sufficient to redirect blood flow from the caudal vena cava to the vertebral venous plexuses. Abdominal tumors,⁷⁸ position of the viscera,⁴¹ pregnancy,⁷⁹ activity of the abdominal muscles,⁸⁰ normal respiration,⁴¹ and manual application of external pressure can also induce this phenomenon. Under these various conditions, caval venous pressures rise sharply and blood is forced out of the thoracolumbar veins and is shunted into the venous plexus.³⁶ Because of its vast connections throughout the body and lack of valves, the vertebral venous plexus has been implicated in the

multidirectional transfer of metastases and air emboli between distant organs and systems.⁸¹

Radiographic and flowmetric studies have verified different directions of flow through spinal veins under various conditions in primates, dogs, cats, sheep, goats and seals.⁷⁶ In addition, the Queckenstedt maneuver, which tests patency of the spinal subarachnoid space by compressing the jugulars or intra-abdominal veins, causes an increase in cerebrospinal fluid pressure through dural compression from expansion of the epidural venous plexus.⁵² Many authors assume the vertebral venous plexus can be a pressure regulating system that buffers volume and pressure peaks from intra-abdominal, intrathoracic, intracranial, and intraspinal spaces in order to protect the spinal cord from pressure injury.^{37,82} The plexus is capable of handling large quantities of blood flow without developing varices. Some authors claim this feature is due to the complex network of collagenous fibers that support the thin walls of the sinuses.⁵²

In human beings, the cervical venous plexus receives numerous nerve endings from the sinuvertebral nerves and is associated with glomerular arteriovenous anastomoses. This suggests a possible baroreceptive function as well.⁵²

Blood flow through the vertebral plexus is affected by gravitational stress induced by posture.⁸³ In human beings and other primates, the plexus is a gravity-sensitive network and has been demonstrated radiographically to be the

principal route of cerebral venous drainage in an upright position.^{82,83} Although it is primarily the jugular veins that drain the head in horizontal subjects, direct observations reveal gravity causes the jugular vein to collapse, at least partially, in upright human beings, giraffes, and dogs.⁷⁶ These radiographic studies support the observation that little if any jugular filling activity is observed during upright posture. The rigid bone cage of the spine, similar to the skull and the cerebral veins, may protect the vertebral venous plexus from collapse.⁸³ Recently, Valdueza et al.,⁸³ and Schreiber et al.,⁸⁴ using color-coded duplex ultrasound in young human beings demonstrated that spinal epidural veins are the most probable alternative cerebral drainage route in the upright position. Individuals showed an increase in vertebral venous flow from 40 ml/min in horizontal position to 210 ml/min in an upright position. Simultaneously, internal jugular veins decreased flow from 700 ml/min to 70 ml/min respectively. Considering that human beings spend most of their time in vertical sitting or standing postures, the vertebral venous plexus must be considered the primary avenue of venous return from the head.^{82,83} No studies have been published in dogs testing the physiological effect of head position on vertebral venous plexus flow.

The role of the vertebral venous plexus in reabsorption of cerebrospinal fluid has been also studied.⁸⁵ Other authors consider the vertebral venous plexus can act as a cooling mechanism of the spinal cord in a similar way as the dural sinuses in the brain.^{34,86} An ancillary function of the vertebral venous plexus may

be to act in a mechanical capacity as a hydraulic shock-absorbing sheath that buffers the spinal cord and the spinal nerves during movements of the vertebral column.^{5,34,52}

Clinically, in human beings and animals rupture of the IVVP has been associated with the etiology of spontaneous spinal epidural hematomas.^{32,65,87,88} Oldenkott et al.⁸⁹ proposed that a “locus minoris resistentiae” in the wall vasculature is required to predispose human beings to hemorrhage. Levy and Stula⁹⁰ related the cause of spinal hemorrhage in human beings to old age (with relative fragility of blood vessels) and chronic inadequate adjustment of coagulation parameters. Doberman pinschers with a deficiency of von Willebrand factor (Factor VIII-related antigen) can develop significant spinal epidural hemorrhage due to laceration of the IVVP which result in progressive neurological deficits.⁶⁵ Epidural or subarachnoid punctures in dogs, at the cisternal region also have a risk of producing spinal epidural hemorrhage since at the atlanto-occipital space the IVVP is well developed and encircles the dural tube.⁵ Following a Hansen type I intervertebral disk herniation, extruded nucleus pulposus can be expelled laterally and rupture the IVVP.⁹¹ This can result in bleeding, hematoma formation and subsequent extradural spinal cord compression.⁹¹ This type of extradural mass constitutes the second most frequent cause of extradural spinal cord compression, after disk material.⁹¹

The continuity of the valveless vertebral venous plexus throughout the length of the neuroaxis enables bacteria or tumor cells to travel from the thorax,

abdomen or pelvis and into the head or vertebral column when intrathoracic or intra-abdominal pressure is increased.¹⁹ This phenomenon has been termed paradoxical embolism, retrograde venous invasion or Batson's phenomenon.¹⁹ Coman and De long⁹² first demonstrated Batson's theory on the spread of metastases to the vertebral column, by experimentally creating, through injection of Walker rat breast carcinoma into the femoral vein of rats with manual abdominal compression.⁹³ In human beings, vertebral metastasis of renal cell carcinoma has been explained by this model of spread.⁹⁴ In dogs, metastasis of osteosarcomas and pheochromocytomas into the central nervous system^{95,96} is suggested to occur by retrograde venous spread through the vertebral venous plexus. Diskospondylitis, vertebral osteomyelitis, and infectious diskitis in dogs with primary sites of infection elsewhere in the body has been explained by this mechanism.⁹⁷

The vertebral venous plexus may participate in the etiology of fibrocartilaginous embolism of spinal cord vasculature (also known as embolic myelopathy) in dogs.⁹⁸ One hypothesis is that disk material ruptures through and into the internal vertebral venous plexus and may then be driven retrograde into leptomeningeal vessels and internal plexus of the spinal cord through interarcuate veins.⁹⁹ Basivertebral veins may also play an important role for entry of fibrocartilaginous emboli into the spinal cord.^{98,100} In these cases the embolic nucleus pulposus material may be extruded into intraosseous veins close to the disk and then into the spinal cord.

The vertebral venous plexuses also participate in the pathophysiology of other spinal cord vascular lesions such as arteriovenous fistulas and venous malformations in human beings.¹⁰¹ Extradural arteriovenous fistulas are characterized by a direct connection between an extradural artery and vein producing a high-flow fistula. This produces engorgement of the epidural venous system, compression of the spinal cord, and progressive myelopathy.¹⁰¹ Also, the high venous pressure in the vertebral venous plexus can lead to intradural venous hypertension by increasing resistance to outflow. Although not common, arteriovenous malformation has been reported in the dog.¹⁰² Other types of malformation of the vertebral venous plexus described in human beings are spinal epidural venous angiomas that can result in foraminal enlargement and erosion of the lumbar vertebral body, causing lumbar pain.¹⁰³

Some uncommon venous disorders in human beings that involve the vertebral venous plexus are congenital dilation of the cervical epidural venous plexus, epidural varices, Foix-Alajuanine syndrome, and venous infarction.⁶³ Spinal cord alterations in decompression sickness¹⁰⁴ may cause compromise of the vertebral venous plexus.

Also in human beings, dilatation of the cervical vertebral venous plexus has been described as an indicator of spontaneous intracranial hypotension syndrome (SIH syndrome, orthostatic headache).¹⁰⁵ To explain these abnormalities, some authors have suggested that the Monro-Kellie hypothesis is applicable.¹⁰⁶ According to this doctrine, with an intact skull, the sum of the

volume of the brain plus the CSF volume plus intracranial blood volume is constant.¹⁰⁶ So, a reduction of CSF (through dural tears) requires a compensatory increase in the venous system. This sign (cervical epidural venous engorgement) has been postulated as a radiographic sign for diagnosis of the sudden intracranial hypotension syndrome.¹⁰⁵

Congenital inheritable connective tissue disorders in human beings, such as Marfan syndrome, predispose to the formation of enlarged cervical anterior IVVP causing neurologic symptoms.⁵⁹ This could be due to alterations in the venous connective tissue, compensatory mechanism (Monro-Kellie hypothesis), herniated disk or compressive lesions.

1.3 PATHOPHYSIOLOGIC MECHANISMS OF ACUTE SPINAL CORD INJURY

It is generally accepted from both clinical and experimental studies that acute spinal cord injury (SCI) is a neuropathologic process involving primary and secondary events.¹⁰⁷⁻¹¹¹ The primary mechanism involves an initial mechanical injury due to local and mechanical deformation. Secondary mechanisms include a cascade of biochemical and cellular processes that are initiated by the primary process or injury and cause ongoing cellular damage and even cell death. This concept of a secondary mechanism to acute SCI was first proposed by Allen in 1911 where he observed there was an improvement in neurologic function after removal of post-traumatic intraparenchymal hematomas in dogs subjected to experimental acute SCI.¹¹² Later, Allen theorized there was a noxious agent that was present in the hemorrhagic necrotic area at the lesion epicenter and may be initiating ongoing damage. This concept of a primary and secondary mechanism and their duality in acute SCI has since been included in the understanding of the pathophysiology of subarachnoid hemorrhage, cerebral and spinal ischemia, and head trauma.¹¹⁰

A variety of experimental models have been developed to study SCI.¹⁰⁷ The most common model is the weight-drop model introduced by Allen which causes impact without significant persisting compression since the weight is removed quickly.¹¹³ Basically, the model consists of dropping a known calibrated weight from a defined distance over an exposed vertebral canal. Several other models of impact plus persisting compression have been created including

electromagnetic devices,^{114,115} blocking-weight technique, extradural clip compression technique,¹⁰⁷ and epidural balloon inflation in rats,¹¹⁶ ferrets,¹¹⁷ and dog.^{118,119} Transection or hemisection of the spinal cord are experimental models also used to study SCI.¹²⁰ The hemisection model allows study of the reactions in the contralateral spinal cord side.

1.3.1 Primary injury

Primary injury is produced by the forces that cause initial mechanical injury in the spinal cord, such as compression, shear, laceration, bending, and distraction.^{27,107,110,121} A common example of these forces in veterinary medicine is acute intervertebral disk herniation, which causes compressive or concussive trauma to the spinal cord.¹²¹ These initial forces lead to complete or incomplete transection of the spinal cord. Primary SCI is most commonly a combination of the initial impact as well as subsequent persisting compression. This typically will occur with fracture dislocation and acutely ruptured disk. Similarly, spinal cord laceration from sharp bone fragments can produce a mixture of spinal cord laceration, contusion, and compression or concussion.¹¹⁰ The nature of the primary injury varies from initial dynamic spinal cord contusion to long term sustained cord compression. Morphologic characteristics and clinical outcomes vary with the forces of spinal cord compression, duration of compression, displacement of the cord, acceleration of impacting forces, and kinetic energy absorbed at the time of spinal cord impact.¹¹¹ The primary injury after SCI tends

to damage the central gray matter first with compromise of the peripheral white matter.¹²² The softer consistency of the gray matter and its vascular density are factors that contribute to its susceptibility to primary damage.¹²²

1.3.2 Secondary injury

There is considerable evidence that primary mechanical injury initiates a cascade of secondary injury mechanisms, including: ischemia, impaired autoregulation, neurogenic shock, hemorrhage, microcirculatory derangements, vasospasm, and thrombosis.¹²² Ionic derangements, including increased intracellular calcium, increased extracellular potassium, increased sodium permeability, neurotransmitter accumulation, including serotonin or catecholamines and extracellular glutamate, also participate in this secondary damage. Arachidonic acid release and free radical production, eicosanoids production, lipid peroxidation, endogenous opioids, edema, inflammation, loss of adenosine triphosphate-dependent cellular processes, and programmed cell death or apoptosis are also mechanisms mentioned as critical in the development of this ongoing process.^{108,110} All of these mechanisms are considered as parallel events that act sequentially.¹²³

1.3.2.1 Biochemical changes

1.3.2.1.1 Free radicals

Free radicals are reactive molecules that possess an extra electron in their outer orbit.¹¹⁰ There is considerable evidence for early involvement and pathophysiologic importance of oxygen free radical formation with cell membrane lipid peroxidation in CNS injury. Free radicals commonly originate from molecular oxygen. Superoxide (O_2^-) is the primary reactive oxygen species (ROS) generated in the body, and is formed by incomplete electron transport in the mitochondria. Superoxide is converted to H_2O_2 by superoxide dismutase, and this is turned into H_2O and O_2 by catalase or glutathione peroxidase.¹²⁴ In the presence of free iron, released from hemoglobin, transferrin, or ferritin by either lowered pH or oxygen radicals, H_2O_2 forms highly reactive hydroxyl radicals (HO). These molecules, if not eliminated, result in progressive lipid peroxidation. This can spread over cellular surfaces causing destruction of phospholipid-dependent enzymes, and disruption of ionic gradients. If severe, membrane lysis can also occur. This process in turn can form more lipid peroxides and consequently more free radicals.^{110,125}

After experimental contusive or compressive injuries to the spinal cord, there is an increase in polyunsaturated fatty acid oxidation products, such as malonyldialdehyde. Early inhibition of the Na^+/K^+ ATPase pump, which is lipid peroxidase-sensitive, and decrease in tissue antioxidant levels (e.g., α -tocopherol) are events that facilitate increases in free radicals. These processes

are markers of early oxygen radical reactions. Lipid peroxidation may also play a role in post-traumatic hypoperfusion after SCI. Free radical mediation occurs through disruption of cell and mitochondrial membranes, denaturation of proteins, and DNA breakdown.¹¹¹

High doses of steroids (methylprednisolone) may improve spinal cord blood flow (SCBF) and microvascular perfusion, as well as clinical neurologic recovery after experimental SCI. These compounds may also provide cytoprotection through inhibition of lipid peroxidation, inhibition of inflammatory cytokines, modulation of inflammatory/immune cells, facilitation of spinal cord impulse generation, and inhibition of prostaglandin-induced vasoconstriction.¹²⁶ Because lipid peroxidation begins within the first 5 minutes after acute SCI, administration of high doses of steroids should occur as close to the time of injury as possible for maximal efficacy. In clinical situations, findings using methylprednisolone are more variable than experimental studies. Some clinical trials have demonstrated efficacy while others have not.^{107,126}

One free radical of considerable interest is nitric oxide (NO). Nitric oxide is a small, relatively unstable, diatomic, free radical and it is also an inorganic gas.¹²⁷ It is produced in a variety of tissues (endothelial cells, smooth muscle cell, epithelial cell, fibroblast, cardiomyocytes, hepatocytes, and macrophages) and has a wide range of physiologic activities. These include vasodilation, immune activation, and neurotransmission. Nitric oxide is formed by nitric oxide synthase (NOS), of which there are several forms. One specific form to neurons, L-

arginine, constitutes the substrate for NO formation and citrullate is the metabolite originated after its production.¹²⁷ Synthesis of excess NO leads to production of radical NO^\cdot , which can damage cells in a number of ways. Damage can result from combining with O_2^- to produce the highly reactive peroxynitrite radical ONOO^\cdot . As with other free radicals, this can lead to lipid, protein, and nucleic acid damage. Besides increases in free radicals, SCI is associated with increased NO production, both in the injury epicenter and adjacent cord. Production of NOS is upregulated in motoneurons and in the dorsal horn after injury. Moreover, spinal cord swelling and cell damage are reduced by application of NOS antiserum.¹¹¹ In normal conditions, NO in the nervous system produces cerebral vasodilation and regulates spinal cord and cerebral perfusion. This helps to protect these structures from ischemia.¹²⁷

There is an interesting link between glutamate induced neurotoxicity and NO-mediated cell damage. Activation of NOS is dependent on cellular calcium levels and calcium-calmodulin binding. Thus, increased intracellular calcium, from NMDA activation, leads to stimulation of NOS and increased NO production. This further exacerbates cell injury. Inhibitions of NOS reduce glutamate and NMDA-induced cell damage in brain cell cultures. However, effect of NOS inactivation in CNS trauma and ischemia is complicated by conflicting neurotoxic actions of excess concentrations of NO in neurons and neuroprotective actions of NO on vasodilation and improved perfusion.^{111,128}

1.3.2.1.2 Neurotransmitter excitotoxicity

The excitatory pathway mediated by neurotransmitters glutamate and aspartate have been described as the important mediators of neuronal cell death.^{110,111} Glutamate, which constitutes the principal excitatory neurotransmitter in the CNS, is released primarily from neuronal cells after SCI.¹²² One of the most important biochemical derangements in the injured spinal cord is the accumulation and subsequent damage exerted by the excitatory aminoacid neurotransmitter, glutamate. Glutamate causes an elevation of intracellular calcium. Increases in extracellular glutamate are believed to be caused by cellular lysis, increased exocytosis and impaired re-uptake of the neurotransmitter.

Increased intracellular calcium in turn causes activation of calcium dependent proteases, lipases, and endonucleases. These can cause further damage by breaking down cytoskeletal components such as neurofilaments, and by dissolving cell membranes, and DNA. Intraspinal injection of glutamate results in a significant loss of neurons around the injection site. This effect demonstrates the neurotoxic capabilities of this excitatory amino acid. There are several types of glutaminergic receptors. However, the N-methyl-D-aspartate (NMDA) receptor appears to be the principal receptor involved in glutamate induced excitotoxicity in neurons. Blockage of this receptor with MK-801, a specific NMDA receptor antagonist, has a protective effect on experimental SCI.¹⁰⁷ NBQX (2,3-dihydro-6-nitro-7-sulfamoyl-benzo(f)quinoxaline) is another more selective and potent

antagonist of NMDA receptors when, administered intravenously in rats after experimental SCI, results in improved distal neurologic function.¹²⁹ Also, non-NMDA receptors such as alpha-amino-3-hydroxy-5-methyl-4-isoazolepropionic acid (AMPA)/kainite type glutamate receptor have been implicated in the detrimental effect of glutamate on oligodendroglia.¹³⁰ Lumbar CSF fluid analysis in dogs with acute intervertebral disk herniation has found increased concentrations of glutamate¹⁰⁸. The neurotransmitter concentration has been correlated with severity of clinical signs.^{131,132} Concentrations of extracellular glutamate in the white matter after experimental SCI in rats are high enough to destroy oligodendrocytes, contributing to the functional damage after injury.¹³⁰

1.3.2.1.3 Endogenous opioids

Increased elevation of endogenous endorphins have been found in plasma after experimental SCI with endogenous opioid dynorphin A and is implicated as the most likely to be involved in SCI secondary injury.¹³³ This is supported by findings of selectively increased dynorphin immunoreactivity immediately after SCI.^{134,135} Opioid dynorphin has been found at the area of SCI in concentrations proportional to the severity of injury. The kappa opioid receptor system is apparently involved in SCI. Naloxone and thyrotropine-releasing hormone (TRH) are kappa opioid receptor antagonists, and both have proven beneficial in treatment of experimental SCI.¹³⁶ These antagonists also improve post-traumatic spinal cord blood flow independent of systemic vascular effects.

Although, there is considerable evidence for an opioid-mediated component to SCI, a clinical trial comparing naloxone and methylprednisolone with a placebo did not demonstrate a significant improvement in neurologic function in the naloxone treatment group.^{111,135,137}

TRH, initially hypothesized to act as a physiologic opioid antagonist, has demonstrated neuroprotective benefits in experimental models of SCI¹³⁷. A small clinical trial with TRH did not show significant neuroprotective effects in human patients with neurologic injuries.¹¹⁰ Because the effective half-life of TRH is short, experimental studies have focused on synthetic analogs (CG-3703) with longer effective duration of actions.^{110,135,137}

1.3.2.1.4 Electrolyte disturbances

Important electrolyte variations (ion dyshomeostasis) exist between extracellular and intracellular compartments and vice versa after SCI.¹²² One of the best defined electrolyte variations is a marked increase of intracellular calcium (Ca^{++}). Evidence exists that excess free intracellular calcium ions plays a fundamental role in mediating the pathogenesis of all neural injuries, especially ischemic and traumatic injuries.¹²² After trauma, calcium concentrations increase in neurons in a variety of ways such as disrupted cell membranes, by depolarization and entry through voltage sensitive calcium channels, or through receptor mediated calcium channels activated by glutamate (NMDA and AMPA). Secondary ischemia can also increase intracellular calcium through glutamate

release.¹²² In turn, increased intracellular calcium appears to trigger neurotoxicity in a variety of ways including activation of proteases such as; phospholipases, plasmalogenase, calpains, protein kinases, guanylate cyclase, nitric oxide synthetase, calcineurins, and endonucleases.¹³⁸ It is also possible that SCI increases intracellular calcium in vascular smooth muscle in the microcirculation at the site of injury which results in vasospasm and post-traumatic ischemia. Studies in experimental SCI have confirmed the damaging effects of glutamate with increased intracellular calcium in cultured spinal cord neurons.¹⁰⁷ An increase in intracellular calcium results in binding of mitochondrial membranes, decreasing ATP production, and increase of free radicals. These substances in turn may directly damage or destroy cell membranes, mediate platelet aggregation, vasospasm, and lead to lysosomal enzyme release.¹¹¹

1.3.2.1.5 Energy depletion

Injury to the CNS tissue creates significant energy demands on cells attempting to regulate normal ionic balance.¹¹¹ Acute energy demands are met with hyperglycolysis, which leads to accumulation of lactic acid and development of acidosis. ATP stores are depleted in the hypoxic environment, leading to inactivation of calcium-dependent ATP and sodium/potassium ATP-activated channels. This may precipitate cellular membrane depolarization and uncontrolled influx of calcium ions and a toxic accumulation of sodium (with water).^{109,111,126}

1.3.2.2 Cellular changes

1.3.2.2.1 Vascular mechanism

Changes in spinal cord blood flow (SCBF) and perturbations that follow are an important change induced by acute SCI.¹³⁹ The changes that occur in SCBF after an acute SCI can be divided into systemic and local. Precise mechanisms behind this ischemia are unclear. Vasospasm secondary to mechanical damage or by vasoactive amines (catecholamines, serotonin) may be partially responsible for the local ischemic process.²⁷ Hemorrhage may also promote ischemia, or thrombosis may occur via platelet aggregation mediated by endothelial damage. Finally, excitatory amino acids, particularly glutamate, may be involved as well. Ischemia may play a role in the formation of local spinal cord edema. Whether edema formation is injurious in itself, or a collateral phenomenon is still unclear.²⁷

Because of differences in vascularity, the central gray matter and adjacent white matter are more severely affected by acute SCI than peripheral white matter.²⁷ In the normal animal, ratios of gray matter to white matter blood flow are maintained at a 3:1 or 5:1 ratio¹⁴⁰. Studies in vivo have confirmed this dichotomy between central gray matter and surrounding white matter.²⁷

White matter perfusion typically decreases within 5 minutes of acute SCI and begins to return to normal within 15 minutes.¹³⁹ Perfusion remains near pre-injury levels during the first 24 hours. In contrast, numerous hemorrhages occur in central gray matter, as early as 5 minutes after acute SCI. Using techniques

such as microangiography, fluorescent tracer studies, and the operating microscope, blood flow in the gray matter is relatively absent 1 hour after SCI.²⁷ Blood flow in the spinal cord gray matter remains absent for at least the first 24 hours after SCI. It has been suggested that peripheral white matter changes in SCBF are due to initial vasospasm, but it seems unlikely this reaction alone causes the central phenomenon.^{107,111}

Using silicon rubber microangiography, Tator and Koyanagi²⁷ demonstrated the role of the sulcal (central) spinal arterial system and pial arteries in the spinal cord. The centrifugal sulcal arterial system supplies the anterior (ventral) gray matter, the anterior (ventral) half of the posterior gray matter, the inner half of the anterior (ventral) and lateral white columns, and the anterior (ventral) half of the posterior white columns (Fig 1.1). Traumatized spinal cords show severe hemorrhages predominantly in the gray matter. It may be that obstruction of these sulcal arteries leads to the hemorrhagic necrosis and subsequent central myelomalacia seen at the site of injury.²⁷

Alteration in endothelial cell function causing an increase in vascular permeability and edema formation are well documented in SCI.^{27,139} Endothelial damage occurs early, with formation of craters, adherence of noncellular debris, alteration of endothelial cell junctions, and microglobular formations occurring 1 to 2 hours after acute SCI.¹¹¹

Early and progressive hemorrhage develops in the central region of the spinal cord (especially in the gray matter).¹⁰⁷ It is likely that this occurs because

of the forces imparted by the primary injury, with direct mechanical disruption of the capillaries and venules. Angiographic studies in human spinal cords confirm that the large arteries remain patent but that a major change occurs in the local microcirculation (mainly capillaries and venules) in the vicinity of the injury. In human SCI, the anterior spinal artery is rarely thrombosed.^{111,141}

Autoregulation is impaired after acute SCI.¹⁰⁷ Systemic hypotension can cause decreases in spinal cord blood flow (SCBF), which then triggers systemic hypertension. This induced hypertension does not necessarily reverse the ischemia, but rather causes marked hyperemia at adjacent sites. Experimental studies in animals show that autoregulation is intact during the initial 60 to 90 minutes after SCI but is then lost suggesting that ischemic responses to SCI are mediated both by the loss of autoregulation and by constriction of the resistance vessels.¹¹⁰

Disturbances of venous drainage may play a role in the secondary damage that occurs after acute SCI, particularly in terms of exacerbating ischemia of the dorsal (posterior) columns.¹⁴² This hypothesis is supported by studies that show that venous occlusion in various human pathological conditions causes white matter lesions.¹¹¹ It may be that peculiarities of the venous drainage of the spinal cord make it more susceptible to damage.¹¹¹

Of all proposed mechanisms of secondary injury, the vascular hypothesis has considerable weight, with biochemical, angiographic, histopathologic, and clinical support for its key role in damage after acute SCI.¹⁰⁷ Proven effects

include loss of microcirculation, direct disruption of small vessels and hemorrhage, failure of autoregulation, and a glutamate-mediated excitotoxicity. Ischemia is a direct linear dose-response association, with severity of the injury becoming progressively worse a few hours after SCI, and persisting for ≥ 24 hours. Like so many secondary mechanisms of acute SCI, the precise mechanisms of vascular damage are still unclear.²⁷

1.3.2.2.2 Immune response

The inflammatory response involves activation of resident and recruited immune cells.¹⁴³ One of the first inflammatory events occurring after SCI is the activation of the complement cascade. This is followed by the cellular response: first by local resident microglia and neutrophils, then by infiltration of T lymphocytes and macrophages, and finally by reactive astrocytes. Neutrophils and macrophages, when activated, produce ROS and lipid peroxidation. The presence of neutrophil migration into the injury zone peaks within 24 hours of injury. The amount of phagocytic cell at the injury site correlates with quantitative damage.¹¹¹ Popovich et al.¹⁴³ demonstrated peak microglial activation within the lesion epicenter between 3 and 7 days after SCI, preceding the increase of monocyte influx and macrophage activation that occurred 7 days after injury. In response to local trauma, expression of cytokine transforming growth factor- β 1 (TGF- β 1) can enhance immune cell infiltration and intensify the impairment resulting from immune response.¹¹¹

Recruitment of leukocytes from blood to the site of inflammation in the injured spinal cord has been attributed to locally generated chemotaxis agents (i.e., cytokines and chemokines).¹¹¹ Using a chemokine antagonist, vMIPII after experimental SCI, Ghirnikar et al.¹⁴⁴ demonstrated a decrease in infiltrating hematogenous cells at the site of injury and increased expression of Bcl-2 gene, an endogenous inhibitor of apoptosis. This supports the argument that disrupting chemokine-receptor interaction may be an effective approach in reducing secondary damage after SCI.^{110,111}

1.3.2.2.3 Apoptosis

Apoptosis, a mechanism of cellular death determined by the genetic program and dependent on active protein synthesis, is characterized by nuclear fragmentation and histologic appearance of basophilic apoptotic bodies. In contrast to necrotic cell death, which is characterized by cellular swelling and nuclear shrinkage without apoptotic bodies, apoptosis results in cellular shrinkage and eventual phagocytosis by macrophages. Cells undergoing necrosis release chemicals that injure the surrounding tissue and produce an inflammatory response typified by polymorphonuclear cells.¹⁰⁹

Apoptosis is observed after human SCI.¹⁰⁹ Emery et al.¹⁴⁵ evaluated the spinal cord of 15 human patients who died after traumatic SCI and described evidence of apoptotic cells at the edges of the lesion epicenter and in adjacent white matter. Oligodendrocytes, microglia, and neurons are susceptible to

apoptosis.¹²² Apoptotic mechanisms of cell death are implicated in delayed Wallerian degeneration of white matter after SCI.¹⁰⁹ The process of apoptosis associated with CNS injury is complex with numerous key molecules up-regulated after injury. Therapeutic benefits may be achieved with development of protease inhibitors to prevent programmed cell death.^{109,110}

The caspases, a family of cysteine proteins, are thought to play an important role in apoptosis.¹⁴⁵ Caspase-3 cleaves several essential downstream substrates involved in the apoptosis pathway, including PAK2, fodrin, and gelosin. Caspase-3-activation in vitro can be triggered by upstream events, leading to release of cytochrome C from mitochondria and subsequent transactivation of procaspase-9 by Apaf-1. These upstream and downstream components of the caspase-3 apoptotic pathway are activated after traumatic SCI in rats and may occur early in neurons in the injury site and hours to days later in oligodendroglia adjacent to and distant from the injury site.¹¹⁰

Oligodendrocytes are thought to be the major cell type in compressive SCI that undergo apoptosis.¹⁴⁶ This is observed in areas of Wallerian degeneration and detectable between 24 hours and 3 weeks post-injury. Apoptosis in oligodendrocytes may occur as a result of axonal demyelination, Wallerian degeneration or both.¹⁴⁶ It is suggested that this death of oligodendrocytes may be as consequence of microglial activation that peaks at 8 days post-injury.¹¹¹ This latter hypothesis is suggested by observation of activated microglia in the same regions undergoing apoptosis, with apparent contact between some of the

microglial process and apoptotic oligodendrocytes.¹⁴⁷ Recent work has suggested a role for the FAS and p75 death receptors in mediating post-traumatic apoptosis of oligodendrocytes, thus contributing to axonal degeneration.^{110,146}

Apoptosis occurs around the lesion epicenter and within areas of Wallerian degeneration in both ascending white matter tracts¹⁴⁶. Targeting of upstream events of the caspase cascade to protect neurons and oligodendrocytes from undergoing apoptotic death may have therapeutic potential in treatment of acute SCI. Agents such as the oncogene Bcl2 have limited the degree of histologic injury in acute experimental SCI in rats, possibly by regulating antioxidant pathway that limits free radical generation. Similarly, cycloheximide, an apoptosis inhibitor drug can improve outcome after contusion trauma in the spinal cord of rats.^{109,111,148}

1.3.3 Neuropathology of the spinal cord injury

The sequential events after spinal cord injury include hemorrhage, edema, neuronal necrosis, axonal fragmentation, demyelination, and eventually cyst formation.^{111,149-151} Studies using electron microscopy demonstrate erythrocyte distension of the venules of the gray matter within 5 minutes after injury.¹¹¹ This is followed by small hemorrhages within the perivascular spaces and axonal changes 15 to 30 minutes after injury. Within 1 hour after injury, damage characteristic of chromatolysis and ischemia begins to appear in ventral (anterior)

horn cells. By 4 hours after SCI, a central region of hemorrhagic necrosis forms and extends centrifugally and proximally in the shape of spindle. White matter breakdown begins at the gray matter junction with progressive edema noted as spongiform changes on light microscopy. Axonal swelling attributed to axoplasmic stasis contains multiple organelles, mitochondria, neurofilaments, and smooth endoplasmic reticulum that undergo glandular dissolution. Damage to the myelin sheath occurs through vesicular disruption. Initially, polymorphonuclear cells infiltrate the injured region. These are replaced by macrophages within days after the injury. Within 4 weeks chronic changes occur, and a cystic cavity remains with astrocytic gliosis and demyelination of the remaining axons.¹⁴⁹

1.3.4 Gene expression during spinal cord injury

Several studies have investigated gene expression changes taking place from 30 minutes to 6 hours after injury in the spinal cord of adult rats and mice.¹⁵² Four major categories of genes sustained major changes in this acute period. First, transcriptional changes in inflammation-related molecules were observed at early time points. As soon as 30 minutes following injury, a strong (threefold) upregulation of cyclooxygenase 2 (COX2), which intensified (fivefold) by 4 hours, was seen.¹⁵² Levels of the pro-inflammatory cytokines interleukin (IL)-1 β and IL-6 and interleukin receptors (IL-4R and IL-2R α) were elevated threefold to nine fold between 30 minutes and 6 hours following SCI. Immediate-early genes such as

c-fos, nerve-growth factor-induced proteins (NGFI-A and NGFI-B), monocyte chemo-attractant protein 1 (MCP-1), activity and neurotransmitter induced early genes 4 and 6 (ANIA-4 and ANIA-6) and fos-related antigen (Fra-1) are upregulated to high levels after 30 minutes post-injury. Activation of these immediate-early genes with concomitant expression of inflammation-related genes and transcription factors involved in cell death and survival (e.g. the c-jun-AP-1 complex and NF- κ B) all illustrate efforts of the injured tissue to survive.¹⁵²

One common finding of studies investigating early transcriptional changes after SCI is the down-regulation of ion channels and transporters involved in cell excitability¹⁵². One hour after SCI, mRNA of several ion channels (e.g. K⁺, Na⁺ and Ca⁺⁺ channels), transporters (e.g. GABA and glutamate transporter) and receptors were downregulated. *In situ* hybridization will now be required to decide whether these processes reflect the cell loss at the lesion epicenter, or a specific dysregulation in the surrounding tissue. Interestingly, other authors reported contradictory findings: they described acute upregulation of several excitatory amino acid receptors (e.g. glutamate, benzodiazepine and gonadotropin receptors) that could represent a compensatory attempt of the CNS to overcome ion disturbances.¹⁵²

Few investigators have evaluated transcriptional changes occurring in the chronic phase following SCI. Seven days after SCI, inflammation and oxidative-stress genes, such as encoding leukocyte antigen MRC-OX44, complement protein C1q, major histocompatibility complex (MHC) class I and II antigens and

IL-6, were upregulated.¹⁵³ Expression of several proteases (cathepsins C, K and L, preprocathepsin D and caspase 6) was increased, most likely contributing to secondary damage or tissue remodeling. Angiogenic and neuritogenic genes are strongly expressed, reflecting an attempt of the spinal cord to repair its tissue integrity. Genes such as those encoding GAS-7, epitelins 1 and 2 and platelet-factor are likely to be indicative of this attempt, as is the upregulation of protein kinase C and their substrates. Bareyre et al.,¹⁵² found that one week following denervation, the spinal cord showed prominent upregulation of growth factors and receptors (e.g. trkB (25-fold), vascular endothelium growth factor (VEGF) receptor, and BDNF and axonal guidance molecules (e.g. decorin, lumican and collagens).¹⁵² The upregulation of these molecules involved in axonal targeting, neural survival and neurite outgrowth demonstrate spinal cord adaptation to the lesion. Limited growth processes for some types of axons could contribute to the functional recovery observed during this time.¹⁵²

In summary, early stages after SCI are characterized by strong upregulation of genes involved in transcription and inflammation, and a general down-regulation of structural proteins and proteins involved in neurotransmission. Later, an increase in expression of growth factors, axonal guidance factors, extracellular matrix molecules and angiogenic factors reflect attempts for repair, while upregulation of stress genes and proteases and down-regulation of cytoskeletal and synaptic mRNA reflect the struggle of the tissue to survive. DNA

microarrays have potential to assist in the discovery of new targets for neuroprotective or restorative therapeutic approaches.¹⁵²

1.3.5 Pharmacology research and clinical trials in spinal cord injury

Although results in animal studies have identified many potentially useful therapeutics strategies, most human beings trials to date have been disappointing and few have translated into clinically useful treatments.¹⁰⁹ However, understanding the precise molecular and biochemical mechanisms by which cells die may improve the ability to design more effective and targeted therapies. At present, methylprednisolone is the only therapeutic agent that has shown efficacy in the treatment of acute SCI. Methylprednisolone has been the subject of three clinical trials by the National Acute Spinal Cord Injury Study Group (NASCIS).¹²⁶ High-dose, intravenous administration of methylprednisolone partially improved neurologic function in human patients when therapy was begun within 8 hours of the injury and continued for 24 hours. However, patients beginning treatment with methylprednisolone more than 8 hours after SCI, did not differ in neurologic outcomes from those administered a placebo.¹⁰⁹ A recent study of the effect of intravenous (30 mg/kg) methylprednisolone on regional spinal cord blood flow in dogs did not provide a significant lasting benefit in relation to neurological preservation or restoration.¹⁵⁴ The conclusion of that study was that methylprednisolone may reduce regional spinal cord blood flow through mechanism affecting normal autoregulatory blood-flow function.^{154,155}

Gangliosides are complex acidic glycolipids that comprise a major component of cell membranes.¹⁵⁶ These compounds are present in important concentrations in cells of the CNS, located primarily in the outer leaflet of bilayer cell membrane. Gangliosides are thought to induce neuronal regeneration of neurons and restore function after SCI. In vitro studies have demonstrated that GM-1 ganglioside protects against excitatory amino-acid related neurotoxicity. In animal models, GM-1 ganglioside reduces acute nerve cell damage and aids in functional recovery after trauma. In the Sygen[®] (GM-1 Ganglioside) Multicenter Acute Spinal Cord Injury Study that included 797 human patients with no penetrating SCI at or superior to T10, GM-1 ganglioside exerted a moderately beneficial effect. This was most apparent in motor-incomplete patients.^{156,157}

A meta-analysis that included 70 neuroprotective agents (between agents or agents with other protective strategies), and 18 combinations from 103 different studies between 1966 and 1999 was reviewed.¹²³ Neuroprotective agents included in this meta-analysis were: excitatory amino acid receptors blockers (*MK-801, magnesium, CGS-19755, Ketamine, LY-293558, NBQX*), free radical scavengers (*SOD, PEG-SOD, tirilazad, allopurinol, deferoxamine, dimethylurea, U-74289G, DMSO, caffeic acid phenethyl ester*), calcium channels blockers (*KB-2796, nimopidine, flunarizine, zionitide, lidoflazine, conotoxin, verapamil*), anesthetics (*thiopental, halothane, isoflurane, methohexital*), opiate receptor antagonist (*naloxone, WIN-44,441-3, M-154,129, nalmefene*), inhibitors of leukocytes and monocytes (*anti-CD, doxycycline, pentoxifylline*),

corticosteroids (*methylprednisolone, dexamethasone*), prostaglandins (*prostaglandin E1, prostacyclin*), alternative oxygen carriers (*Fluosol DA, diaspirin cross-linked hemoglobin*), adenosine (*propentofylline*), modulators of coagulation (*tissue pathway factor inhibitor, aprotinine, heparin*), serotonin antagonists (*lysergic acid diethylamide, 2-bromolysergic acid diethylamide, cinanserin, cyproheptadine*), sodium channels inhibitors (*riluzole, CPP, QX*), local anesthetic (*tetracaine, lidocaine*), pH modulators (*dichloroacetate, CO₂*), modulator of glucose metabolism (*2-deoxyglucose, 3-O-methylglucose, insulin*), protein kinase C modulators (*staurosporine, H-7, 1,2-oleoylacetylgllycerol*), GABA modulators (*muscimol, bicuculine*), nitric oxide synthase inhibitor (*N(G)-nitro-L-arginine-methyl ester*), regenerative agents (*A4 protein precursor, gangliosides*), vasodilators (*poloxamer 188, papaverine*), plasma expanders (*pentastarch, 6% hydroxyethyl starch*), phenothiazines (*chlorpromazine, trifluoperazine*), inhibition of apoptosis (*cycloheximide*) and additional agents (*deprenyl, phenylephrine*).¹²³

This analysis demonstrated that the number of studies with positive results exceeded the number of studies with negative results. The authors of that publication stated that bias was a distinct possibility, implying selective reporting of studies favoring protection and consequently under-reporting studies with negative results. Overall this systematic review suggested that numerous agents may protect the spinal cord from transient ischemia. However, in a substantial number of studies, the lack of statistical power (due to small experimental groups) and poor control of temperature were shortcomings that had influence on

the validity of the results. These authors suggested that before results from experimental studies involving neuroprotective agents justify initial clinical evaluation, individual studies should at least comply with the following criteria: demonstration of histopathological protection and neurological improvement, adequate statistical power, meticulous temperature control, and a sufficient duration of post-ischemic survival. In addition, to avoid investigator bias, they propose that both the investigator and the observer responsible for the neurological evaluation are blinded regarding treatment.¹²³

New promising therapies for SCI include neutralization of myelin-associated proteins (Nogo, Myelin-associated glycoprotein and Oligodendrocyte Myelin Glycoprotein) that block axonal regeneration using agents such as monoclonal antibodies and inhibitors of the glial scar.^{111,153,158} Cellular transplants at the site of spinal cord lesions have also been used as a mechanism to provide a growth promoting tissue bridges for nerve fiber growth.¹⁵⁸ Neurotrophins, including nerve growth factor (NGF), brain derived growth factor (BDNF), neurotrophin -3 (NT-3) and NT4/5 have been used to promote recovery and regeneration in the CNS. Neurotrophins are responsible for stimulating neurite outgrowth needed for reorganization of injured CNS tissue and expression of key enzymes for neurotransmitter synthesis that may need to be upregulated to compensate for reduced innervation.¹¹¹ Transplantation of Schwann cells, olfactory ensheathing glial cells, fibroblasts, stem cells, fetal

tissue and peripheral nerves are among the techniques used to provide support for axonal regeneration and replacing neuronal tissue.^{158,159}

1.4 GENERAL PHYSIOLOGIC EFFECTS OF ACUTE SPINAL CORD INJURY

1.4.1 Cardiovascular complications

Experimental studies in dogs and mice have shown that acute experimental spinal cord transection consistently results in two distinct and consequential phases of cardiovascular changes.^{120,160}

Initial phase

This phase lasts between 3 to 8 minutes post-injury and is characterized by sudden slowing of the heart rate by 52% compared to normal individuals. Sinus tachycardia can also be observed during this phase.¹⁶⁰ Dogs with bradycardia can develop arrhythmias, predominantly due to escape rhythms associated with sinus arrest and subsequent junctional pacemaker capture. Short episodes of ventricular tachycardia can occur in these animals. These changes in cardiac rhythm begin immediately after experimental spinal cord transection and last 45 seconds to approximately 3 minutes.¹⁶⁰

Marked arterial hypertension occurs in experimental animals approximately 3 to 6 seconds after spinal cord transection.¹²⁰ Mean arterial pressure (MAP) can rise to 145% of control values reaching a peak within 45 seconds post-injury. Pulse pressure increases to 208% of baseline values, with increases in both systolic and diastolic pressures (70% and 30%, respectively). Systemic vascular resistance (SVR) increases rapidly to 134% of pre-transection levels.¹⁶⁰

The brief initial phase is presumably due to generalized sympathetic neurotransmitter release (noradrenalin).¹⁶⁰ The associated bradycardias and escape rhythms may be derived from concomitant increases in parasympathetic activity. Apparently, the mechanical deformation of vasoactive neurons and tracts by compression or transection of the cervical or upper thoracic spinal cord initiates this early “pressor response”. The thoracolumbar sympathetic outflow is thought to be the effector limb for this hypertensive reaction, which can be prevented by treatment with α -adrenergic receptor blocking agents. A similar mechanism is responsible for the Cushing reflex which follows increased intradural pressure.¹⁶¹ Experimental data indicate that injury of the cervical spinal cord initially results in stimulation of both α and β sympathetic receptor mediated effects. These effects are manifested by simultaneous increases in peripheral vasoconstriction as well as cardiac contractility. Experiments in cats, where thoracic sympathectomy and adrenalectomy were performed, demonstrate that the combination of both procedures abolish the initial hypertensive phase.¹⁶² This study suggests that thoracic sympathetic ganglia and the adrenal glands participate in the pressor response in cats.¹⁶² It is postulated the hypertensive response to SCI is due to stimulation of preganglionic sympathetic neurons in the thoracic spinal cord, either directly or indirectly, via descending sympathetic efferent. It is of interest that this efferent pathway probably accounts for hypertension of the Cushing’s response (discussed later in this chapter).^{120,139} The descending vasomotor pathways in human beings and cats are located in

the dorsal aspect of the lateral funiculus.¹⁶³ Severity of cardiovascular complication in SCI is related to severity of damage in descending vasomotor pathways. Some authors have referred to this state as “sympathetic shock”.¹⁶⁴ Due to its extremely short duration, the initial rise in systemic arterial pressure may not be seen in human beings or veterinary patients with SCI, but may be important in determining the amount of intramedullary hemorrhage.¹²⁰ Some experiments in animals have not documented this initial pressure response after experimental compression of the spinal cord, only the second hypotensive phase.¹⁶⁵ It is probable that factors like location of the spinal cord lesion, duration of the compression, and time of initial recording for systemic blood pressure could contribute to that lack of detection of the initial hypertensive phase.

Second phase

Resolution of the initial pressor phase is followed by a more prolonged second period, which includes a drop in arterial pressure (70%) and narrowing of pulse pressure.¹⁶⁰ Mean SVR decreases and further cardiac arrhythmias are usually not observed. By 2 hours after spinal cord transection, sustained sinus bradycardia is established.

In rats, acute changes in cardiac output (CO) parallel changes in main arterial pressure after spinal cord injury (SCI). An abrupt and persistent decline of CO and MAP is observed in rats 5 minutes after spinal cord injury.¹²⁰ However, experiments in dogs have shown no significant changes in CO between

experimental spinal cord injury animals and control animals.¹⁶⁰ Possibly, the maintenance of normal CO in dogs after SCI is due to the Frank-Starling effect.¹⁶⁰ Nevertheless, in animals presenting low CO, a decrease in sympathetic tone cannot fully explain the persistently low CO. Some investigators suggest that direct myocardial injury, similar to that shown after intracranial injury (brain heart-syndrome), may contribute to variations in cardiac activity observed in SCI in humans and animals.^{120,166} Studies have shown significant myofibrillar degeneration and other indications of myocardial damage in dogs after SCI, and postulate that myocardial damage in both SCI and brain injury are due to large catecholamine releases following injury to the neuroaxis.¹⁶⁷

In human beings, after the second phase, some individuals with cervical or high thoracic SCI present with a volatile arterial pressure.¹⁶⁸ This is characterized by episodes of marked hypertension, pounding headache, baroreceptor-mediated vagal bradycardia and upper body flushing. This condition is known as autonomic dysreflexia, and has not been described in animals. Usually some stimulus such as cutaneous touch or distension of the urinary bladder or bowel triggers this response.

Cardiac activity

Effects of SCI on heart rate are variable.¹²⁰ Using an experimental model Guha et al.,¹²⁰ found there is a significant decline in HR in animals with severe spinal cord damage.¹²⁰ Injured animals present a delayed bradycardia beginning

about 45 minutes post SCI. Evans et al.,¹⁶⁹ noted an immediate bradycardic response which preceded a rise of systemic arterial pressure, which was followed by both bradycardic and tachycardic arrhythmias.^{107,169} Other authors have not observed bradycardia. Instead, sinus tachycardia was found to accompany the rise in systemic arterial pressure, followed by a variety of dysrhythmias.¹⁷⁰ In some human patients with SCI, varying degrees of heart block, ventricular or sinus arrhythmia, and asystole have been observed which required implantation of a cardiac pacemaker.¹³⁹

1.4.2 Regulation of perfusion in the spinal cord vasculature.

The spinal cord and the brain require a constant supply of oxygen and glucose to provide for their high energy requirements.¹⁷¹ Normal physiologic values for spinal cord blood flow are between 45-55 cc/100gr/min, similar to values for cerebral blood flow. Blood flow values in the gray matter are higher than in white matter. Several efficient mechanisms in the spinal cord are present to protect central nervous system perfusion from fluctuations in systemic blood pressure (pressure autoregulation). Spinal cord perfusion is also regulated when conditions of systemic hypoxia and hypercapnia, and local metabolic requirements (metabolic autoregulation).¹⁶⁶

Pressure autoregulation

In the normal dog, perfusion of the brain remains constant despite fluctuations in MAP between 50 and 160 mm Hg. As a result, vasodilation occurs during hypotension and vasoconstriction during hypertension.¹⁶⁶ This implies, if mean arterial pressure lowers to < 50 mmHg or increases to > 150 mmHg, cerebral blood flow is maintained at normal levels. This autoregulatory mechanism is also present in the spinal cord.^{111,172}

Spinal cord perfusion pressure (SCPP) is the principal determinant of spinal cord blood flow, spinal cord oxygenation, and nutritional support. SCPP is represented by the difference between MAP and spinal CSF pressure (CSFP). In dogs, normal CSF pressure in the spinal subarachnoid space ranges from 6-7 mmHg in a standing position.¹⁷³ However, local variation in CSF pressure can occur in the spinal subarchanoid space during different body positions.¹⁷³ Assuming a MAP of 70 mmHg in a dog with a standing position, the spinal cord perfusion pressure should be approximately 60 mmHg.

The mechanisms that control autoregulation are unclear, however, myogenic and metabolic theories have been implicated.¹⁶⁶ The myogenic mechanism is the most accepted and explains the phenomenon by pressure sensitive smooth muscle cells in the CNS blood vessels. Other theories implicate reliance on metabolite concentrations such as nitric oxide.

Histopathologic and physiologic studies demonstrate loss of autoregulation in the spinal cord after 4 hours post injury. Animals with normal

blood pressure and hypotensive animals, demonstrate a relative lack of hemorrhage in peripheral spinal cord white matter after SCI. Hypertensive animals show a marked increase in peripheral white matter and gray matter hemorrhage. This finding is probably secondary to absence of autoregulatory mechanisms and rupture of damaged endothelial tight junctions.¹⁴⁰ Elevations of systemic blood pressure in the post-injury period after a concussive-type of SCI may be harmful. Disruption of damaged vasculature with increased hemorrhage and enhancement of edema formation results in severe neuronal changes. However, lowering blood pressure in affected patients in order to retard hemorrhage and edema formation is not indicated, since ischemic changes in the white matter vasculature may occur in the presence of impaired autoregulation. Maintenance of normotensive ranges in blood pressure is probably optimal in the treatment of acute SCI.¹⁴⁰ Loss of autoregulation and regional end-capillary blood flow became passively dependent on systemic arterial pressure. Vasospasm, mediated through increased neurotransmitter accumulation (i.e., noradrenalin, dopamine, and serotonin), may further restrict blood flow and delivery of oxygen to an already ischemic environment.¹¹¹

Metabolic autoregulation

The mechanism that couples metabolic requirements of the spinal cord and blood flow may be related to accumulation of metabolites such as hydrogen, potassium, and adenosine. In the spinal cord, dilation and constriction of

pressure vessels are mediated by endothelial factors such as endothelium-derived relaxing factor or arginine-nitric oxide-cyclic guanosine monophosphate (cGMP) system and endothelin. There is still controversy about the predominant factor that is responsible for metabolic autoregulation.¹⁶⁶

Spinal cord perfusion pressure is also sensitive to changes in arterial partial pressure of carbon dioxide ($p\text{CO}_2$), displaying marked increases during hypercapnia and reductions during hypocapnia.¹⁶⁶ Spinal cord vasculature responds in a similar manner to cerebral circulation when there are changes in $p\text{CO}_2$, $p\text{O}_2$, and MAP.¹¹¹ In conditions of high levels of CO_2 (>35 mmHg) in arterial blood of the spinal cord parenchyma, there is an increase in spinal cord blood flow. The mechanism of producing arterial vasodilatation implicates formation of carbonic acid from carbon dioxide and the later dissociation of the acid generates H^+ ions. Hydrogen ions are among vasodilator agents of the spinal cord vessels. Other acidic metabolic substances such as lactic acid and pyruvic acid are also shown to increase spinal cord blood flow. Nitric oxide (NO), especially from neural origin, is also considered a mediator of CO_2 -induced vasodilatation.

Oxygen deficiency, manifested by $p\text{O}_2$ values below 60 mmHg (normal value 80-100 mm Hg), is also responsible for a rapid increase in spinal cord blood flow.¹⁷⁴ However, oxygen tensions greater than 60 mm Hg do not change spinal cord blood flow significantly. Mechanisms that produce vasodilation during

hypoxia are unclear but, chemoreceptors in the spinal cord that induce a neurogenic response are believed to be involved.

1.4.3 Cushing reflex

The Cushing reflex or response, is a powerful mechanism that regulates arterial pressure in order to maintain cerebral perfusion.^{161,175} If cerebral perfusion is reduced enough to cause ischemia of neurons of the medulla, an increase in systemic vasomotor tone (from nerves cells of the medullary vasomotor center) increases arterial blood pressure and therefore cerebral perfusion pressure.¹⁶⁶ The Cushing reflex appears after a latent period of 20-30 seconds after initiation of the stimulus.¹⁷⁵ This suggests that either a reduction in local O₂ or metabolic fuel supply; or an increase in local pCO₂ or H⁺ ion activity are responsible.¹⁶¹ The rise of MAP during the Cushing reflex is mediated by α -adrenergic vasoconstriction and β -cardiac stimulation.¹⁷⁵ Increase in MAP activates baroreceptors, causing a reflex bradycardia. This response is selective and preserves brain and heart blood flow at expense of other tissues.

1.4.4 Monro-Kellie hypothesis and cerebrospinal fluid pressure

The Monro-Kellie hypothesis states that, with an intact skull, the sum of the volume of the brain, plus CSF volume, plus intracranial blood volume is constant.¹⁰⁶ This hypothesis has also been applied to the vertebral canal. The spinal cord is confined in a slightly elastic bony and fibrous channel, the vertebral

canal. The canal contains the spinal cord, cerebrospinal fluid, fatty areolar tissue and the internal vertebral venous plexus. Therefore, a mild degree of dural collapse in response to CSF volume depletion can occur and is compensated by engorgement of the internal vertebral venous plexus.¹⁰⁶ An increase in one volume must be accompanied by a decrease in another to minimize any increase in the pressure within the vertebral canal.¹⁰⁶ This may be a compensatory mechanism for intracranial and intraspinal compliance. The purpose of this compensatory mechanism is to maintain normal intracranial or intraspinal pressures.¹⁷⁶

1.4.5 Respiratory complications

Two respiratory complications may occur in patients with cervical spinal disorders. Some patients experience ventilatory failure associated with a physical inability to move sufficient amounts of air into the lungs secondary to paralysis or paresis of the respiratory musculature.¹⁷⁷ In these animals, parenchymal lung disease is usually absent or mild, pulmonary gas exchange function is normal, and hypoxia is caused by hypoventilation. The severity of hypoventilation is determined by measuring the arterial partial pressure of carbon dioxide (pCO₂). Alternatively, some patients may ventilate normally, but because of lung disease such as pneumonia, atelectasis, hemorrhage, or edema, they have abnormal pulmonary gas exchange and hypoxia caused by ventilation-perfusion mismatch or pulmonary shunting. Complications involving the pleura and thromboembolism

can also be present in patients with SCI.¹⁷⁸ Also, airway hyper-responsiveness subsequent to loss of sympathetic innervation to the airway can be present. Airway hyper-responsiveness associated with cervical SCI is attributed to unopposed parasympathetic tone and subsequent cholinergic bronchoconstrictor activity.¹⁷⁹ Respiratory compromise is also a potential sequela with acute or chronic atlantoaxial subluxation.¹⁷⁹ A recent retrospective study showed that approximately 5% of dogs with cervical spinal cord disorders may need ventilatory support perioperatively.¹⁷⁷ Studies in human beings have shown that respiratory complications occurred in 62% of patients with acute cervical SCI, with the amount of compromise being associated with the severity of the injury.¹⁸⁰

The mechanism of hypoventilation in dogs with cervical spinal cord disorders is not completely understood and is likely multifactorial. In human beings, possible causes include failure of the respiratory muscles (intercostals muscles, diaphragm) and failure of feedback mechanisms for sustaining ventilation. In dogs, neurons of the medullary respiratory center enter the spinal cord via the reticulospinal tracts and give rise to the phrenic nerve through segments C5 through C7 of the spinal cord (over cervical vertebral bodies 4 through 6). Spinal cord injury cranial to the phrenic nerve nuclei (located at the level or cranial to, the cervical intumescence) may interrupt all or part of descending respiratory drive to phrenic motor neurons. Injury at the level of the phrenic nerve nuclei can lead to damage of both descending respiratory axons and phrenic motor neurons.¹⁷⁹ Reticulospinal tracts also give rise to neurons that

innervate the intercostal muscles via the segmental intercostal nerves. The reticulospinal tract also has projections to both sides of the body and, as a result, clinical manifestations of autonomic motor dysfunction occur bilaterally even in dogs with unilateral lesions. Dogs with a SCI cephalad to the origin of the motor neurons for the muscles of respiration should be more likely to experience respiratory compromise than a more caudal spinal cord lesion. Factors that depress reticular formation activity (sleep, narcotics) could result in clinical manifestations of hypoventilation, as evidenced by increased PaCO₂ necessary to drive ventilation in such patients. Treatment of patients with respiratory compromise due to cervical SCI consists of removing the inciting cause and providing supportive ventilatory care.¹⁷⁹

1.4.6 Spinal shock

Spinal shock is a phenomenon that results from interruption of ascending and descending nerve fibers below the site of SCI, resulting in temporary flaccid paralysis of limbs with loss or depression of all or most spinal reflexes below the level of the injury.¹⁸¹ Impaired sympathetic outflow, in combination with unopposed action by the parasympathetic nervous system, may be present and result in hypotension and bradycardia.¹⁷⁷ Spinal shock is associated with respiratory failure in human beings; however, this phenomenon has yet to be well-documented in veterinary medicine, although it has been induced experimentally in animals.¹⁸²

It is believed that alteration in intrinsic spinal cord pathways is the mechanism of depression of spinal cord reflexes in human beings.¹⁸¹ In animals, the Schiff-Sherrington posture is a phenomenon characterized by flaccid hindlimb paralysis, and sometimes hyporeflexia of the hindlimbs due to lesions in the thoracolumbar spinal cord region. This neurologic condition is probably an example of spinal shock in animals.¹⁸³

1.5 IMAGING OF THE CERVICAL SPINAL REGION IN DOGS

1.5.1 Principles and technical considerations for imaging modalities used in evaluation of the canine cervical spine.

1.5.1.1 Radiology

The X-ray constitutes a type of electromagnetic radiation discovered during the 19th century that can be used for medical diagnostic imaging.^{184,185} X-rays are produced by collisional phenomenon or radiative interactions.¹⁸⁵ The X-rays are generated by interaction of high speed electrons that strike a metal target. For the creation of high speed electrons, an electronic current is generated and conducted toward a filament located in the X-ray tube. The amount of electrons generated is directly proportional to the applied electric current.¹⁸⁴ The electric current is regulated by mA (milliamperage) adjustments by an operator, using the control panel of the x-ray machine. The area where the filaments and the electrons are generated is termed the cathode. The area where electrons interact with the metal target is termed the anode. Stationary electrons produced at the cathode are directed to the anode by application of a voltage differential between the cathode and the anode.^{184,185} The difference in voltage is controlled by the kilovoltage peak (KVp). Large differences in voltage (high KVp) produce an increase in the acceleration of electrons toward to the anode and a subsequent increase in the energy that hits the metal target.¹⁸⁵ This results in improving efficiency of production of X-ray's.

The process of x-ray generation is at the expense of heat production. In order to minimize heat generated during the metal-electron interaction, targets are made of metals with a high melting point, such as tungsten. Use of a rotational anode also increases the heat dissipation capacity of the target metal.¹⁸⁴

The X-ray beam exits the tube, penetrates the patient and is differentially absorbed or transmitted by tissues within the patient.¹⁸⁴ This differential absorption is affected primarily by x-ray beam energy and tissue properties such as relative tissue density, thickness, and atomic number. Scatter radiation is also produced during tissue interactions but does not contribute to image production. Scatter radiation can be absorbed by a grid that is positioned between patient and film cassette. Since film emulsion is more sensitive to light photons than X-rays, it is more efficient to transform X-rays into light photons. For that purpose, intensifying screens convert X-rays into light photons and are used in conventional radiography. These intensifying screens are made of compounds (phosphorescent crystals) that fluoresce when they are struck by X-rays. According to their capacity of absorption of X-rays, physical density and effective atomic number, tissues are classified as radiolucent or radiopaque. Tissues or structures with low physical densities such as air or fat are considered radiolucent and appear black on the radiographs.¹⁸⁵ Tissues with high physical densities and high effective atomic number such as bone are considered radiopaque and are white on the radiographic film. Thus, there are 5 degrees of

radiopacity that can be perceived on a radiograph: air, fat, soft tissue, bone and metal.¹⁸⁵

In dogs, heavy sedation or general anesthesia is recommended to prevent movement and facilitate proper positioning.¹⁸⁶ Elements such as radiolucent sponges, tape, or gauze can assist in correct positioning and decreasing personnel x-ray exposure. Use of a small focal spot and large object-film distance (air gap) may be used to magnify smaller structures of interest. Areas of clinical concern should be centered in the x-ray beam in order to minimize geometric distortion and maximize spatial resolution.¹⁸⁷ Use of high milliamperage, moderate to low Kvp, and high-detail film and screens, are protocols that contribute to ideal film detail. Centering the beam directly over the area of interest and evaluation of several spinal segments are common radiographic techniques that improve examination of the spine.²⁰

Spinal survey radiographs should be performed after a complete clinical examination.¹⁸⁶ The clinical examination should indicate a tentative anatomic localization of the lesion and assessment of the most likely etiology. Interpretation of survey radiographs of the spine requires the radiologist to understand anatomy and function of all components of the axial skeleton.^{185,186}

Recommended radiographic views for the cervical region include; ventrodorsal, and lateral views.¹⁸⁵ Special views include the lateral stress view (dynamic radiography), with options of hyperextension or hyperflexion. Also, traction views and oblique views from the ventrodorsal position are

recommended.¹⁸⁸ The basilar view for the occipital condyles, lateral view with rotation of the head for the odontoid process, and open-mouth view for examining of the odontoid process are other recommended positions for evaluating the occipito-atlanto-axial region.¹⁸⁸ Important basic anatomic principles regarding the normal canine cervical spine are: the cervical segment is formed by 7 bones; the dorsal spinous process of C2 should be contiguous with, or overlap the dorsal arch of the atlas (C1);¹⁸⁵ the lateral views the cervical articular processes are positioned obliquely across and superimposed over the intervertebral foramina and vertebral canal; and the lamina of C6 vertebra is prominent and ventral to its transverse process. Number, alignment, size, shape and radiopacity are radiographic signs that should be considered in evaluation of the cervical spine.¹⁸⁵

1.5.1.2 Myelography

Myelography is an invasive radiographic technique that consists of injection of contrast medium into the spinal subarachnoid space.^{185,186} This technique should be considered if clinical signs and survey radiographs of the spine appear inconclusive. Cervical myelography is performed by injecting non-ionic iodinated isosmolar contrast medium into the cerebellomedullary cistern through the atlanto-occipital space. Iohexol and iopamidol are the most common contrast media used in small animal myelography. A 20 to 22 gauge, 1 to 1.5 inch short bevel spinal needle is adequate for cervical subarachnoid injection of

contrast medium. The patient, under general anesthesia, is placed in lateral or sternal recumbency. The head should be elevated to facilitate opacification of the cervical segments. The head and neck should be flexed to facilitate injection of contrast medium. The needle is inserted percutaneously on the dorsal midline of the neck at its intersection with an imaginary line traced at the cranial limits of the wings of the atlas. The needle should be directed slightly cranial. Entry of the needle into the dorsal subarachnoid space is recognized by a characteristic popping noise made by the friction when the needle penetrates the dorsal atlanto-occipital membrane. Removal of the stylet is followed by a drip or steady flow of CSF unless low CSF pressure is encountered, in which case gentle aspiration may be required. Hemorrhagic CSF or blood indicates the needle has deviated lateral to the midline and entered the internal vertebral venous plexus.¹⁸⁶ A volume of CSF equal to the intended dose of contrast agent may be removed if cranial hypertension is not present. If cranial hypertension is present aspiration should not be performed as this may increase the risk of brainstem herniation. The dose of contrast medium is approximately 0.3 ml/kg. Injection of contrast medium should be made slowly to avoid increasing CSF volume and thus increasing intracranial pressure. One should expect little resistance during injection. The total volume for injection is variable and depends on the area of the spinal cord to be visualized and operator experience.^{185,186} The normal myelogram is characterized by sharply margined, radiopaque, and thin columns of contrast medium within the subarachnoid space. In small sized dogs,

columns are thinner than large sized dogs since the former have relatively large spinal cords. Ventral epidural space is normally wide in the caudal cervical region giving a false impression of dorsal spinal cord displacement. The dorsal subarachnoid space is widest at the C1-C2 level and tends to be wider than the corresponding ventral subarachnoid space in the thoracolumbar region. Normal epidural soft tissue causes a filling defect in the ventral medium column at C1-C2 and should not be confused with an extradural lesion. However, smaller filling defects are often seen dorsal to cervical disks C3-C7 and are the result of hypertrophy of the ligamentum flavum or annulus fibrosus. An abnormal myelogram is characterized by changes in the size and location of the subarachnoid contrast medium columns, and the width and opacity of the spinal cord. Myelographic lesions can be grouped into the following patterns: extradural, intradural-extramedullary, intramedullary swelling, and intramedullary opacification.¹⁸⁵ The extradural pattern, in the lateral view, shows that subarachnoid contrast columns are displaced and thinner or absent in the area of compression. In the ventrodorsal view, the extradural pattern shows spinal cord swelling. In the intradural-extramedullary pattern the compressive mass is visible inside the subarachnoid space, causing dilatation of the columns cranially and caudally (golf tie sign). In intramedullary swelling, contrast columns are obliterated dorsally and ventrally on lateral and ventrodorsal myelographic views. Intramedullary opacifications are characterized by opacification of the spinal cord due to diffusion of contrast medium into the spinal cord parenchyma.

1.5.1.3 Computed tomography

Computed tomography (CT) is the process of production of cross sectional (transverse) images using X-rays and computer acquisition.¹⁸⁹ Formation of CT images by a CT machine or scanner involves 3 steps: data acquisition, image reconstruction, and image display.¹⁹⁰ The data acquisition (collection of data) from the patient is made using a conventional X-ray tube. This process includes the collection of x-ray transmission measurements from the patient. After X-rays pass through the patient they stimulate special detectors that measure transmission values or attenuation values of the tissues. This constitutes an indirect representation of the density of the tissues. The detectors can be scintillation crystals or xenon gas ionization chambers.¹⁹¹ The detector converts the x-ray photons into electrical or analog signals, which are converted into digital (numeric) data. During image reconstruction, the computer uses special mathematical techniques to reconstruct CT images in a finite number of steps called reconstruction algorithms (or reconstructions techniques). Simple back projection, iterative methods, and analytical methods are the algorithms most frequently used.

The computer automatically evaluates and manipulates digital data before image display. The final image (image display) is made up of numerous rows and columns of picture elements (pixels) each representing a small block of tissue (volume element or voxel). The computer assigns a number to each pixel that represents the linear attenuation coefficient and thus the density of the tissue

in the voxel. The tissue in each voxel or the linear attenuation coefficient for that tissue in each voxel is determined by making multiple projections through the same voxel. This is accomplished as the tube circles the patient and data is collected from angles around the patient.¹⁸⁹ Linear attenuation is expressed in CT numbers or Hounsfield units (HU). The CT numbers are assigned to the different tissues, their values run from +1000 to -1000. The range of displayed CT numbers is termed the Hounsfield scale. In this scale, water is set at 0 HU, cortical bone +1000 HU, and air -1000 HU. Other tissues are assigned Hounsfield units according to their densities relative to these tissues. Computed tomography has a superior contrast resolution than conventional x-ray techniques.^{187,189}

Computed tomography scanners were initially classified in generations, according with technologic advances in x-ray tube movement and detector design.^{187,189,192} For instance, third generation scanners are constructed in a way that the x-ray tube and arc of detectors rotate together around the patient for each slice. Fourth generation scanners have an x-ray tube that rotates around a stationary ring of detectors. In spiral (helical) CT, the table moves continuously while the x-ray tube rotates around the patient. This allows acquisition of all the volume data at one time. In some spiral scanners, slice thickness can be manipulated retrospectively if necessary. In spiral CT, the table speed can be adjusted to optimize scan protocols (collimator pitch). The lower the pitch (<1.0), the greater the number of samples are obtained per unit of tissue and the higher

the image resolution, but also higher radiation dose to the patient.¹⁸⁷ Pitch values greater than 1.0 yield some degree of partial scanning for the patients, but with the benefit of faster scan time, and fewer motion artifacts.

Multichannel CT scanners (MCCT) are the newest technique among helical scanners. They have a very fast image-acquisition phase. With MCCT (also called multislice CT, multidetector row CT, or multisection CT) the single row of detectors is replaced by multiple rows of detectors. These multiple rows of detectors allow registration of more than one image per gantry rotation. A four-channel detector (detector row is equipped with the capacity to collect four simultaneous images of information during each gantry rotation) compared with a single channel scanner, has a four fold capacity to register slices during each gantry rotation. If the number of simultaneous registered channels is increased to 8 or 16 by adding more electronics to the detector system, the capacity to register images increases similarly. Total body scanning for human patients can be reduced to less than 30 seconds. Multichannel CT allows scans with submillimeter section thickness, which creates ultra high resolution images.¹⁹³

Technical parameters (kVp, mAs), slice thickness, slice interval, field of view, region of interest, angulation of the gantry, and the number of scans per slice are parameters controlled by the operator console. Digital information generated in the computer may be used to reformat data in a set of CT images in order to view structures in the sagittal, dorsal, or oblique planes. Post-processing

techniques also allow 3D reconstruction, selective color display, and morphometric analysis on CT images.¹⁸⁷

An optimal CT scanning protocol of the spine considers features such as the size of the animal, the image processing techniques used and the type of the possible lesion. In conventional CT, noise can be reduced using a relatively high mA with the major trade off being excessive tube heating.¹⁹⁴ Computed tomographic imaging of the spine should be performed with the slice orientation perpendicular to the vertebral canal or parallel to the intervertebral disk space to minimize distortion.^{187,194,195} For evaluation of small areas such as intervertebral disk spaces or articular facets, thin slices are selected to avoid partial volume averaging, with the disadvantages of reducing image quality because of increased noise. For evaluation of larger areas, like the vertebral bodies and paraspinal soft tissue, thicker slices are preferred to reduce noise and decrease the total number of slices.¹⁹⁴ Intrathecal and intravenous contrast agents are additional techniques used in CT spinal examinations. Spinal CT images are typically viewed with both bone and soft tissue window settings.¹⁹⁴

Computed tomographic examination of the spine allows a detailed evaluation of the vertebral osseous anatomy.¹⁹⁴ Cortical bone of the vertebrae is observed as thin and hyperdense (uniformly high density) with smooth margins. Cancellous bone has a porous (trabecular) appearance. The intervertebral foramina, basivertebral venous canal, and vertebral processes are components also visualized on CT examination of the spine.¹⁹⁴ Diarthrodial joints of the

vertebral column are described as having thin, smooth subchondral bone of the articular facets separated by a hypodense zone of synovial fluid and articular cartilage. Intervertebral disk and dorsal longitudinal ligaments are not consistently visualized. Margins of the dorsal annulus of the intervertebral disk and dorsal longitudinal ligament, and the ventral annulus and ventral longitudinal ligament are seen as linear or thin elliptical soft tissue densities. The interarcuate ligament appears at some disk spaces as curvilinear soft tissue opacity spanning the dorsal laminae and blending with joint capsules of the diarthroidal joints. The ventral, dorsal, interspinous, and intertransverse ligaments are not often identified. Epidural fat is seen as a hypoattenuating tissue surrounding and contrasting soft tissue opacities within the vertebral canal. The dural sac, consisting of the spinal cord, blood vessels, and meninges, appears as a round to oval uniform soft tissue opacity. Nerve roots are observed as circular or linear soft tissue opacity structures, that extend from the dural sac, traverse caudally, and then exit the intervertebral foramen.¹⁹⁴ Computed tomographic myelography is a more detailed evaluation of the dural sac and extradural abnormalities of the vertebral canal.¹⁹⁴

1.5.1.4 Magnetic resonance imaging

Magnetic resonance imaging (MRI) is a technique where images are produced by interaction of radiofrequency waves and hydrogen ions of tissue within a magnetic field. Hydrogen is the most abundant component of biological tissue and MRI uses properties of this atom for image production.¹⁸⁴

After positioning the patient inside the MRI gantry the protons of the tissue align with the magnetic field of the MRI unit. The alignment of the protons may be in the same direction as the magnetic field or the opposite.¹⁹⁶ Normally, a few more protons are aligned with the magnetic field, because this group has a slightly lower energy level. When protons are in alignment, the protons wobble similar to a spinning top. This movement is called precession. Protons precess with a constant rate determined by the Larmor frequency. This frequency is determined by the gyromagnetic properties of the atom and the strength of the magnetic field. The greater the strength of the magnetic field, the faster the precession. Application of a radiofrequency pulse induces rotation of the atoms from their initial stationary alignment position. Radiofrequency pulses are sent with the same frequency as the precessing protons, i.e., their Larmor frequency.¹⁹⁶ After discontinuation of the radiofrequency pulse the atoms realign with the main magnetic field. A weak energy signal (resonance) is released from tissues as the hydrogen atoms realign themselves to the main magnetic field. A receiver coil is located over the area of interest to detect waves or signals coming from tissues, which are later transmitted to a computer. The computer converts

those radiofrequency signals using Fourier software program, which generate digital data for the construction of the final image.

The most common magnetic pulse sequence used for MRI is the spin echo pulse sequence.¹⁸⁴ For this sequence, an initial pulse of 90° is used to rotate the atoms away from the longitudinal main magnetization field. After a defined period, a second pulse of 180° is applied to the tissue. There is a small period of time before the receiving coil measures a signal after application of the first 90° pulse. This delay time is referred to as echo time or TE. Typical TE times vary from 30 to 150 ms. The time between the two 90° pulses is the repetition time or TR. In most clinical spin echo pulse sequences the TR intervals vary between 500 ms (0.5 s) and 2000 to 3000 ms (2-3 s).. Contrast resolution in the image is controlled by modifying TR and TE variables. Different combinations of TR and TE produce images with different contrast in the same tissue due to exploitation of tissue properties such as proton density, T1 relaxation time and T2 relaxation time.¹⁸⁴

Tissues that have high intensity (hyperintense, white) on T1-weighted images include fat, gadolinium contrast medium, and proteinaceous fluid. Tissues that have low intensity (hypointense, black) on T1-weighted images include all other fluids, edema, air, bone, and fast-flowing blood. Proton-density weighted images are created using short TE and long TR intervals (e.g., 20 - 35 ms and 1500 - 2500 ms respectively). Fluid appears dark, fat appears white, and gray matter appears brighter than white matter. Hyperintense tissues on T2-

weighted images include fluid and edema. Hypointense tissues on T2-weighted images include soft tissue, air, bone, and fast-flowing blood.

Magnetic resonance imaging provides better anatomic assessment of the spinal cord and other soft tissues since contrast resolution is better than CT. The appearance of the normal vertebral column on MR images varies according with the image sequence. On spin echo T1W images, intervertebral disks are of nearly uniform medium signal intensity, slightly greater than that of the spinal cord. The spinal cord, nerve roots, and bone marrow are isointense and of slightly lesser signal intensity in comparison to the intervertebral disk. Epidural fat, due to its short T1 relaxation time, is hyperintense and provides excellent contrast with other vertebral canal structures. A low signal shell representing a chemical shift artifact and/or possibly CSF is observed surrounding the spinal cord, sharply contrasted by epidural fat. Cortical bone of the vertebral bodies appears as marked hypointense borders in all image sequences because of the lack of mobility of its H₂ protons. This shell is distinctly contrasted with the medium-signal bone marrow and the high signal paraspinal fat. Dorsal and ventral longitudinal ligaments and interarcuate ligaments are low signal and not distinguishable from adjacent cortical bone of the vertebrae. These ligaments are distinctly visible where separated from the bone over the intervertebral disk space and interarcuate foramen. The low-signal joint capsules and synovial fluid are not distinguishable from the low-signal cortical bone of the articular facets. On spin echo T2 images, normal intervertebral disks are characterized by a high-

signal central portion surrounded by an intermediate-signal outer portion. This finding is essentially the same as that seen in human intervertebral disks, which are anatomically and histologically similar.¹⁹⁷ This appearance is due to biochemical differences between the outer annulus, the inner annulus, and the nucleus pulposus. The inner annulus contains less collagen and a larger proportion of chondrocytes and ground substance. The nucleus is similar to the annulus in its ground substance content while having less organized collagen. Ground substance is composed of hyaluronic acid and glycosaminoglycans that, by virtue of a strong negative charge, attract and hold water.¹⁸ On T2 weighted images, epidural fat has an intermediate signal intensity, considerably lower than that seen on T1W images, and is well contrasted from lower signal spinal cord and nerve roots. Vertebral bone marrow is lower signal intensity than either fat or the spinal cord. Heavily T2W images show an area of high signal surrounding the spinal cord, creating a natural myelogram effect. As in T1 images, cortical bone, ligaments of the spine, and capsules of the diarthroidal joints are low signal intensity and cannot be delimited.¹⁹⁴

1.5.1.5 Vertebral intraosseous venography

Vertebral intraosseous venography is performed by injecting contrast medium into the marrow cavity of bony components (spinous processes, vertebral body, pedicles) of the vertebral column.¹⁹⁸ In the early 1960s, publications describing intraosseous venography in human beings began to appear on its use in human medicine. Most authors were satisfied with results of the technique saying that it compared favorably with myelography.^{199,200} However, others questioned the adequacy of the technique in diagnosis of herniated intervertebral disk lesions since the technique did not provide regular filling of the epidural veins. Technical problems also occurred due to thickness of the spinous process in some regions (cervical) or because of preferential filling of extradural veins.²⁰¹

Contrast media injected into the marrow cavity is cleared more rapidly than from muscles or soft tissue. The rapidity with which large quantities of fluids could be introduced into the marrow space and cleared reflected the capacity of venous outflow of the system. It was this property of the marrow circulation which made intraosseous venography practical.⁵²

In human beings, a spinous process located preferably one or two vertebral spaces inferior to the level of the suspected or radiographically evident pathologic condition is first identified.¹⁹⁸ After proper positioning and under aseptic technique, 1 to 2 ml of procaine 2% is injected into the skin, subcutaneous tissues and periosteum. A water-soluble contrast medium is

injected into the marrow cavity of the dorsal spine of either the fourth or fifth lumbar vertebra. A 16 gauge bone marrow needle with obturator in place is introduced by a rotary motion of the hand into the spinous process. The patient is positioned on an inflated bladder that occludes blood flow into the inferior vena cava. Radiographs are taken as the last 2 or 3 mls of contrast medium is being injected. Contrast medium is cleared quickly from the marrow cavity via the vertebral venous system. If a herniated disk is present, the filling of the vertebral sinuses is incomplete in the area of the compression.

If aseptic technique is used, intraosseous vertebral venography is a innocuous procedure.¹⁹⁸ If contrast medium spills into the epidural space or soft tissue, no complications have been observed. Also, no changes in subarachnoid pressure have been observed after injection of contrast medium.¹⁹⁸ Reported contraindications are infection in the area of injection or coagulation dyscrasia due to the contrast agent.¹⁹⁸ A reported complication was mild discomfort and pain of short duration after the procedure. Marrow cells, bone spicules, and fat have been reported to be embolized to pulmonary vessels during the course of intraosseous contrast studies.^{202,203} Other complications rarely reported are thrombophlebitis, thrombosis, and osteomyelitis.¹⁹⁸

Today, intraosseous venography in human beings is used sometimes as an ancillary technique to help physicians in percutaneous vertebroplasty techniques.^{204,205} Usually 3-5 ml of iohexol for venography are used during vertebroplasty and a biplane digital subtraction angiography unit at a frame rate

of 2 frames per second. The venographic study is helpful for assessing cannula location required for minimizing risk of cement leakage outside the vertebrae. The venographic technique allows easy identification of the junction between the basivertebral veins and the anterior vertebral venous plexus, giving the operator a reference point to observe during polymethylmethacrylate injection.²⁰⁴⁻²⁰⁷

Transosseous vertebral venography has been used in dogs for evaluating the lumbosacral area.^{49,200} This technique involves placement of a 1.6 gauge 7.6 cm needle with a grip handle. Others authors recommend a 15 cm long biopsy needle.⁶² In an anesthetized dog, the injection is made through the skin in a depression between the cranial margin of the sartorius muscle and abdominal wall muscles with extension of the hip joints. The needle is inserted through the skin and psoas muscle into the deepest part of this depression. The needle should be redirected if contraction of the quadriceps muscle occurs because this indicates impingement of the femoral nerve. Contact of the needle with the vertebral body is determined by palpating the concavity of the bone (ventral to the transverse process) or by using fluoroscopy or radiographs. Once the injection site is located, drilling of the vertebral body cortex is accomplished by rotating the needle 180°. When the cortex is penetrated, a decrease in resistance is felt. The needle should then be stabilized and resist lateral forces if placed correctly. The stylet is then removed. In order to facilitate injection of the contrast medium, flushing of the marrow cavity is made with heparinized saline solution using a 6 ml syringe. Blood from the marrow cavity is aspirated to determine

correct placement of the needle. Approximately 7-10 ml of contrast medium is slowly injected through the extension catheter attached to the needle. This extension tubing is used in order to minimize operator exposure to the primary x-ray beam. Radiographic exposures are made as the last ml of contrast medium is injected. This time of injection varies from 2 to 20 seconds.⁴⁹ The transosseous technique is preferred by some authors over catheterization of the veins because there is less filling of venous radicals peripheral to the spinal cord that can obscure the vertebral venous plexus.^{199,200}

Cervical venographic examination has been performed in dogs and other species by drilling the wing of the atlas and injecting the contrast material.⁶² Flushing with normal saline prior to injection is recommended. In cervical venography compression of the external jugular veins during the procedure is considered essential, otherwise contrast material drains into the external jugular veins and the vertebral venous plexus does not adequately opacify.

1.5.1.6 Epidural venography

Epidural venography (phlebography, sinus venography) is an indirect technique for investigating the intervertebral disk, vertebrae, spinal cord, and other neural elements by visualizing the vertebral venous plexus.⁵⁶ It is performed by selective intravenous injection of contrast medium that will allow opacification of the vertebral venous plexus. The principal indication for lumbar

epidural venography is to confirm the presence and location of a suspected disk herniation in a patient whose myelographic study is normal or equivocal.^{56,75}

Intraosseous vertebral injection of contrast medium has been recently replaced by selective and super-selective catheter venography.⁵⁶ Advantages of catheterization are that it is easy to perform, allows more consistent visualization of the veins, and causes fewer post-procedural complications.⁵⁶ The internal vertebral venous plexus of the lumbar spine can be opacified by catheterization and injection of contrast material into ascending lumbar, intervertebral or internal iliac veins.⁵⁶ The left femoral vein is often chosen since it is always present, and has an adequate size compared to the inconstant right ascending lumbar vein. Transfemoral catheterization of either the vertebral or anterior condyloid vein are used for cervicovertebral phlebography.^{201,208} In human beings, a 5, 6 or 7 French flexible tip, end hole catheter is utilized for transfemoral ascending lumbar catheterization.²⁰⁹ Originally bilateral catheterization of the ascending lumbar vein was performed but this was abandoned when it became apparent that even contralateral catheterization of the lumbar vein produced opacification of the vertebral venous plexus, bilaterally. Meglumine has been employed in human beings as contrast material. It is mixed with lidocaine hydrochloride to obtain a relatively painless injection. Contrast medium is injected at a rate of 4 to 8 ml/sec,²⁰⁹ with a total volume of 40 to 50 mls. Five to 10 radiographic films are taken over a period of 10 seconds. This permits evaluation of contrast progression and minimizes unpredictable flow inherent in venous systems. The

radiographic tube is tilted 15 degrees cranial to demonstrate the two inferior (caudal) intervertebral disk spaces. A lower abdominal compression device, similar to those used in intravenous urography, plus performance of the Valsalva maneuver, facilitates filling of epidural veins. This additional combination promotes a reverse venous flow from the external vertebral venous plexus to the epidural veins. The procedure is completed when all lumbar veins on the symptomatic side are visualized.⁵⁶ The procedure is usually performed in 30 minutes. Examination is usually well tolerated in patients, and patients who have had both venography and myelography frequently prefer the former. This procedure does not require heavy sedation or anesthesia of the intraosseous procedure and the injection site, the rate, and the amount of administered contrast agent are better controlled.²⁰⁹

The venographic signs that are consistent with a lumbar disk herniation are.^{56,75}

1. Unilateral or bilateral block of the anterior (ventral) internal vertebral veins as they cross an interspace.
2. Abnormal curvature of the anterior (ventral) internal vertebral veins.
3. Failure of visualization of the intervertebral veins (only with occlusion of the anterior (ventral) internal vertebral vein as well).
4. Demonstration of collateral circulation.
5. Excessive caudal flow of contrast agent.

6. Narrowed caliber of the anterior internal vertebral vein.
7. Localized dilatation or phlebectasia of an epidural vein.

In human beings, epidural venoraphy is shown to be more accurate than myelography in the diagnosis of far lateral disk herniation and of central disk herniation in cases having a large epidural space cranial to L5-S1, a short dural sac, or a very large dural sac.⁵⁶ Other conditions where epidural venography has been valuable in human beings are diskitis, lateral nerve root entrapment,²⁰¹ spinal stenosis,²¹⁰ spondylolithesis, epidural tumor (primary or secondary),²⁰¹ epidural venous malformation,⁵⁶ sacral neoplasms and post-operative patients.²⁰⁸

Opacification of the lumbar vertebral venous plexus via catheterization (phlebography, vertebral sinus venography) also has been reported in dogs.^{37,211,212} The procedures involve catheterization of the caudal vena cava, non selective injections of peripheral limb veins,^{37,211} or bilateral femoral vein catheterization. Catheterization of other veins such as the seventh lumbar vein, right cranial gluteal vein, right internal iliac vein, right common iliac vein and caudal vena cava has been shown to produce incomplete filling of the vertebral venous plexus. In general, these techniques do not appear to be practical for routine diagnostic use since they do not consistently outline the vertebral venous system in the lumbosacral-region. Catheterization via fluoroscopy of the median sacral vein provides a consistent filling of the epidural veins if temporary occlusion of the caudal vena cava is maintained during injection.²¹² This extra-

abdominal compression can be obtained in these cases by a Velcro belly-band placed over a radiolucent sponge, or by means of a wooden instrument.²⁰⁰

Repeatability and sensitivity were evaluated for myelography, vertebral venography and epidurography in 12 normal dogs; before and after experimental placement of silicone masses in the lumbosacral epidural spaces.²¹³ Technical repeatability was highest for epidurography (96%) and lowest for vertebral venography (42%). Diagnostic sensitivities (true positives/[true positive + false negative]) were low for all three procedures.

1.5.1.7 Digital subtraction epidural venogram (DSEV)

In human beings, use of digital subtraction instead of conventional film epidural venography is preferred for a number of reasons. DSEV allows more rapid examination; is less expensive because it requires less film and contrast material, and it is safer since radiation dose rates are lower.⁵⁶ Other advantages of DSEV are the ability to manipulate the image by changing the window level and width, changing pixel sizes, edge enhancement, and use of various filters. For DSEV the technique of catheter placement is precisely the same as that used for the conventional study and the same volume of contrast material is injected. However, a much lower concentration of contrast medium is used, namely, 15% rather than 76%, and the injections are, therefore less likely to cause pain. Gershater et al.,⁵⁶ indicated that results using DSEV for evaluation of

the vertebral venous plexus are similar to those produced by the conventional technique.

1.5.2 Imaging Characteristics of Common Diseases in the Cervical Spine of the Dog

1.5.2.1 Congenital anomalies

Most congenital anomalies of the spine in dogs are vertebral anomalies caused by disturbances during embryonic development.²¹⁴ The majority of vertebral anomalies are not clinically significant unless there is instability or deformity of the vertebral canal. The most frequently recognized vertebral anomalies in the cervical region of dogs are; spina bifida, block vertebrae and hemivertebrae.²¹⁴ Another malformation associated with the cervical spine is the Chiari malformation.¹⁷¹ This anomaly includes herniation of the caudal cerebellum and brainstem through an enlarged foramen magnum.

Spina bifida is a spinal developmental disorder characterized by defective closure of the two halves of the vertebral arch through which the spinal cord and meninges can protrude.³ Spina bifida is usually an incidental finding. However, if neurological signs are present the possibility of concomitant spinal cord malformation or herniation should be suspected (spina bifida manifesta, spina bifida aperta).²¹⁵ Among malformations of the dens, atlanto-axial luxation is one of the most commonly seen in miniature and toy breeds. Block vertebra is an anomalous spinal development in which two or more vertebrae are fused.³ Hemivertebrae are short and misshapen vertebra formed by normal bone tissue with smooth cortical margins.³ Although, apparently rare, hemivertebrae may be

associated with malformations of the neural tissue, for example, spinal dysraphism and spinal arachnoid cyst.^{185,216} Arnold-Chiari malformation is a congenital anomaly in which the cerebellum and medulla oblongata protrude caudally into the cervical vertebral canal through the foramen magnum. It is associated with syringohydromyelia, spina bifida, and hydrocephalus. Syringohydromyelia has been observed in other abnormalities such as Dandy-Walker syndrome, Chiari malformation and arachnoid cyst.¹⁷¹

1.5.2.1.1 Radiographic signs of congenital anomalies

Radiographic features of spina bifida include absence of fusion of the lamina or spinous process. End plates and intervertebral disk spaces are normal and no alteration in the vertebral angulation is observed.^{185,215,216}

Atlantoaxial luxation is demonstrated by an increased distance between the C1 lamina and C2 spinous process, with malalignment of C1 and C2 in lateral views.²¹⁶ In order to demonstrate the odontoid process clearly, a lateral oblique radiograph can be performed.¹⁸⁵ Dogs with odontoid process malformation can also show a malformed atlas (hypoplastic atlas) or occipital dysplasia.²¹⁶ Other dens-associated anomalies in dogs are abnormal (dorsal) angulation of the dens and absence of the transverse ligament of the atlas.²¹⁶

Congenital block vertebrae are usually incidental radiographic findings characterized by complete or partial fusion of two or more vertebral bodies, arches or spines. Other radiographic signs are absence or narrowing of the disk

space; decreased opacity (osteopenia) of endplates; absence of periosteal or reactive new bone; continuous trabecular pattern; focal scoliosis (caused by associated spinal angulation), and kyphosis or lordosis. The vertebral arch may be incorporated into the anomaly.^{185,215}

In radiographs, adjacent disk spaces of a hemivertebrae are usually normal but may be wider or narrower than normal.²¹⁶ Vertebral end plates are smooth and may have a normal thickness or be sclerotic. Sometimes the contiguous vertebra exhibits a compensatory shape. Vertebral osteophytes may be seen due to abnormal distribution of mechanical forces in the malformed area of the spine.

1.5.2.1.2 Myelographic signs of congenital anomalies

If hemivertebrae, block vertebrae, or spina bifida cause malalignment or spinal stenosis, myelography will reveal elevation of the ventral contrast column and thinning of both contrast columns indicative of a spinal compression.²¹⁶ Lateral cervical myelography in patients with dorsal angulation of the dens shows severe spinal cord compression dorsal to the dens and widening of the spinal cord at the C1-2 space.²¹⁷

In cases of Arnold-Chiari malformation, syringohydromyelia can be observed in the cranial cervical region as focal or linear accumulations of contrast medium within the spinal cord parenchyma or in the central canal (canalogram).²¹⁸

1.5.2.1.3 CT signs of congenital anomalies

Computed tomographic imaging can demonstrate the bone defects associated with vertebral malformations. Three dimensional reconstructions allow a better surface appearance of the vertebral column defect including spina bifida, hemivertebrae and others.²¹⁹

Bony lesions as small caudal fossa, narrow foramen magnum, and cranial vertebral stenosis are CT features observed in cases of Chiari syndrome of Cavalier King Charles Spaniels.¹⁷¹ Hydrocephalus can also be present. For better evaluation of this pathology, a recent method using CT morphometry was developed to quantify the absolute and relative size of the cerebral cavity and caudal fossa in dogs.²²⁰

1.5.2.1.4 MRI signs of congenital anomalies

If spinal cord anomalies (meningocele, myelomeningocele) or spinal cord compression are suspected with vertebral anomalies, MRI offers a better alternative than radiographs or CT for spinal imaging.²¹⁹

Magnetic resonance images also show the cavitory lesions in Chiari patients, and additionally this imaging modality can demonstrate fluid filled spinal cord lesions such as syringohydromyelia.¹⁷¹ In sagittal MRI images, the central canal of the cervical region appears dilated and can be contiguous with a dilated fourth ventricle rostrally.²²¹ Post-contrast T1W spin echo transverse plane

images show a thin rim of isointense spinal cord surrounding a hypointense dilated central canal.²²¹ Transverse T2W images demonstrate a central hyperintense circular area in the cervical spinal cord parenchyma also indicative of syringohydromyelia.¹⁷¹ Gliosis is commonly associated with syringohydromyelia in human beings and appears as areas of increased signal intensity surrounding the syrinx on T2W images.²²¹ Sagittal T2W images characteristics include rostral indentation of the caudal cerebellum by the occipital bone, obliteration of the dorsal subarachnoid space at the cervicomedullary junction, and hydrocephalus.¹⁷¹

1.5.2.2 Intervertebral disk disease

Intervertebral disk disease (IVD) is a syndrome characterized by pain and neurologic deficits resulting in displacement of part or all the nucleus pulposus of the intervertebral disk. A system of classification for IVD is called the Hansen classification.²²² Hansen type I is characterized by complete rupture of the annulus with an extrusion of the nucleus pulposus into the vertebral canal. Disk extrusion, prolapsed disk, disk explosion, and blown out disk are synonyms for Hansen type I disk disease. Hansen type II protrusions occur in nonchondrodystrophoid breeds usually as a feature of advancing age. These protrusions are the result of fibrinoid metaplasia and consist of partial rupture of the annulus fibers and bulging of the dorsal annulus. Disk protrusion or disk bulging are synonyms for Hansen type II disk protrusion.

1.5.2.2.1 Radiographic signs of intervertebral disk disease

Radiographic signs consistent with Hansen type I intervertebral disk disease include: narrowing of the disk space, narrowing of the intervertebral articular process joint space (collapse of articular facets), reduced intervertebral foramen, increased opacity in the intervertebral foramen, and extruded mineralized disk material within the cervical canal or superimposed over the intervertebral foramen.^{20,185} Survey radiographs indicate the presence of intervertebral disk disease but may lack accuracy in identifying the exact location of the extruded disk.^{20,185,215}

Width of the intervertebral disk is an important parameter to be evaluated on survey radiographs. Narrowing of the width of the disk space can be confirmed by noting a normal disk width in adjacent intervertebral disk spaces. In older dogs with Hansen type II disk disease, decreased width is a frequent finding since disks slowly degenerate. This finding is not a reliable radiographic sign of disk herniation and occurs in older dogs with or without the presence of vertebral osteophytes on adjacent vertebral end plates or sclerosis of the end plates.²¹⁵ Thus, a narrowed disk space with or without calcification in a young dog is more suggestive of an acute disk protrusion than is narrowing of the disk space in an older patient. A narrow disk space can also be associated with traumatic disk herniation or can be an early sign of diskitis.²¹⁵

The shape of the disk space can be a diagnostic aid. Usually adjacent vertebral endplates are parallel to each other, indicating the disk has the same width dorsally as ventrally. A Hansen type I disk herniation often appears to have a decrease in the width of the disk dorsally and the disk appears wedge-shaped. In young patients without presence of secondary changes associated with chronic disk degeneration, this wedging can be an important diagnostic finding on the radiograph.²¹⁵

Calcification within the nucleus pulposus follows chondroid metaplasia and is more extensive in some breeds than in others. The appearance of calcification of the nucleus pulposus may be seen better on the lateral projections and appears as a foggy, well defined density in the dorsal or ventral portion of the nucleus, ring shadow around the noncalcified center nucleus, or amorphous pattern of calcification. Associated with these features, sharp spikes of calcified tissue within the disk may extend dorsally toward the vertebral canal and suggest early nuclear herniation. Calcification of the disk can take many appearances and can be clinically insignificant when rupture or significant herniation has not occurred. Superimposition of the ribs heads may cause the disk space at C6-C7 to appear mineralized.¹⁸⁵

Following further degeneration of the disk, the calcified nucleus may be displaced dorsally and cause clinical signs.²¹⁵ Lateral and intraforaminal protrusions of the cervical disks may escape detection by standard, 90-degree orthogonal space projections. The ratio of the vertebral canal diameter to the

spinal cord diameter is greatest in the caudal cervical spinal canal region, which allows for greater capacity of spinal cord displacement secondary to extradural lesions.²⁰ Oblique radiographic projections (ventral 45-degree left-dorsal right or ventral 45-degree right dorsal left) allow assessment of the left and right intervertebral foramina, enabling identification of an opaque foramen.¹⁸⁵

1.5.2.2.2 Myelographic signs of the intervertebral disk disease

Abnormal myelographic patterns associated with disk extrusion or protrusion include extradural and intramedullary swelling and opacification. The most common myelographic pattern characterizing an intervertebral disk protrusion is the extradural pattern. Extradural lesions involve tissue outside the dura and displacement of the subarachnoid space. The subarachnoid space is partially or completely attenuated depending on the severity of compression. Ventrodorsal views frequently show widening of the spinal cord segment. Chronic Hansen type II, annular disk protrusion or gradual onset Hansen type I disk extrusion are most likely to show an extradural pattern.²⁰

Intramedullary patterns are commonly associated with acute extrusions (Hansen type I) and spinal cord edema. This pattern occurs over several vertebral segments and can obscure visualization of extradural lesions. Intramedullary lesions are characterized by widening of the spinal cord and deviation of the subarachnoid spaces away from the central canal on all radiographic views. In some instances, swelling may completely obliterate the

subarachnoid space.¹⁸⁵ The subarachnoid space is attenuated on all views. If an intramedullary pattern is present and there are no obvious extradural signs, careful examination of the myelogram may identify the site of disk protrusion. Slight axial deviation of the contrast medium column at the site of spinal cord swelling suggests the site of the extradural disk mass.¹⁸⁵ Hemorrhage from rupture of the internal vertebral venous plexus is a complication of acute disk disease and may cause an extradural lesion.¹⁸⁵ Evaluation of myelographic spinal cord swelling may assist in establishing a prognosis. Increased opacity of the spinal cord after injection of contrast medium indicates leakage of contrast medium into the spinal cord parenchyma, and possible myelomalacia.^{20,218}

1.5.2.2.3 CT signs of intervertebral disk disease

Noncontrast CT is able to adequately document the anatomy of the vertebrae and is capable of detecting herniation of mineralized intervertebral disk (Hansen type I).¹⁹⁴ Herniated mineralized disk material is clearly visible as a heterogeneous, hyperattenuating mass (mean attenuation: 219 ± 95 HU; range: 104-407) within the vertebral canal causing severe spinal cord compression. Sometimes, herniated material is not distinguishable and is only slightly more attenuating than spinal cord (mean attenuation: 59 ± 17 HU; range: 38-98 HU). Disk material can also extend over distances of up to 5 vertebrae.²²³ A heterogeneous appearance in the dural sac and lack of visualization of epidural fat are CT findings also associated with disk herniation. Sometimes the spinal

cord is outlined by a rim of increased attenuation cranial and caudal to the acutely herniated disk material. This is believed to represent blood in the epidural or subarachnoid space. At surgery these animals often have extensive epidural hemorrhage around the herniated disk material.²²³ Computed tomographic myelography is considered superior to conventional radiography and myelography for localizing asymmetric (foraminal or lateral disk extrusion) spinal cord compression and for surgical planning.^{20,194} Spinal cord swelling or atrophy, intervertebral foraminal changes and dural sac displacement are abnormalities detected accurately by CT myelography.²⁰ This imaging technique can be used postoperatively to assess effectiveness of spinal cord decompression, particularly when substantial spinal cord swelling is present.¹⁹⁴ Computed tomographic myelography is helpful in discriminating between primary intramedullary and extradural causes of spinal cord swelling and in definitively determining location of a herniated disk when conventional myelograms are equivocal.¹⁹⁴

1.5.2.2.4 MRI signs of intervertebral disk disease

Disk degeneration is best observed on sagittal T2W images as partial or complete loss of the normal high signal within the nucleus pulposus and inner annular portion of the disk.¹⁹⁴ These findings are related to the loss of hyaluronic acid and glycosaminoglycans from the disk and resultant dehydration.¹⁹⁴ Presence of normal signal within a disk on T2W images basically rules out disk

degeneration.¹⁹⁴ In addition a focal signal void can be identified within the vertebral canal and correspond to a free fragment of mineralized nucleus pulposus. Presence of extradural masses of low signal intensity near the mineralized disk material on the spin echo images are suggestive of recent hemorrhage or hematoma.²²⁴ This is specially true for T2W images, as other soft tissue masses such neoplasia are expected to be isointense or hyperintense in relation to the spinal cord.²²⁴ Recent hematomas (hours or days) typically appear hypointense on both T1W and T2W spin echo images until conversion of deoxyhemoglobin to methemoglobin.²²⁴ In sagittal images, intervertebral disk protrusion appears as varying degrees of dorsal displacement of the intervertebral disk into the vertebral canal, fragmentation and loss of normal ovoid shape of the disk, and dorsal and/or lateral deviation of adjacent epidural fat and nerve roots or spinal cord.¹⁹⁴ Sagittal images are valuable for localizing the side of a herniated disk. Sagittal and transverse images also show occlusion of the intervertebral foramen by laterally herniated disks as a loss of visualization of normal epidural and periradicular fat within the foramen. Transverse images are the most useful in evaluating the degree of narrowing of the vertebral canal by permitting visualization of the relative cross-sectional area of the vertebral canal occupied by herniated disk material, epidural fat, and proliferative bone or soft tissue structures. Spinal cord and nerve root compression can be assessed in both sagittal and transverse images as deviation of these structures and loss of visualization of epidural fat interposed between neural structures and spinal

canal. When examined on T2W images herniated portions of the disk may show higher signal than the parent disk, most likely related to increased water content or the formation of associated granulation tissue.¹⁹⁴ T1W postgadolinium contrast images help in differentiation of nerve root tumors from lateral disk herniation and differentiation of scar or granulation tissue from residual or recurrent disk herniation.¹⁹⁴

1.5.2.3 Cervical vertebral stenosis (CVS)

Cervical vertebral stenosis (wobbler's syndrome, cervical spondylopathy, cervical spondylomyelopathy, cervical vertebral instability, cervical vertebral malformation/malarticulation, cervical vertebral subluxation, cervical spondylolisthesis, cervical stenotic myelopathy, progressive caudal cervical spinal cord compression) is a compression of the caudal cervical spinal cord caused by cervical vertebral malformation-malarticulation or instability.²²⁵ It is caused by a combination of bone and soft tissue encroachment due to hypertrophy of the pedicles, lamina, and articular processes; the ligamenta flava, dorsal longitudinal ligament, and dorsal annulus fibrosus may also be hypertrophied or protruded. The etiology of CVS is not well understood, and nutritional factors have been associated in Great danes, as well as genetic and conformation factors in Doberman pinschers.²²⁶

1.5.2.3.1 Radiographic signs of CVS

Diagnosis of cervical vertebral stenosis (CVS) can be sometimes made from a non-contrast study that includes lateral, and VD views. Some animals with signs of CVS have normal plain radiographs.²²⁵ Radiographic changes of CVS may consist of: malalignment of cervical vertebrae, change in shape of the vertebral body, apparent loss of vertebral foramina creating a funnel shape to the vertebral canal, marked asymmetry of articular facets with secondary periarticular bone proliferation, sclerosis of vertebral endplates, vertebral osteophytes on the cranial ventral aspect of the vertebral body often appearing to be responding to a bony defect in this location, end plate sclerosis resulting from instability of the affected disk, and type II degeneration of the intervertebral disk including narrowing of the disk space and calcification of the nucleus pulposus.²¹⁵ Severe malalignment can appear as subluxation.²²⁵ Spondylosis deformans may be seen ventral to the intervertebral disk space, with associated changes in the opacity of the vertebral body.^{185,225} On correctly positioned radiographs the sagittal diameter of the canal can be measured and these dimensions can be used for assessment of cervical stenosis.²²⁵ In normal Dobermans pinschers, differences between the diameter of the cranial orifice and the caudal orifice is less than 2 mm, and in affected Dobermans pinschers differences are 3 mm or more.²²⁶ Canal:body ratios are also used for diagnosis of CVS. Vertebral canal diameter and vertebral body height of C6 ratio with values < 0.6 have been shown to be

significantly different in Doberman pinschers affected with cervical vertebral stenosis.²²⁷

1.5.2.3.2 Myelographic signs of CVS

Chronic changes including hypertrophy of the annulus fibrosus, ligamentum flavum, and joint capsule of the dorsal intervertebral articular process joint, cause circumferential compression of the spinal cord also known as an “hour glass” appearance sign.¹⁸⁵ A ventral extradural compression is suggestive of Hansen type II disk herniation or a misshapen cranial dorsal vertebral body. Dorsal extradural compression is indicative of ligamentum flavum hypertrophy or articular facet hypertrophy. In oblique VD views, dorsolateral extradural compression is suggestive of hypertrophied fibrous joint capsule of the articular facets. Annular extradural compression is indicative of impaired growth of the pedicles.^{215,225} If there is instability, the use of stress positioning demonstrates an increase in vertebral canal stenosis and cord compression when the neck is extended. Use of hyperflexed lateral projections demonstrates reduction in the degree of spinal cord compression. The VD view during myelography shows lateral compression associated with articular facets and hypertrophy of the adjoining soft tissue. Traction radiographs demonstrate whether the stenosis is dynamic or static. If dynamic, a soft tissue compressive mass (such as excess ligamentum flavum or annulus fibrosus) can be reduced by this type of

positioning.^{215,225} Traction must be applied with caution since this can worsen the lesion.²²⁶

1.5.2.3.3 CT signs of CVS

Non-contrast CT is adequate to document the shape and transverse diameter of the spinal canal as well as the anatomy of the vertebrae, and is capable of detecting severe canal stenosis.¹⁹⁴ Computed tomographic abnormalities include oblong to triangular shape of the vertebral canal, reduced interpedicular space, reduced dorsoventral diameter of the vertebral canal, dorsoventral flattening of the spinal cord, thinning of the ventral subarachnoid space, reduced epidural fat, dorsoventral elongation of the cranial and caudal cervical endplates, bulbous asymmetrical articular processes and decreased size of the cervical intumescence.^{194,228} A proposed system to classify appearance of CT myelographic images for human CVS has been used in veterinary patients.²²⁹ The classification is composed of 4 patterns being A; a central spinal cord deformity, B; unilateral spinal cord deformity; C; bilateral deformity of the spinal cord and D; spinal cord atrophy.²²⁹ Computed tomographic myelography in CVS provides more information than conventional myelography on the exact location and degree of spinal cord compression. In particular, it distinguishes spinal cord atrophy from reversible spinal cord compression where conventional myelography may fail to do so. Another advantage of this technique is that, because of the superior contrast definition of CT, CT myelography may provide a

diagnostic image when obstruction of contrast medium flow is encountered.²²⁹ However, CT myelography is an invasive procedure and does not show parenchymal spinal cord changes.²³⁰

1.5.2.3.4 MRI signs of CVS

MRI characteristics of CVS include decreased signal intensity from new bone formation, and increased signal intensity from edema, erosion, and bone defects. Spinal stenosis secondary to ligamentous hypertrophy is identified based on dorsal or ventral compression of the spinal cord by linear hypointense structures that correspond to thickened ligaments.²²¹ Major abnormalities on sagittal T1W and T2W images are dorsolateral compression of the spinal cord by hypointense soft tissue associated with articular processes and the interarcuate ligament.²³¹ Articular process hypertrophy and soft tissue proliferation can also be detected on parasagittal images. Transverse plane images are useful for evaluating the degree of spinal cord compression. On transverse T1W images, the hypointense interarcuate ligament or periarticular tissues decrease the amount of epidural fat and compress the spinal cord. On T2W images, soft tissue proliferation associated with the articular processes and interarcuate ligament is also hypointense but difficult to differentiate from the surrounding vertebral column. Dorsal T2W images of the cervical spine have been shown to be helpful in showing lateral compression of the spinal cord resulting from abnormal pedicle growth.²³² The degree of spinal cord compression can be

evaluated on T2W images as a loss of hyperintense CSF signal around the spinal cord, or a change in shape of the spinal cord from round to oval.²³¹ Spinal cord atrophy is indicated by a decrease in spinal cord diameter with preservation of fat and fluid signal around the cord.²³² Degeneration (dehydration) of the intervertebral disk is best evaluated in the sagittal plane as a loss of signal intensity in the nucleus pulposus on T2W spin echo images. Loss of epidural fat and deviation of the spinal cord can be seen on both sagittal T1W and T2W images.²³¹ Vertebral endplates adjacent to the degenerated disk can appear sclerotic (markedly hypointense). Focal areas of hyperintensity in the spinal cord can be indicative of edema, malacia, gliosis, or early syrinx/cyst formation.²²¹ The use of traction in MR imaging can assist in the diagnosis of dynamic cases of cervical spinal stenosis.²³³

1.5.2.4 Spinal neoplasia

Spinal neoplasia is defined as abnormal growth of tissue involving the spine. Spinal neoplasms can be benign or malignant, primary or secondary to other tissues.³ In dogs, osteosarcoma is the most frequent primary vertebral neoplasia, although sarcoma can be also present.¹⁸⁵ Secondary vertebral neoplasms include carcinoma and sarcoma. Osteosarcomas usually are located in one or more vertebrae and are more frequent in large dogs.¹⁸⁵ Lymphosarcoma is the most common soft tissue extradural tumors in dogs.²³⁴ In dogs, nerve sheath tumor (Schwannoma, neurofibroma) is one of the two most

common neoplasias in the intradural/extramedullary location.²³⁴ Meningiomas and hemangiomas are reported to occur with equal frequency as the second most common intradural extradural neoplasm. Myxoma and myxosarcoma have also been reported in this location.¹⁸⁵ Astrocytoma and ependymoma are the most common intramedullary tumors, but other histologic types include oligodendroglioma, undifferentiated sarcoma, choroid plexus papilloma and meningeal sarcoma. These tumors are more common in the cervical intumescence region (C6-T2).²³⁴

1.5.2.4.1 Radiographic signs of spinal neoplasia

Radiographic features of primary and secondary tumors of vertebrae include destructive lesions with cortical destruction, pathologic fractures, endplate destruction, and adjacent disk space collapse.²¹⁵ Others tumors have productive new bone as the major radiographic pattern, or have a mixed pattern of bony destruction and production. In primary and secondary neoplasms there is often alteration in shape of the vertebrae. In some cases, a paraspinal soft tissue mass can be present and mineralization of soft tissue can occur. Spinal neoplasia, contrary to diskospondylitis, does not typically present with endplate lysis cranial and caudal to the intervertebral disk simultaneously. In the cervical region enlargement of the intervertebral foramen is evident in cases where the foramen is occupied by nerve roots tumors such as meningiomas and neurofibromas.¹⁸⁵ Spinal cord neoplasms may increase the diameter of the

vertebral canal as a result of soft tissue expansion. Metastatic lesions are seen together with multiple lesions in the pelvis, sacrum or other vertebral regions.²¹⁵ Well defined focal regions of decreased bone opacity in the spine can be due to lymphoreticular neoplasia such as myeloma and lymphoma which are usually multiple. Single isolated radiolucent lesions may be due to primary or metastatic solid tumors.¹⁸⁵

1.5.2.4.2 Myelographic signs of spinal neoplasia

Vertebral tumors usually exhibit an extradural pattern that is not associated with the disk space. These can be multiple and associated with surrounding destructive or productive patterns in the bone.²¹⁵ Neoplasms usually presenting with an extradural pattern are osteosarcomas, fibrosarcomas, hemangiosarcomas, multiple myeloma and chondrosarcomas. Other metastatic tumors, including mammary carcinomas, perianal gland adenocarcinomas, transitional carcinomas, Sertoli cell carcinoma, thyroid carcinoma and pheochromocytoma can also produce an extradural mass effect. Intradural-extramedullary neoplasms include those outside the spinal cord but within the subarachnoid space. In this case, a typical pattern with filling defects in the subarachnoid space at the area of location of the tumor is observed. An intramedullary pattern can be observed with neoplasms within the spinal cord parenchyma and are predominantly glial in origin.²³⁴

1.5.2.4.3 CT signs of spinal neoplasia

The ability to detect and characterize primary and secondary osseous neoplasms using CT is excellent and exceeds that of plain radiographs. Computed tomography has particular value in detecting extension of the lesion, spinal cord involvement and soft tissue extension.¹⁹⁴ Computed tomography can be used for guiding biopsies of spinal lesions.²³⁵ Soft tissue neoplasms of the spine are often evaluated with intrathecal contrast medium to obtain a better evaluation of the relationship between the tumor and the spinal cord. Use of intravenous contrast medium with CT is also beneficial for assessing the nature and extension of tumors in the vertebral canal.^{194,236} Most of the brachial plexus and contributing nerve root masses enhance after intravenous contrast medium administration.¹⁹⁴ Enhancement of the brachial plexus tumors is often non-uniform with areas of decreased enhancement.²³⁶ Hypoattenuating areas are believed to be areas of necrosis. Significant atrophy of the shoulder muscles is a key sign in the clinical evaluation that justifies use of planar imaging of brachial plexus tumors.²³⁶ Although not all the neoplasms enhance, post-contrast CT helps delineate tumor extent and differentiation of solid versus cystic lesions.

1.5.2.4.4 MRI signs of spinal neoplasia

Primary and metastatic vertebral tumors in dogs present similar imaging characteristics to those observed in human patients.^{194,237} The most consistent findings are a hypointense signal from tumors on T1W images, and iso or

hyperintense appearance on T2W images. Malignant peripheral nerve sheath tumors present uniform contrast enhancement that helps distinguish the intradural component of the tumor from the spinal cord. Meningiomas in dogs present variable degrees of intensity after intravenous contrast medium, while meningiomas in human beings are reported to enhance intensely after Gd-DTPA administration.²³⁷ Determination of an intradural extramedullary pattern is reported to be difficult to observe on MR images.²³⁷ Images in which CSF has a high signal (MR myelogram, heavily T2W images) may be helpful for defining parts of the tumor that are intradural-extramedullary. Transverse images give detailed information on the relationship between the tumor and spinal cord, and determine the degree of spinal cord compression. Intramedullary tumors have a hyperintense signal on T2W images and often an isointense signal on T1W images. Administration of intravenous Gd-DTPA may result in contrast-enhancement, improving lesion detection, extent and differentiation from surrounding edema and gliosis.²³⁷ T2W transverse images provide the best definition of peritumor edema in the spinal cord. Absence of spinal cord compression from disk material helps in ruling out intervertebral disk disease. Post-contrast T1W images with fat suppression are also useful in helping distinguish tumor from surrounding fat.²³⁵ In human beings, MRI is found to have an accuracy rate of greater than 95% in detecting metastases when images are of good diagnostic quality.¹⁹⁴ In a recent retrospective study, 7 out of 24 dogs with brachial plexus tumors presented with initial or subsequent spread to the

vertebral canal or spinal cord.²³⁶ Brachial plexus tumors in dogs are usually well margined, ovoid to fusiform masses, isointense to hypointense on T1W, and isointense to hyperintense on T2W images. Additionally, post-contrast T1W images help to show the extension of the tumor along the nerves.²³⁶

1.5.2.5 Spinal infections

Spinal infection may include several infectious processes of the bony and soft tissue components of the vertebral canal.⁹⁷ Spondylitis is an osteomyelitis of the vertebrae. Diskospondylitis is a destructive, inflammatory, and proliferative process involving the intervertebral disk, associated endplates and vertebral bodies. Bacteremia is an important cause of spondylitis/diskospondylitis where venous drainage of the pelvic region may extend to the vertebral column with bacterial embolus via the vertebral venous system. *Brucella canis* is responsible for diskospondylitis due to bacteremia secondary to genital infection. *Staphylococcus intermedius*, *Staphylococcus aureus*, *Streptococcus sp*, *Escherichia coli* are other bacterial agents commonly isolated.^{97,185,215} In cases of secondary infectious processes with a hematogenous origin, noncontiguous vertebra are frequently involved. Primary sites of infection include the genitourinary system, skin, heart valves, and oral cavity. In cases of direct infection of the intervertebral disk or vertebrae; penetrating wounds, surgery and plant material migration are the most common causes involved. Some viral, fungal rickettsial and parasitic infections may produce meningomyelitis

(distemper virus, *Cryptococcus neoformans*, *Rickettsia rickettsii*, *Toxoplasma gondii*) or meningoencephalomyelitis (rabies virus, *Erlichia canis*, *Toxoplasma gondii*).^{171,214,238,239}

1.5.2.5.1 Radiographic signs of spinal infection

Since infection can reach the vertebrae or intervertebral disk by several different pathways, the radiographic appearance of the lesions varies widely. The radiographic appearance of infections following inhalation of plant material as a foreign body (paravertebral abscess) is not specific. Initially, fine periosteal new bone forms along the ventral aspect of the midportion of the affected vertebral bodies.²¹⁵ New bone continues to form, often reaching a thickness of one-half of the height of the vertebral body. At this point the inflammatory process can penetrate the vertebral body and it may be possible to identify underlying destructive changes within the vertebral body. If not treated, the combination of osteolysis and osteoproliferation can involve the lamina and articular processes.²¹⁵ The disk is usually not initially affected by the inflammatory process, but in chronic cases narrowing of the disk space followed by the appearance of small punctuate lucent foci within the normally dense vertebral endplates are indicative of disk involvement. Progression of the lesion can produce disk collapse, eventual end plate destruction and shortening of the vertebral bodies. Healing can occur during the evolution of the disease showing

smooth periosteal new bone formations on the vertebral body. If healing occurs late in the process a large callus forms around the destructive disk lesion.²¹⁵

The earliest radiographic sign of diskospondylitis is subtle irregularity of the vertebral end plates.⁹⁷ Common patterns are widening of the disk space and endplate destruction. Inflammatory lesions that first start in the vertebral body (spondylitis, vertebral osteomyelitis) are present as focal destructive lesions that later expand to the disk and vertebral endplates. Regardless of the origin of the lesion, advancement of infection usually leads to destruction (lysis) of vertebral end plates and adjacent trabecular bone. In later stages, there is also collapse of the disk space. Spondylosis may develop on adjacent ends of affected vertebrae.¹⁸⁵ Sequestration is often seen in subchondral bone adjacent to the disk. Periosteal new bone is not obvious early, and the lesion remains centered around the intervertebral disk until the later stages of the disease when involvement of adjacent vertebrae and new bone formation has occurred.²¹⁵ Healing may occur at any stage in this form of vertebral infection and results in a bony reaction that typically appears as bridging vertebral osteophytes. Healing is often associated with bony ankylosis across the disk space. Another vertebral infectious entity is vertebral physisitis. Initial signs consist of radiolucent widening of the caudal vertebral physis and lack of definition of the physeal margins.⁹⁷ Later radiographic signs include bone lysis, initially of the caudal physeal region of the affected vertebral body, with sparing of the vertebral end plates.⁹⁷

1.5.2.5.2 Myelographic signs of spinal infections

Epidural abscesses and granulomas often cause attenuation and dorsal deviation of the ventral contrast column over the affected disk space or vertebra consistent with an extradural pattern.⁹⁷ Chronic focal meningomyelitis may result in obstruction of CSF flow and blockage of contrast medium due to arachnoid adhesions.²¹⁴

1.5.2.5.3 CT signs of spinal infections

Early findings for spondylitis and discospondylitis detected with non-contrast CT include osteolysis, osteoproliferation, and intervertebral disk hypodensity.¹⁹⁴ In cases of discospondylitis transverse CT images show destruction of the end plate with irregularities or multiple hypoattenuating areas.⁹⁷ Alterations of the adjacent paravertebral soft tissue may include swelling and abscess formation. Computed tomographic myelography helps to demonstrate areas of compression of neural components caused by abscess, granulation tissue or bone impingement.⁹⁷ Computed tomography can also facilitate collection of biopsy samples in the affected region and post-treatment evaluations where increased opacity of the vertebrae and reduction of soft tissue swelling are seen.¹⁹⁴ A recent report of a cervical epidural empyema in a dog showed a soft tissue mass in the left dorsal aspect of the epidural space with loss of normal attenuating epidural fat.²⁴⁰ In human beings, contrast injection usually shows intense enhancement of the lesion and helps in evaluating the extension

of the process inside the vertebral canal.²⁴¹ However, CT is not specific and differential diagnosis between non-infectious or lesions produced by tumors may sometimes be extremely difficult. Intra-canal infectious lesions, such as epidural abscess and spinal cord lesions may be poorly detected on non-contrast CT. If available, MRI is preferred in those cases.²⁴¹ Reported CT findings for spinal epidural abscess include loss of the low attenuating epidural fat, poorly defined hypodense lesions in the paraspinal region, ring enhancement of the abscess and gas in the adjacent soft tissues.¹⁹⁴ Occasionally, CT images show a soft tissue density mass in the epidural space that corresponds to granulation tissue in the vertebral canal.⁷²

1.5.2.5.4 MRI signs of spinal infection

Magnetic resonance imaging is the diagnostic imaging procedure of choice in evaluation of spinal infections in human patients.^{97,241,242} Direct assessment of the disk space on sagittal images allows early diagnosis of endplate destruction.²⁴¹ This technique also allows evaluation of large areas of the spine on a single set of images and helps in determining the extent of infection.⁹⁷ The earliest response to vertebral osteomyelitis is accumulation of water in extracellular bone marrow, responsible for bone marrow edema.²⁴¹ This edema is easily detected as areas of decreased intensity (hypointense areas) and definition on T1W images and high signal intensity (hyperintense areas) on proton density or T2W images.^{97,194,241,242} Later, destruction of the vertebral end

plates can be appreciated with post gadolinium T1W images where there is often enhancement of the interface between the disk and end plate.⁹⁷ Enhancement also helps demonstrate presence and extent of epidural involvement.²⁴¹ Fat suppression techniques used with enhancement can improve contrast between hyperemic osseous tissue and soft tissue components and surrounding normal structures.²⁴¹ Abscesses usually demonstrate a ring enhancing pattern.^{194,241} Although, MR imaging is accurate in the diagnosis of vertebral infection, it does not differentiate between bacterial and fungal infections and does not eliminate the need for culture or biopsy.⁹⁷ Distribution of the lesion and signal intensity are essential MR parameters for differentiation between neoplasia and infection. In cases of neoplasia, involvement of the disk is rarely seen, but it is common in infectious processes.¹⁹⁴ Spinal lesions with involvement of two adjacent vertebrae and the intervertebral disk are more likely to be seen with spinal infection than neoplasia. Signal intensity in T2W images is usually more pronounced in infectious processes than with neoplastic diseases.¹⁹⁴

1.5.2.6 Fibrocartilaginous embolism (FCE)

Fibrocartilaginous embolism (fibrocartilaginous embolic myelopathy, ischemic myelopathy) is caused by an extrusion of degenerative intervertebral disk material into meningeal or intramedullary blood vessels, which results in ischemic myelopathy. A characteristic finding is the presence of fibrocartilage in the lumen of spinal cord arteries or veins, which cause ischemia or hemorrhage.

This disease usually affects nonchondrodystrophic dogs, mainly large and giant dogs, however small dogs (ie. Miniature Schnauzers) have been also affected.

1.5.2.6.1 Radiographic signs of FCE

Survey radiographs are generally non diagnostic for FCE. Occasionally mild collapse of an intervertebral disk space may be seen.²⁴³

1.5.2.6.2 Myelographic signs of FCE

Focal myelomalacia may be seen as accumulation of contrast medium in the spinal cord. More commonly in FCE cases the only convincing myelographic sign is spinal cord swelling.²¹⁸ Myelography is normal in more than 40% of confirmed cases of FCE, specially if myelography is performed 12-24 hrs post injury where spinal cord swelling has resolved.^{100,243}

1.5.2.6.3 CT signs of FCE

Computed tomography is not useful in identification of FCE but can help in excluding other causes of spinal cord damage.¹⁰⁰At our veterinary hospital, we have seen hypoattenuation of the spinal cord and areas of poor enhancement in CT images of dogs with FCE^c .

^c Dr Jeryl Jones, personal communication.

1.5.2.6.4 MRI signs of FCE

MR features of FCE include a focal hyperintense lesion on T2W and post-gadolinium T1W images suggestive of an intraparenchymal spinal ischemic lesion.^{100,194} These lesions are usually isointense on T1W images.¹⁹⁴

1.5.2.7 Spinal trauma

Several causes produce acute spinal cord trauma in dogs, and is commonly caused by automobile, fighting or falling injuries.¹⁷¹ External forces (ie. automobile) can produce spinal cord injury with or without evidence of vertebral instability. The pathophysiology associated with acute spinal trauma is similar to injury associated with head trauma, in that it also involves primary and secondary mechanisms. Another cause of trauma may include subluxation of the atlantoaxial joint. This can be caused by agenesis, fracture or fusion failure of the odontoid process or by rupture of the stabilizing ligaments (apical liagement of the axis, lateral ligaments of the axis, transverse ligaments of the axis).¹⁸⁵

1.5.2.7.1 Radiographic signs of spinal trauma

Radiographic features in spinal fracture-luxation complex include: disruption of the line indicating the floor of the vertebral canal, kyphosis, shortening of a vertebral body, separation of an end plate, fracture lines, vertebral displacement, canal stenosis, and disk space collapse. Ventrodorsal views can also show disruption in the line between adjacent spinous processes

or pedicles.²¹⁵ Horizontal beam techniques may be preferred to prevent unsafe manipulation of the vertebral column.¹⁸⁵ Separation of the odontoid process is a particular type of physeal fracture usually recognized by ventral displacement of the axis and marked narrowing of the vertebral canal. Use of a lateral view with the head flexed and a ventrodorsal open-mouth projection may clearly demonstrate the free fragment.²¹⁵ Sometimes, the centrum of the proatlas (ossification center) is not fused with centrum I of the axis and may appear as separate fracture fragment without causing dislocation.⁷ Caudodorsal displacement of the cranial portion of the lamina of C2 in relation with the lamina of C1 is suggestive of subluxation. Traumatic atlanto-occipital luxation is evaluated on lateral views where it shows rotation on the long axis of the atlas with one wing being more dorsal than the other.²⁴⁴ Ventrodorsal views show evidence of displacement of the atlas to the right or left with widening of one of the joint spaces.²⁴⁴

1.5.2.7.2 CT signs of spinal trauma

Computed tomography provides superior anatomic detail of multiple comminuted fractures of the pedicle, transverse process, lamina and spinous process.²¹⁹ Also, CT is useful in demonstrating fractures involving the dorsal compartment of the vertebrae, since this compartment cannot be adequately evaluated with plain radiographs.²¹⁹ Three-dimensional CT reconstruction is a useful procedure that displays the surface of the bony components of the

vertebral column with different degrees of rotation without superimposition of soft tissue.²⁴⁵ This post processing technique allows assessment of the extent of bony lesions (fractures) and helps to determine the level of spinal instability (luxation/subluxation). This methodology can be valuable as both a diagnostic aid as well as a surgical planning aid.²⁴⁵ In cases of traumatic atlanto-occipital luxation, CT (specially 3D reconstructed myelography images) has been shown to be an excellent diagnostic aid to exclude fractures not detected by conventional radiography and to demonstrate the spatial orientation of the luxation.^{244,246} Computed tomographic myelography can demonstrate the level of narrowing of the vertebral canal and corresponding lateral compression of the spinal cord.²⁴⁴ Information gained from CT can facilitate planning for closed reduction of atlanto-occipital luxation.²⁴⁴ Occasionally CT can demonstrate acute hematomas.²¹⁹

1.5.2.7.3 MRI signs of spinal trauma

Magnetic resonance imaging has the advantage of providing information regarding intramedullary spinal disease.²⁴⁶ Focal contusion, resulting in swelling of the spinal cord is seen as isointense or mildly hyperintense signal on T1W images. Hyperintensity of signal within the spinal cord on T1W images usually indicates hemorrhage of > 72 hours (see below).²¹⁹ On T2W sequences, both edema and ischemia or hemorrhage due to trauma have a hyperintense signal in the subacute settings.²¹⁹ Magnetic resonance imaging of the whole spine can

identify presence of multilevel injury (i.e. occult vertebral fractures) in human patients with more confidence than conventional radiographs.²⁴⁷ In a trauma patient with neurologic compromise, MRI is superior to CT in diagnosing presence and extension of an acute epidural mass, such as disk extrusion or epidural hematoma, compressing the cervical spinal cord. Distinction between spinal cord contusion, hemorrhage, or transection has an important prognostic value. In the acute stage (within the first 72 hours), a complex fibrin mass is formed consisting of red and white blood cells, platelets, and serum. The clot subsequently retracts with hemoconcentration, red blood cell deformation, and hemoglobin desaturation from oxyhemoglobin (diamagnetic) to deoxyhemoglobin (strongly paramagnetic). The acute clot is isointense with gray matter on T1-weighted sequences, and markedly hypointense on T2-weighted sequences. In the subacute phase (4 days to 4 weeks), denaturation of deoxyhemoglobin to methemoglobin (paramagnetic) occurs, with subsequent red blood cell lysis and release of methemoglobin into the extracellular space.²³⁰ In this stage, the hematoma gradually becomes uniformly hyperintense on T1W and T2W sequences but remains markedly hypointense on gradient echo images. In the chronic stage (months to years), the extracellular methemoglobin is surrounded by a vascularized wall of macrophages containing iron products such as ferritin and hemosiderin. The hematoma is replaced by fibrosis with iron-laden macrophages. During this time, the hematoma progressively changes from

hyperintense to hypointense on T1W and T2W images and remains markedly hypointense on gradient echo sequences.²³⁰

1.5.2.8 Arachnoid cysts

An arachnoid cyst (spinal subarachnoid cyst, arachnoid diverticulae, arachnoid pseudocyst, leptomeningeal cavitation)³ is a cyst of the pia and arachnoid membranes, containing cerebrospinal fluid. Many times, the cyst gradually causes increased pressure on nervous tissue and subsequent neurological signs.²⁴⁸ In dogs, cysts occur most often in the dorsal subarachnoid space between C1 to C3 and T11 to T13.²⁴⁸ The pathophysiology of this disease process is not well understood but congenital and acquired causes have been proposed.^{248,249}

1.5.2.8.1 Radiographic signs of arachnoid cysts

Survey radiographs may or may not contribute to the diagnosis of arachnoid cysts in animals.²⁵⁰ In human beings, erosion of the pedicles and widening of the vertebral canal are not uncommon.²⁵¹ A few cases in the veterinary literature have reported expansion of the vertebral canal associated with arachnoid cyst.²⁵² A recent study identified the presence of spina bifida on survey radiographs of one case of arachnoid cyst supporting the etiology of a congenital lesion.²⁴⁹

1.5.2.8.2 Myelographic signs of arachnoid cysts

Frequently it is possible to see bulbous dilation (focal accumulation of contrast medium) of the dorsal subarachnoid space with marked attenuation of the adjacent spinal cord in the lateral view.^{250,253} A dorsolateral extradural pattern has been reported.²⁵⁴ Opacification of the cyst is evident with image intensification immediately following completion of contrast medium injection. Sometimes there is a partial block to flow of contrast medium beyond the level of the cyst. Myelography can be non-diagnostic if the cysts do not fill with contrast medium. Sometimes, the cyst wall is not visualized and there is no central canal opacification.¹⁸⁵

1.5.2.8.3 CT signs of arachnoid cysts

Computed tomography can provide additional information to myelography by improving visualization of the limits of the cyst. Computed tomography allows accurate measurement of the degree of spinal cord compression. Changes in the spinal cord attenuation (hypoattenuating areas) seen on CT can be attributed to myelomalacia.²⁵⁰ Computed tomographic attenuation coefficients vary with the degree of communication of the cyst with the normal subarachnoid space and in some human beings the cyst has low attenuation values consistent with delayed or absent diffusion of contrast medium into them.²⁵⁰ An irregular and triangular shape of the spinal cord indicative of spinal atrophy has been noted in some dogs affected by arachnoid cysts.²⁵³

1.5.2.8.4 MRI signs of arachnoid cysts

On MRI images arachnoid cysts appear as focal, well circumscribed lesions that are isointense to CSF on both T1W and T2W images.¹⁹⁴ Sometimes cysts can be hyperintense on T2W images.²⁵³ Since the cyst contains fluid that is isointense to CSF it can be difficult to differentiate the cyst from the subarachnoid space.²⁵³ Associated thinning of the spinal cord may be present. This lesion does not enhance on T1W postcontrast studies. MR images can also detect syringohydromyelia sometimes associated with the cyst.^{249,250} One dog had a circumscribed T1 and T2 hypointense signal dorsal to the cyst and extradural to the spinal cord, which did not show gadolinium enhancement. This finding correlated with to postmortem histopathological finding of fibrosis of extradural connective tissue.²⁴⁹

1.5.2.9 Schmorl's nodes

Schmorl's nodes are caused by a defect of the vertebral endplate where the nucleus pulposus herniates into the vertebral body. They are also known as intravertebral disk herniation.^{3,255} Defects of the cartilaginous endplate may occur from any disorder that weakens the endplate itself, or subchondral bone of the vertebral body, allowing herniation of the disk material into the spongiosa.²⁵⁶ Defects can be caused by trauma or by a congenital defect of the vertebral endplates due to incomplete reabsorption of the notochord.²⁵⁶

1.5.2.9.1 Radiographic signs of Schmorl's nodes

Intravertebral disk herniations or Schmorl's nodes appear radiographically as spheroidal, radiolucent vertebral endplate defects with sclerotic borders.^{257,258} Vacuum phenomenon (vertebral osteonecrosis) may also be observed on radiographs in patients with Schmorl's node. Vacuum phenomenon is due to the accumulation of gas, mainly nitrogen, in fissures within the intervertebral disk or vertebral body.²⁵⁸ Schmorl's nodes are common in the lumbar region, although they are also seen in the thoracic and cervical region.²¹⁹ In human beings, only 5 to 35% of Schmorl's nodes can be detected by conventional radiography.²⁵⁹

1.5.2.9.2 Myelographic signs of Schmorl's nodes

Normally Schmorl's nodes do not show myelographic signs.²⁵⁶ However, if a herniation of the calcified nucleus pulposus occurs into the vertebral canal, it is possible to see an extradural myelographic pattern associated with the Schmorl's node.²⁵⁹

1.5.2.9.3 CT signs of Schmorl's nodes

On CT, a Schmorl's node appears as a sharply marginated sclerotic lesion with a central hypodense region located at the vertebral end plate.²¹⁹ Sagittal reformatted CT images can also show the extension of the intravertebral disk herniation.²¹⁹ Due to bone destruction, Schmorl's nodes can be confused with infectious and neoplastic processes on CT images.⁷² However, Schmorl's

nodes are located closer to the intervertebral disk than neoplastic lesions and are associated with more sclerosis than diskospondylitic lesions.

1.5.2.9.4 MRI signs of Schmorl's nodes

On MRI a Schmorl's node appears as a focus of isointense to slightly hyperintense signal surrounded by a margin of low signal intensity on T1W images and marked hypointensity on T2W images. The hypointensity is further accentuated in the GRE sequences. The disk space is usually narrowed with some loss of the normal disk signal in the T2W images.²¹⁹

CHAPTER 2:
COMPUTED TOMOGRAPHIC ANATOMY OF THE CANINE CERVICAL
VERTEBRAL VENOUS SYSTEM

Marcelo Gómez DVM,¹ Larry Freeman DVM MS,¹ Jeryl Jones DVM PhD
DACVR,² Otto Lanz DVM DACVS,² Pam Arnold.¹

From Departments of Biomedical Science and Pathobiology¹ and Small Animal
Clinical Sciences², Virginia-Maryland Regional College of Veterinary Medicine,
Virginia Polytechnic Institute & State University.

Published in: *Veterinary Radiology & Ultrasound*, Vol 41, No. 1, 2004, pp 29-37

2.1 Abstract

Computed tomographic (CT) venography of the cervical vertebral canal was performed in six, clinically normal, adult mixed-breed dogs from 14 to 23 kg. After dogs were euthanized and saline perfused, a gelatin and iohalamate mixture was injected into the right external jugular vein. Contiguous, 4 mm thick CT images were obtained with dogs in sternal recumbency. Dogs were kept in the same position as for the CT scan and frozen to approximately -8°C . All post-contrast CT images were analyzed using similar bone window and level settings. Additional multiplanar reformatted dorsal images were obtained in all dogs. The frozen cadavers were sectioned through the cervical region extending from the occiput to T1 at approximately 8 mm intervals. The frozen sections were then compared to the CT images. The CT appearance of the normal cervical vertebral venous system was described and illustrated. Components such as the internal vertebral venous plexus, interarcuate veins, intervertebral veins and vertebral veins were clearly identified on the CT images.

Key Words: vertebral venous plexus, computed tomography, cervical, dog, anatomy

2.2 Introduction

The canine vertebral venous system is composed of three intercommunicating networks: the external vertebral venous plexus (*plexus vertebralis externus ventralis* and *dorsalis*) that encloses the outer portion of the vertebral column, the internal vertebral venous plexus (*plexus vertebralis internus ventralis*) that surrounds the dura mater within the vertebral canal, and the basivertebral veins (*Vv. basivertebrales*) that extend through the vertebral bodies.⁵⁰ The vertebral venous system constitutes an alternative route for the return of blood from the body to the heart via anastomoses with the rostral systemic veins and the azygos vein. This, in effect bypasses the caval system.^{50,51} The veins drain blood from the vertebral column, adjacent epaxial and hypoaxial spinal musculature and the spinal cord.⁵¹ In addition to the normal drainage function, some authors have suggested that the venous plexus could be participating in the cooling mechanism of the spinal cord in a role similar to that of the cranial dural sinus for the brain.⁸⁶ The venous plexus also appears to play a critical role in postural hemodynamics.⁴⁸ In human beings positioned upright, the vertebral venous system represents the major outflow pathway for the cerebral venous blood.⁸³ The vertebral plexuses are in direct communication with the cranial venous sinuses and, since no valves exist in either, blood may flow cranially or caudally, depending on pressure relations.^{50,51}

The vertebral venous system also appears to be important in the etiology of some spinal disorders. Pelvic tumors may spread into the vertebral canal via

connections between the pelvic veins and the cranial sinuses via the vertebral venous plexus.³¹ Other spinal cord conditions related to the vertebral venous system include spontaneous spinal epidural hematoma,⁸⁷ congenital dilation of the cervical epidural venous plexus,²⁶⁰ arteriovenous malformations,¹⁰² and fibrocartilaginous embolism.¹⁰⁰ Congestion of the intra and intervertebral veins has also been proposed as a mechanism for development of epidural fibrosis²⁶¹ and intermittent claudication.²⁶²

In human beings, computed tomographic (CT) venography has been used to study the relationship between internal vertebral veins and disk herniation.^{68,263} In dogs, nonselective contrast-enhanced CT has been used to identify compressive soft tissues in the cervical²²⁹ and lumbosacral spine.²⁶⁴ Atlases of the normal CT anatomy of the canine spine have been published; however, little detailed information on the normal CT appearance of vertebral venous structures could be found.²⁶⁵⁻²⁶⁷ Also, to our knowledge, no information has been published on the use of selective CT venography to evaluate the normal vertebral venous system in dogs.

The purpose of this study was to develop a technique for selective venography of the cervical vertebral venous system and to describe the normal CT anatomy of venous structures in the canine cervical spine. This information may provide an important basis for future studies evaluating the role of the vertebral venous system in canine cervical spinal disease.

2.3 Material and Methods

Animals

Six, young-adult, mixed-breed dogs were used. All animals were clinically normal. The dogs weighed between 14 to 23 kg. The protocol used was in accordance with Virginia Tech Animal Care and Use Committee guidelines. The dogs were pre-medicated with acepromazine, (0.1 mg/kg, IV) and then injected with sodium pentobarbital (30 mg/kg) via cephalic vein until a surgical plane of anesthesia was achieved. To prevent clot formation, each dog was injected intravenously with 6000 IU of heparin. An incision of the skin at the right mid cervical region, ventral to the jugular groove, was performed to identify the right external jugular vein. Then after separating the fibers of the belly of the sternomastoideus muscle, the right common carotid artery was also identified. A flexible polyvinyl chloride cannula (outer and inner diameters, 6.35 mm x 3.18 mm, respectively) was inserted in the right common carotid artery and the dog was exsanguinated through this cannula.

Another cannula was inserted in the right external jugular vein and directed craniad toward its rostral bifurcation. To remove the residual venous blood, dogs were perfused via the right common carotid artery; using a 0.9% saline solution until clear fluid was seen coming from right external jugular vein cannula. The right common carotid artery, caudal end of the right external jugular vein, right internal jugular vein, left common carotid artery, left external jugular vein, and left internal jugular vein were ligated in order to facilitate the

symmetrical filling of the vertebral venous system with the contrast medium. The cannula in the right external jugular vein was kept in place, and a standard bore 4-way stopcock with rotating male luer lock adapter was added to the free end for further adaptation of a 60 cc plastic syringe containing the contrast medium.

Contrast medium solution

The contrast medium was made with 500 ml of boiling sterile saline solution (0.9%) mixed with 50 grams of granular gelatin^a and 25 cc of iothalamate.^{b,268} After cooling the solution, acrylic blue dye^c was added to assist visualization of the veins on anatomic slices. The solution was prepared in a glass beaker and gently agitated using a magnetic stirrer to obtain a homogeneous suspension. 5 mg of arabic gum^a were added to the solution prior to the injection. Approximately 200 cc of this solution was used in each animal.

CT scanning

All dogs were scanned using the same fourth generation CT scanner^d and protocol. Each animal was positioned in sternal recumbency on a positioning wooden board (approximately 65 cm wide and 137 cm long and 2 cm thick). The

^a Acros®, New Jersey

^b Conray 400®, Mallinckrodt Inc, St Louis.

^c Rowney Blue 119, Daler-Rowney, Bracknell, England.

^d Picker IQXtra, Picker Medical System, Cleveland, Ohio

dogs, with the positioned board, were then placed on the CT table. Lateral and ventrodorsal CT pilot images were used to make any adjustments needed to minimize slice plane obliquity. After final positioning, the dogs were taped to the positioning board to prevent further movement. The contrast medium was injected gently into the right external jugular vein catheter using a 60 cc syringe with Luer-Lock tip. Immediately after injection, 4 mm thick transverse images were obtained at 4 mm intervals from the external occipital protuberance to the spinous process of T1. Localizer lights in the CT gantry were used to guide placement of hypodermic needles into the skin, marking the anatomic locations of the most rostral and caudal CT slices. All the cadavers were scanned using similar bone window setting (Window Width: 1300-1753, Window Level: 300-466). Dorsal plane images were also generated from a reformatting workstation.

Anatomic sections

Cadavers were kept on the positioning board in the same position as that used for scanning and frozen at approximately -8° C. Specimens were cut beginning at the needle markers into approx. 8 mm thick transverse contiguous sections with a circular band saw. The cranial and caudal faces of each anatomic slice were later photographed using a digital camera^d. Structures visible in CT images were identified in the gross anatomic sections and then labeled. The

^d Olympus Camedia, 3,3 Megapixels

terminology used herein is in accordance with the *Nomina Anatomica Veterinaria*.¹

2.4. Results

Injection technique

Relatively consistent and symmetric filling of the majority of the cervical vertebral venous plexus vessels was obtained in all specimens with manual injection of contrast medium. In one animal, few air bubbles appeared as small sharply marginated filling defects in the lumen of the venous plexus. In the other 5 dogs, uniform opacification was obtained for the following vessels: internal vertebral venous plexus, interarcuate veins, intervertebral veins, and vertebral veins.

CT anatomy of cervical vertebral venous system

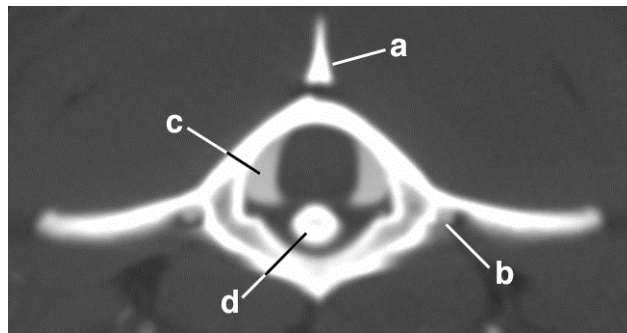
The junction of the vertebral venous plexus with the occipital sinus was visualized within the foramen magnum. At the level of the atlas, the continuation of the occipital veins appeared as two symmetrical, smoothly marginated, oval opacities. These vessels were positioned ventral to the dorsal arch of the atlas and dorsolateral to the dens of the axis (Fig 2.1). Plexus vessels covered the dorsal surface of the vertebral bodies and the medial surface of the pedicles for the entire length of the cervical vertebral column. In all dogs, the rest of the internal vertebral venous plexus at the mid vertebral body level was visualized

ventral to the spinal cord and in contact with the floor of the vertebral canal (Figs 2.3, 2.5, 2.7, 2.9, 2.11, 2.13). The imaging appearance of the internal vertebral venous plexus at the interspace levels consisted of two symmetric hyperattenuating ovoid structures, sharply margined, that diverged slightly from the ventral location (Figs. 2.4, 2.6, 2.8, 2.10, 2.12). That pattern was observed also in reformatted dorsal images of the cervical vertebral canal (Fig 2.14). A connection was seen between the plexus and the vertebral veins through the intervertebral foramen between the adjacent pedicles (Figs. 2.3, 2.5, 2.7, 2.9, 2.11, 2.13). Basivertebral veins were not visible in CT images, probably due to partial volume averaging with the bodies of the cervical vertebrae. Interarcuate branches arising from the dorsal surface of the plexus and coursing dorsad along the interior of the vertebral arch were observed at the intervertebral regions (Figs 2.4, 2.6, 2.8, 2.10).

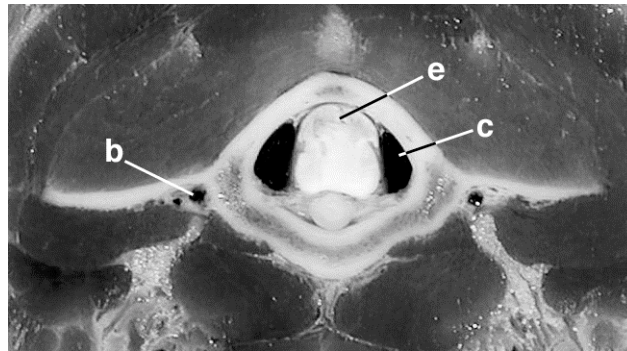
External vertebral venous plexus

The vertebral veins could be seen connecting with the veins of the hypoglossal canal. The vertebral veins appeared as round homogeneous, markedly enhanced structures of about 1.5 mm in diameter. They were visualized coursing caudally across the ventrolateral part of the atlanto-occipital joint and then ventral to the wing of the atlas and into the transverse foramen. The bilateral vertebral veins were seen from C1-C6 inside the transverse canal

(Figs 2.1, 2.2, 2.4-2.12). These veins connected with the intervertebral venous plexus via the intervertebral veins.

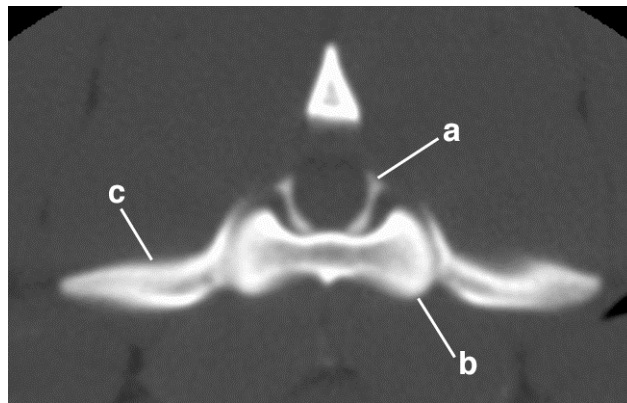


A

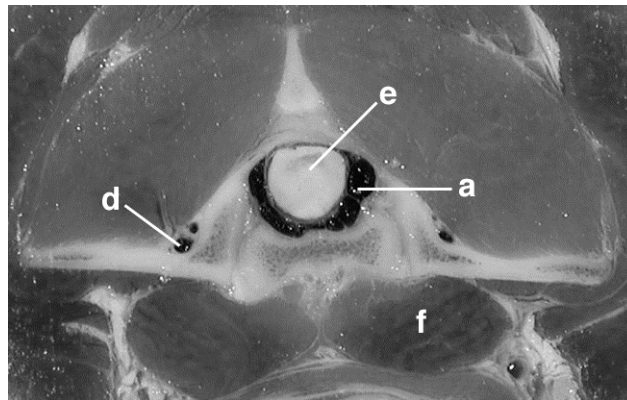


B

Figure 2.1 – Transverse, contrast-enhanced CT image (A) and anatomic section (B) through C1. Spinous process of the axis (a), vertebral vein (b), internal vertebral venous plexus (c), dens (d), spinal cord (e).

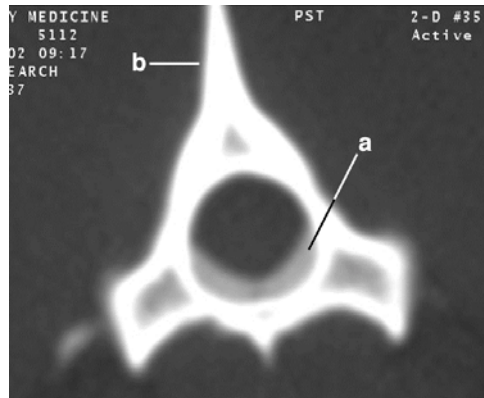


A

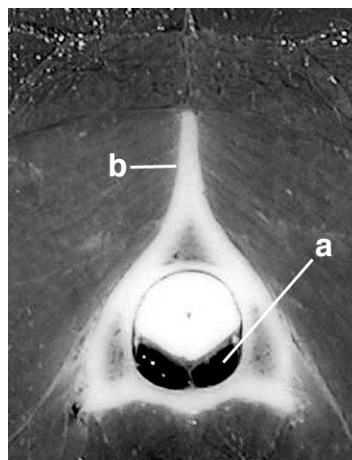


B

Figure 2.2 – Transverse, contrast-enhanced CT image (A) and anatomic section (B) through C1-C2. Internal vertebral venous plexus (a), cranial articular process of C2 (b), wing of C1 (c), vertebral vein (d), spinal cord (e), longus capitis muscle (f).

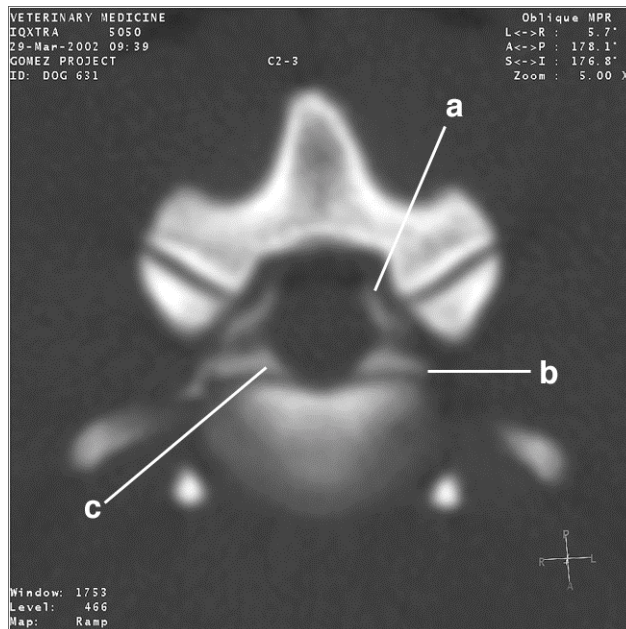


A

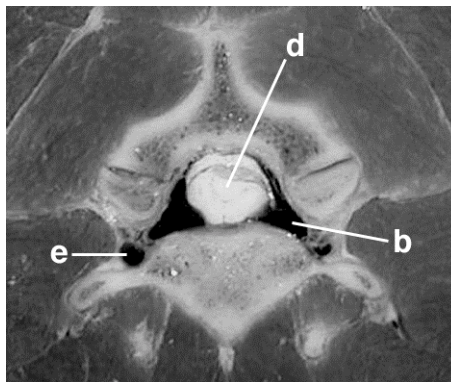


B

Figure 2.3 – Transverse, contrast-enhanced CT image (A) and anatomic section (B) through C2. Internal vertebral venous plexus (a), spinous process of C2 (b).

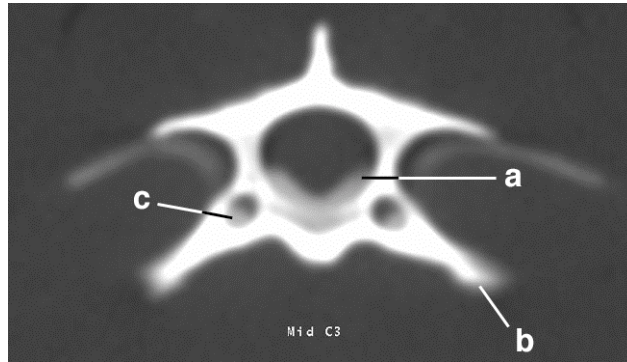


A

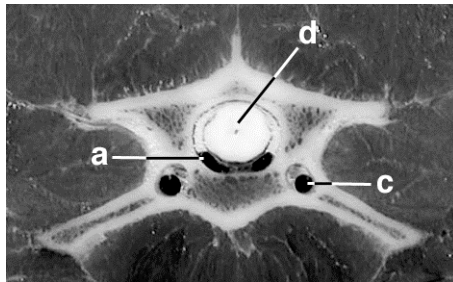


B

Figure 2.4 – Transverse, contrast-enhanced CT image (A) and anatomic section (B) through C2-3. Interarcual vein (a), intervertebral vein III (b), internal vertebral venous plexus (c), spinal cord (d), vertebral vein (e).

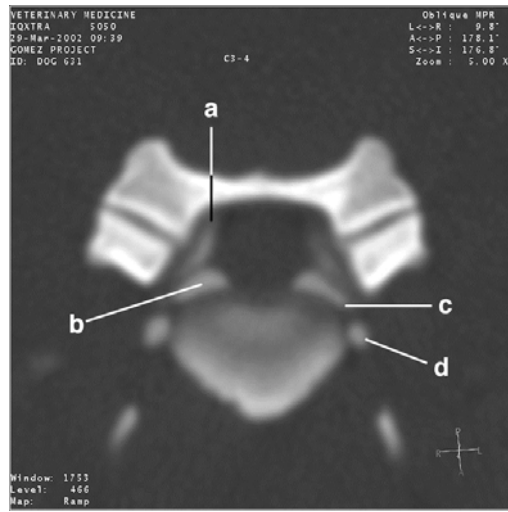


A

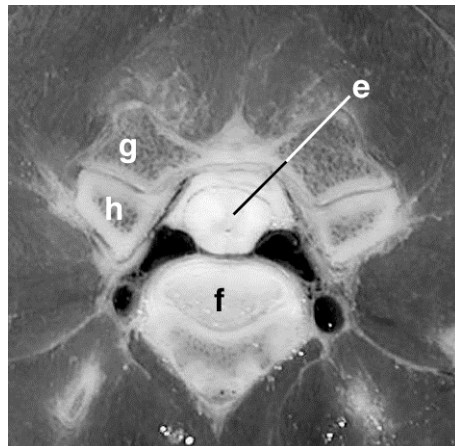


B

Figure 2.5 – Transverse, contrast-enhanced CT image (A) and anatomic section (B) through C3. Internal vertebral venous plexus (a), transverse process of C3 (b), vertebral vein (c), spinal cord (d).

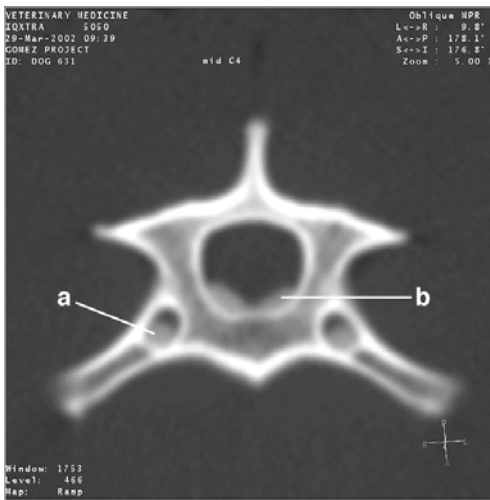


A

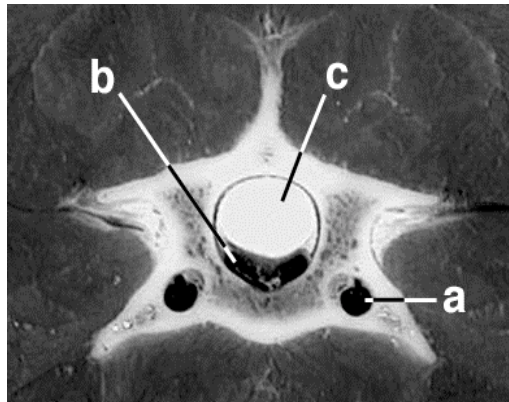


B

Figure 2.6 – Transverse, contrast-enhanced CT image (A) and anatomic section (B) through C3-4. Interarcual vein (a), internal vertebral venous plexus (b), intervertebral vein IV (c), vertebral vein (d), spinal cord (e), intervertebral disk (f), caudal articular process of C3 (g), cranial articular process of C4 (h)

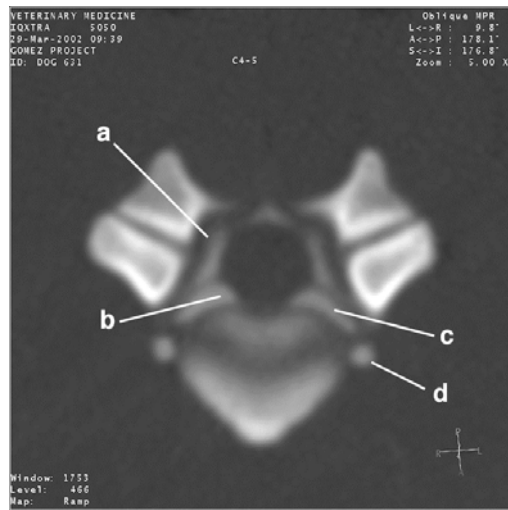


A

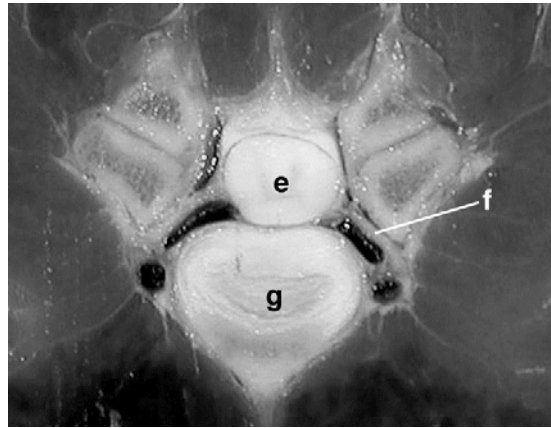


B

Figure 2.7 – Transverse, contrast-enhanced CT image (A) and anatomic section (B) through C4. Vertebral vein (a), internal vertebral venous plexus (b), spinal cord (c).

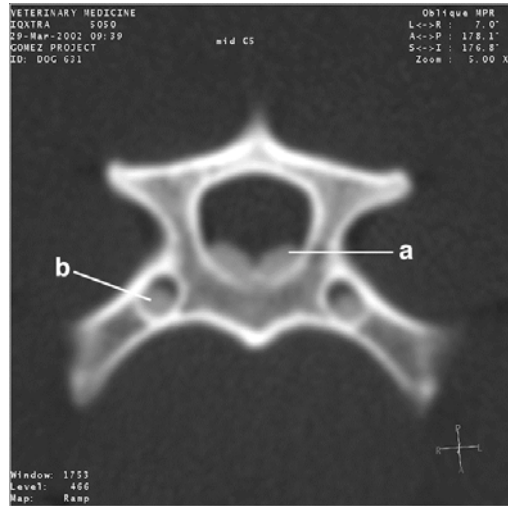


A

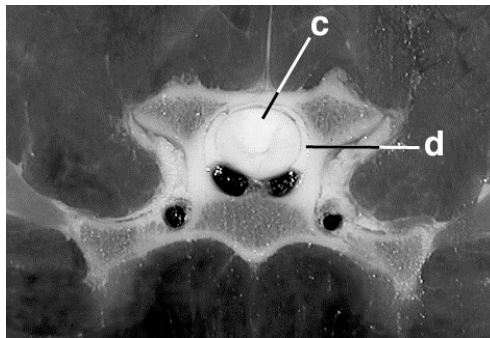


B

Figure 2.8 – Transverse, contrast-enhanced CT image (A) and anatomic section (B) through C4-C5. Interarcual vein (a), internal vertebral venous plexus (b), intervertebral vein V (c), vertebral vein (d), spinal cord (e), cranial spinal nerve VI (f), intervertebral disk (g).

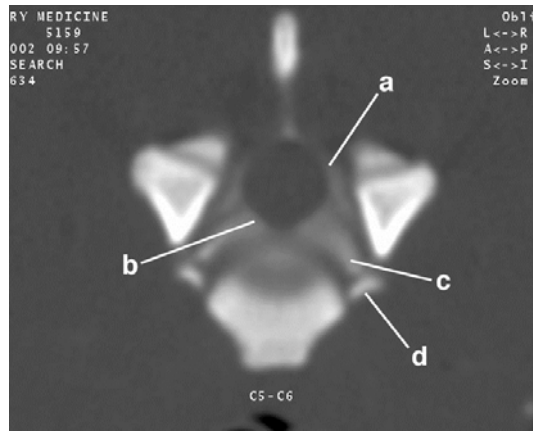


A

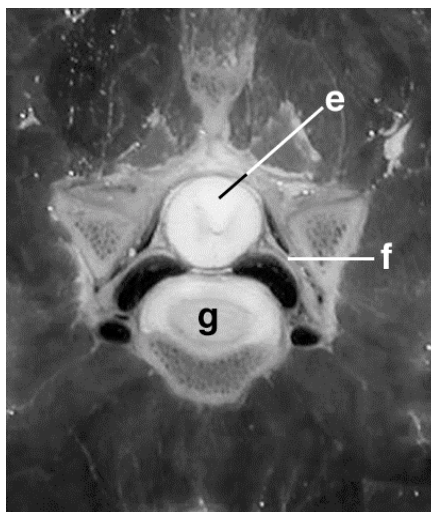


B

Figure 2.9 – Transverse, contrast-enhanced CT image (A) and anatomic section (B) through C5. Internal vertebral venous plexus (a), vertebral vein (b), spinal cord (c), epidural fat (d).

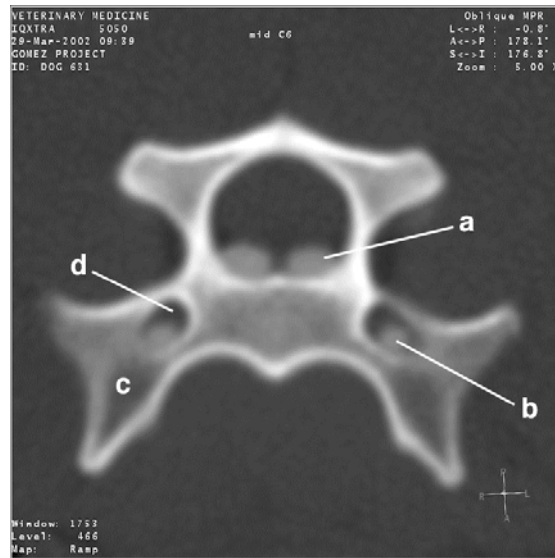


A

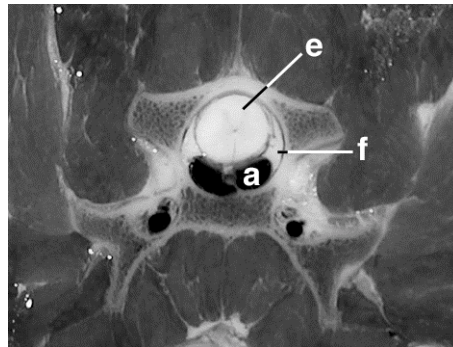


B

Figure 2.10 – Transverse, contrast-enhanced CT image (A) and anatomic section (B) through C5-C6. Interarcual vein (a), internal vertebral venous plexus (b), intervertebral vein VI (c), vertebral vein (d), spinal cord (e), cranial spinal nerve VI (f), intervertebral disk (g).

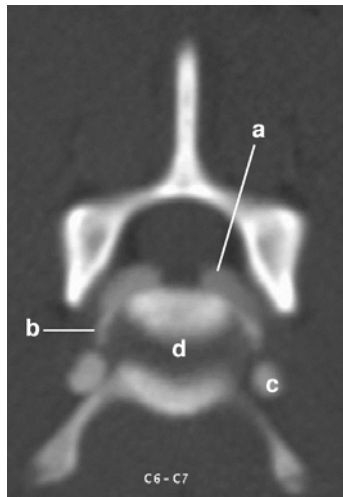


A

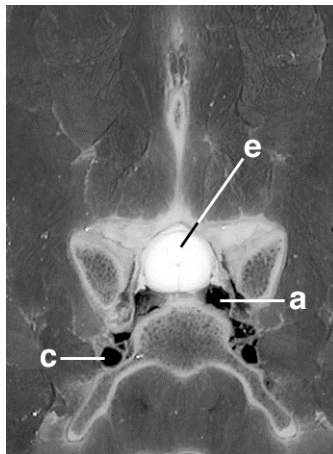


B

Figure 2.11 - Transverse contrast-enhanced CT image (A) and anatomic section (B) through C6. Internal vertebral venous plexus (a), vertebral vein (b), transverse process of C6 (c), transverse foramen (d), spinal cord (e), epidural fat (f).

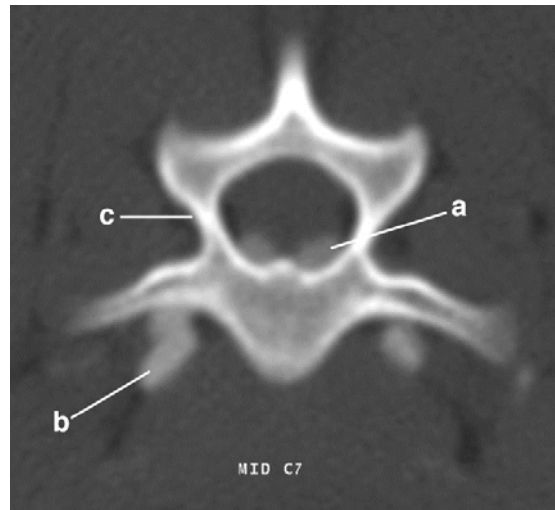


A

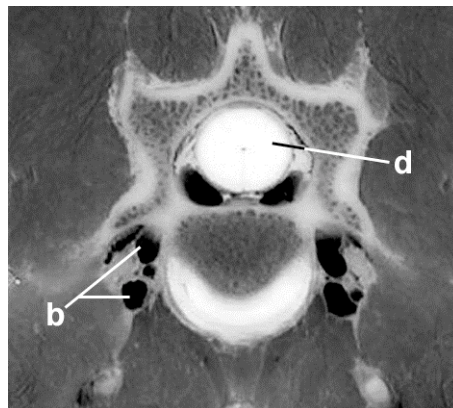


B

Figure 2.12 - Transverse contrast-enhanced CT image (A) and anatomic section (B) through C6-7. Internal vertebral venous plexus (a), intervertebral vein VII (b), vertebral vein (c), intervertebral disk (d), spinal cord (e).



A



B

Figure 2.13 – Transverse, contrast-enhanced CT image (A) and anatomic section (B) through C7. Internal vertebral venous plexus (a), vertebral vein (b), pedicle of C7 (c), spinal cord (d).

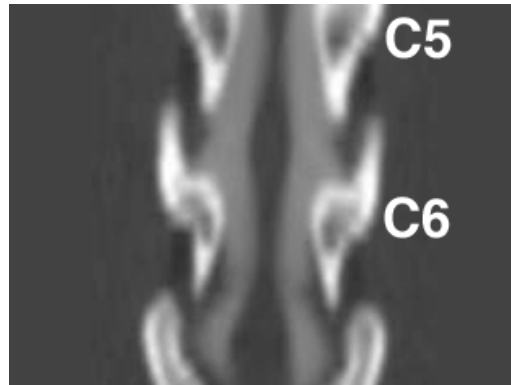


Figure 2.14 - Dorsal plane view of the C5-C7 vertebral canal. The ventral internal vertebral venous plexus is depicted as two, undulating, columns of contrast material on the ventral aspect of the vertebral canal, medial to the pedicles. Fifth cervical vertebra (C5), sixth cervical vertebra (C6).

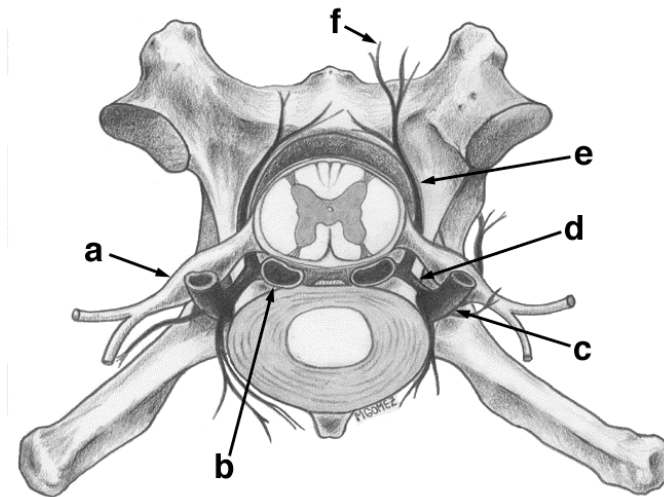


Figure 2.15 - Schematic illustration of the vertebral venous plexus. Spinal nerve (a), internal vertebral venous plexus (b), vertebral vein (c), intervertebral vein (d), interarcuate vein (e), muscular branches (f). (Drawing made by the first author).

2.5 Discussion

Epidural venography was once valuable in investigation of numerous spinal disorders.²⁶⁹ Injection of contrast medium into a spinous process of a lumbar vertebra in human cadavers resulted in opacification of parts of the vertebral venous plexus.²⁷⁰ By this technique, veins of the spine were visualized for the first time in a human living subject. Based on these investigations in human beings and working with dogs, transosseous vertebral venography was used to localize intervertebral disk lesions.¹⁹⁹ If a protruding or herniated intervertebral disk is present, the blood flow in these associated venous system should be occluded.¹⁹⁹ The venous system anatomy in dogs opacified by epidural venography using percutaneous transfemoral ascending lumbar catheterization, was later described.²¹²

In human beings, intravenous injection of iodine in CT studies allows visualization of lumbar and cervical epidural veins if certain conditions such as abdominal compression are used.²⁶³ Injection of the support agent araldite did not provide satisfactory CT or MRI studies of the internal vertebral venous plexus. A technique for injection of the vertebral venous plexus that allows anatomic, CT and MRI studies in human cadavers was developed.²⁷¹ Demonstration of the human vertebral venous plexus in these three types of investigation was obtained combining gelatin, gadolinium, and minium.²⁷¹ In the present study a good filling was obtained in the cervical internal vertebral venous plexus using gelatin and iothalamate.

In the present study, the venous system of all dogs was carefully perfused and flushed before injection of contrast medium. Quality of irrigation and injection has been stressed because of the potential clots or introduction of air that can interfere with the interpretation.^{73,271} For the route of injection in this study the right external jugular vein was used; however, other sites (the *angularis oculi* vein or the temporomandibular articular vein) may also be suitable for injecting these plexus vessels. Extensive communications exist and the non-valvular nature of the system facilitates complete filling.

Throughout the vertebral column the cervical internal vertebral venous plexus or epidural cervical veins are located inside the vertebral canal between the dura mater and the epidural space²⁷² (Fig 2.15). The plexus receives branches from the spinal cord, vertebral body, and extends from the foramen magnum through the fourth to sixth caudal vertebra.^{51,73} Plexus vessels are largest in the cervical region in dogs while in human beings the cervical plexus constitutes the smallest part.^{32,50} In the present study these longitudinal venous trunks appeared as symmetric, paired uniformly enhanced structures. Both channels deviated laterodorsally at the level of each intervertebral disk and converged medially at the midportion of the vertebral body, where they united with the basivertebral veins.^{32,50,51} Evidence of the dorsal internal vertebral venous plexus was the presence of interarcuate veins that joined the internal vertebral venous plexus at the vertebral arch. Numerous transverse connections exist between these two longitudinal networks in mammals, especially in the

cervical region.¹⁹ Within the arch of the atlas we observed that in all of the specimens the internal vertebral venous plexus was laterally positioned in relation to the spinal cord. The internal vertebral venous plexus communicates rostrally with the intracranial basilar venous plexus, which connects with the petrosal, cavernous and the occipital sinuses.⁵¹ The continuation of the internal vertebral venous plexus at the junction with the basilar sinuses often appeared ampullated.^{50,82} The vertebral veins were observed ventrally located inside the transverse channel of the vertebrae C1 through C6. These veins are part of the external vertebral venous plexus. They communicate with the internal vertebral venous plexus via the segmental intervertebral veins before they escape from the vertebral canal by passing through the intervertebral foramina with the spinal nerves.^{19,73} These connections through the intervertebral foramina form a plexus around the emerging spinal nerves, protecting them from injury.^{5,34,36}

In human beings, contrast-enhanced CT of epidural venous plexuses has been performed to evaluate intervertebral disk pathology in the lumbar spine²⁷³ and cervical nerve roots.²⁷⁴ Contrast-enhanced CT examinations of the vertebral venous system in the thoracic inlet also allow the study of important venous conditions in human patients.⁶⁹ Venographic CT studies in human patients with cervical spinal injury have also been used to demonstrate abnormal vertebral venous hemodynamics.²⁷⁵

The findings herein reported indicate that cervical spine CT venography is an effective technique for evaluating vertebral venous plexus anatomy in normal

dogs. This preliminary study provides reference normals that may assist interpretation of venous abnormalities in dogs with spinal diseases. An understanding of normal venous anatomy may also be helpful for precise surgical planning in the cervical region. Future studies are needed to develop a cervical spine CT venography technique for use in live dogs and to determine the effects of spinal cord compressive lesions on cervical venous structures.

CHAPTER 3

MORPHOMETRY OF THE VERTEBRAL VENOUS PLEXUS, VERTEBRAL CANAL, DURAL SAC, AND VERTEBRAL BODY IN THE NORMAL CANINE CERVICAL SPINE: EVALUATION USING NON-SELECTIVE CT VENOGRAPHY

Marcelo A. Gómez DVM,¹ Jeryl C. Jones DVM PhD DACVR,¹ Richard V. Broadstone DVM PhD DACVA,¹ Karen D. Inzana DVM PhD DACVIM,¹ Larry E. Freeman DVM MS.²

Departments of Small Animal Clinical Sciences¹ and Biomedical Sciences and Pathobiology,² Virginia-Maryland Regional College of Veterinary Medicine, Virginia Polytechnic Institute & State University.

Portions of this study were presented at the Experimental Biology Meeting, Washington D.C., April 17-21, 2004.

3.1 Abstract

The objectives of this study were to evaluate non-selective CT venography as a technique for quantifying the cervical vertebral venous plexus (IVVP) in dogs, define the normal diameter and area dimensions of the canine cervical IVVP, and determine the relationship between dimensions of the cervical IVVP and other vertebral components. Pre- and post-contrast helical CT scans were performed in 6 clinically normal dogs, from C1 to C7, using 3 mm thick slices, 2 mm intervals, and a pitch of 1.25. Post-contrast images were obtained immediately following a bolus intravenous injection of 480 mgI/kg iodinated contrast medium. A continuous infusion of an additional 240 mgI/kg was administered during scans. Image data from each dog were transferred to a CT workstation and measurements were performed on displayed transverse images using computer software for distance and area calculations. Diameter and area measurements of the vertebral canal, dural sac, IVVP and vertebral body were measured at the C3-C7 vertebral locations. Measurements were repeated three times by the same observer. Epidural space dimensions were calculated by subtracting dural sac dimensions from vertebral canal dimensions. Means for all dimensions were compared using Pearson correlation analysis. Significance was set at $r > 0.7$ and $p < 0.0001$.

Optimal opacification of vertebral venous structures was achieved in all dogs with no adverse reactions. Sagittal diameters of the IVVP for the C3 to C7 vertebral segments ranged from 0.6 mm to 3.2 mm. Transverse diameters

ranged from 2.32 mm to 5.74 mm. For all dogs and all vertebral segments, the mean transverse area for the IVVP was 13.38 mm² (6.69 mm² each for left and right components). The IVVP area represented 12.4% of the mean vertebral canal transverse area (107.9 mm²) and 30.61% of the mean cervical vertebral epidural space area (43.7 mm²). Vertebral venous plexus area represented almost 40% of the epidural space area at the C5 vertebral segment. At each vertebral location, no significant correlation was found between dimensions of the venous plexus and dimensions of other components. However, when all the segments (C3-C7) were considered as a group, area measurements of the IVVP were significantly correlated ($r > 0.7$, $p < 0.0001$) with vertebral canal area and dural sac area. Significant correlations were also identified between the following dimensions: transverse diameter of the dural sac and mid-sagittal diameter of the vertebral canal; mid-sagittal diameter of the IVVP, mid-sagittal diameter of vertebral canal and area of the vertebral canal; transverse diameter of the dural sac and transverse diameter of vertebral body; mid-sagittal diameter of dural sac and mid-sagittal diameter of vertebral body; and area of the vertebral canal and area of the dural sac.

Results indicate that non-selective CT venography is a safe, sensitive method for performing morphometry of cervical IVVP in dogs. Dimensions of the cervical IVVP are correlated with dimensions of other C3-7 vertebral components in the normal dog. Further investigations are needed to determine whether these relationships change in dogs with cervical spinal disease.

3.2 Introduction

The canine vertebral venous plexus (VVP) is a large valveless collateral network that is composed of the internal vertebral venous plexus (IVVP; i.e. epidural veins, vertebral venous sinuses), the external vertebral venous plexus and the basivertebral veins.⁵⁰ The IVVP is clinically important in dogs because it has been associated with pathologic conditions such as spontaneous epidural hematoma,⁶⁵ arteriovenous malformation,¹⁰² fibrocartilaginous embolism,¹⁰⁰ and lumbosacral stenosis.²⁶⁴ In a prospective cohort study of canine lumbosacral stenosis,²⁶⁴ 33% (5/13) of the cases were found to have congestion of the IVVP and intervertebral veins at surgery. Epidural venous congestion has also been identified in dogs with experimental compression of the cauda equina.²⁷⁶ In human beings, the IVVP has been implicated as a direct cause of spinal cord or nerve root compression (lumbar radiculopathy).^{67,277} Under compression, VVP veins collapse easily due to the laxity of their walls and low internal pressure.²⁷⁸ Absence of valves in the vertebral venous plexus and flow deviation create localized venous dilation and stasis above and around the compression.²⁷⁹ Venous congestion may be responsible for acute intraneural edema and nerve function alteration.²⁸⁰

The normal appearance of the cervical IVVP has been described in human and canine post mortem specimens using intravenous contrast-enhanced CT.^{271,281} Computed tomography with intravenous contrast-enhancement also has been used in human beings and dogs for demonstrating extradural

compressive lesions, including disk herniations.^{68,264,273,282,283} Kaiser et al.,²⁷⁹ postulated that epidural venous stasis in human beings is a CT sign of clinically significant narrowing of the vertebral canal. These authors also recommended that a CT examination be performed before and after injection of intravenous contrast medium to differentiate protruded disk from prominent epidural veins.²⁷⁹

Normal ratios and measurements between cervical spinal cord diameter and vertebral body diameter have been reported from myelographic studies in small and large breed dogs.²⁸⁴ However, radiographic measurements are subject to errors due to rotation, superimposition, and projection.²⁸⁵ The ratio of the sagittal diameter of the human cervical canal to the corresponding diameter of the vertebral body has been calculated by CT and described as a reliable method for assessing stenosis of the cervical vertebral canal.²⁸⁶ Computed tomographic morphometry also has been used to describe stenosis of the canine lumbosacral vertebral canal.²⁸⁷ Calculating ratios of lumbosacral vertebral canal diameter and area versus vertebral body diameter and area was found to be an effective method for correcting for differences in dog body sizes.²⁸⁷ No morphometric computed tomographic studies relating soft tissue (neural, vascular) and bony components of the cervical spine in dogs were found at the time of this study.

We hypothesized that non-selective CT venography could be used to quantify IVVP collapse or congestion in dogs. Since the IVVP drains components of the vertebral canal, we also hypothesized that changes in the IVVP size would vary with changes in dimensions of these structures. However, before abnormal

venous plexus dimensions could be established, it would first be necessary to establish normal values for vertebral venous plexus dimensions and the relationships to other vertebral components. The objectives of this study were to evaluate non-selective CT venography as a technique for performing morphometry of the cervical IVVP, to describe normal ranges for cervical IVVP dimensions, and to determine the relationship of these dimensions to the dimensions of the vertebral canal, dural sac, epidural space, and vertebral body.

3.3 Material and Methods

Dogs

This prospective and non-terminal study was performed in 6 clinically normal research dogs. All animals were examined by a board-certified veterinary neurologist (KI) and determined to be free of any signs of spinal disease. All procedures were approved by the Virginia Tech Institutional Animal Care and Use Committee.

Anesthetic protocol

The dogs were fasted for 12 hours prior to anesthesia. Each dog was premedicated with butorphanol¹ (0.2 mg/kg, intramuscular (IM)), diazepam^b (0.2 mg/kg), and atropine sulfate^c (0.02 mg/kg). After placement of an indwelling 20-gauge cephalic vein catheter^d, anesthesia was induced by titrating 2% thiopental^e intravenously (IV) at a dose just sufficient to allow tracheal intubation (average: 9.6 ± 1.3 mg/kg). Anesthesia was maintained with Isoflurane^f (1.1 to 1.2 % end-tidal (ET) in 100% O₂ (30-40 ml/kg)) delivered by a calibrated precision vaporizer^g, using a semiclosed system with a CO₂ absorber system. Normal

¹ Torbugesic^R Butorphanol Tartrate (10 mg/ml), Fort Dodge Animal HealthFort Dodge, Iowa

^b Diazepam Injection USP (5 mg/ml) Abbott Laboratories, North Chicago, IL

^c Atropine Sulfate Injection (0.54 mg/ml) Phoenix Pharmaceutical, Inc, St. Joseph, MO

^d Becton Dickinson Angiocath, Sandy, Utah

^e Pentothal Thiopental Sodium for injection, Abbott Laboratories, North Chicago, IL

^f Isoflo^R Isoflurane, USP, Abbott LaboratoriesNorth, Chicago, IL

^g Isoflurane Vapor 19.1, North American Drager, Dragerweck AG, Lubeck, Germany

saline (0.9%) solution^h was administered IV at a rate of 10ml/kg/hr. A 20 gauge catheter was placed in a lingual artery for direct arterial blood pressure measurement. Tidal volume and respiratory rate were controlled to maintain an end-expired CO₂ (28-32 mmHg) using a volume-controlled ventilatorⁱ. The partial pressure of CO₂ in end-expired gas was measured by an infrared analyzer^j. Heart rate, respiratory rate, direct arterial pressure, ET CO₂ levels, and oxygen saturation^k were recorded every 5 minutes during the entire procedure.

Non-selective CT venography protocol

All dogs were scanned using the same helical CT scanner^l. Dogs were positioned in sternal recumbency with their necks extended. Thoracic limbs were pulled caudally and slight traction force was maintained using duct tape. Pre- and post-contrast CT scans were obtained using 3 mm slice thickness, 2 mm slice interval, and a table pitch of 1.25. The scanned region began at the external occipital protuberance and ended at the spinous process of the first thoracic vertebra (T1). The CT gantry was angled to generate slices that were as perpendicular to the vertebral canal as possible.²⁸⁸ For post-contrast images, iodinated contrast medium^m was administered intravenously via a 20-gauge right

^h 0.9% Sodium Chloride Injection, USP Baxter Healthcare Corporation, Deerfield, IL

ⁱ Hallowell EMC Model 2000™ Veterinary Anesthesia Ventilator Hallowell Engineering and Manufacturing Corp. , Pittsfield, MA

^j Datex Ohmeda AS/3™ Anesthesia Monitor Datex Ohmeda Instrumentation Corp Helsinki, Finland

^k Nellcor N-20PA, Nellcor Puritan Bennett Inc, Pleasanton, CA

^l Picker PQ5000, Philips Medical Systems, Cleveland, OH

^mConray 400, 400 mgI/kg, Mallinckrodt Medical Inc., St Louis, Mo

lateral saphenous vein catheter. A manual bolus injection of 480 mgI/kg was administered at a rate of approximately 2 ml/sec.^{289,290} Spiral scanning was initiated immediately following the bolus injection. Infusion of an additional 240 mgI/kg of contrast medium was administered during the CT scan by means of a constant-rate infusion pump.ⁿ

CT morphometry:

Image data from CT scans were transferred to a remote workstation via Ethernet. From transverse CT images displayed on the computer monitor, diameter and area dimensions of the IVVP, vertebral canal, dural sac and vertebral body at each vertebral level were measured. Window and level settings were standardized for all measurements (WW: 300 HU, WL: 40 HU). All CT transverse images were magnified by a factor 3 to improve visualization of the structures. Diameter and area measurements were performed manually using an electronic cursor and the workstation's software for diameter and area calculations. Since C1 and C2 vertebrae have unique morphologic features that differ from other cervical vertebrae, measurements were made from C3 to C7. All the measurements were made at the midpoint of each cervical vertebral body using transverse CT images. Each parameter was measured 3 times by the same observer (MG). The following measurements from the CT images were recorded for each vertebral level (Fig 3.1):

ⁿ Baxter, Model AS50 Infusion Pump, Baxter Healthcare Corp., IV System Division, Deerfield, IL

1. Transverse and sagittal diameter of the internal vertebral venous plexus. (TIVVP, SIVVP; left and right components).
2. Transverse and sagittal diameter of the vertebral canal (TVC, SVC)
3. Transverse and sagittal diameter of the dural sac (TDS, SDS)
4. Sagittal diameter of the vertebral body (SVB)
5. Area of the internal vertebral venous plexus, vertebral canal, dural sac and vertebral body (AIVVP, AVC, ADS, AVB).

Statistical analysis:

Epidural space areas were calculated by subtracting dural sac areas from vertebral canal areas. Means \pm standard deviations (SD), and ranges for all dimensions were calculated for the C3-7 vertebral locations in all dogs. To test the hypothesis that a significant relationship was present between dimensions of the IVVP and other vertebral components, a Pearson's correlation coefficient analysis^o was performed. Significance was set at $r > 0.7$, $p < 0.0001$. Ratios of some vertebral components were calculated and compared with those reported in previous studies.

^o The SAS System (version 9.12) SAS Institute Inc., Cary, NC

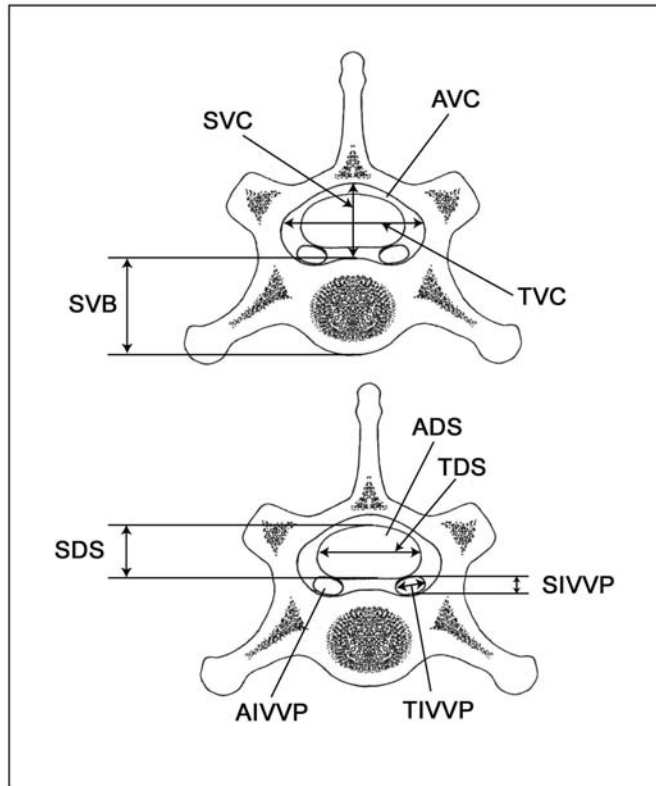


Figure 3.1 - Illustration demonstrating the diameter and area dimensions measured. (Drawing made by the first author).

TIVVPI= transverse diameter of the left internal vertebral venous plexus; TIVVPr= transverse diameter of the right internal vertebral venous plexus; TVC= transverse diameter of vertebral canal; TDS= transverse diameter of the dural sac; SIVVPI= sagittal diameter of the left internal vertebral venous plexus; SIVVPr= sagittal diameter of the right internal vertebral venous plexus; SVC= sagittal diameter of the vertebral canal; SDS= sagittal diameter of the dural sac; SVB= sagittal diameter of the vertebral body; AIVVPI= area of the left internal vertebral venous plexus; AIVVPr= Area of the right internal vertebral venous plexus; AVC= Area of the vertebral canal; ADS= Area of the dural sac; AVB= Area of the vertebral body.

3.4 Results

Dogs

Weights of dogs ranged from 18-27 Kg, with a mean weight of 21.5 kg. Breeds represented included Labrador retriever, German shepherd, and mixed. There were 2 male and 4 female dogs.

CT venography

The range of total contrast medium dosages administered per animal was 31 to 48 ml (12,400 to 19,200 mgI), with a mean of 38.3 ml (15,320 mgI). In five dogs, the contrast-enhancement protocol resulted in good opacification of all veins. Intra-vascular CT density values of the IVVP ranged from 210 - 300 HU after contrast administration. The dural sac was visualized as a round or elliptical structure inside the vertebral canal with a CT density of 30 to 40 HU. In one of the dogs, a double dose of contrast medium was necessary because the first injection failed to opacify the vessels. This problem was found to have been caused by an error in setting parameters on the infusion pump. However, none of the dogs exhibited signs of adverse reactions during or following the procedure. All dogs recovered routinely from anesthesia and were clinically normal at 24 and 48 hours post CT examination.

CT Morphometry (Table 3.1)

Vertebral venous plexus

The sagittal diameters of the vertebral venous plexus for the C3 to C7 vertebral segments ranged from 0.6 mm to 3.2 mm (mean= 1.84 mm). The larger sagittal diameters were found at the C6 vertebral level (2.32 ± 0.44 mm), corresponding to the location of the C7 spinal cord segment. Transverse diameters ranged from 2.32 mm to 5.74 mm (mean= 4.0 mm). The maximum transverse diameters were found at the level of C5 (4.19 ± 0.48 mm for the left IVVP, 4.80 ± 0.75 mm for the right IVVP). The mean transverse area for the internal vertebral venous plexus was 13.38 mm^2 (approx. 6.69 mm^2 for each left and right component). This represented approximately 12.4% of the vertebral canal transverse area (mean= 107.9 mm^2), 20.84% of the dural sac area (mean= 64.18 mm^2) and 30.61% of the cervical vertebral epidural space area (area vertebral canal-area dural sac: 43.7 mm^2). This former percentage increased to nearly 40% at the C5 level (Fig 3.2). Maximum areas of the internal vertebral venous plexus were measured at the C6 vertebral segment, at the location of the cervical intumescence (Fig 3.3). Vertebral vein measurements were not obtainable, primarily due to a silhouette effect with vertebral arteries (Fig 3.4 and 3.5)

Dural sac

The maximum mean mid-sagittal diameter of the dural sac was observed at the level of C6 vertebra (8.45 ± 0.57 mm) and the lowest was observed at C4 (7.01 ± 0.57 mm) (Fig 3.6). For the transverse diameter, minimum values were seen at the C3 vertebral level (8.89 ± 0.97 mm) and the maximum at C6 vertebral level (11.29 ± 0.91 mm). The mean area for the dural sac between C3 to C7 was 64.18 ± 10.48 mm². The largest area was observed at the C6 level (78.9 ± 13.18 mm²).

Vertebral canal

The maximum mean mid-sagittal diameter of the vertebral canal was found at C6 (11.56 ± 0.36 mm) and the minimum at C3 (9.12 ± 0.34 mm) (Fig 3.6). The maximum transverse diameter was observed at C7 (14.99 ± 1.82 mm). The minimum transverse diameter was found at C3 (10.46 ± 1.13 mm). The mean vertebral canal area between C3 to C7 was 107.87 ± 24.44 mm². The vertebral canal averaged its largest area dimension at C7 (134 ± 17.06 mm²).

Vertebral body

The maximum mean mid-sagittal diameter for the vertebral body was observed at C7 (12.14 ± 1.37 mm) and the minimum value was at C3 (8.29 ± 1.57 mm) (Fig 3.6). Transverse diameters of the vertebral body were subjectively

considered similar to transverse diameters of the vertebral canal at all cervical vertebral levels. The largest area of the vertebral bodies was found at C7 ($151.6 \pm 28.6 \text{ mm}^2$) and the minimum value at C3 ($73.8 \pm 13.21 \text{ mm}^2$).

Statistical analysis (Table 3.2)

When vertebral segments were analyzed individually, no significant correlations were found between dimensions of the IVVP and dimensions of other vertebral components. When all segments (C3-C7) were analyzed as a group, area measurements of the venous structures were significantly correlated ($r > 0.7$, $p < 0.0001$) with vertebral canal area and dural sac area. Significant correlations were also identified between the following dimensions: transverse diameter of the dural sac and mid-sagittal diameter of the vertebral canal; mid-sagittal diameter of the IVVP, mid-sagittal diameter of vertebral canal and area of the vertebral canal; transverse diameter of the dural sac and transverse diameter of vertebral body; mid-sagittal diameter of dural sac and mid-sagittal diameter of vertebral body; and area of the vertebral canal and area of the dural sac.

TABLE 3.1 - Dimensions of C3-7 vertebral components in 6 normal adult dogs
(mean \pm SD)

Dimension	C3	C4	C5	C6	C7
TIVVPI (mm)	3.72 \pm 0.60	3.70 \pm 0.75	4.19 \pm 0.48	3.95 \pm 0.59	3.50 \pm 0.58
TIVVPr (mm)	4.16 \pm 0.50	3.92 \pm 0.83	4.80 \pm 0.75	4.48 \pm 0.58	3.57 \pm 0.52
TVC (mm)	10.46 \pm 1.13	10.65 \pm 1.31	12.13 \pm 1.55	13.54 \pm 1.63	14.99 \pm 1.82
TDS (mm)	8.89 \pm 0.97	9.05 \pm 1.08	10.06 \pm 1.09	11.29 \pm 0.91	9.78 \pm 0.93
SIVVPI (mm)	1.2 \pm 0.31	1.45 \pm 0.19	1.87 \pm 0.26	2.32 \pm 0.44	2.17 \pm 0.22
SIVVPr (mm)	1.17 \pm 0.22	1.34 \pm 0.23	2.02 \pm 0.40	2.32 \pm 0.50	2.47 \pm 0.22
SVC (mm)	9.12 \pm 0.34	9.16 \pm 0.50	10.68 \pm 0.25	11.56 \pm 0.36	10.48 \pm 1.22
SDS (mm)	7.14 \pm 0.62	7.01 \pm 0.57	7.88 \pm 0.53	8.45 \pm 0.57	7.87 \pm 0.95
SVB (mm)	8.29 \pm 1.57	8.50 \pm 1.03	8.74 \pm 0.84	10.04 \pm 0.72	12.14 \pm 1.37
AIVVPI (mm ²)	4.10 \pm 1.29	4.33 \pm 1.22	7.01 \pm 1.16	8.24 \pm 1.63	7.38 \pm 1.61
AIVVPr (mm ²)	4.47 \pm 1.30	5.20 \pm 1.94	9.22 \pm 2.64	9.52 \pm 2.39	7.40 \pm 1.79
AVC (mm ²)	82.05 \pm 11.84	84.49 \pm 14.95	108.76 \pm 16.35	129.98 \pm 18.49	134.07 \pm 17.06
ADS (mm ²)	53.54 \pm 9.92	54.49 \pm 10.88	67.44 \pm 10.64	78.88 \pm 13.18	66.55 \pm 11.69
AVB (mm ²)	73.75 \pm 13.21	74.36 \pm 10.51	78.52 \pm 10.45	100.79 \pm 11.66	151.60 \pm 28.56

See Figure 1 for abbreviation keys

TABLE 3.2 - Correlations between dimensions of the vertebral venous plexus, vertebral canal, dural sac, and vertebral body between C3 and C7 vertebral segments. * indicates $r > 0.7$ and $p < 0.0001$

	TIWPI	TIVPr	TVC	TDS	SIVPI	SIVPr	SVC	SDS	SVB	AIVPI	AIVPr	AVC	ADS	AVB
TIWPI		*0.79	0.12	0.51	0.16	0.1	0.33	0.25	-0.04	0.54	0.51	0.19	0.39	-0.08
TIVPr			0.2	0.64	0.26	0.23	0.35	0.28	-0.08	0.54	*0.72	0.25	0.48	-0.13
TVC				*0.7	0.66	*0.81	0.56	0.62	*0.85	0.66	0.61	*0.93	*0.72	*0.86
TDS					0.61	0.62	*0.74	*0.77	0.44	*0.74	*0.77	*0.78	*0.92	0.39
SIVPI						*0.85	*0.79	0.61	0.55	*0.86	*0.76	*0.79	0.61	0.5
SIVPr							*0.72	0.58	0.64	*0.83	*0.81	*0.87	0.62	0.66
SVC								*0.87	0.33	*0.81	*0.75	*0.8	*0.83	0.33
SDS									0.31	0.64	0.6	*0.79	*0.93	0.35
SVB										0.47	0.31	*0.76	0.43	*0.94
AIVPI											*0.87	*0.78	*0.7	0.49
AIVPr												*0.72	*0.7	0.29
AVC													*0.85	*0.76
ADS														0.43

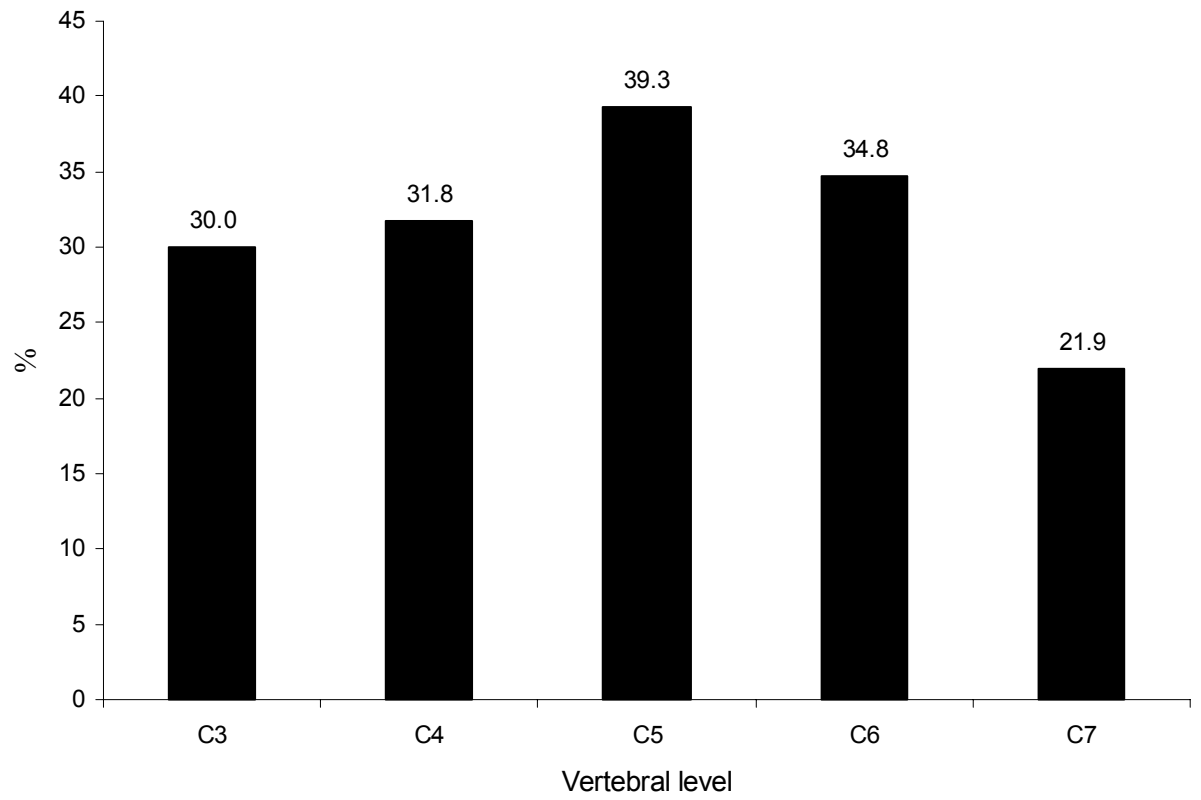


Figure 3.2 – Percent of the C3-C7 epidural space area occupied by the vertebral venous plexus.

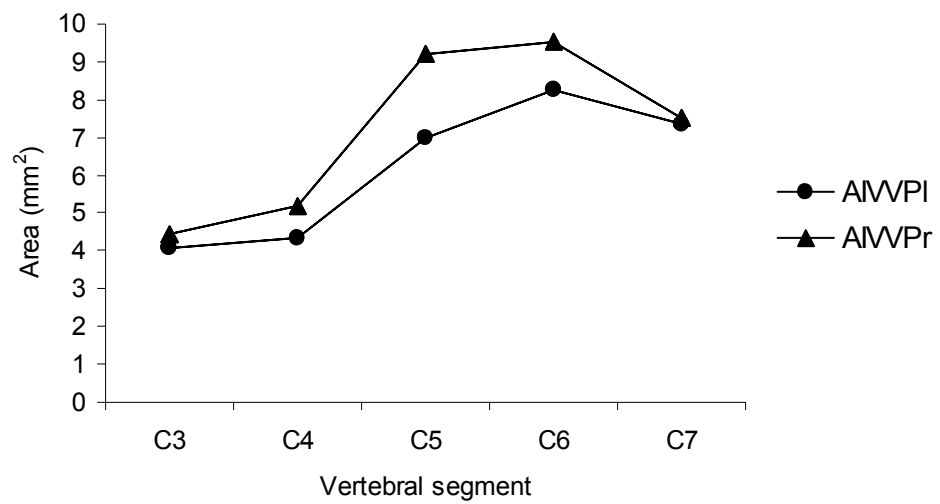
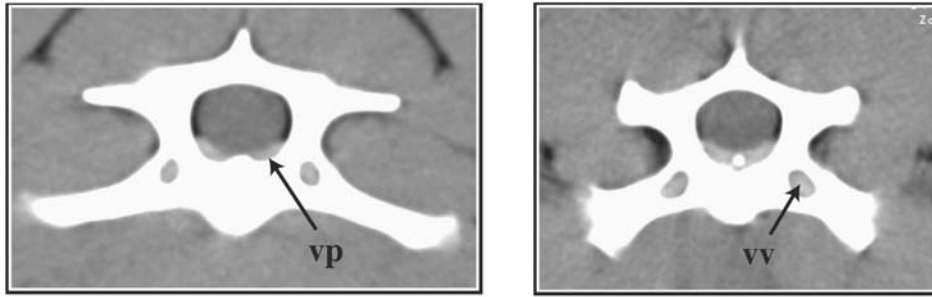


Figure 3.3 – Mean areas values of the right and left IVVP in the vertebral segments C3 to C7.



A

B

Figure 3.4 - Transverse CT images obtained at the mid-vertebral bodies of C4 (A) and C5 (B). Notice that the ventral epidural space is nearly completely occupied by the internal vertebral venous plexus (vp). Vertebral veins (vv) are difficult to distinguish due to the silhouette effect with the vertebral arteries.

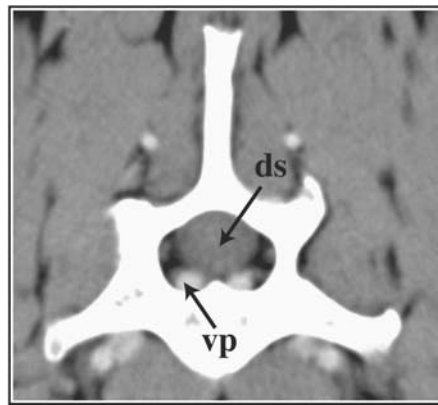


Figure 3.5 - Transverse CT image obtained at the mid-vertebral body of C7. There is an increase in the lateral epidural space due to an increase in the transverse diameter of the vertebral canal (compare with Fig 3.4). The internal vertebral venous plexus (vp) is clearly observed as two hyperattenuating oval opacities ventral to the dorsal sac (ds).

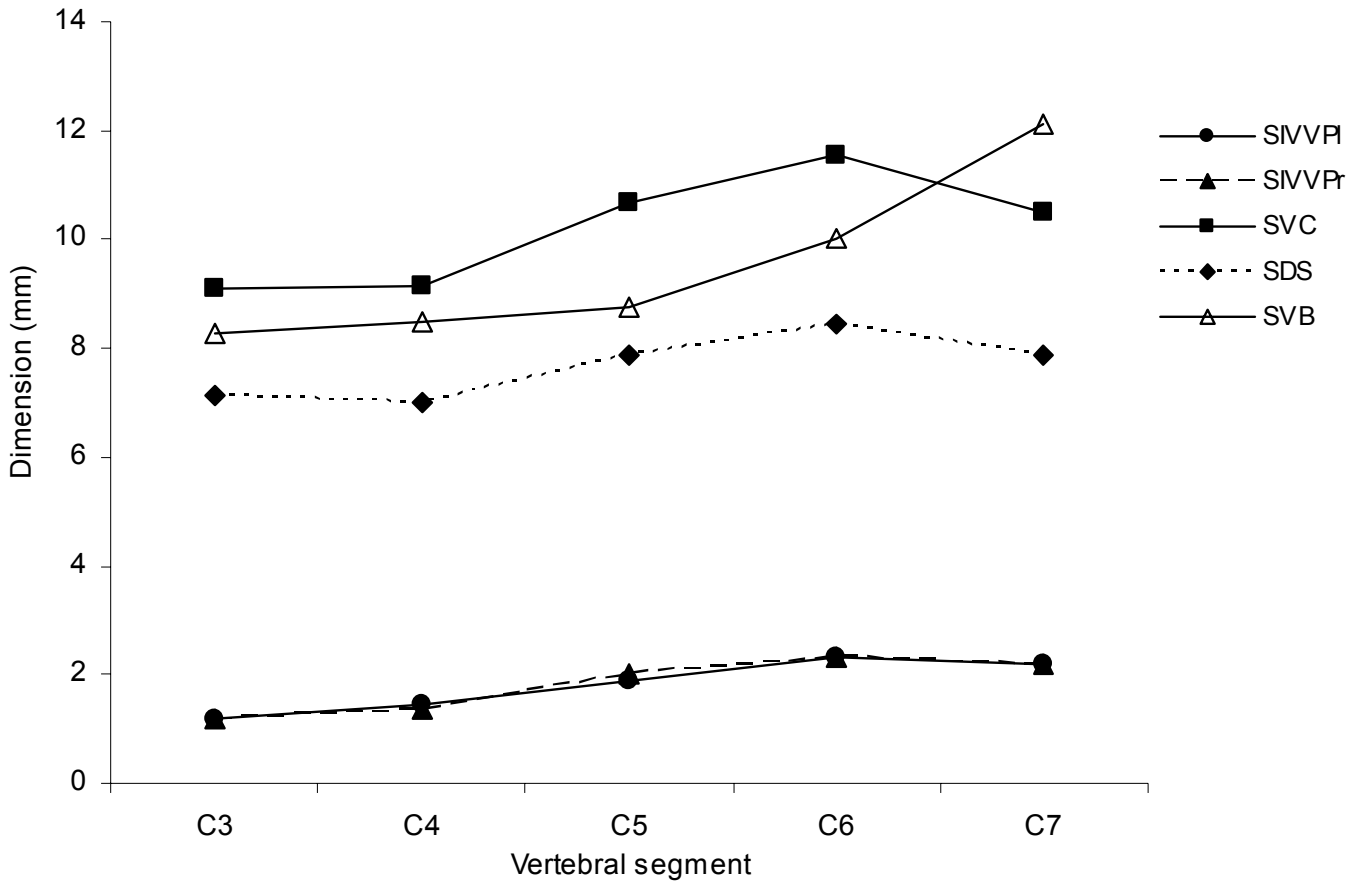


Figure 3.6 – Mean values for sagittal diameters of the vertebral venous plexus, vertebral canal, dural sac and vertebral body from C3 to C7.

3.5 Discussion

Evaluation of CT venography technique

Our CT venography protocol achieved IVVP CT density values of 210-300 HU. A value of 240 HU has previously been reported to be optimal for vessel enhancement and measurements.^{291,292} No adverse effects after administration of contrast medium were seen in any dog. Morphology and location of the veins were consistent with those seen in our previous anatomy study performed in dog cadavers.²⁸¹ In that study, selective CT venography was performed using a single manual injection into the external jugular vein. This was performed after occluding the ipsilateral internal jugular vein, and occluding the contralateral internal and external jugular veins.²⁸¹ In our current study, non-selective CT venography was performed using an injection into the saphenous vein. A manual bolus injection of contrast medium was followed by a continuous infusion.

Several factors may affect the accuracy of measurements in CT morphometric studies. Variations in window level and window width selections can influence the measurements due to a blooming artifact.²⁹³ In this artifact there is variation in the attenuation outside the real border of the vessel altering the apparent size of its lumen.²⁹⁴ Also, diameter and area dimensions of objects located in the transverse plane can be altered if they are not perpendicular to the scan plane.²⁹⁵ Oblique slices in those cases can produce falsely elongated images. Operator factors can also influence the variability in the accuracy of the measurements, even when there is one observer performing the

measurements.²⁹⁶ In a morphometric study of the canine lumbosacral spine, Jones et al.²⁸⁷ determined that the accuracy of transverse area measurements was lower than diameter measurements. This was considered most likely due to operator error related to hand tracing irregular regions of interest. Imprecision of the device used for manual measuring can also affect the measurements. One study proposed that, when the cursor or electronic caliper is positioned at the edges of the object being measured, there is often an unstable jittering of the instrument that can limit precise outlining of the object.²⁹⁶

Normal dimensions of the vertebral venous plexus and other vertebral components

The range of dimensions we measured for the cervical IVVP in our dogs (0.6 to 3.2 mm) was similar to that reported for human beings.²⁹⁷ Based on sagittal T1-weighted post Gd-DTPA MRI, human cervical SIVVP diameters ranged between 1-3 mm. No normal veins were identified in human beings with diameters larger than 4 mm and less than 1 mm. However, the relative size of the IVVP we measured in our dogs was greater than the relative size of the IVVP reported in human beings.³² Our observations also indicated that diameter dimensions for the IVVP changed gradually between adjacent segments. No abrupt changes in linear dimensions were found. Maximum cross-sectional areas of the IVVP were identified at the caudal cervical region (C5-C7). These results

were consistent with findings from anatomic studies in dogs made by Crock.⁴⁰ The relative epidural space occupied by the venous plexus was approximately 30% in the cranial cervical region and almost 40% in the caudal cervical region (C5 level). It is possible that this relative increase in size of caudal cervical venous structures is related to protection and drainage of the cervical intumescence. It is also probable that the increased size of veins in this region is associated with the increased size of vertebral bodies.³²

Engorgement of the IVVP can occur due to congenital or acquired causes.²⁹⁸ In human beings, localized congestion of the IVVP can produce sciatica symptoms and may resemble a prolapsed intervertebral disk on MRI images.²⁷⁷ Reports indicate that human patients with obstruction of the inferior vena cava due to caval thrombosis and gestation presented enlargement of the IVVP and clinical signs of radicular compression or spinal stenosis.²⁹⁹ Spinal epidural varices are a rare condition in human beings that can cause neurologic symptoms due to a dilated IVVP.³⁰⁰ However, increased diameter of the IVVP can be asymptomatic in others conditions such as congestive heart failure, hepatic failure, obesity, pregnancy, and positioning with abdominal compression.

In human beings, measurement of the area and sagittal dimensions of the IVVP has been shown to be a good indicator for diagnoses of spinal diseases with CSF fluid leakage such as spontaneous intracranial hypotension syndrome.^{58,301} The Monro-Kellie hypothesis established that cerebral CSF volume fluctuates inversely to cerebral blood volume.¹⁰⁶ So, a decrease in CSF

volume leads to compensatory vasodilation in the brain and meninges. Since these vessels are closely associated with intraspinal vessels, venous dilation will also affect the cervical IVVP.

Vertebral canal

In dogs studied, lower mid-sagittal diameters of the vertebral canal occurred at C3 the level and higher values occurred at the C6 level. This finding is consistent with previous radiographic studies in dogs.^{302,303} However, measurements of vertebral canal mid-sagittal diameters were on average 1 or 2 mm smaller than values measured in previous radiographic studies. This difference could be the result of the smaller size of our dogs and/or absence of magnification of CT measurements compared to radiographs.²⁸⁶

Mid-sagittal diameter measurements of the vertebral canal were nearly constant in this group of dogs from C3 to C4 and were increased from C5 to C7. In human beings, vertebral canal quantitative data are controversial. Some studies found smaller sagittal dimensions in the superior cervical region and others studies found smaller sagittal dimensions in the inferior cervical region.^{304,305} Our observation that maximum transverse diameter and area of the cervical vertebral canal occurred at C7 also supports results of other CT studies in dogs.^{229,306} Transverse diameters of the vertebral canal were greater than mid-sagittal diameters in all cervical segments. In CT images, the epidural space was visible only in the lateral portions of the canal at most cervical vertebral

locations measured. In human beings, this finding is believed to be the reason why lateral displacement of caudal cervical neural structures is more likely to occur than displacement in the sagittal plane.²⁸⁶ In our dogs, a relative increase in transverse diameter of the caudal cervical vertebral canal was also associated with an increase in size of vertebral veins. It is possible this potential space helps to protect the spinal cord at the vertebral level where segmental motion of the spine is generally the greatest.

Sagittal and transverse diameters of the dural sac in our dogs were more circular in shape at the cranial cervical segment, and more oval in shape in the caudal cervical segments, a finding also reported in previous studies.^{283,306} Epidural space areas were calculated by subtracting dural sac area from vertebral canal area. Mean epidural space areas represented approximately 30% of the vertebral canal area for the C3-C7 vertebral segment in dogs. Epidural space areas were lower in the cranial cervical region (C3) than in the caudal cervical region (C6-7). This finding suggests that an epidural mass of similar size should be more compressive to neural and vascular tissues in the cranial cervical region than it would be in the caudal cervical region. We estimated the sagittal diameter of the epidural space by subtracting dural sac sagittal diameter from vertebral canal sagittal diameter. Cervical epidural space values in dogs ranged from 1.9 to 3.11 mm with the greatest value at C6. Smaller values were found at C3-C5 and are similar to SAC values in people.³⁰⁷ The SAC value is defined as

the space available for the spinal cord and is recommended to be an effective indicator of cervical spinal stenosis in human patients.³⁰⁷

Correlation results

Calculation of ratio between mid-sagittal diameter of the dural sac and the vertebral canal (VDS:VVC), revealed values of 0.73 and 0.78 for the cervical segments. These values are greater than ratios of spinal cord and vertebral canal diameter reported by Fourie et al.²⁸⁴ Discrepancies are likely due to the fact that the dural sac includes both the spinal cord and spinal subarachnoid space.

In our dogs, the calculated ratios between sagittal diameter of vertebral canal and sagittal diameter of vertebral body ranged between 0.8 and 1.22. In human beings, this ratio is termed the Torg ratio and is used for determining spinal stenosis.³⁰⁷⁻³⁰⁹ Torg ratios < 0.8 or 0.7 are considered to be indicative of spinal stenosis.³⁰⁹ However, one CT study demonstrated a low positive predictive value for this ratio in predicting human cervical spinal stenosis.³¹⁰ In a radiographic study including Doberman pinschers, Drost et al.²²⁷ demonstrated that the ratio between mid-sagittal diameter of the vertebral canal and mid-sagittal diameter of the vertebral body were statistically different at C5 and C7 levels in dogs affected with caudal cervical stenosis versus unaffected dogs.²²⁷ However, their measurements were performed at the cranial endplate of the vertebrae while ours were performed at the mid-vertebral region. Drost et al. concluded that the presence of spondylosis deformans in the cranio-ventral

portion of the vertebral bodies could affect the accuracy of these vertebral body measurements.

Values for the mid-sagittal, transverse and area dimensions of the vertebral bodies in this study increased between C3 and C7. In human beings, mid-sagittal diameters of the vertebral bodies do not differ between C3 and C6, and slightly increase at C7.³¹¹ In human beings, many patients with cervical stenotic myelopathy have larger cervical vertebral bodies than normal individuals.³¹¹ Previous studies demonstrate that an increase in size of the vertebral bodies can result in proportionally larger osteophytes or protruded disks.^{311,312} This has been proposed to be caused by a higher area for mechanical stress or biomechanical forces affecting the vertebral bone mass.

One limitation of our study was the small sample size and low breed variation. In order to overcome the problem of small sample size, significance for the correlation analysis was set using a high r value (> 0.7) and a low p value (< 0.0001). The high correlation between sagittal and transverse diameters of the vertebral canal and its components (dural sac and vertebral venous plexus) support the theory that bony spinal canal morphology may be related to the development of the neural and vascular structures of the canal.²⁸⁶

In conclusion, findings from our study indicate that non-selective CT venography is an effective and safe technique for morphometric evaluation of the cervical vertebral venous plexus in dogs. Findings also indicate the relative size of the normal cervical vertebral venous plexus increases from C3 to C7 in normal

dogs. When all segments were evaluated as a group, a significant correlation was identified between venous plexus dimensions and dimensions of other components of the C3-7 vertebral region. This findings support the theory there may be a physiologic or developmental relationship between cervical vertebral canal components. Future research is needed to determine how these relationships change in dogs with developmental or acquired cervical spinal disease.

CHAPTER 4

EFFECTS OF ACUTE SPINAL CORD COMPRESSION ON THE MORPHOLOGY OF THE CANINE CERVICAL VERTEBRAL VENOUS PLEXUS: EVALUATION USING COMPUTED TOMOGRAPHIC VENOGRAPHY AND DIGITAL SUBTRACTION VENOGRAPHY

Marcelo Gómez DVM,¹ Otto Lanz DVM, DACVS,¹ Jeryl Jones DVM, PhD, DACVR,¹ Richard Broadstone DVM, PhD, DACVA,¹ Karen Inzana DVM, PhD, DACVIM,¹ Mary Jensen MD, DACR,³ Larry Freeman DVM, MS.²

From Departments of Small Animal Clinical Sciences¹ and Biomedical Sciences and Pathobiology,² Virginia-Maryland College of Veterinary Medicine, Virginia Polytechnic Institute & State University. From the Department of Radiology, University of Virginia, School of Medicine, Charlottesville.³

4.1 Abstract

The internal vertebral venous plexus (IVVP) is a vascular network located along the vertebral canal. Information is scarce in relation to the role of the IVVP in cases of acute spinal cord injury in dogs. The present study was designed to assess variation in morphology of the cervical IVVP under experimental acute spinal cord conditions in dogs. Eleven beagle dogs were used, with two dogs used in pilot studies and nine dogs used in the experimental spinal cord compression portion. Experimental spinal cord compression was induced at C3/4 vertebral canal level using a modified angioplasty balloon catheter technique. Dogs were evaluated prior to, during and post spinal cord compression using vertebral intraosseous digital subtraction venography (DSV) and computed tomographic (CT) venography. DSV was successful in 3 dogs and unsuccessful in 3. In the 3 successful dogs, DSV demonstrated significant and immediate lack of opacification of the cervical IVVP at the site of compression. CT venography was performed in 3 dogs and was more consistent compared to DSV in demonstrating opacification of the cervical IVVP. CT venography also demonstrated a similar lack of filling of the IVVP in areas of balloon compression. DSV images demonstrated the hemodynamic changes of the IVVP and their collateral veins during compression. During post-compression, DSV and CT venography images revealed that some dogs exhibited lack of filling of the cervical IVVP at the previously compressed area. Increases in physiological variables such as systolic, diastolic, and mean arterial pressure were observed

after induction of experimental spinal cord compression in all dogs. Results indicate that CT venography and DSV accurately depict the IVVP in dogs, and demonstrate early changes of IVVP morphology under acute spinal cord compression conditions. The modified angioplasty balloon catheter technique used for acute spinal cord compression was a reliable and consistent method for inducing acute cervical spinal cord compression in all dogs. Intraosseous vertebral venography was not a consistent method for evaluating the cervical IVVP morphology. Further studies are needed to test the specific venous flow changes that occur during spinal cord compression, and the physiological effects of acute spinal cord compression in dogs.

4.2 Introduction

The vertebral venous plexus (VVP) is a network of valveless veins surrounding the vertebral canal, spinal cord and spinal nerves.⁵⁰ Normal anatomy of the cervical vertebral venous plexus in dogs was described macroscopically^{36,38,51} and more recently by computed tomography (CT):²⁸¹ However, little is known how acute spinal cord compression alters vertebral venous plexus morphology. Previous clinical studies in human beings suggest the VVP may play a role in spinal cord injuries.^{276,280} In a study involving six human patients, enlarged VVP vessels were found during lumbar disk decompression, and were implicated as the primary cause of neurologic signs in each of these six patients.²⁷⁷ In human beings⁸⁷ and dogs,⁶⁵ rupture of the internal vertebral venous plexus (a component of the VVP) was associated with spontaneous spinal epidural hematoma formation, which led to extradural compression of the spinal cord. Other spinal cord conditions that may produce abnormalities of the vertebral venous system in human and veterinary patients include spontaneous congenital dilation of the cervical epidural venous plexus,²⁶⁰ arteriovenous malformations,¹⁰² and fibrocartilaginous embolism.¹⁰⁰

Previous reports describe intraosseous vertebral venography as a technique for diagnosing extradural compression (intervertebral disk disease, vertebral body malformation, and tumors) involving the spinal cord and nerve root compression in both human beings and dogs.^{49,56,198,200,201} Intraosseous vertebral venography performed at the seventh lumbar vertebra (L7) consistently localized

spinal cord compression in the lumbar and thoracic region of dogs.²⁰⁰ Digital subtraction venography diameter measurements have been found to be similar to those obtained using CT venography.³¹³ In human beings, DSV is considered to be the gold standard procedure in evaluation of detailed anatomy and flow dynamics of vascular structures.³¹⁴ Computed tomography has the advantage over DSV to be less invasive and vascular abnormalities can be related to the adjacent parenchymal tissue.³¹⁵ In our Veterinary Teaching Hospital, DSV is a less expensive imaging modality than CT venography. However, to our knowledge, vertebral intraosseous venography combined with a digital subtraction technique has not been used to evaluate morphological changes of the VVP in dogs with acute spinal cord compression involving the cervical region.

Epidural balloon catheter inflation is an established technique for experimentally inducing extradural compression in the thoracolumbar region in both rats¹¹⁶ and dogs.^{119,316} This procedure is preferable to other experimental models because it does not require surgical exposure of the spinal cord and allows a gradual and controlled degree of spinal cord compression.³¹⁷

Based on a review of the literature, we theorized the vertebral venous plexus system may play an important role in the pathophysiology of acute cervical spinal injury in dogs. Extradural compressive lesions (herniated disks, hematomas, neoplasms, and vertebral malformations) may cause congestion and/or collapse of vessels in this valveless venous system, which in turn may exacerbate or complicate cervical spinal cord and/or nerve root compression.²⁰⁸

Venous congestion and/or collapse may also extend beyond the site of compression and persist after surgical removal of the original inciting cause.²⁷⁶

The objectives of this study were to test the effects of acute cervical spinal cord compression on the morphology of the canine vertebral venous plexus, refine an experimental method for inducing acute cervical extradural compression in the dog, and evaluate vertebral intraosseous DSV versus CT venography as possible techniques for demonstrating morphological changes in the IVVP caused by acute spinal compression in dogs. The null hypothesis was that quantitative and qualitative morphology of the cervical vertebral venous plexus would not differ prior to, during, or post acute experimental extradural spinal cord compression in the canine cervical vertebral canal.

Results of this study may explain the immediate effects of acute extradural compressive lesions on venous morphology in the cervical spine, and improve the experimental compression and imaging techniques required for future studies of acute spinal cord compression in dogs.

4.3 Material and Methods

Animals

Eleven adult beagle dogs, weighing between 9 and 11 kgs, were used in this study. All animals had normal physical and neurological examinations prior to inclusion in the study. Dogs were allowed at least 3 days to acclimate to new surroundings prior to entering the study. Two dogs were used in pilot studies to standardize the experimental procedures and techniques (see below). The remaining 9 dogs were tested using the protocols established during the pilot studies. All study protocols were approved by the Virginia Tech Institutional Animal Care and Use Committee.

Pilot studies

For elaboration of a standard experimental protocol, 2 dogs were used in 2 separate pilot studies.

Dog 1 (cadaver)

In order to determine the site of injection for cervical intraosseous vertebral venography, we conducted a pilot study in a dog cadaver using plain radiographs and fluoroscopic guidance. The test site for intraosseous injection was the vertebral body of C3. The intraosseous injection was made using a 13-gauge x 3.5 inches bone marrow biopsy/aspiration needle (Jamshidi needle). Introduction of the Jamshidi needle was made at a point located 1 cm cranio-

ventral to the palpable ventral prominence of the transverse process of C3. After percutaneous introduction of the Jamshidi needle through the right mid-cervical region, the vertebral body of C3 was located by palpating the bone with the Jamshidi and confirmed by fluoroscopy. Once the site of intraosseous injection was determined, drilling of the cortical bone of C3 vertebral body was performed by use of clockwise rotation of the Jamshidi needle. Reduction of resistance during the drilling was indicative of penetration of vertebral cortical bone. Correct placement of the Jamshidi into the center of the vertebral body was confirmed when the hub was resistant to lateral forces. A 6 cc syringe was attached to the Jamshidi hub and presence of blood after aspiration was considered indicative of correct intraosseous placement. A second syringe filled with 7 cc of contrast medium was attached to the jamshidi for manual injection of contrast. Contrast medium was injected rapidly and radiographic exposures were made at the end of contrast injection. Post-contrast radiographs showed the entire cervical IVVP and its cranial communication with the cerebral veins, including the confluence of sinus (*confluens sinuum*) and transverse sinus (*sinus transversus*) (Fig 4.1). Results from this pilot study indicated that intraosseous vertebral venography could be used to opacify the cervical IVVP with contrast medium (Fig 4.1 and 4.2).

Dog 2 (live dog)

The second dog was used to develop the location for experimental spinal cord compression, grade of spinal cord compression, and anesthesia protocol in vivo. A 6 French angioplasty balloon catheter was positioned under fluoroscopy over the mid-vertebral body of C5. Compression was created by inflating the angioplasty balloon to 2 atmospheres of pressure for 2 minutes, 4 atmospheres for 2 minutes and 4 atmospheres for 5 minutes. Location of the angioplasty balloon catheter at C5 and intraosseous injection at C3 was found to be too close for adequate visualization of the IVVP. Therefore, a more separate distance between the 2 objects was proposed for the final protocol. Also, placement of the angioplasty balloon catheter cranial to the injection site was chosen. For inducing spinal cord compression a pressure of 2 atmospheres was found insufficient for adequate balloon inflation and 4 atmospheres allowed satisfactory balloon inflation. Previous studies indicated that 10 minutes of spinal cord compression was the minimum time necessary to induce spinal cord compression injury in experimental studies.¹¹⁶ Therefore the duration of balloon inflation used in the second pilot study was also adjusted for the final protocol.

Experimental protocol

Anesthesia:

The dogs were fasted for twelve hours prior to anesthesia. Each dog was premedicated with butorphanol^a (0.2mg/kg, intramuscular [IM]), diazepam^b (0.2mg/kg IM), and atropine sulfate^c (0.02 mg/kg IM). After placement of an indwelling 20-gauge cephalic vein catheter^d, anesthesia was induced by titrating 2% thiopental^e intravenously (IV) at a dose just sufficient to allow tracheal intubation (13.6 ± 4.3 mg/kg). Anesthesia was maintained with isoflurane^f (1.1 to 1.2 % end tidal (ET) in 100% O₂ (30-40ml/kg) delivered by a calibrated precision vaporizer^g, using a semiclosed system with a CO₂ absorber system. Oxygen, Normal saline (0.9%) solution^h was administered IV at a rate of 10 ml/kg/hr. A 20-gauge catheter was then placed in a lingual artery for direct arterial blood-pressure measurement. Tidal volume and respiratory rate were controlled to maintain arterial eucapnia (PaCO₂, 35 to 45 mm Hg) using a volume-controlled ventilatorⁱ. The partial pressure of CO₂ in end-expired gas (ETCO₂) and isoflurane was measured, using an infrared analyzer^j.

^a Torbugesic[®] Butorphanol Tartrate (10mg/ml), Fort Dodge Animal Health, Fort Dodge, Iowa

^b Diazepam Injection USP (5mg/ml), Abbott Laboratories, North Chicago, IL

^c Atropine Sulfate Injection (0.54mg/ml), Phoenix Pharmaceutical, Inc. St. Joseph, MO

^d Becton Dickinson Angiocath, Sandy, Utah

^e Pentothal Thiopental Sodium for injection, Abbott Laboratories, North Chicago, IL

^f Isoflo[®] Isoflurane, USP Abbott Laboratories, North Chicago, IL

^g Isoflurane Vapor 19.1, North American Drager, Dragerwerk AG, Lubeck, Germany

^h 0.9% Sodium Chloride Injection USP, Baxter Healthcare Corporation, Deerfield, IL

ⁱ Hallowell EMC Model 2000[™] Veterinary Anesthesia Ventilator, Hallowell Engineering and Manufacturing Corp., Pittsfield, MA

^j Datex Ohmeda AS/3[™] Anesthesia Monitor, Datex Ohmeda Instrumentation Corp Helsinki, Finland

Monitoring and stabilization of physiologic parameters

Following a stabilization period of at least 45 minutes, baseline values for each of the following physiologic parameters were obtained after induction: temperature, pulse, respiration, heart rate, systolic and diastolic blood pressure, and arterial blood gases (HCO_3 , pH, pCO_2 , pO_2 , O_2 saturation). Measurements of all physiologic parameters were repeated at 5 minute intervals during pre and post-compression treatments and at 1 minute intervals during compression. Arterial blood gas analyses^k performed 5 minutes prior to compression, 5 minutes following initial compression, and 10 minutes after compression. All arterial blood samples were collected into heparinized syringes and stored on ice for no longer than 5 minutes prior to analysis.

Experimental spinal cord compression technique

The spinal cord compression model used in our study was a modified technique initially described by Purdy.^{119,318} Materials used in the experimental spinal cord compression study are shown in Figure 4.3. The lumbosacral space of each dog was clipped and aseptically prepared for angioplasty balloon catheter introduction. A 6 French introducer was percutaneously inserted into the lumbosacral space using fluoroscopic guidance, and a 145 cm Teflon coated

^k Rapid Lab, Bayer 348, Medfield, MA

guidewire^l was then introduced and directed cranially (Fig 4.4). A 6 French angioplasty balloon catheter^m (2 cm long and 6 mm diameter) was inserted over the guidewire until the radiopaque markers of the balloon were located between the third and fourth cervical vertebral bodies (Figs 4.5 and 4.6). The guidewire was then removed. Following stabilization of physiologic parameters (mean arterial pressure, heart rate, respiratory rate, end tidal CO₂, O₂ saturation) in each dog, extradural spinal cord compression over caudal C3 vertebral body, C3/4 vertebral level, and cranial C4 vertebral body was induced. Extradural compression was applied by rapid inflation of the balloon. Saline solution was injected manually through syringe with an attached manometer until 4 atmospheres of pressure was achieved. Balloon inflation at this pressure was maintained for a period of 10 minutes.

Digital subtraction venography

Vertebral intraosseous injection of contrast medium was performed in 6 dogs. Three dogs were excluded due to insufficient opacification of the IVVP. Two of these 3 dogs had incomplete venograms of the cervical IVVP immediately after intraosseous injection of contrast medium in the C6 vertebral body. In the first of the 3 dogs, a protruded annulus fibrosus at C4/5 was identified on necropsy. The contrast medium flowed in a retrograde fashion after injection toward the thoracic vertebral venous plexus and costocervical vein. In the second

^l Cook Group Company, Bloomington, IN

dog no cause for the lack of opacification was determined. In the third dog, extravasation of contrast medium from the C6 vertebral body made the evaluation of the cervical venogram difficult. On necropsy, placement of the biopsy needle ventral to the body of C6 was present and accounted for the extravasation of contrast medium in this particular case.

Three dogs exhibited sufficient opacification for inclusion in the experiment. For the 3 included dogs, digital subtraction venograms (DSV) images were exposed for each treatment (pre-compression, compression, and post-compression) using a digital fluoroscopic unitⁿ. After surgical preparation, a small skin incision was made in the left mid-cervical region. Using fluoroscopic guidance, a Jamshidi^o (13-gauge x 3.5 inches bone marrow biopsy/aspiration needle) was introduced manually into the vertebral body of the sixth cervical vertebra (C6). The position of the biopsy needle was checked in both dorso-ventral and lateral projections during introduction of the needle to ensure proper placement of the tip of the needle into the center of the vertebral body. The needle was flushed with heparinized saline solution to confirm proper needle placement. A syringe filled with 16 cc of contrast medium (meglumine iothalamate, 2 mgI/kg) was connected to a 55 cm extension set and then attached to the bone biopsy needle. The extension set was used in order to reduce radiation exposure during manual injection. To facilitate intraosseous

^m Boston Scientific Corporation, Fremont, CA

ⁿ Shimadzu YSF120, Shimadzu Medical Systems, Torrance, CA

^o Tyco Healthcare Group, Mansfield, MA

injection, contrast medium was pre-warmed to approximately 42°C. Immediately before and during rapid injection of the contrast medium, dorso-ventral DSV images were acquired at a rate of 2 frames per second over a period of 10 seconds. To remove bone superimposition a precontrast digital radiograph or mask was subtracted from the subsequent frames exposed during the injection of contrast medium. The pre-compression venograms were performed following the placement of the angioplasty balloon catheter. Compression venograms were acquired following inflation of the angioplasty balloon catheter to a pressure of 4 atmospheres. Post-compression venograms were acquired following deflation of the balloon, and after each dog's physiological parameters approached normal values. Each set of images was assigned a random identification number, and images were evaluated on a computer monitor using a window width of 1024 and a window level of 2048.

Computed tomographic venography

Computed tomographic (CT) venography images of 3 dogs were obtained using the protocol previously described in our CT morphometry experiment (see Chapter 3). Computed tomographic venography was performed prior to compression, during compression, and post-compression using the same compression and anesthesia protocols as those used for the DSV dogs.

Scanning protocol

Dogs were scanned using a helical CT scanner^p and a standardized scanning protocol. Dogs were placed in sternal recumbency with the cervical spine extended. Thoracic limbs were extended in a caudal direction. Lateral and dorsoventral pilot images were obtained to facilitate alignment of the neck and selection of slice locations. Precontrast computed tomographic scans were obtained using 3 mm slice thickness at 2 mm slice intervals, with a table pitch of 1.25. The scanned region extended from the external occipital protuberance to the spinous process of the first thoracic vertebra (T1) in all dogs. The CT gantry was angled as necessary to ensure slices were perpendicular to the vertebral canal. For CT venography images, scans were repeated after ionic contrast medium^q was intravenously administered through the previously placed lateral saphenous catheter. A manual bolus injection of 480 mgI/kg was administered at a rate of 2 ml/sec and spiral scanning was initiated immediately following bolus injection. Intravenous infusion of an additional 240 mgI/kg of contrast medium was administered during the scan by means of a constant-rate infusion pump^r. During CT acquisition, mechanical ventilation was suspended to minimize breathing motion artifacts and to maximize filling of the cervical vertebral venous plexus.

^p Picker PQ5000, Philips Medical Systems, Cleveland, OH

^q Conray 400, 400 mgI/kg, Mallinckrodt Medical Inc., St Louis, Mo

^r Baxter, Model AS50 Infusion Pump, Baxter Healthcare Corporation, IV System Division, Deerfield, IL

Data obtained

For the C1 to C7 vertebral levels, the following data were recorded from DSV and CT venograms:

- a) Presence of right and left components of the IVVP.
- b) Transverse diameters of the right and left IVVP at the midvertebral level and intervertebral space level.
- c) Distance between right and left components of the IVVP at the midvertebral level and intervertebral space level from C1 to C7.
- d) Presence of subjective abnormalities (occlusion, dilation, displacement or presence of collateral vessels) of the IVVP.

For measurements of the veins on DSV images, a calibration reference was used. The reference was defined as the distance between the 2 radiopaque markers of the angioplasty balloon catheter. These markers are known to be 2 cm apart and were located in the epidural space at the same geometric plane as the internal vertebral venous plexus. This technique allowed correction for magnification effects produced in the DSV images.

Calculations of the parameters in the post-contrast CT images were made using software for distance calculations. A window width of 300 HU and a window level of 100 HU were used during data measurements. Measurements of vein diameters from the DSV and post-contrast CT images were performed by a single observer (MG).

Statistical significance between the differences in values of pre-compression, compression, and post-compression in DSV and CT venograms were analyzed using a paired t test with a $p < 0.05$. Data analysis was performed using SAS statistical analysis system^s. A post hoc statistical analysis of the physiological parameters observed during pre-compression, compression, and post-compression was performed using a paired t test.

Histological analysis

At the conclusion of the experimental studies, all dogs were euthanized by an intravenous overdose of sodium pentobarbital^t (390 mg/ml). For the 6 included dogs (3 DSV and 3 CT) with diagnostic imaging studies, the cervical spinal cord was removed from the vertebral canal, fixed in 10 % buffer formalin and embedded in paraffin. Samples were obtained from the following sites; the site of compression (spinal cord segment C3 and C4), cranial to the site of compression (spinal cord segment C2), caudal to the site of compression (spinal cord segment C8) and, a site distant to compression (spinal cord segment L4). Serial transverse sections (4 μ m) were selected and stained with hematoxylin and eosin. Histological sections were evaluated by a board-certified veterinary pathologist.

^s The SAS System (version 9.12) SAS Institute Inc., Cary, NC

^t Fatal Plus^R Solution, Vortech Pharmaceuticals, Dearborn, MI

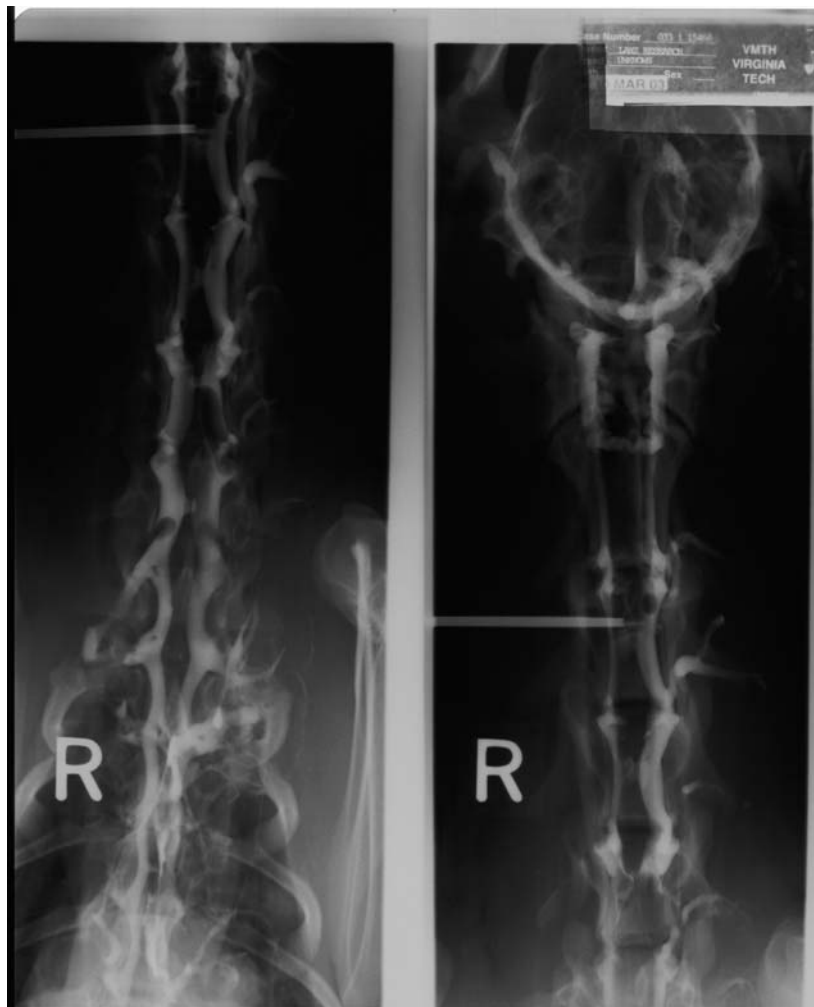


Figure 4.1 - Dorsoventral post-contrast radiographs of the cervical region in the first pilot dog. Opacification of the cervical and cranial thoracic vertebral venous plexus is observed after injection of contrast medium into the vertebral body of C3. Cranial communication of the cervical vertebral venous plexus with the cerebral veins (confluence of sinus and transverse sinuses) is also observed.

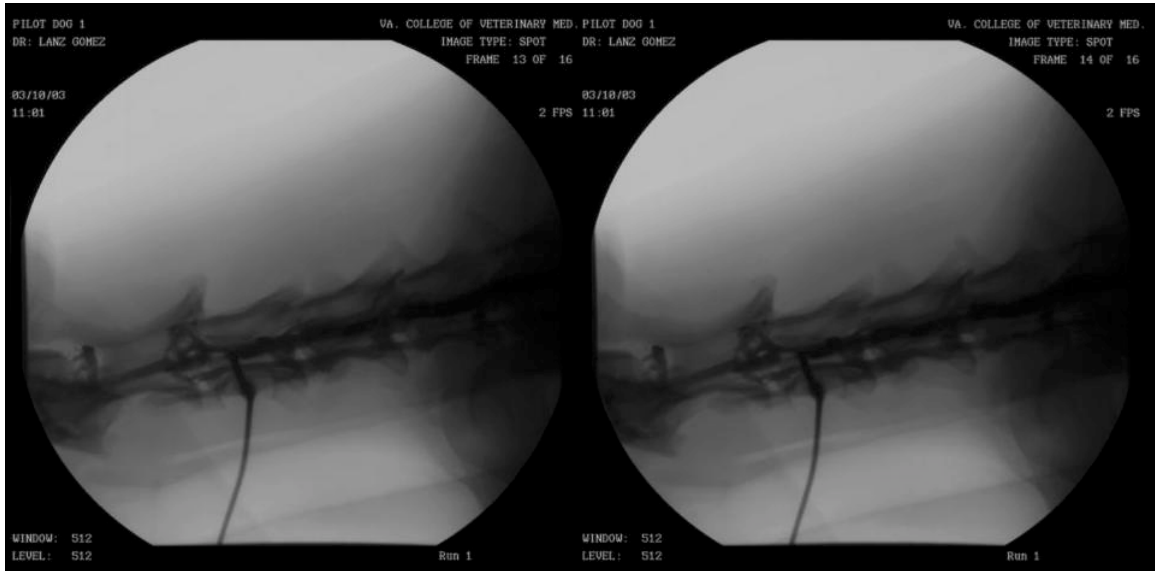


Figure 4.2 – Lateral reverse window, digital images of the cervical region from the first pilot dog. Both images show filling of the vertebral venous plexus after contrast medium injection into the vertebral body of C3.

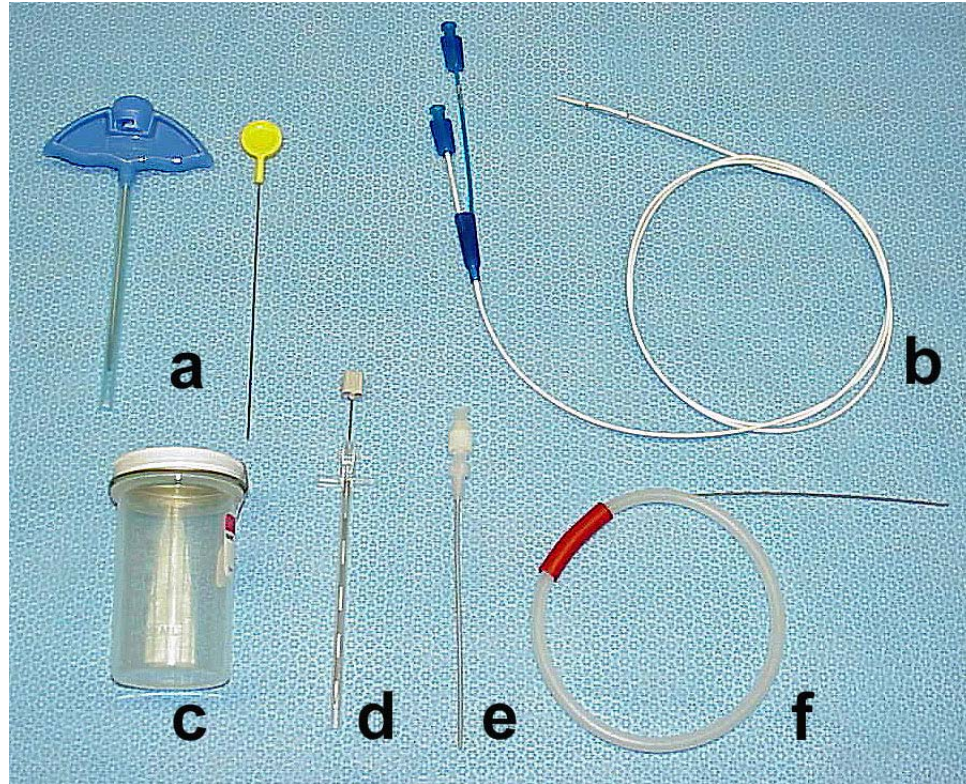


Figure 4.3 - Materials used in the spinal cord compression experiment.

Biopsy needle (Jamshidi) (a), Angioplasty balloon catheter (b), Sterile specimen container (c), Epidural needle (d), 6 French introducer (e), Guidewire (f)

4.4 Results

Digital subtraction venography (DSV)

Evaluation of the vertebral venous plexus was successful in 3 of 6 dogs in which DSV was performed. Evaluation of pre-compression images revealed maximal opacification of the cervical vertebral venous plexus in the 3 dogs in frames 11 (5.5 seconds) and 12 (6 seconds) of the 20 frames (10 seconds) of the DSV sequence. Vascular anatomy pattern of the cervical IVVP during pre-compression was consistent between the 3 dogs. The DSV images clearly depicted symmetrical right and left components of the IVVP and the intervertebral veins (Fig 4.7). Intervertebral veins located between C2/3, C3/4, C4/5, and C5/6 vertebral levels were represented by double vessels, visible on both sides of the cervical vertebral canal (Fig 4.7). Opacification of the external jugular veins was observed at the end of the DSV sequence, with maximal opacification in frames 16 to 20 (8 to 10 seconds). Transverse diameters of the IVVP ranged from 1.72 mm to 3.2 mm, with a mean of 2.54 ± 0.29 mm for the right IVVP, and 2.59 ± 0.45 mm for the left IVVP. Transverse diameters were maximal in the C1/2 vertebral region with a mean diameter of 3 ± 0.07 mm. The smallest diameter of the IVVP was observed at the C2/3 vertebral level with a mean diameter of 1.95 ± 0.31 mm. Distances between the right and left components of the IVVP was maximal over the atlas (C1) with a mean distance of 12.3 ± 0.73 mm. Distances between IVVP components had a mean of 8.5 ± 1.31 mm over the intervertebral spaces at C1/2; C2/3; C3/4; C4/5, C5/6. The distances between IVVP

components had a mean value of 1.02 ± 0.16 mm over vertebral bodies from C2 to C7. The vertebral veins were also identified on both sides of the vertebral canal, communicating with the IVVP via the intervertebral veins (Fig 4.7). The mean diameter of vertebral veins was 1.35 ± 0.28 mm.

The cervical IVVP, during compression, appeared optimal for evaluation at frame 12 (6 seconds) of the total 20 frames (10 seconds) of the DSV. Vertebral veins were also observed in these frames. Internal jugular veins were depicted at frames 11 (5.5 seconds) through 20 (10 seconds). The right external jugular vein was evident in frames 12 (6 seconds) through 20 (10 seconds). Transverse diameter of the left IVVP on the compression images had significantly lower values between the segments of C3 to C5 compared with pre-compression images. The mean transverse diameter of the IVVP for this region (C3-C5) was 1.25 ± 0.62 mm. Compression DSV images in all 3 dogs showed total or partial lack of filling with contrast medium of IVVP in areas of compression and segments adjacent to it (Fig 4.8). Post-compression images revealed maximal opacification of the IVVP in frames 11 (5.5 seconds) and 12 (6 seconds) of the DSV sequence. Vertebral veins were clearly visible in those frames. The right internal jugular vein was identified in frames 9 (4.5 seconds) through 20 (10 seconds) of the DSV run obtained during post-compression. The right external jugular veins were identified in frames 10 (5 seconds) through 20 (10 seconds) of the DSV series. Mean values of transverse diameters of the IVVP between C3 and C5 during post-compression were 1.75 ± 0.4 mm for the left side, and $1.55 \pm$

0.4 mm for the right side. Both diameter values were lower than pre-compression values but higher than compression values.

Computed tomographic venography

Evaluation of the postcontrast CT compression images revealed adequate visualization of the veins of the cervical spinal canal in 2 of the 3 dogs. One problem in images was the presence of hypoattenuating areas (-764 Hounsfield units) in the epidural space between C4-C7 in 2 dogs. These areas were most likely due to epidural air introduced during catheter placement (Fig 4.9). Also, streak artifacts due to hyperdense radiopaque markers of the angioplasty balloon catheter degraded soft tissue detail within the vertebral canal and made CT images of the IVVP difficult. However, evaluation of the IVVP in the remaining cervical vertebral segments was possible in all dogs (Fig 4.10). Mean transverse diameters of the IVVP for C1 to C7 in pre-compression CT venograms were 3.2 ± 0.98 mm for the right IVVP and 2.93 ± 1.39 mm for the left IVVP. The maximal transverse diameter of the IVVP was observed at C6 with a mean of 4.42 ± 0.20 mm for the right and left IVVP. The minimal transverse diameter of the IVVP during pre-compression was observed at C1 with a mean of 1.91 ± 0.39 mm for both components of the IVVP. Distance between medial borders of the IVVP was maximal over the atlas with 10.56 ± 1.12 mm between the right and left IVVP.

An additional CT venographic finding at the C2 level was the presence of two small ovoid enhanced structures each of about 0.3 mm in transverse

diameter (Fig 4.11). They were located dorsal to the IVVP and inside the dural sac. Those structures were interpreted to represent paired ventral spinal arteries based on the anatomical location and histologic examination of the spinal cord samples.

Computed tomographic venography images during compression showed no opacification of the right and left IVVP between C3-C5 vertebral levels in all 3 dogs (Fig 4.12). Measurements of transverse diameter of IVVP (mean: 3.16 ± 0.93 mm for left component, and 3.6 ± 1.06 mm for right component) and distance (mean: 7.45 ± 1.48 mm at intervertebral level, and 1 mm over the vertebral bodies) between right and left components of the IVVP during compression at C1, C1/2, C2 and C2-C3 vertebral segments were similar to pre-compression CT venography values. The transverse diameters values between C5 and C7 in one dog were also similar to pre-compression values (from all dogs) with a mean diameter of 4.32 ± 0.28 mm. In the other 2 dogs, gas in the epidural space seemed to collapse the IVVP.

Post-compression CT venography images did not demonstrate the IVVP between C3 and C4-C5 vertebral segments. Presence of epidural air within the

C6 and C7 vertebral canal in 2 dogs made it difficult to visualize the IVVP on post-compression CT venography images.

Digital subtraction venography and CT venography images demonstrate that in all 6 dogs the angioplasty balloon was located in the left side of the C3/4 vertebral canal. After experimental spinal cord compression 3 dogs presented spasmodic contraction of the neck toward the left side.

Histological examination

In all 6 dogs (3 DSV and 3 CT venography), spinal cord examination from the areas in direct contact with the angioplasty balloon catheter during compression were consistent with acute spinal cord trauma. Some of the transversely sectioned specimens revealed a central hemorrhagic core on gross examination (Fig 4.13). Under microscopic examination, 3 dogs had spinal cord samples with central tissue disruption, and cavitary lesions in the gray matter (Fig 4.14) with multiple areas of adjacent recent perivascular hemorrhage. Hemorrhage was principally located in the dorsal horn and central intermediate substance that surrounds the central canal (Fig 4.14). In 2 of these dogs, the presence of debris in the central canal was observed in areas cranial to the compression (C2). Also in 2 dogs, areas of hemorrhage in the epidural and subarachnoid space were identified in spinal cord samples cranial to compression (C2) (Table 4.1). The remaining 3 dogs showed unilateral and bilateral areas of recent perivascular hemorrhage. No abnormalities were

observed in the L4 spinal cord samples.

Statistical analysis

Measured values of vein diameters were compared between treatments (pre-compression, compression, and post-compression) in the DSV group and the CT venography group. Significant differences in the transverse diameters were found between pre-compression and compression in the left IVVP at the C3 vertebral level ($p = 0.048$) (Fig 4.15). Also, the transverse diameter of the right IVVP at the C3/4 vertebral level differed ($p = 0.033$) between pre-compression and post-compression treatments.

Physiologic parameters

Evaluation of physiologic parameters showed a significant increase of mean arterial pressure (mean: 153 ± 62 mm Hg) during experimental spinal cord compression in all 6 included dogs (Table 4.2). A rapid increase in the systolic (mean: 203 ± 76 mm Hg) and diastolic (mean: 136 ± 39 mm Hg) blood pressures were observed immediately after inflation of the balloon catheter (Fig 4.16). Mean peak values during compression for systolic, diastolic and MAP were 239.5 ± 71.9 mm Hg, 149.7 ± 43.7 mm Hg, and 185 ± 56.9 mm Hg respectively. In 2 dogs, peak systolic pressures > 300 mm Hg were recorded at the middle of the compression period. Heart rates showed also a significant increase during compression (mean: 140 bpm) compared with pre-compression values (mean:

112 bpm). However, heart rates were within the referenced physiological ranges for the dog (70-150 bpm).

Mean end-tidal carbon dioxide concentrations (ETCO₂) were statistically different among pre-compression, compression and post-compression treatments (Table 4.2). However, mean values of ETCO₂ for the 3 periods were within the reference ranges for the dog. Following deflation of the angioplasty balloon, MAP, systolic pressure, diastolic pressure and heart rate values decreased gradually for a period of approximately 10 minutes until baseline values were reached (Fig 4.16).

Analysis of temperature, HCO₃, pH, pCO₂, pO₂, and O₂ saturation showed values for all treatments (pre-compression, compression, and post-compression) and dogs to be within references ranges (Table 4.3).

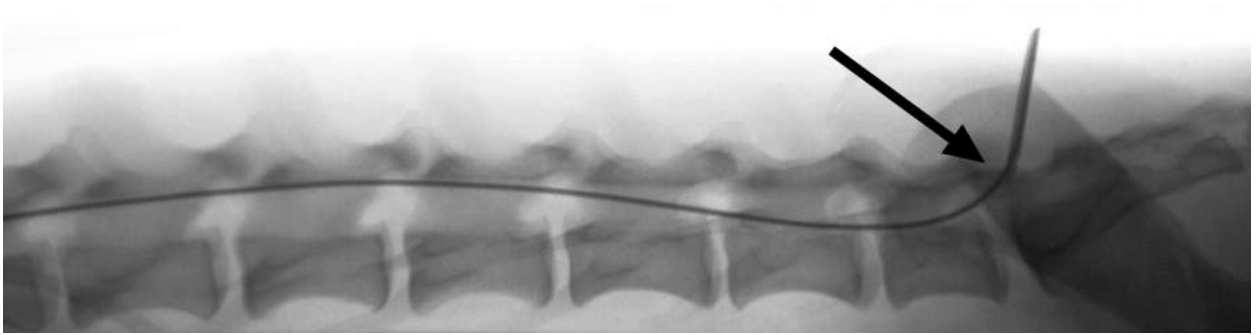


Figure 4.4 - Lateral digital radiograph of the lumbosacral area demonstrating a guidewire in place in the lumbar vertebral canal extending from the lumbosacral space (arrow).

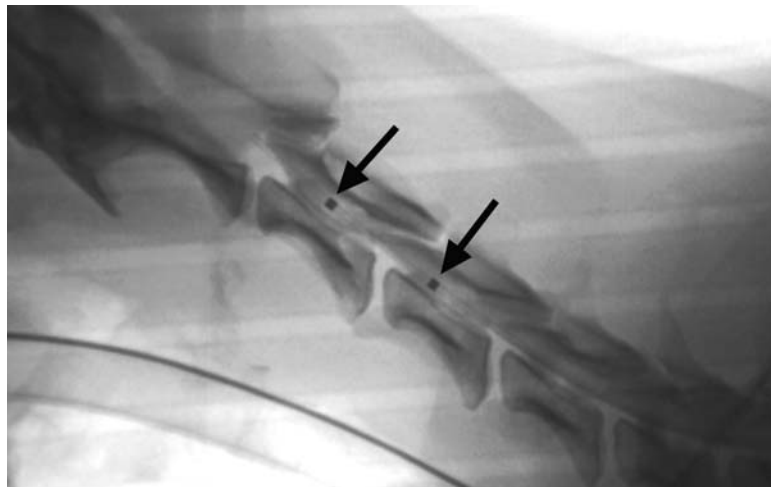


Figure 4.5 - Lateral digital radiograph of the cervical region in a dog showing the position of the angioplasty balloon catheter at C3/4. Arrows indicate the radiopaque markers of the angioplasty balloon catheter.

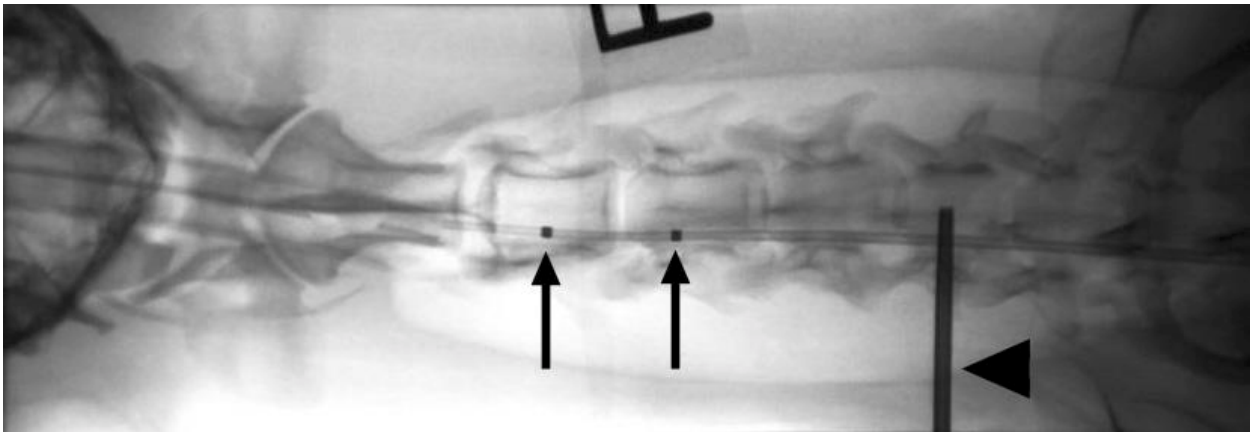
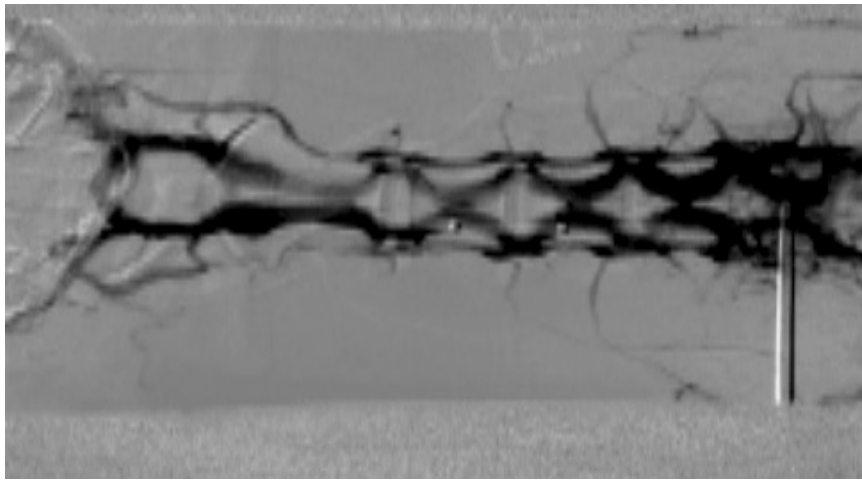
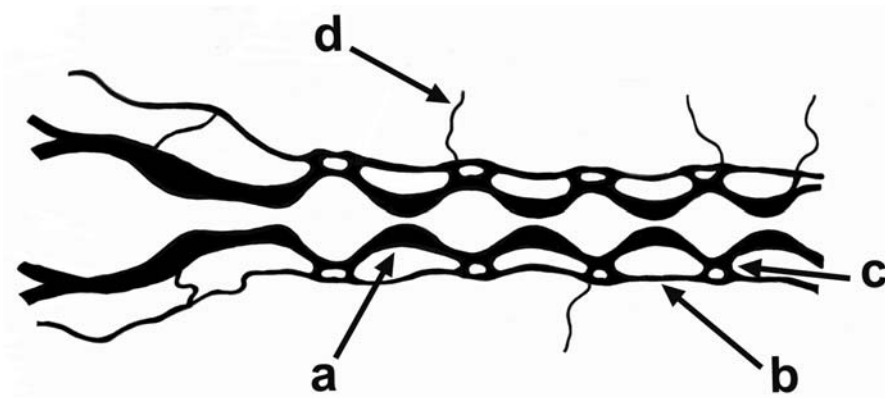


Figure 4.6 – Dorsoventral digital radiograph of the cervical region demonstrating the position of the angioplasty balloon catheter with its radiopaque markers (arrows) inside the C3/4 vertebral canal. The tip of the jamshidi is positioned within the body of C6 (arrowhead).

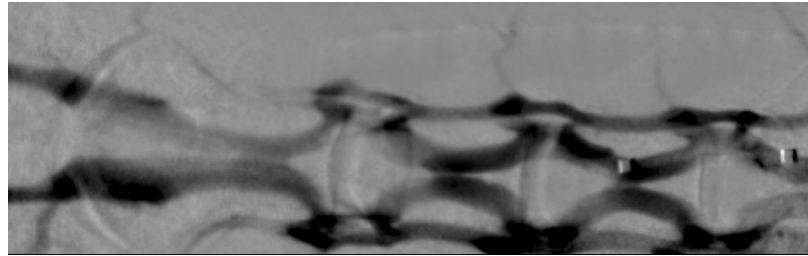


A

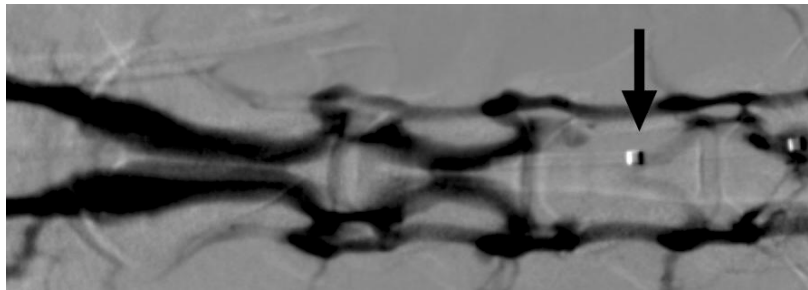


B

Figure 4.7 – Pre-compression digital subtraction venogram (A) and diagram (B) of the IVVP in the cervical region of a dog. Notice the symmetrical and undulating appearance of the cervical internal vertebral venous plexus. Internal vertebral venous plexus (a), vertebral vein (b), intervertebral vein (c), muscular branches (d). (Drawing made by the first autor).



A



B

Figure 4.8 - Magnified pre-compression (A) and compression (B) digital subtraction venograms of the cranial cervical region obtained from the same dog. Notice the bilateral lack of filling of the vertebral venous plexus in the area of compression (arrow) on image B.

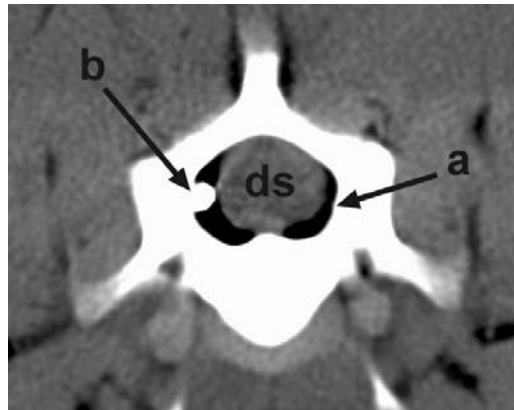


Figure 4.9 - Pre-compression transverse CT venographic image at the mid-portion of C7. Epidural air (a), angioplasty balloon catheter (b), dural sac (ds)

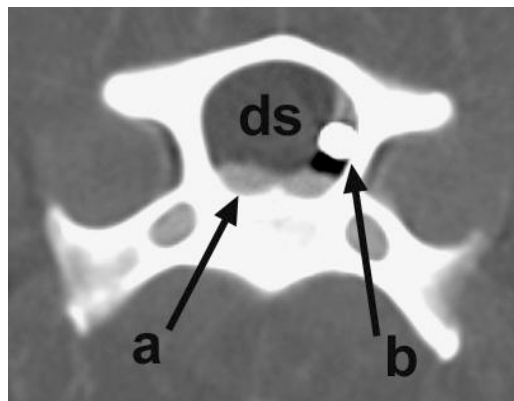


Figure 4.10 - Pre-compression transverse CT venographic image at the mid-portion of C5. Internal vertebral venous plexus (a), angioplasty balloon catheter with small air bubble in the epidural space (b), dural sac (c)

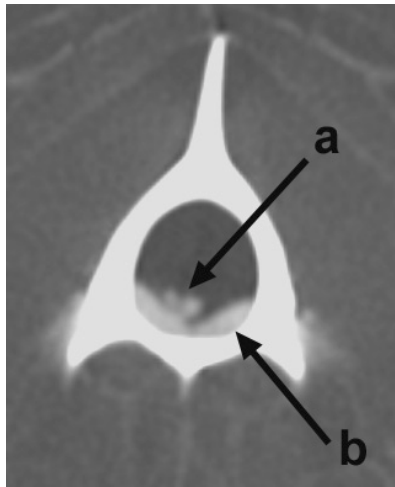


Figure 4.11 - Pre-compression transverse CT venographic image at the mid-portion of C2. Paired ventral spinal artery (a), internal vertebral venous plexus (b)

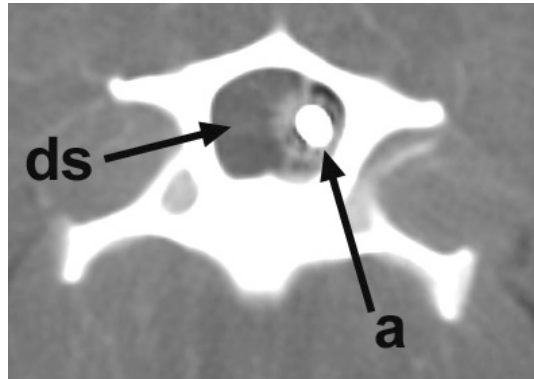


Figure 4.12 - Transverse CT venographic image at C4 during compression. Balloon radiopaque marker (a), dural sac (ds). Notice the right ventrolateral displacement of the dural sac, and the lack of filling of the internal vertebral venous plexus. The balloon radiopaque marker is surrounded by a hyperattenuating halo probably due to acute epidural hemorrhage. Radiating streak artifacts are also noted.

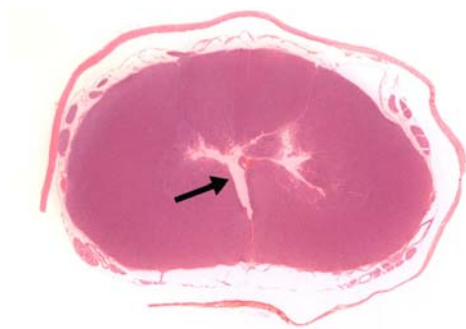


A

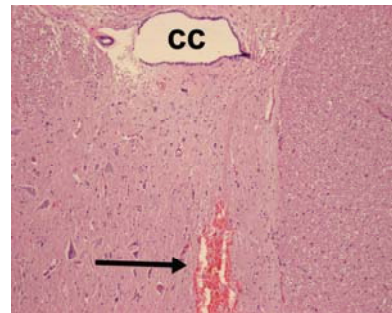


B

Figure 4.13 - Transverse views of compressed spinal cord sections obtained at C4 (A) and C5 (B) spinal cord segments from 2 dogs. Notice the central area of hemorrhage in both cases.



A



B

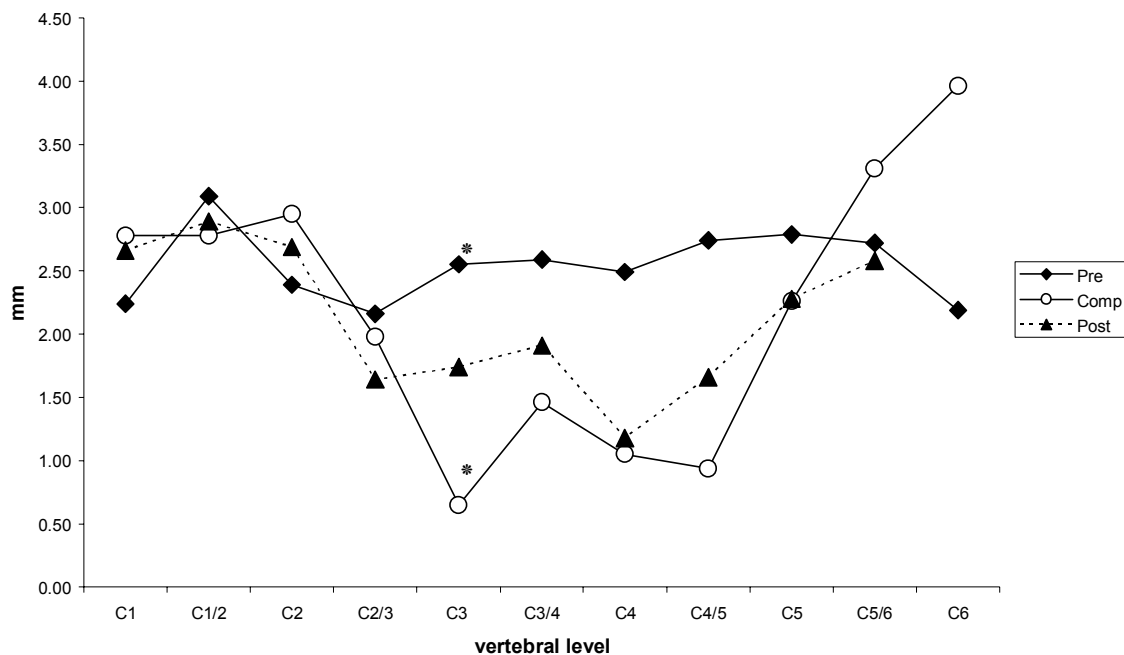
Figure 4.14 - Histological images from two different C4 compressed spinal cord samples (Hematoxyline and eosin).

A. Histological transverse image of C4 spinal cord segment showing a cavitory central lesion (arrow) (4x). B. Area of hemorrhage (arrow) located at the intermediate central substance and adjacent to the central canal (cc)(10x).

Dog N	Imaging Technique	Imaging Findings	Histopathologic Findings
1	DSV	<u>Compression:</u> Lack of filling of IVPr between C2/3 and C4/5. IJV evident in right side. EJV evident in right side. <u>Post-compression:</u> Lack of filling between C2/3 and C5/6.	Small areas of hemorrhage in dorsal horn at C4. Areas of hemorrhage in intermediate substance at C6. Debris in central canal at C8 spinal cord segment
2	DSV	<u>Compression:</u> Lack of filling of IVVP between C2/3 and C4/5. <u>Post-compression:</u> Lack of filling of IVVP between C2/3 and C5.	Focal perivascular hemorrhage in ventral horn of C5. Areas of hemorrhage at intermediate substance at C7. Small dorsal subarachnoid hemorrhage at C1.
3	DSV	<u>Compression:</u> Lack of filling of IVVP at C3, IVPr at C3/4 and from C4 to C4/5. <u>Post-compression:</u> Lack of filling of IVVP at C4.	Perivascular hemorrhages in dorsal horn and intermediate gray matter of C7. Bilateral recent hemorrhage at C2.
4	CT venography	<u>Compression:</u> Presence of hypodense areas of -764 HU (air bubbles) in ventral epidural space between C3 to C4/5 obstructs the IVVP. Also at C6/7. <u>Post-compression:</u> Presence of hypodense round areas (air bubbles) in epidural space between C2 and C7 that obstructs the IVVP.	Tissue disruption and cavitary lesion with hemorrhage in dorsal horn and intermediate substance at C4. Small unilateral hemorrhage in dorsal horn of C8. Nervous tissue in central canal of C2, probably from a cavitary lesion.
5	CT venography	<u>Compression:</u> Small air bubbles at C1/2 and C4 and C5/6. Big vertebral veins at C4/5 <u>Post-compression:</u> Hypodense areas (air bubbles) in epidural space of C3 to C4. Central hyperattenuating area in spinal cord at C3/4 vertebral level.	Unilateral area of tissue disruption and multiple and extensive area of hemorrhage in dorsal horn of C3. Normal C8 spinal cord segment.
6	CT venography	<u>Compression:</u> Lack of filling with contrast medium of the IVVP bilaterally between C3 and C4/5. <u>Post-compression:</u> Lack of observation of the IVVP bilaterally between C3 and C7.	Tissue disruption of gray and white matter with areas of hemorrhage in C4 and C8. Focal recent areas of hemorrhage in ventral horn of C2.

Table 4.1 - Imaging and histopathological findings for 6 dogs, after experimental acute cervical spinal cord compression.

Figure 4.15 - Mean transverse diameters (mm) of the left IVVP measured from DSV and CT venograms during precompression, compression, and postcompression of the cervical spinal cord in 6 dogs (#)



*Indicate vertebral canal levels with statistically significant difference between treatments ($p \leq 0.05$)

#Data from 3 DSV and 3 CT venograms dogs were pooled for analysis

TABLE 4.2 - Physiological parameters recorded during pre-compression, compression, and post-compression

	Physiologic Parameters*				Blood Pressure		
	HR (bpm)	FR (bpm)	T (°F)	ETCO ₂ mm Hg	Systolic mm Hg	Diastolic mm Hg	MAP mm Hg
Pre-compression	112±12.6 ^a	9.2±2.8	96.2±3.1	37.1±4.4 ^a	106.6±16.8 ^a	73.4±16 ^a	86.8±15.8 ^a
Compression	140.3±23.9 ^b	9.7±2.7	95.1±3.1	42.1±9.5 ^b	203.4±76.4 ^b	136.8±58.5 ^b	153.2±61.5 ^b
Post-compression	130.6±15.6 ^b	9.7±2.1	95.0±3.6	40.5±6.5 ^b	124.5±23.97 ^c	83.6±20.1 ^a	99.9±21.4 ^a
References values ³¹⁹	50-170	9-20	99.5-102.6	35-45	120-140	80-100	100-110

Measures represent mean ± standard deviation values of the 6 dogs obtained at 5 minutes intervals during pre-compression and post-compression, and 1 minute intervals during compression (*)

HR= heart rate, FR= respiratory rate, ETCO₂= end-tidal carbon dioxide, MAP= mean arterial pressure, bpm= beats per minute or breaths per minute

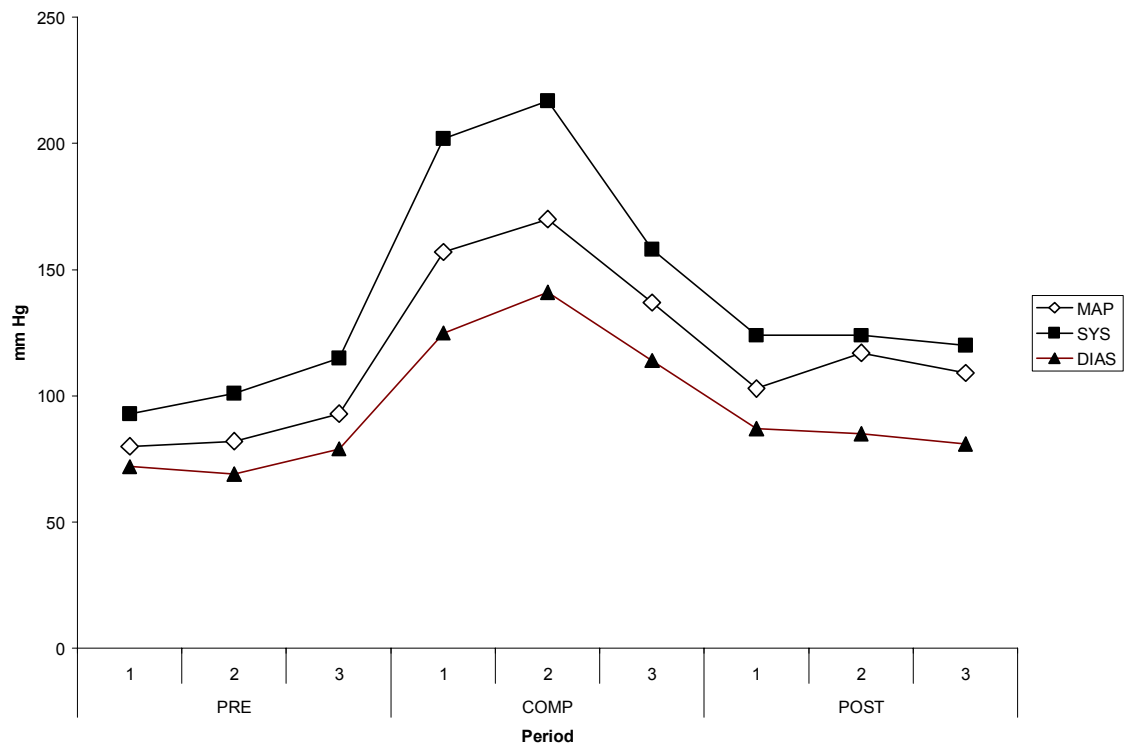
Significance set at $p < 0.05$. Different superscripts (^{a,b,c}) indicate significance differences in parameters between treatments

TABLE 4.3 - Arterial gas analysis results recorded during pre-compression, compression, and post-compression.

	Arterial Gas Analysis*				
	HCO ₃ mmHg	pH	pCO ₂ mmHg	pO ₂ mmHg	O ₂ Sat (%)
Pre-compression	20.2	7.4	36.0	516.0	99.9
Compression	20.6	7.28	44.4	519.8	99.8
Post-compression	19.4	7.3	37.5	515.7	99.9
Reference values ³¹⁹	16.6-22.8	7.32-7.46	27.7-41.2	> 100	96-98.2

Measured 10 minutes before compression (Pre-compression), 5 minutes after initiated compression (Compression), and 10 minutes after compression (Post-compression) in 6 dogs (*)

Figure 4.16 – Mean values for arterial blood pressure during pre-compression, compression and post-compression. Values from the 6 dogs were taken at the beginning (1), middle (2), and end (3) of the different periods. After initiated compression, systolic pressure increased markedly as is shown by the error bars in periods 1 and 2 of compression.



4.5 Discussion

Digital subtraction venography

In this study, DSV was one of two imaging modalities used to assess morphological variation of the cervical IVVP under experimental spinal cord compression. To our knowledge, this study represents the first report describing DSV for evaluation of the cervical IVVP in dogs. In our study, 3 DSV cases were successful. From 3 unsuccessful venograms, two had incomplete filling of the cervical IVVP immediately after intraosseous injection of contrast. One dog had a protruded annulus fibrosus, 1 dog had a misplacement of the biopsy needle into the C6 vertebra, and in the third dog no cause could be determined. In the 3 successful cases, intraosseous injection of contrast medium into the C6 vertebral body provided adequate opacification of the basivertebral veins and the rest of the cervical IVVP. Another reported site of injection for cervical venography in dogs is the wing of the atlas.⁶² The vertebral body of C6 was chosen based on results obtained on pilot study. The C6 vertebral body was easy to access from a midcervical lateral approach, and the position of the biopsy needle was caudal to the location of the angioplasty balloon catheter. Having at least one vertebral segment distance between the biopsy needle and balloon catheter was considered necessary to avoid superimposition of the 2 objects, and to facilitate visualization of the IVVP on dorsoventral DSV views. The valveless condition of the IVVP allows a single intraosseous injection to sufficiently opacify the venous plexuses.²⁰⁰ Some authors recommend that, during canine vertebral venography,

compression of the external jugular veins is essential, otherwise contrast material drains into the external jugular veins and the IVVP does not opacify.^{49,62} In our experiment we did not compress the jugular veins because we wanted to insure that the contrast medium would flow into the IVVP in a cranial direction. Digital subtraction venography was chosen over conventional venography for various reasons. Digital images obtained on DSV studies allowed manipulation of certain variables such as contrast, brightness and size of images that facilitate clarity and measurement of the selected object.^{56,320} Software for calibration allowed us to use distance between the radiopaque markers of the angioplasty balloon catheter as a magnification correction factor. These markers were located in the same geometric plane as the target IVVP.

Several factors can influence values of IVVP dimensions besides spinal cord compression or magnification. We designed our protocol to minimize the effects of these other factors as much as possible. The IVVP tends to collapse during inspiration and dilate during expiration.⁴¹ To minimize the effect of respiration, DSV and CT venography images in our study were obtained during induced apnea. Cardiopulmonary conditions in human beings can alter dimensions of the IVVP.³²¹ Congestive heart failure or chronic obstructive lung disease may elevate right atrial pressure, and subsequently venal caval pressure.³²¹ Elevation of central venous pressure is transmitted by collateral veins into the IVVP, thus producing distension of the IVVP. Dogs used in this

study were of the same breed, size and weight. This helped to minimize effects of normal anatomic variation on IVVP measurements.

Our results showed that the morphology of the cervical IVVP on pre-compression DSV images was in accordance with anatomical descriptions from the literature.^{36,38,50,51} Pre-compression DSV sequences also clearly demonstrated the anastomoses of the cervical IVVP with the intervertebral veins, vertebral veins, and cerebral veins. Transverse diameter measurements of the IVVP were slightly smaller than those measured in our previous CT morphometry study (see Chapter 3). The discrepancy between the 2 studies may be due to differences in sizes of the 2 dog populations under study or anatomic variation between subjects.

The current study indicated that DSV imaging characteristics and some dimensions of the cervical IVVP were affected by acute, experimental, extradural compression of the cervical spinal cord. Digital subtraction venography images showed regions of complete or partial lack of filling of the IVVP in areas associated with balloon compression. Previous studies in monkeys, using conventional venography and a similar balloon compression model in the lumbar region, also demonstrated total obstruction of the IVVP during balloon inflation.³²² Intraosseous and catheter epidural venography in human beings and dogs have been reported to display unilateral or bilateral block of the IVVP at the site of disk herniation.^{200,201,208,209} Venographic studies in human beings have also demonstrated that, in cases of cervical disk disease, interruption of the IVVP

usually occurs at multiple vertebral levels.²⁰⁸ Apparently, this multiple IVVP interruption pattern is observed more often than a single pattern. In human patients with intermittent claudication, magnetic resonance phlebography has shown areas of extensive filling defects of the IVVP at the lumbosacral region.⁶⁰

During compression, veins easily collapse due to their low internal pressure and wall laxity.²⁷⁹ Extradural compression induces a rapid increase of epidural pressure. Wolfa et al.,³²³ indicated that ventral cervical epidural pressure increases sharply when an epidural mass occupies more than 20% of the cervical vertebral canal space. According to our data, we estimate that our experimental model compromised more than 40% of the vertebral canal over C3 and C4 vertebral bodies. Therefore, our model seems to apply considerable pressure on cervical vertebral canal components.

During compression, distance between the components of the IVVP did not show variation comparative with compression or post-compression values. However, spinal conditions such as central protruded disk material or neoplastic masses inside the vertebral canal can increase the distance between IVVP components.²⁰⁸ The increase in distance between IVVP components was not observed in our dogs. This was probably caused by our lateral positioning of the angioplasty balloon catheter in the vertebral canal.

Our DSV findings during compression demonstrated increases in transverse diameters of the IVVP in areas immediately cranial or caudal to the spinal cord compression. Those values, were not statistically significant.

Magnetic resonance imaging studies in human beings have demonstrated that spinal compression from masses produce IVVP congestion.³²⁴ The venous congestion is due to blood accumulation in the venous sinuses cranial to the site of compression.³²⁵ We did not observe congestion of the IVVP during compression in our dogs. The most likely reason for this is that we only applied compression for 10 minutes. Probably, a longer period of experimental spinal cord compression would have been needed to cause venous congestion adjacent to the site of compression.

Post-compression DSV images of the cervical IVVP were variable. One dog had no change in IVVP morphology and 2 dogs had complete lack of opacification of the IVVP at the site of compression. This late and persistent lack of filling of the IVVP may have been due to spinal cord swelling following compression that constricted the IVVP. Similar observations were found by Doppman³²² who observed obstruction of the lumbar IVVP in primates, 4 hours after experimental spinal cord compression. In human beings with disk herniation or spinal neoplasia, long standing compression of the IVVP may result in irreversible occlusion of the venous plexus at the affected site, despite successful spinal cord decompression.^{142,208} Venous stasis produced during spinal cord compression may lead to white matter edema that subsequently exacerbates the spinal cord secondary damage and IVVP compression.^{27,142,211,280} Vasoactive agents (norepinephrine, serotonin, prostaglandin), known to be released during acute spinal cord compression, may also contribute to the persistent vertebral

venoconstriction observed on post-compression DSV images.³²⁶ Post-traumatic changes in the IVVP due to introduction of the angioplasty balloon catheter may also cause interference in the IVVP circulation and contribute to the post-compression venous collapse.

An interesting and consistent DSV finding was that external jugular veins were filled with contrast medium in earlier frames of compression and post-compression DSV studies (Frame 11) compared to pre-compression DSV studies (Frame 16 through 20). In one animal the internal jugular vein was visualized clearly during compression, but not during pre-compression and post-compression. These observations indicate that compression or factors associated with compression may produce alterations in hemodynamics of the IVVP and increase shunting of blood into communicating veins. Several authors have found that individuals with spinal cord injury presented with abnormal systemic venous circulation.^{275,327} Various factors are proposed for these altered venous hemodynamics findings. Spinal cord injury (SCI) can induce autonomic dysfunction that may alter the passive resistance of veins and promote changes in the IVVP flow.³²⁷ Changes in intra-abdominal pressure, associated with altered diaphragmatic and abdominal muscle function after SCI may also affect the caval and vertebral venous system flow.^{76,275} Viscosity of the contrast medium may be a factor to consider in IVVP venous fluctuations observed during compression. However, warming of the contrast medium at 42° C prior to injection in our study should have minimized the viscosity of iothalamate.

Computed tomographic venography

Non-selective CT venography evaluation of the cervical IVVP was also performed in 3 dogs during pre-compression, compression, and post-compression. The imaging protocol elaborated in our study was less invasive than intraosseous DSV, and more consistently resulted in adequate opacification of the venous structures inside the cervical vertebral canal. The two major limitations of the technique were the presence of epidural gas in the epidural space (discussed below) in 2 dogs, and presence of small streak artifacts produced by the radiopaque markers inside the vertebral canal. Another limitation of the CT venography technique compared with DSV was the inability to measure changes in IVVP flow dynamics for each treatment.

As in DSV, CT venography was able to demonstrate filling defects of the IVVP during experimental spinal compression. In 2 cases, CT venography showed displacement of the spinal cord toward the opposite site of compression; therefore, obliterating the contralateral IVVP. In two of the 3 CT venograms, air bubbles located in the ventral and lateral epidural space of the caudal cervical region were observed. These air filled bubbles adopted the contour of the epidural space and were able to compress the vertebral venous plexus. Air collection in the epidural space is reported to be an incidental finding, usually with no clinical importance.³²⁸ However, in rare occasions air collection can act as a mass lesion and produce clinical signs of radicular pain.^{328,329} This

phenomenon of air collection in the epidural space we believed was due to introduction of atmospheric air during the process of catheterization of the epidural space or via the biopsy needle used for contrast medium administration.

Spinal cord compression model and histological findings

The spinal compression technique used in this study produced consistent spinal cord compression in all 6 included dogs. This technique was modified from previous methods^{119,318} The previous models consisted of a subarachnoid introduction of the angioplasty balloon catheter by a lateral lumbar foraminal approach instead of the lumbosacral and epidural approach used in our study. The balloon model in both cases provided the advantage of avoiding an invasive surgical intervention such as laminectomy.³¹⁷ Laminectomy could significantly alter the hemodynamics of the IVVP, especially in the post compression period.³²² A previous report³¹⁸ described the grade of balloon expansion by using the spinal canal occlusion ratio (SCO). The SCO ratio was defined as the ratio of the balloon area to the spinal canal area, expressed as a percentage of occlusion. In their study, SCO ratios ranged from 12% in cases of compression using a 2 mm angioplasty balloon to 82% in cases using 7 mm angioplasty balloon. In this study we did not calculate the SCO. However, according with the SCO obtained from Purdy³¹⁸ for a 4 mm (28-56%) and 7 mm (62-82%) angioplasty balloon catheters, we believe the 6 mm balloon used in our study would likely have induced a SCO between 56 to 62%.

The model used in this study created similar histopathological changes to those seen in previous reports of dogs and human beings with acute spinal cord compression.¹⁴¹ Areas of perivascular hemorrhage and cavitory lesions, mainly in the gray matter, were identified. Central hemorrhage is believed to be due to rupture of post-capillary venules and sulcal arterioles, by either mechanical disruption directly from trauma, or from intravascular coagulation leading to venous stasis and distention.²⁷ Studies indicate that the degree of compression (balloon inflation) seems to be more important than the duration of compression in determining the severity of spinal cord damage.³¹⁸ However, in a clinical setting, spinal cord compression lesions are many times more complex and their duplication in experimental studies is impossible.¹⁶⁵

Physiological parameters

In all dogs, our compression model caused increases in systolic, diastolic and mean arterial pressure (MAP). The arterial hypertension occurred immediately after inflation of the balloon and persisted until approximately 10 minutes following deflation of the balloon. Many authors describe an initial decrease in MAP following spinal cord lesions.^{120,330,331} Other studies have encountered a hypertensive response initially.^{140,160,332} This cardiovascular response is believed to be due to alteration in sympathetic nervous system. Some authors suggest that compression produces deformation of the vasoactive sympathetic neurons and tracts at the cervical region and initiation of a pressure response.¹⁴⁰ Another

possible explanation is an increase in epidural pressure producing a Cushing response, similar to cases with increased intracranial pressure and subsequent increased MAP.^{161,175}

Additional findings

In 3 dogs from our study a spasmodic contraction of the neck was observed during the experimental compression. The torticollis was toward the side of the balloon catheter location. It is possible the inflated balloon produced a unilateral compression or irritation of the spinal branches of the ipsilateral accessory nerve.^{333,334} These spinal branches originate from the lateral portion of the ventral gray column from the first to the seventh cervical spinal cord segment.³³⁵ The excessive accessory nerve activity in the compressed area will respond with contraction of the ipsilateral brachiocephalicus (*m. cleidocephalicus*) and trapezius (*m. trapezius*) muscles.³³³

Our study had several limitations. The study population was small. The data obtained from this small number of dogs was not intended to describe DSV or CT venographic findings on IVVP morphology in all cases of acute spinal cord compression. Rather, this was an exploratory study designed to evaluate a spinal cord compression model and 2 imaging techniques. Reports suggest agreement between CT angiography and digital subtraction angiography are very high ($r > 90\%$) for evaluation of vascular components.^{336,337} Despite the relative small study population, DSV and CT venography consistently demonstrated changes in

IVVP morphology during experimental spinal cord compression. Additionally, the spinal cord compression model used in our study represented a simple model for creating acute spinal cord damage in dogs. This experimental model has several advantages. First, this model provides an easy method to change the selected site of spinal cord compression. Under fluoroscopic guidance, the guidewire can be directed cranially or caudally without problems, facilitating placement of the angioplasty balloon catheter over the desired vertebral canal location. Second, radiopaque markers of the angioplasty balloon catheter are recognized on DSV images and can be used as reference objects if measurements are required. Finally, the model is minimally invasive, and produced consistent spinal cord lesions.

In conclusion, our study demonstrates alterations in cervical vertebral venous plexus morphology under experimental spinal cord compression in dogs. These variations in venous morphology were detected using digital subtraction venography and CT venography. The study also showed that the spinal cord compression model used in our study represents a consistent and reliable method for studying acute spinal cord injuries in dogs. We also found that acute spinal cord compression alters some physiological parameters. Further studies are needed to evaluate specific hemodynamic changes of the canine cervical IVVP under acute spinal cord compression conditions, and effects of acute spinal cord compression on physiologic parameters.

CHAPTER 5 GENERAL CONCLUSIONS

1 - The selective CT venography technique developed in our first experiment consistently opacified the internal vertebral venous plexus (IVVP), the external vertebral venous plexus, and the intervertebral veins in 6 canine cadavers. The injection technique was elaborated after selective ligation of major veins in the neck and administration of contrast medium plus gelatine mixture into the right external jugular vein. The scan protocol included contiguous 4 mm thick sections from the occipital region to the first thoracic vertebra and dogs positioned in sternal recumbency. CT scans depicted the cervical IVVP as symmetric, paired, uniformly hyperattenuating structures inside the cervical vertebral canal. Basivertebral veins were not visible in CT images, probably due to partial volume averaging with the bodies of the cervical vertebrae. Cadavers were later frozen and sectioned in the cervical region at 8 mm intervals. Localization and morphology of the cervical IVVP on transverse CT scans correlated well with that seen in frozen anatomic sections. Computed tomographic images of the cervical IVVP were in accordance with the anatomic descriptions reported in the literature. Results from this study provide a new anatomic reference for CT imaging studies of the morphology of the cervical vertebral venous plexus in dogs.

2 - The non-selective CT venography procedure developed in our second experiment was found to be an adequate imaging technique for visualization of the cervical IVVP in 6 live dogs. Peripheral intravenous administration of contrast medium was performed by an initial bolus injection followed by a continuous infusion. This injection technique produced consistent opacification of the IVVP structures. The injection protocol did not produce adverse reactions in the 6 dogs under study. Vertebral veins were not recognized on CT images, primarily due to a silhouette effect with the vertebral arteries. Non-selective CT venography allowed morphometric evaluation of the IVVP on transverse CT images. Computed tomography venography allowed quantitative evaluation of the vertebral canal, dural sac and vertebral bodies of the C3-C7 cervical segments. Findings indicate the size of the IVVP increases from C3 to C7 in normal dogs. The area of the epidural space occupied by the IVVP is relatively constant for the cervical segment with minor increases in the caudal cervical region. Comparison of the morphometric parameters at each cervical vertebral location demonstrated no correlation between dimensions of the IVVP and dimensions of other components of the vertebral canal. When C3-C7 vertebral segments were considered as a group, area measurements of the IVVP were significantly correlated with vertebral canal area and dural sac area. Significant correlations were also identified between the following dimensions: transverse diameter of the dural sac and mid-sagittal diameter of the vertebral canal; mid-sagittal diameter of the IVVP, mid-sagittal diameter of vertebral canal and area of

the vertebral canal; transverse diameter of the dural sac and transverse diameter of vertebral body; mid-sagittal diameter of the dural sac and mid-sagittal diameter of the vertebral body; and area of the vertebral canal and area of the dural sac. Results from this experiment indicated that non-selective CT venography is a safe, sensitive method for performing qualitative and quantitative analysis of the cervical IVVP in dogs.

3 - The digital subtraction venography technique (DSV), used in our third experiment, was successful in providing consistent opacification of the IVVP in 3 of 6 dogs. In 3 dogs, failure of the technique was attributable mainly to the vertebral intraosseous injection procedure. However, when intraosseous injection was successful, DSV images showed excellent visualization of the cervical IVVP morphology. Digital subtraction venography was valuable in providing information related with flow dynamics of the cervical IVVP. In dogs with experimental spinal cord compression, DSV demonstrated partial filling defects of the vertebral venous plexus in areas associated with compression. Also, during experimental compression, DSV was able to demonstrate a different venous flow pattern than that initially observed in pre-compression DSV images. Post-compression DSV images showed a persistent lack of filling of the IVVP in the cervical area previously subjected to compression.

4 - Non-selective CT venography was a less invasive and more consistent technique for observing the cervical IVVP than DSV in 3 out of 3 dogs with experimental compression. Computed tomographic images demonstrated, in areas of experimental compression, displacement of the dural sac and occlusion of both components of the IVVP. Radiopaque markers of the angioplasty balloon catheter used for experimental compression, produced small streak artifacts on CT scans that sometimes obscured visualization of the cervical IVVP.

5 - The modified experimental spinal cord compression technique used in our study was a reliable and consistent method for inducing acute cervical spinal cord compression in dogs. The angioplasty balloon catheter device used for spinal cord compression was easily introduced into the lumbar epidural space and advanced to the cervical region. Use of a guidewire and fluoroscopic equipment were necessary for advancement and proper placement of the angioplasty balloon catheter into the cervical epidural space. Inflation of the balloon and, gradation of compression was easy to perform and control. Inflation of the angioplasty balloon to a pressure of 4 atmospheres was adequate for producing consistent spinal cord compression. Additionally, the radiopaque balloon markers provided a good reference for calibrating vein diameter measurements. Histological examination of the compressed spinal cord areas demonstrated that our experimental model produced lesions consistent with

acute spinal cord injury, similar to those observed in previously reported clinical and experimental studies.

6 - The experimental spinal cord compression model produced alteration in blood pressure physiological parameters. Immediately after inflation of the angioplasty balloon, dogs experienced an increase in diastolic, systolic, and mean arterial pressure. Those parameters returned to baseline values after 10 minutes following the balloon deflation. Other variables such as heart rate and end-tidal carbon dioxide concentration had significantly different values between groups (pre-compression, compression and post-compression) but values were within references ranges reported for dogs.

7 – Comparision of mean IVVP transverse diameters between treatments (pre-compression, compression, and post-compression) indicated that: transverse diameters differed between compression and post-compression treatments for the left IVVP at the C3 vertebral level, and also between pre-compression and post-compression treatments for the right IVVP at the C3/4 vertebral level. Changes in the distance between the left and right IVVP for the treatments were also observed, but changes were not statistically significant.

In summary:

1. Computed tomographic venography is a safe and sensitive imaging modality for qualitative and quantitative evaluation of vertebral venous plexus morphology in the cervical region of dogs.
2. Computed tomographic venography and vertebral intraosseous digital subtraction venography are able to demonstrate early alterations in morphology of the cervical internal vertebral venous plexus under experimental extradural spinal cord compression.
3. Vertebral intraosseous digital subtraction venography was less consistent than computed tomographic venography in demonstrating complete opacification of the cervical IVVP in dogs.
4. The angioplasty balloon catheter model is a consistent and reliable technique for inducing acute cervical experimental extradural spinal cord compression in dogs.
5. Experimental acute cervical spinal cord compression produces alterations of diastolic, systolic and mean arterial pressure in dogs.

6. Experimental cervical spinal cord compression at C3/4 produced significant differences in the transverse diameter of the left IVVP at the C3 vertebral level compared to pre-compression values.

BIBLIOGRAPHY

1. World Association of Veterinary Anatomists. *Nomina Anatomica Veterinaria 4th ed, Nomina Histologica 2nd ed, Nomina Embryologica Veterinaria*. Zurich and Ithaca: World Association of Veterinary Anatomists, 1994.
2. Federative Committee on Anatomical Terminology. *Terminologia Anatomica*. Stuttgart: Thieme, 1998.
3. Dorland W. *Dorland's Illustrated Medical Dictionary*. 27th ed. Philadelphia: WB Saunders, 1988.
4. Noden D, Delahunta A. *The Embryology of Domestic Animals*. Baltimore: Williams & Wilkins, 1985.
5. Dyce K, Sack W, Wensing C. *Textbook of Veterinary Anatomy*. Third ed. Philadelphia: Elsevier Science, 2002.
6. Webb AA. Potential sources of neck and back pain in clinical conditions of dogs and cats: a review. *Vet J* 2003;165:193-213.
7. Evans H. The skeleton In: Evans H, ed. *Miller's Anatomy of the dog*. 3rd ed. Philadelphia: WB Saunders, 1993;122-218.
8. Watson AG, Evans HE, de Lahunta A. Ossification of the atlas-axis complex in the dog. *Anat Histol Embryol* 1986;15:122-138.
9. Burbidge HM, Thompson KC, Hodge H. Post natal development of the canine caudal cervical vertebrae. *Res Vet Sci* 1995;59:35-40.
10. Nickel R, Schummer A, Seiferle E. *The Anatomy of Domestic Animals: The Locomotor System of Domestic Mammals*: Blackwell Science, 1995. 1-487
11. Nickel R, Schummer A, Seiferle E. *Lehrbuch der anatomie der haustiere*. Berlin & Hamburg: Paul Parey, 1975. 1-522
12. Evans H. *Miller's Anatomy of the Dog*. Third ed. Philadelphia: WB Saunders Company, 1993. 1-1113
13. Watson AG, Stewart JS. Postnatal ossification centers of the atlas and axis in miniature schnauzers. *Am J Vet Res* 1990;51:264-268.
14. Schaller O. *Illustrated Veterinary Anatomical Nomenclature*. Stuttgart: F. Enke Verlag, 1992.1-614

15. Thacher C. Neuroanatomic and pathophysiologic aspects of intervertebral disc disease in the dog. *Probl Vet Med* 1989;1:337-357.
16. Evans H. Arthrology In: Evans H, ed. *Miller's Anatomy of the Dog*. 3rd ed, Philadelphia: WB Saunders, 1993;219-257.
17. Watson AG, Evans HE, de Lahunta A. Gross morphology of the composite occipito-atlas-axis joint cavity in the dog. *Anat Histol Embryol* 1986;15:139-146.
18. Bray JP, Burbidge HM. The canine intervertebral disk: Part one: structure and function. *J Am Anim Hosp Assoc* 1998;34:55-63.
19. King AS. *Physiological and Clinical Anatomy of the Domestic Mammals*. New York: Oxford University Press, 1987.24-30.
20. Coates JR. Intervertebral disk disease. *Vet Clin North Am Small Anim Pract* 2000;30:77-110.
21. Lammi P, Inkinen RI, von der Mark K, et al. Localization of type X collagen in the intervertebral disc of mature beagle dogs. *Matrix Biol* 1998;17:449-453.
22. Hermanson J, Evans H. The muscular system In: Evans H, ed. *Miller's Anatomy of the Dog*. 3rd ed, Philadelphia: WB Saunders, 1993;258-384.
23. Fletcher T. Spinal cord and meninges In: Evans HE, ed. *Miller's Anatomy of the Dog*. 3rd ed, Philadelphia: WB Saunders, 1993;800-828.
24. Catala M. Embryonic and fetal development of structures associated with the cerebro-spinal fluid in man and other species. Part I: The ventricular system, meninges and choroid plexuses. *Arch Anat Cytol Pathol* 1998;46:153-169.
25. Caulkins SE, Purinton PT, Oliver JE, Jr. Arterial supply to the spinal cord of dogs and cats. *Am J Vet Res* 1989;50:425-430.
26. Wells-Roth D, Zonenshayn M. Vascular anatomy of the spine. *Oper Tech Neurosurgery* 2003;6:116-121.
27. Tator CH, Koyanagi I. Vascular mechanisms in the pathophysiology of human spinal cord injury. *J Neurosurg* 1997;86:483-492.
28. Naka Y, Itakura T, Nakai K, et al. Microangioarchitecture of the feline spinal cord. Three-dimensional observation of blood vessel corrosion casts by scanning electron microscopy. *J Neurosurg* 1987;66:447-452.

29. Ireland WP, Fletcher TF, Bingham C. Quantification of microvasculature in the canine spinal cord. *Anat Rec* 1981;200:102-113.
30. Soutoul JH, Gouaze A, Castaing J, et al. The arteries of the cervical spinal cord in several experimental animals. Comparative study with human vascularization. *Arch Anat Histol Embryol* 1965;48:77-93.
31. Batson OV. The vertebral vein system. *Am J Roentgenol* 1957;78:195-212.
32. Groen RJ, Groenewegen HJ, van Alphen HA, et al. Morphology of the human internal vertebral venous plexus: a cadaver study after intravenous Araldite CY 221 injection. *Anat Rec* 1997;249:285-294.
33. Parkinson D. History of the extradural neural axis compartment. *Surg Neurol* 2000;54:422-431.
34. Smuts MM. The venous drainage of the cervical vertebrae of the ox (*Bos taurus* L.). *Onderstepoort J Vet Res* 1977;44:233-247.
35. Drager K. Uber die sinus columnae vertebralis des hundes und ihre Verbindungen zu Venen der Nachbarschaft. *Morphol Jb* 1937;80:579-598.
36. Worthman RP. The longitudinal vertebral venous sinuses of the dog: I. Anatomy. *Am J Vet Res* 1956;17:341-348.
37. Worthman RP. The longitudinal vertebral venous sinuses of the dog: II. Functional aspects. *Am J Vet Res* 1956;17:349.
38. Reinhardt K, Miller M, Evans H. The craniovertebral veins and sinuses of the dog. *Am J Anat* 1962;111:67-87.
39. Wieboldt A. Venen der koperwand des hundes un der katze. Thesis, Hannover, 1966.
40. Crock H. The arterial supply and venous drainage of the vertebral column of the dog. *J Anat* 1960;94:88-99.
41. Herlihy J. Experimental studies on the internal vertebral venous plexus. *Essays Biol* 1948;1:152-163
42. Wiley A, Trueta J. The vascular anatomy of the spine and its relationship to pyogenic vertebral osteomyelitis. *J Bone Joint Surg* 1959;41B:796-809.

43. Konerding MA, Blank M. The vascularization of the vertebral column of rats. *Scanning Microsc* 1987;1:1727-1732.
44. Dommissie GF. The arteries, arterioles, and capillaries of the spinal cord. Surgical guidelines in the prevention of postoperative paraplegia. *Ann R Coll Surg Engl* 1980;62:369-376.
45. Rauhut D. Venen der Koperwand der kleinen Wiederkäuer: Ziege und Schaf. Thesis, Hannover, 1962.
46. Harrison R, Tomlinson J. Observations on the venous system in certain Pinnipedia and Cetacea. *Proc Zool Soc Lond* 1956;126:205-233.
47. Baumel J. Aves heart and blood vessels In: Getty R, ed. *Sisson and Grossman's the Anatomy of the Domestic Animals*. 5th ed, Philadelphia: WB Saunders, 1975;1968-2009.
48. Zippel KC, Lillywhite HB, Mladinich CR. New vascular system in reptiles: anatomy and postural hemodynamics of the vertebral venous plexus in snakes. *J Morphol* 2001;250:173-184.
49. Sturion DJ. Estudo anatomico dos plexos venosos vertebrais no cao. *Ciência Rural* 1993;23.
50. Evans H. Veins In: Evans H, ed. *Miller's Anatomy of the Dog*. 3rd ed, Philadelphia: WB Saunders, 1993;682-716.
51. Barone R. *Anatomie Comparee des Mammiferes Domestiques*. Paris: Vigot, 1996.575-579.
52. Parke W. Applied anatomy of the spine In: Herkowitz H, Garfin S, Balderston R, et al., eds. *The Spine*. 3rd ed, Philadelphia: WB Saunders Company, 1992.35-88
53. Reesink EM, Wilmsink JT, Kingma H, et al. The internal vertebral venous plexus prevents compression of the dural sac during atlanto-axial rotation. *Neuroradiology* 2001;43:851-858.
54. Gray H, Bannister L, Berry M, et al. *Gray's Anatomy: The Anatomical Basis of Medicine & Surgery*. 38th ed: Churchill Livingstone, 1995.1593-1595
55. Ghoshal N. *The Venous Drainage of the Domestic Animals*. Philadelphia: WB Saunders, 1981.84-89

56. Gershater R, St. Louis E. Lumbar epidural venography In: Kricun ME, ed. *Imaging Modalities in Spinal Disorders*. Philadelphia: WB Saunders, 1988. 557-573.
57. Crock HV, Goldwasser M. Anatomic studies of the circulation in the region of the vertebral end-plate in adult Greyhound dogs. *Spine* 1984;9:702-706.
58. Forderreuther S, Yousry I, Empl M, et al. Dilated cervical epidural veins and extra arachnoid fluid collection in orthostatic headaches. *Neurology* 2001;57:527-529.
59. Chun JY, Dillon WP, Berger MS. Symptomatic enlarged cervical anterior epidural venous plexus in a patient with Marfan syndrome. *AJNR Am J Neuroradiol* 2002;23:622-624.
60. Manaka M, Komagata M, Endo K, et al. Assessment of lumbar spinal canal stenosis by magnetic resonance phlebography. *J Orthop Sci* 2003;8:1-7.
61. Okumura R, Asato R, Fukuyama H, et al. Epidural venous system (meningorachidian venous plexus) in juvenile amyotrophy of distal upper extremity: assessment with GD-DTPA enhanced volumetric MR study. *Comput Med Imaging Graph* 1994;18:193-202.
62. Singh G, Bhargava A, Mogha I. Note on experimental intraosseous vertebral venography in dogs, goats and pigs. *Indian J Anim Sci* 1982;52:611-613.
63. Sliwa JA, Maclean IC. Ischemic myelopathy: a review of spinal vasculature and related clinical syndromes. *Arch Phys Med Rehabil* 1992;73:365-372.
64. Pluhar GE, Tucker RL, Gavin PR, et al. Cerebral sinus venography in the dog: a new technique. *Vet Radiol Ultrasound* 1997;38:112-115.
65. Applewhite AA, Wilkens BE, McDonald DE, et al. Potential central nervous system complications of von Willebrand's disease. *J Am Anim Hosp Assoc* 1999;35:423-429.
66. Testut L, Latarjet A. *Tratado de Anatomia Humana*. Barcelona: Salvat editores SA, 1979.
67. LaBan MM, Wilkins JC, Wesolowski DP, et al. Paravertebral venous plexus distention (Batson's): an inciting etiologic agent in lumbar

radiculopathy as observed by venous angiography. *Am J Phys Med Rehabil* 2001;80:129-133.

68. Russell EJ, D'Angelo CM, Zimmerman RD, et al. Cervical disk herniation: CT demonstration after contrast enhancement. *Radiology* 1984;152:703-712.

69. Ibukuro K, Fukuda H, Mori K, et al. Topographic anatomy of the vertebral venous system in the thoracic inlet. *AJR Am J Roentgenol* 2001;176:1059-1065.

70. Macnab I, St Louis EL, Grabias SL, et al. Selective ascending lumbosacral venography in the assessment of lumbar-disc herniation. An anatomical study and clinical experience. *J Bone Joint Surg Am* 1976;58:1093-1098.

71. Grenier N, Greselle JF, Douws C, et al. MR imaging of foraminal and extraforaminal lumbar disk herniations. *J Comput Assist Tomogr* 1990;14:243-249.

72. Haughton V, Williams A. *Computed tomography of the spine*. St. Louis: The C.V. Mosby Co, 1982.1-252.

73. Demondion X, Delfaut EM, Drizenko A, et al. Radio-anatomic demonstration of the vertebral lumbar venous plexuses: an MRI experimental study. *Surg Radiol Anat* 2000;22:151-156.

74. Genevay S, Palazzo E, Hutten D, et al. Lumboradiculopathy due to epidural varices: two case reports and a review of the literature. *Joint Bone Spine* 2002;69:214-217.

75. Gargano FP, Meyer JD, Sheldon JJ. Transfemoral ascending lumbar catheterization of the epidural veins in lumbar disk disease. Clinical application and results in the diagnosis of herniated intervertebral disks of the lumbar spine. *Radiology* 1974;111:329-336.

76. Eckenhoff JE. The physiologic significance of the vertebral venous plexus. *Surg Gynecol Obstet* 1970;131:72-78.

77. Suzuki T, Kurokawa K, Okabe K, et al. Correlation between the prostatic vein and vertebral venous system under various conditions. *Prostate* 1992;21:153-165.

78. Pritchard JA, Barnes AC, Bright RH. The effect of the supine position on renal function in the near-term pregnant woman. *J Clin Invest* 1955;34:777-781.
79. Hirabayashi Y, Shimizu R, Fukuda H, et al. Effects of the pregnant uterus on the extradural venous plexus in the supine and lateral positions, as determined by magnetic resonance imaging. *Br J Anaesth* 1997;78:317-319.
80. Youmans WB, Murphy QR, Turner JK, et al. Activity of abdominal muscles elicited from the circulatory system. *Am J Phys Med* 1963;42:1-70.
81. Suzuki T, Shimizu T, Kurokawa K, et al. Pattern of prostate cancer metastasis to the vertebral column. *Prostate* 1994;25:141-146.
82. Eckenhoff JE. The vertebral venous plexus. *Can Anaesth Soc J* 1971;18:487-495.
83. Valdueza JM, von Munster T, Hoffman O, et al. Postural dependency of the cerebral venous outflow. *Lancet* 2000;355:200-201.
84. Schreiber SJ, Lurtzing F, Gotze R, et al. Extrajugular pathways of human cerebral venous blood drainage assessed by duplex ultrasound. *J Appl Physiol* 2003;94:1802-1805.
85. Zenker W, Bankoul S, Braun JS. Morphological indications for considerable diffuse reabsorption of cerebrospinal fluid in spinal meninges particularly in the areas of meningeal funnels. An electronmicroscopical study including tracing experiments in rats. *Anat Embryol (Berl)* 1994;189:243-258.
86. Zenker W, Kubik S. Brain cooling in humans--anatomical considerations. *Anat Embryol (Berl)* 1996;193:1-13.
87. Groen RJ, Ponssen H. The spontaneous spinal epidural hematoma. A study of the etiology. *J Neurol Sci* 1990;98:121-138.
88. Kreppel D, Antoniadis G, Seeling W. Spinal hematoma: a literature survey with meta-analysis of 613 patients. *Neurosurg Rev* 2003;26:1-49.
89. Oldenkott P, Driesen W. Spontaneous epidural hematoma in the thoracic spinal canal during long-term therapy with anticoagulants. *Med Welt* 1966;6:305-307.
90. Levy A, Stula D. Neurosurgical aspects of central nervous system hemorrhages due to anticoagulants. *Dtsch Med Wochenschr* 1971;96:1043-1048.

91. Amsellem P, Toombs J, Laverty P, et al. Loss of deep pain sensation following thoracolumbar intervertebral disk herniation in dogs: Pathophysiology. *Compend Contin Educ Pract Vet* 2003;25:256-264.
92. Coman DR, de LR. The role of the vertebral venous system in the metastasis of cancer to the spinal column; experiments with tumor-cell suspensions in rats and rabbits. *Cancer* 1951;4:610-618.
93. Shevrin DH, Kukreja SC, Ghosh L, et al. Development of skeletal metastasis by human prostate cancer in athymic nude mice. *Clin Exp Metastasis* 1988;6:401-409.
94. Oeppen RS, Tung K. Retrograde venous invasion causing vertebral metastases in renal cell carcinoma. *Br J Radiol* 2001;74:759-761.
95. Poncelet A, Coppens A, Grauwels M, et al. Metastases d'un pheochromomocytome entreprenant le systeme nerveux central chez un chien. *Annales de Medecine Veterinaire* 2000;144:95-98.
96. Moore GE, Mathey WS, Eggers JS, et al. Osteosarcoma in adjacent lumbar vertebrae in a dog. *J Am Vet Med Assoc* 2000;217:1038-1040.
97. Thomas WB. Diskospondylitis and other vertebral infections. *Vet Clin North Am Small Anim Pract* 2000;30:169-182.
98. Penwick R. Fibrocartilaginous embolism and ischemic myelopathy. *Compend Contin Educ Pract Vet* 1989;11:287-297.
99. Zaki FA, Prata RG. Necrotizing myelopathy secondary to embolization of herniated intervertebral disk material in the dog. *J Am Vet Med Assoc* 1976;169:222-228.
100. Cauzinille L. Fibrocartilaginous embolism in dogs. *Vet Clin North Am Small Anim Pract* 2000;30:155-167.
101. Spetzler RF, Detwiler PW, Riina HA, et al. Modified classification of spinal cord vascular lesions. *J Neurosurg* 2002;96:145-156.
102. Hayashida E, Ochiai K, Kadosawa T, et al. Arteriovenous malformation of the cervical spinal cord in a dog. *J Comp Pathol* 1999;121:71-76.
103. Decker RE, San Augustin W, Epstein JA. Spinal epidural venous angioma causing foraminal enlargement and erosion of vertebral body. Case report. *J Neurosurg* 1978;49:605-606.

104. Hallenbeck JM, Bove AA, Elliott DH. Mechanisms underlying spinal cord damage in decompression sickness. *Neurology* 1975;25:308-316.
105. Miyazawa K, Shiga Y, Hasegawa T, et al. CSF hypovolemia vs intracranial hypotension in "spontaneous intracranial hypotension syndrome". *Neurology* 2003;60:941-947.
106. Mokri B. The Monro-Kellie hypothesis: Applications in CSF volume depletion. *Neurology* 2001;56:1746-1748.
107. Tator CH. Update on the pathophysiology and pathology of acute spinal cord injury. *Brain Pathol* 1995;5:407-413.
108. Kraus KH. The pathophysiology of spinal cord injury and its clinical implications. *Semin Vet Med Surg (Small Anim)* 1996;11:201-207.
109. Lu J, Ashwell K, Waite P. Advances in secondary spinal cord injury: role of apoptosis. *Spine* 2000;25:1859-1866.
110. Sekhon LH, Fehlings MG. Epidemiology, demographics, and pathophysiology of acute spinal cord injury. *Spine* 2001;26:S2-12.
111. Carlson GD, Gorden C. Current developments in spinal cord injury research. *Spine J* 2002;2:116-128.
112. Allen AR. Surgery of experimental lesion of spinal cord equivalent to crush injury of fracture dislocation of spinal column: preliminary report. *J A M A* 1911;57:878.
113. Wrathall JR. Spinal cord injury models. *J Neurotrauma* 1992;9 Suppl 1:S129-134.
114. Bresnahan J, Beattie M, Todd F, et al. A behavioral and anatomical analysis of spinal cord injury produced by a feed-back controlled mechanism. *Exp Neurol* 1987;95:548-570.
115. Fiford RJ, Bilston LE, Waite P, et al. A vertebral dislocation model of spinal cord injury in rats. *J Neurotrauma* 2004;21:451-458.
116. Vanicky I, Urdzikova L, Saganova K, et al. A simple and reproducible model of spinal cord injury induced by epidural balloon inflation in the rat. *J Neurotrauma* 2001;18:1399-1407.
117. Eidelberg E, Staten E, Watkins CJ, et al. Treatment of experimental spinal cord injury in ferrets. *Surg Neurol* 1976;6:243-246.

118. Tarlov IM. Acute spinal cord compression paralysis. *J Neurosurg* 1972;36:10-20.
119. Purdy PD, Duong RT, White CL, 3rd, et al. Percutaneous translumbar spinal cord compression injury in a dog model that uses angioplasty balloons: MR imaging and histopathologic findings. *AJNR Am J Neuroradiol* 2003;24:177-184.
120. Guha A, Tator CH. Acute cardiovascular effects of experimental spinal cord injury. *J Trauma* 1988;28:481-490.
121. Bergman R, Lanz O, Shell L. Acute spinal cord trauma: mechanism and clinical syndromes. *Vet Med* 2000;95:846-849.
122. Dumont RJ, Okonkwo DO, Verma S, et al. Acute spinal cord injury, Part I: pathophysiologic mechanisms. *Clin Neuropharmacol* 2001;24:254-264.
123. de Haan P, Kalkman CJ, Jacobs MJ. Pharmacologic neuroprotection in experimental spinal cord ischemia: A systematic review. *J Neurosurg Anesthesiol* 2001;13:3-12.
124. Vaziri ND, Lee YS, Lin CY, et al. NAD(P)H oxidase, superoxide dismutase, catalase, glutathione peroxidase and nitric oxide synthase expression in subacute spinal cord injury. *Brain Res* 2004;995:76-83.
125. Dirnagl U, Iadecola C, Moskowitz MA. Pathobiology of ischaemic stroke: an integrated view. *Trends Neurosci* 1999;22:391-397.
126. Kwon BK, Tetzlaff W, Grauer JN, et al. Pathophysiology and pharmacologic treatment of acute spinal cord injury. *Spine J* 2004;4:451-464.
127. Howe LM, Boothe HW, Jr. Nitric oxide: A review for veterinary surgeons. *Vet Surg* 2001;30:44-57.
128. Dijkers MP. Searching the literature for information on traumatic spinal cord injury: the usefulness of abstracts. *Spinal Cord* 2003;41:76-84.
129. Wrathall JR, Teng YD, Choiniere D. Amelioration of functional deficits from spinal cord trauma with systemically administered NBQX, an antagonist of non-N-methyl-D-aspartate receptors. *Exp Neurol* 1996;137:119-126.
130. Xu GY, Hughes MG, Ye Z, et al. Concentrations of glutamate released following spinal cord injury kill oligodendrocytes in the spinal cord. *Exp Neurol* 2004;187:329-336.

131. Brand-Schieber E, Lowery SL, Werner P. Select ionotropic glutamate AMPA/kainate receptors are expressed at the astrocyte-vessel interface. *Brain Res* 2004;1007:178-182.
132. Voitenko N, Gerber G, Youn D, et al. Peripheral inflammation-induced increase of AMPA-mediated currents and Ca²⁺ transients in the presence of cyclothiazide in the rat substantia gelatinosa neurons. *Cell Calcium* 2004;35:461-469.
133. De Riu PL, Petruzzi V, Caria MA, et al. Beta-endorphin and cortisol levels in plasma and CSF following acute experimental spinal traumas. *Physiol Behav* 1997;62:1-5.
134. Segatore M, Way C. Neuroprotection after spinal cord injury: State of the science. *SCI Nurs* 1997;14:8-18.
135. Faden AI, Jacobs TP, Smith GP, et al. Neuropeptides in spinal cord injury: Comparative experimental models. *Peptides* 1983;4:631-634.
136. Sandor P, Reivich M, Komjati K. Significance of endogenous opioids in the maintenance of cerebral and spinal vascular CO₂-sensitivity in deep hemorrhagic hypotension. *Brain Res Bull* 2003;59:433-438.
137. Faden AI, Jacobs TP. Effect of TRH analogs on neurologic recovery after experimental spinal trauma. *Neurology* 1985;35:1331-1334.
138. Chu KT, Tator CH, Tymianski M. Calcium and Neuronal Death in Spinal Neurons In: Kalb R, Strittmatter S, eds. *Neurobiology of Spinal Cord Injury*. Totowa: Humana Press, 2000.
139. Guha A, Tator CH, Rochon J. Spinal cord blood flow and systemic blood pressure after experimental spinal cord injury in rats. *Stroke* 1989;20:372-377.
140. Rawe SE, Lee WA, Perot PL, Jr. The histopathology of experimental spinal cord trauma. The effect of systemic blood pressure. *J Neurosurg* 1978;48:1002-1007.
141. Norenberg MD, Smith J, Marcillo A. The pathology of human spinal cord injury: Defining the problems. *J Neurotrauma* 2004;21:429-440.
142. Kato A. Disturbance of the circulation in the spinal cord with epidural neoplasm. *Med J Osaka Univ* 1985;35:63-71.

143. Popovich PG, Wei P, Stokes BT. Cellular inflammatory response after spinal cord injury in Sprague-Dawley and Lewis rats. *J Comp Neurol* 1997;377:443-464.
144. Ghirnikar RS, Lee YL, Eng LF. Chemokine antagonist infusion promotes axonal sparing after spinal cord contusion injury in rat. *J Neurosci Res* 2001;64:582-589.
145. Emery E, Aldana P, Bunge MB, et al. Apoptosis after traumatic human spinal cord injury. *J Neurosurg* 1998;89:911-920.
146. Kim DH, Vaccaro AR, Henderson FC, et al. Molecular biology of cervical myelopathy and spinal cord injury: role of oligodendrocyte apoptosis. *Spine J* 2003;3:510-519.
147. Shuman SL, Bresnahan JC, Beattie MS. Apoptosis of microglia and oligodendrocytes after spinal cord contusion in rats. *J Neurosci Res* 1997;50:798-808.
148. Profyris C, Cheema SS, Zang D, et al. Degenerative and regenerative mechanisms governing spinal cord injury. *Neurobiol Dis* 2004;15:415-436.
149. Balentine JD. Pathology of experimental spinal cord trauma. II. Ultrastructure of axons and myelin. *Lab Invest* 1978;39:254-266.
150. Balentine JD. Pathology of experimental spinal cord trauma. I. The necrotic lesion as a function of vascular injury. *Lab Invest* 1978;39:236-253.
151. Balentine JD, Greene WB, Bornstein M. In vitro spinal cord trauma. *Lab Invest* 1988;58:93-99.
152. Bareyre FM, Schwab ME. Inflammation, degeneration and regeneration in the injured spinal cord: insights from DNA microarrays. *Trends Neurosci* 2003;26:555-563.
153. Merkler D, Oertle T, Buss A, et al. Rapid induction of autoantibodies against Nogo-A and MOG in the absence of an encephalitogenic T cell response: implication for immunotherapeutic approaches in neurological diseases. *Faseb J* 2003;17:2275-2277.
154. Carlson GD, Gorden CD, Nakazawa S, et al. Sustained spinal cord compression: Part II: Effect of methylprednisolone on regional blood flow and recovery of somatosensory evoked potentials. *J Bone Joint Surg Am* 2003;85-A:95-101.

155. Carlson GD, Gorden CD, Oliff HS, et al. Sustained spinal cord compression: Part I: Time-dependent effect on long-term pathophysiology. *J Bone Joint Surg Am* 2003;85-A:86-94.
156. Dumont RJ, Verma S, Okonkwo DO, et al. Acute spinal cord injury, Part II: Contemporary pharmacotherapy. *Clin Neuropharmacol* 2001;24:265-279.
157. Fehlings MG, Bracken MB. Summary statement: The Sygen (GM-1 ganglioside) clinical trial in acute spinal cord injury. *Spine* 2001;26:S99-100.
158. Ferraro G, Alabed Y, Fournier A. Molecular targets to promote central nervous system regeneration. *Current Neurovascular Research* 2004;1:61-75.
159. McDonald J, Holekamp T, Howard M, et al. Repair of the injured spinal cord and the potential of embryonic stem cell transplantation. *J Neurotrauma* 2004. 21:383-393.
160. Tibbs PA, Young B, McAllister RG, et al. Studies of experimental cervical spinal cord transection. Part I: Hemodynamic changes after acute cervical spinal cord transection. *J Neurosurg* 1978;49:558-562.
161. Grady PA, Blaumanis OR. Physiologic parameters of the Cushing reflex. *Surg Neurol* 1988;29:454-461.
162. Young W. Spinal cord contusion models. *Prog Brain Res* 2002;137:231-255.
163. Furlan JC, Fehlings MG, Shannon P, et al. Descending vasomotor pathways in humans: correlation between axonal preservation and cardiovascular dysfunction after spinal cord injury. *J Neurotrauma* 2003;20:1351-1363.
164. Latr I, Nemecek S. Changes in systemic pressure during experimental injury of the thoracic spinal cord. *Sb Ved Pr Lek Fak Karlovy Univerzity Hradci Kralove Suppl* 1991;34:581-585.
165. Hitchon PW, Dyste GN, Osenbach RK, et al. Spinal cord blood flow in response to focal compression. *J Spinal Disord* 1990;3:210-219.
166. Olby N, Jeffery N. Pathogenesis of diseases of the central nervous system In: Slatter D, ed. *Textbook of Small Animal Surgery* 3rd ed: WB Saunders, 2003;1132-1147.

167. Greenhoot JH, Shiel FO, Mauck HP, Jr. Experimental spinal cord injury. Electrocardiographic abnormalities and fuchsinophilic myocardial degeneration. *Arch Neurol* 1972;26:524-529.
168. Krassioukov AV, Furlan JC, Fehlings MG. Autonomic dysreflexia in acute spinal cord injury: An under-recognized clinical entity. *J Neurotrauma* 2003;20:707-716.
169. Evans DE, Alter WA, 3rd, Shatsky SA, et al. Cardiac arrhythmias resulting from experimental head injury. *J Neurosurg* 1976;45:609-616.
170. Greenhoot JH, Mauck HP, Jr. The effect of cervical cord injury on cardiac rhythm and conduction. *Am Heart J* 1972;83:659-662.
171. Dewey CW. *A Practical Guide to Canine and Feline Neurology*. Ames: Iowa State Press, 2003.
172. Griffiths IR, Pitts LH, Crawford RA, et al. Spinal cord compression and blood flow. I. The effect of raised cerebrospinal fluid pressure on spinal cord blood flow. *Neurology* 1978;28:1145-1151.
173. Carlson GD, Oliff HS, Gorden C, et al. Cerebral spinal fluid pressure: Effects of body position and lumbar subarachnoid drainage in a canine model. *Spine* 2003;28:119-122.
174. Brearley J, Walsh K. Neurological disease In: Seymour C, Gleed R, eds. *BSAVA Manual of small animal anesthesia and analgesia*. Cheltenham: British small animal veterinary association, 1999.
175. Dickinson CJ. Reappraisal of the Cushing reflex: The most powerful neural blood pressure stabilizing system. *Clin Sci (Lond)* 1990;79:543-550.
176. Davis H. Nursing Management of traumatic brain injured patients. *Vet Tech* 2004:249-254.
177. Beal MW, Paglia DT, Griffin GM, et al. Ventilatory failure, ventilator management, and outcome in dogs with cervical spinal disorders: 14 cases (1991-1999). *J Am Vet Med Assoc* 2001;218:1598-1602.
178. Winslow C, Rozovsky J. Effect of spinal cord injury on the respiratory system. *Am J Phys Med Rehabil* 2003;82:803-814.
179. Kube S, Owen T, Hanson S. Severe respiratory compromise secondary to cervical disk herniation in two dogs. *J Am Anim Hosp Assoc* 2003;39:513-517.

180. el-Bohy AA, Schrimsher GW, Reier PJ, et al. Quantitative assessment of respiratory function following contusion injury of the cervical spinal cord. *Exp Neurol* 1998;150:143-152.
181. Atkinson PP, Atkinson JL. Spinal shock. *Mayo Clin Proc* 1996;71:384-389.
182. Cash WC, Leipold HW, Blauch BS. Clinical findings in experimental lesions of the bovine spinal cord and dorsal rootlets. *Zentralbl Veterinarmed A* 1986;33:491-503.
183. Schadt JC, Barnes CD. Motoneuron membrane changes associated with spinal shock and the Schiff-Sherrington phenomenon. *Brain Res* 1980;201:373-383.
184. Curry T, Dowdey J, Murry R. *Christensen's Physics of Diagnostic Radiology*. Philadelphia: Lea & Febiger, 1990.
185. Thrall D. *Textbook of Veterinary Diagnostic Radiology*. 4th ed, Philadelphia: WB Saunders, 2002.98-126.
186. Sande RD. Radiography, myelography, computed tomography, and magnetic resonance imaging of the spine. *Vet Clin North Am Small Anim Pract* 1992;22:811-831.
187. Jones J. Neuroimaging In: Braund K, ed. *Clinical Neurology in Small Animals: Localization, Diagnosis and Treatment*. Ivis, 2002. <http://www.ivis.org>.
188. Morgan J, Doval J, Samii V. *Radiographic Techniques: The Dog*. Hannover: Schlutersche, 1998. 101-126.
189. Hathcock JT, Stickle RL. Principles and concepts of computed tomography. *Vet Clin North Am Small Anim Pract* 1993;23:399-415.
190. Seeram E. *Computed Tomography: Physical Principles, Clinical Applications, and Quality Control*. Pennsylvania: WB Saunders Co, 2001.1-430
191. Stickle RL, Hathcock JT. Interpretation of computed tomographic images. *Vet Clin North Am Small Anim Pract* 1993;23:417-435.
192. Assheuer J, Sager M. *MRI and CT atlas of the dog*. Berlin: Blackwell Science, 1997.83-129.
193. Rydberg J, Liang Y, Teague SD. Fundamentals of multichannel CT. *Radiol Clin North Am* 2003;41:465-474.

194. Adams WH. The spine. *Clin Tech Small Anim Pract* 1999;14:148-159.
195. Hofer M. *CT Teaching Manual*. Dusseldorf: Georg Thieme Verlag, 2000.1-176.
196. Snellman M. Magnetic resonance imaging in canine spontaneous neurological disorders: an evaluation of equipment and methods. *Department of Clinical Sciences*. Helsinki: University of Helsinki, 2000.1-74.
197. Sether LA, Nguyen C, Yu SN, et al. Canine intervertebral disks: correlation of anatomy and MR imaging. *Radiology* 1990;175:207-211.
198. Schobinger RA, Krueger EG. Intraosseous epidural venography in the diagnosis of surgical diseases of the lumbar spine. *Acta Radiol Diagn (Stockh)* 1963;11:763-776.
199. Blevins E. The localization of spinal cord compression using transosseous vertebral venography in canis familiaris. Ames, IA: Thesis, Iowa State University, 1970.
200. Blevins E. Transosseous vertebral venography: A diagnostic aid in lumbosacral disease. *Vet Radiol* 1980;21:50-54.
201. Theron J. Cervicovertebral phlebography: Pathological results. *Radiology* 1976;118:73-81.
202. Amsler FR, Jr., Wilber MC. Intraosseous vertebral venography as a diagnostic aid in evaluating intervertebral-disc disease of the lumbar spine. *J Bone Joint Surg Am* 1967;49:703-712.
203. Lessmann FP, Perese DM. Intraosseous vertebral plexus venography, a new diagnostic method. *Neurochirurgia (Stuttg)* 1960;2:175-189.
204. Mathis JM, Barr JD, Belkoff SM, et al. Percutaneous vertebroplasty: a developing standard of care for vertebral compression fractures. *AJNR Am J Neuroradiol* 2001;22:373-381.
205. Jensen ME, Evans AJ, Mathis JM, et al. Percutaneous polymethylmethacrylate vertebroplasty in the treatment of osteoporotic vertebral body compression fractures: Technical aspects. *AJNR Am J Neuroradiol* 1997;18:1897-1904.

206. Jensen ME, Dion JE. Percutaneous vertebroplasty in the treatment of osteoporotic compression fractures. *Neuroimaging Clin N Am* 2000;10:547-568.
207. Peh WC, Gilula LA. Additional value of a modified method of intraosseous venography during percutaneous vertebroplasty. *AJR Am J Roentgenol* 2003;180:87-91.
208. Miyasaka K, Takei H, Ito T, et al. Catheter cervical vertebral venography. *Neuroradiology* 1978;16:413-415.
209. LePage JR. Transfemoral ascending lumbar catheterization of the epidural veins. Exposition and technique. *Radiology* 1974;111:337-339.
210. Bestawros OA, Vreeland OH, Goldman ML. Epidural venography in the diagnosis of lumbar spinal stenosis. *Radiology* 1979;131:423-426.
211. Lindblad G, Ljunggren G, Olsson S. On spinal cord compression in the dog. 1962;3:121-127.
212. Koblik P, Suter P. Lumbosacral vertebral sinus venography via transjugular catheterization in the dog. *Vet Radiol* 1981;22:69-77.
213. Hathcock JT, Pechman RD, Dillon AR, et al. Comparison of three radiographic contrast procedures in the evaluation of the canine lumbosacral canal. *Vet Radiol* 1988;29:4-15.
214. Lecouteur RA, Child G. Diseases of the spinal cord In: Ettinger S, ed. *Textbook of Veterinary Internal Medicine*. 3rd ed, Philadelphia: WB Saunders, 1989;624-701.
215. Morgan J, Bailey C. *Exercise in Veterinary Radiology: Spinal disease*. Napa: Venture Press, 2000.1-325.
216. Bailey CS, Morgan JP. Congenital spinal malformations. *Vet Clin North Am Small Anim Pract* 1992;22:985-1015.
217. Gibson K, Ihle S, Hogan P. Severe spinal cord compression caused by a dorsally angulated dens. *Prog Vet Neurol* 1995;6:55-57.
218. Lu D, Lamb CR, Targett MP. Results of myelography in seven dogs with myelomalacia. *Vet Radiol Ultrasound* 2002;43:326-330.
219. Rao K, Williams J, Lee B, et al. *MRI and CT of the Spine*. Baltimore: Williams & Wilkins, 1994.1-536.

220. Garcia-Real I, Kass PH, Sturges BK, et al. Morphometric analysis of the cranial cavity and caudal cranial fossa in the dog: A computerized tomographic study. *Vet Radiol Ultrasound* 2004;45:38-45.
221. Levitski RE, Lipsitz D, Chauvet AE. Magnetic resonance imaging of the cervical spine in 27 dogs. *Vet Radiol Ultrasound* 1999;40:332-341.
222. Hansen HJ. A pathologic-anatomical study on disc degeneration in dog. *Acta Orthop Scand* 1952;XI.
223. Olby NJ, Munana KR, Sharp NJ, et al. The computed tomographic appearance of acute thoracolumbar intervertebral disc herniations in dogs. *Vet Radiol Ultrasound* 2000;41:396-402.
224. Tidwell A, Specht A, Blaeser L, et al. Magnetic resonance imaging features of extradural hematomas associated with intervertebral disc herniation in a dog. *Vet Radiol & Ultrasound* 2002;43:319-324.
225. Sharp N, Wheeler SJ, Cofone M. Radiological evaluation of wobbler syndrome-cervical spondylopathy. *J Small Anim Pract* 1992;33:491-499.
226. Garosi L, Cauzinille L. Caudal cervical spondylo-myelopathy Part 1: Pathophysiology, diagnostic approach. *Prat Med Chir Anim Comp* 1999;34:129-134.
227. Drost WT, Lehenbauer TW, Reeves J. Mensuration of cervical vertebral ratios in Doberman pinschers and Great danes. *Vet Radiol Ultrasound* 2002;43:124-131.
228. Massicotte C, Jones J, Newman S, et al. Wobbler syndrome due to cervical stenosis in a Great dane puppy. *Canine Practice* 1999;24:18-20.
229. Sharp N, Cofone M, Robertson I, et al. Computed tomography in the evaluation of caudal cervical spondylomyelopathy of the Doberman pinscher. *Vet Radiol Ultrasound* 1995;36:100 -108.
230. Kaiser JA, Holland BA. Imaging of the cervical spine. *Spine* 1998;23:2701-2712.
231. Lipsitz D, Levitski RE, Chauvet AE, et al. Magnetic resonance imaging features of cervical stenotic myelopathy in 21 dogs. *Vet Radiol Ultrasound* 2001;42:20-27.

232. Abramson CJ, Dennis R, Smith KC, et al. Radiographic diagnosis--lateralized vertebral osseous compression causing cervical spondylomyelopathy in a Great Dane. *Vet Radiol Ultrasound* 2003;44:56-58.
233. Penderis J, Dennis R. Use of traction during magnetic resonance imaging of caudal cervical spondylomyelopathy ("wobbler syndrome") in the dog. *Vet Radiol Ultrasound* 2004;45:216-219.
234. Seguin B, Bagley RS, Silver GM. Diagnosis and treatment of spinal neoplasia in dogs and cats. *Waltham Focus* 2000;10:4-9.
235. Tidwell AS, Jones JC. Advanced imaging concepts: A pictorial glossary of CT and MRI technology. *Clin Tech Small Anim Pract* 1999;14:65-111.
236. Rudich SR, Feeney DA, Anderson KL, et al. Computed tomography of masses of the brachial plexus and contributing nerve roots in dogs. *Vet Radiol Ultrasound* 2004;45:46-50.
237. Kippenes H, Gavin PR, Bagley RS, et al. Magnetic resonance imaging features of tumors of the spine and spinal cord in dogs. *Vet Radiol Ultrasound* 1999;40:627-633.
238. Nesbit JW, Lourens DC, Williams MC. Spastic paresis in two littermate pups caused by *Toxoplasma gondii*. *J S Afr Vet Assoc* 1981;52:243-246.
239. Sorjonen DC. Myelitis and meningitis. *Vet Clin North Am Small Anim Pract* 1992;22:951-964.
240. Nykamp SG, Steffey MA, Scrivani PV, et al. Computed tomographic appearance of epidural empyema in a dog. *Can Vet J* 2003;44:729-731.
241. Baleriaux DL, Neugroschl C. Spinal and spinal cord infection. *Eur Radiol* 2004;14:E72-E83.
242. Gonzalo-Orden JM, Altonaga JR, Orden MA, et al. Magnetic resonance, computed tomographic and radiologic findings in a dog with discospondylitis. *Vet Radiol Ultrasound* 2000;41:142-144.
243. Seim HB. Conditions of the thoracolumbar spine. *Semin Vet Med Surg (Small Anim)* 1996;11:235-253.
244. Steffen F, Flueckiger M, Montavon PM. Traumatic atlanto-occipital luxation in a dog: Associated hypoglossal nerve deficits and use of 3-dimensional computed tomography. *Vet Surg* 2003;32:411-415.

245. Kraus MS, Mahaffey MB, Girard E, et al. Diagnosis of C5-C6 spinal luxation using three-dimensional computed tomographic reconstruction. *Vet Radiol Ultrasound* 1997;38:39-41.
246. Bagley RS. Spinal fracture or luxation. *Vet Clin North Am Small Anim Pract* 2000;30:133-153
247. Green RA, Saifuddin A. Whole spine MRI in the assessment of acute vertebral body trauma. *Skeletal Radiol* 2004;33:129-135.
248. Skeen TM, Olby NJ, Munana KR, et al. Spinal arachnoid cysts in 17 dogs. *J Am Anim Hosp Assoc* 2003;39:271-282.
249. Jurina K, Grevel V. Spinal arachnoid pseudocysts in 10 Rottweilers. *J Small Anim Pract* 2004;45:9-15.
250. Galloway AM, Curtis NC, Sommerlad SF, et al. Correlative imaging findings in seven dogs and one cat with spinal arachnoid cysts. *Vet Radiol Ultrasound* 1999;40:445-452.
251. Kendall BE, Valentine AR, Keis B. Spinal arachnoid cysts: Clinical and radiological correlation with prognosis. *Neuroradiology* 1982;22:225-234.
252. Hashizume CT. Cervical spinal arachnoid cyst in a dog. *Can Vet J* 2000;41:225-227.
253. Gnirs K, Ruel Y, Blot S, et al. Spinal subarachnoid cysts in 13 dogs. *Vet Radiol Ultrasound* 2003;44:402-408.
254. Dickinson PJ, Sturges BK, Berry WL, et al. Extradural spinal synovial cysts in nine dogs. *J Small Anim Pract* 2001;42:502-509.
255. Gómez M, Mieres M, Thibaut J. Cervical intravertebral disk herniation (Schmorl's node) in a dog. *Arch Med Vet* 2000;32:115-119.
256. Peng B, Wu W, Hou S, et al. The pathogenesis of Schmorl's nodes. *J Bone Joint Surg Br* 2003;85:879-882.
257. Wise M, Faulkner R. Unusual disc herniation in a dog. *Vet Radiol Ultrasound* 1984;25:280-281.
258. Gashen L, Lang J, Haeni H. Intravertebral disc herniation (Schmorl's node) in five dogs. *Vet Radiol Ultrasound* 1995;36:509-516.

259. Hamanishi C, Kawabata T, Yosii T, et al. Schmorl's nodes on magnetic resonance imaging. Their incidence and clinical relevance. *Spine* 1994;19:450-453.
260. Groen RJ, Batchelor DA, Hoogland PV. RE: Congenital dilatation of the cervical epidural venous plexus: neuroradiology and endovenous management. *Minim Invasive Neurosurg* 2000;43:109-110.
261. Jayson MI. The role of vascular damage and fibrosis in the pathogenesis of nerve root damage. *Clin Orthop* 1992:40-48.
262. Porter RW. Spinal stenosis and neurogenic claudication. *Spine* 1996;21:2046-2052.
263. Dietemann JL, Zöllner G, Dettlof H, et al. Scannographie des veines épidurales rachidiennes. *Radiologie CEPUR* 1989;9:169-181.
264. Jones JC, Shires PK, Inzana KD, et al. Evaluation of canine lumbosacral stenosis using intravenous contrast-enhanced computed tomography. *Vet Radiol Ultrasound* 1999;40:108-114.
265. Feeney D, Fletcher T, Hardy R. *Atlas of Correlative Imaging Anatomy of the Normal Dog: Ultrasound and Computed Tomography*. Philadelphia: WB Saunders, 1991.3-152.
266. George T, Smallwood J. Anatomic Atlas For Computed Tomography In The Mesencephalic Dog: Head and Neck. *Vet Radiol Ultrasound* 1992;33:217-240.
267. Assheuer J, Sager M. *MRI and CT Atlas of the Dog*: Iowa State University Press, 1997.83-129
268. Pagani JJ, Hayman LA, Kelemouridis VL. A technique for preparation, removal, and storage of cadaver spine specimens for CT evaluation. *Invest Radiol* 1984;19:51-53.
269. Roland J, Treil J, Larde D, et al. Lumbar phlebography in the diagnosis of disc herniations. *J Neurosurg* 1978;49:544-550.
270. Fischgold H, Adam H, Ecoiffier J, et al. Opacification des plexus rachidiens et des veines azygos par voie osseuse. *J Radiol Electrol Med Nucl* 1952;33:37-38.

271. Plaisant O, Sarrazin JL, Gillot C, et al. Technique for injection of the lumbar vertebral venous plexuses employed in anatomic, computed tomography and magnetic resonance imaging studies. *Surg Radiol Anat* 1998;20:113-118.
272. Plaisant O, Sarrazin JL, Cosnard G, et al. The lumbar anterior epidural cavity: the posterior longitudinal ligament, the anterior ligaments of the dura mater and the anterior internal vertebral venous plexus. *Acta Anat (Basel)* 1996;155:274-281.
273. Magnaldi S, Pozzi-Mucelli RS, Cova MA, et al. CT study of the cervical spine with intravenous administration of the contrast medium. *Radiol Med (Torino)* 1989;77:329-335.
274. Heinz ER, Yeates A, Burger P, et al. Opacification of epidural venous plexus and dura in evaluation of cervical nerve roots: CT technique. *AJNR Am J Neuroradiol* 1984;5:621-624.
275. Cassar-Pullicino VN, Colhoun E, McLelland M, et al. Hemodynamic alterations in the paravertebral venous plexus after spinal injury. *Radiology* 1995;197:659-663.
276. Delamarter RB, Bohlman HH, Dodge LD, et al. Experimental lumbar spinal stenosis. Analysis of the cortical evoked potentials, microvasculature, and histopathology. *J Bone Joint Surg Am* 1990;72:110-120.
277. Hammer A, Knight I, Agarwal A. Localized venous plexi in the spine simulating prolapse of an intervertebral disc: a report of six cases. *Spine* 2003;28:E5-E12.
278. Ammerich H, Quintana F. Phlebographic signs of the narrow lumbar canal In: Wackenheim A BE, ed. *The Narrow Lumbar Canal*. New York: Springer, 1980.
279. Kaiser MC, Capesius P, Roilgen A, et al. Epidural venous stasis in spinal stenosis. CT appearance. *Neuroradiology* 1984;26:435-438.
280. Olmarker K, Rydevik B, Holm S, et al. Effects of experimental graded compression on blood flow in spinal nerve roots. A vital microscopic study on the porcine cauda equina. *J Orthop Res* 1989;7:817-823.
281. Gomez M, Freeman L, Jones J, et al. Computed tomographic anatomy of the canine cervical vertebral venous system. *Vet Radiol Ultrasound* 2004;45:29-37.

282. Raininko R, Torma T. Contrast enhancement around a prolapsed disk. *Neuroradiology* 1982;24:49-51.
283. Sharp NJH, Cofone M, Robertson ID, et al. Computed tomography in the evaluation of caudal cervical spondylomyelopathy of the Doberman Pinscher. *Vet Radiol Ultrasound* 1995;36:100-108.
284. Fourie SL, Kirberger RM. Relationship of cervical spinal cord diameter to vertebral dimensions: A radiographic study of normal dogs. *Vet Radiol Ultrasound* 1999;40:137-143.
285. Doherty BJ, Heggeness MH. Quantitative anatomy of the second cervical vertebra. *Spine* 1995;20:513-517.
286. Debois V, Herz R, Berghmans D, et al. Soft cervical disc herniation. Influence of cervical spinal canal measurements on development of neurologic symptoms. *Spine* 1999;24:1996-2002.
287. Jones JC, Wright JC, Bartels JE. Computed tomographic morphometry of the lumbosacral spine of dogs. *Am J Vet Res* 1995;56:1125-1132.
288. Schonstrom NS, Bolender NF, Spengler DM. The pathomorphology of spinal stenosis as seen on CT scans of the lumbar spine. *Spine* 1985;10:806-811.
289. Barthez PY, Begon D, Delisle F. Effect of contrast medium dose and image acquisition timing on ureteral opacification in the normal dog as assessed by computed tomography. *Vet Radiol Ultrasound* 1998;39:524-527.
290. Thompson MS, Graham JP, Mariani CL. Diagnosis of a porto-azygous shunt using helical computed tomography angiography. *Vet Radiol Ultrasound* 2003;44:287-291.
291. Kuszyk BS, Fishman EK. Technical aspects of CT angiography. *Semin Ultrasound CT MR* 1998;19:383-393.
292. Foley WD, Karcaaltincaba M. Computed tomography angiography: Principles and clinical applications. *J Comput Assist Tomogr* 2003;27 Suppl 1:S23-30.
293. Nieman K, Cademartiri F, Raaijmakers R, et al. Noninvasive angiographic evaluation of coronary stents with multi-slice spiral computed tomography. *Herz* 2003;28:136-142.

294. Fischer DR, Baltzer P, Malich A, et al. Is the "blooming sign" a promising additional tool to determine malignancy in MR mammography? *Eur Radiol* 2004;14:394-401.
295. Schonstrom N. The significance of oblique cuts on CT scans of the spinal canal in terms of anatomic measurements. *Spine* 1988;13:435-436.
296. Ros L, Mota J, Guedea A, et al. Quantitative measurements of the spinal cord and canal by MR imaging and myelography. *Eur Radiol* 1998;8:966-970.
297. Gelber ND, Ragland RL, Knorr JR. Gd-DTPA enhanced MRI of cervical anterior epidural venous plexus. *J Comput Assist Tomogr* 1992;16:760-763.
298. Rodiek SO, Schmidhuber H, Lumenta CB. Congenital dilation of the cervical epidural venous plexus: neuroradiology and endovenous management. *Minim Invasive Neurosurg* 1999;42:69-73.
299. Paksoy Y, Gormus N. Epidural venous plexus enlargements presenting with radiculopathy and back pain in patients with inferior vena cava obstruction or occlusion. *Spine* 2004;29:2419-2424.
300. Wong CH, Thng PL, Thoo FL, et al. Symptomatic spinal epidural varices presenting with nerve impingement: report of two cases and review of the literature. *Spine* 2003;28:E347-350.
301. Yousry I, Forderreuther S, Moriggl B, et al. Cervical MR imaging in postural headache: MR signs and pathophysiological implications. *AJNR Am J Neuroradiol* 2001;22:1239-1250.
302. Wright JA. A study of the radiographic anatomy of the cervical spine in the dog. *J Small Anim Pract* 1977;18:341-357.
303. Lewis D. Radiological assesment of the cervical spine of the dobermann with reference to cervical spondylomyelopathy. *J Small Anim Pract* 1991;32:75-82.
304. Lee HM, Kim NH, Kim HJ, et al. Mid-sagittal canal diameter and vertebral body/canal ratio of the cervical spine in Koreans. *Yonsei Med J* 1994;35:446-452.
305. Senol U, Cubuk M, Sindel M, et al. Anteroposterior diameter of the vertebral canal in cervical region: comparison of anatomical, computed tomographic, and plain film measurements. *Clin Anat* 2001;14:15-18.

306. Dabanoglu I, Kara ME, Turan E, et al. Morphometry of the thoracic spine in German shepherd dog: a computed tomographic study. *Anat Histol Embryol* 2004;33:53-58.
307. Tierney RT, Maldjian C, Mattacola CG, et al. Cervical spine stenosis measures in normal subjects. *J Athl Train* 2002;37:190-193.
308. Pavlov H, Torg JS, Robie B, et al. Cervical spinal stenosis: determination with vertebral body ratio method. *Radiology* 1987;164:771-775.
309. Keats T, Siström C. *Atlas of Radiologic Measurements*. St Louis: Mosby, 2001.127-176.
310. Blackley HR, Plank LD, Robertson PA. Determining the sagittal dimensions of the canal of the cervical spine. The reliability of ratios of anatomical measurements. *J Bone Joint Surg Br* 1999;81:110-112.
311. Hukuda S, Xiang LF, Imai S, et al. Large vertebral body, in addition to narrow spinal canal, are risk factors for cervical myelopathy. *J Spinal Disord* 1996;9:177-186.
312. Breit S, Kunzel W. The position and shape of osteophyte formations at canine vertebral endplates and its influence on radiographic diagnosis. *Anat Histol Embryol* 2001;30:179-184.
313. Kim H, Chung JW, Park JH, et al. Role of CT venography in the diagnosis and treatment of benign thoracic central venous obstruction. *Korean J Radiol* 2003;4:146-152.
314. Josephson SA, Bryant SO, Mak HK, et al. Evaluation of carotid stenosis using CT angiography in the initial evaluation of stroke and TIA. *Neurology* 2004;63:457-460.
315. Wetzel SG, Kirsch E, Stock KW, et al. Cerebral veins: Comparative study of CT venography with intraarterial digital subtraction angiography. *AJNR Am J Neuroradiol* 1999;20:249-255.
316. Tarlov I, Klinger H, Vitale S. Spinal compression studies. I. Experimental techniques to produce acute and gradual compression. *AMA Arch of Neurol Psychiatry* 1953;70:813-819.
317. Schwartz ED, Himes BT. New model of minimally invasive experimental spinal cord injury. *AJNR Am J Neuroradiol* 2003;24:166-168.

318. Purdy PD, White CL, 3rd, Baer DL, et al. Percutaneous translumbar spinal cord compression injury in dogs from an angioplasty balloon: MR and histopathologic changes with balloon sizes and compression times. *AJNR Am J Neuroradiol* 2004;25:1435-1442.
319. Johnson C. Patient monitoring In: Seymour C, Gleed R, eds. *BSAVA Manual of small animal anesthesia and analgesia*. Cheltenham: British Small Animal Veterinary Association, 1999.
320. Rosenstein DS, Bowker RM, Bartlett PC. Digital angiography of the feet of horses. *Am J Vet Res* 2000;61:255-259.
321. LaBan MM, Wesolowski DP. Night pain associated with diminished cardiopulmonary compliance. A concomitant of lumbar spinal stenosis and degenerative spondylolisthesis. *Am J Phys Med Rehabil* 1988;67:155-160.
322. Doppman JL. Angiographic changes following acute spinal cord compression: an experimental study in monkeys. *Br J Radiol* 1976;49:398-406.
323. Wolfla CE, Snell BE, Honeycutt JH. Cervical ventral epidural pressure response to graded spinal canal compromise and spinal motion. *Spine* 2004;29:1524-1529.
324. Morikawa M, Sato S, Numaguchi Y, et al. Spinal epidural venous plexus: Its MR enhancement patterns and their clinical significance. *Radiat Med* 1996;14:221-227.
325. Zimmerman GA, Weingarten K, Lavyne MH. Symptomatic lumbar epidural varices. Report of two cases. *J Neurosurg* 1994;80:914-918.
326. Osterholm JL, Mathews GJ. Altered norepinephrine metabolism following experimental spinal cord injury. 1. Relationship to hemorrhagic necrosis and post-wounding neurological deficits. *J Neurosurg* 1972;36:386-394.
327. Chantraine A, van Ouwenaller C, Hachen HJ, et al. Intra-medullary pressure and intra-osseous phlebography in paraplegia. *Paraplegia* 1979;17:391-399.
328. Hjarbaek J, Kristensen PW, Hauge P. Spinal gas collection demonstrated at CT. *Acta Radiol* 1992;33:93-96.
329. Giraud F, Fontana A, Mallet J, et al. Sciatica caused by epidural gas. Four case reports. *Joint Bone Spine* 2001;68:434-437.

330. Teasell RW, Arnold JM, Krassioukov A, et al. Cardiovascular consequences of loss of supraspinal control of the sympathetic nervous system after spinal cord injury. *Arch Phys Med Rehabil* 2000;81:506-516.
331. Bravo G, Guizar-Sahagun G, Ibarra A, et al. Cardiovascular alterations after spinal cord injury: an overview. *Curr Med Chem Cardiovasc Hematol Agents* 2004;2:133-148.
332. Piepmeier JM, Lehmann KB, Lane JG. Cardiovascular instability following acute cervical spinal cord trauma. *Cent Nerv Syst Trauma* 1985;2:153-160.
333. Shima F, Fukui M, Matsubara T, et al. Spasmodic torticollis caused by vascular compression of the spinal accessory root. *Surg Neurol* 1986;26:431-434.
334. Shima F, Fukui M, Kitamura K, et al. Diagnosis and surgical treatment of spasmodic torticollis of 11th nerve origin. *Neurosurgery* 1988;22:358-363.
335. Evans HE, Kitchell R. Cranial nerves and cutaneous innervation of the head. *Miller's Anatomy of the Dog*. 3rd ed, Philadelphia: WB Saunders, 1993.829-893.
336. Link J, Muller-Hulsbeck S, Wesner F, et al. Spiral CT angiography versus DSA in detection of carotid stenoses. *Zentralbl Chir* 1996;121:1018-1022.
337. Kaatee R, Beek FJ, de Lange EE, et al. Renal artery stenosis: detection and quantification with spiral CT angiography versus optimized digital subtraction angiography. *Radiology* 1997;205:121-127.

VITA

Marcelo Gomez Jaramillo was born in Panguipulli, Chile. After finishing high school in Valdivia, in December 1988, he attended Austral University of Chile, Valdivia, Chile, where he graduated from Veterinary Medical School in 1995. He worked as a large animal practitioner in his hometown for one year. Then, he joined the Veterinary Anatomy Institute, Austral University of Chile, where he has been a faculty member since 1997. In August of 2000, he enrolled in the Master of Veterinary Science program at the VA-MD Regional College of Veterinary Medicine, Department of Biomedical Sciences and Pathobiology. He was transferred to the doctoral program in 2002. He continued his academic pursuit under Dr. Jeryl Jones supervision. He will return to Chile and Austral University of Chile after completing his Ph.D.